

General Disclaimer

One or more of the Following Statements may affect this Document

- This document has been reproduced from the best copy furnished by the organizational source. It is being released in the interest of making available as much information as possible.
- This document may contain data, which exceeds the sheet parameters. It was furnished in this condition by the organizational source and is the best copy available.
- This document may contain tone-on-tone or color graphs, charts and/or pictures, which have been reproduced in black and white.
- This document is paginated as submitted by the original source.
- Portions of this document are not fully legible due to the historical nature of some of the material. However, it is the best reproduction available from the original submission.

Princeton University

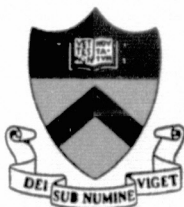
Part I

(NASA-CR-146083) A SEARCH FOR CHEMICAL
LASER ACTION IN LOW PRESSURE METAL VAPOR
FLAMES Ph.D. Thesis (Princeton Univ.)
403 p HC \$11.00

N76-15450

CSSL 20E

G3/36 Unclass
07417



Department of
Aerospace and
Mechanical Sciences

A SEARCH FOR
CHEMICAL LASER ACTION IN
LOW PRESSURE METAL VAPOR FLAMES

Melvin L. Zwillenberg

A DISSERTATION
PRESENTED TO THE
FACULTY OF PRINCETON UNIVERSITY
IN CANDIDACY FOR THE DEGREE
OF DOCTOR OF PHILOSOPHY
RECOMMENDED FOR ACCEPTANCE BY THE
DEPARTMENT OF
AEROSPACE AND MECHANICAL SCIENCES

September 1975

ABSTRACT

Reactions of the alkaline earth metals with various oxidizers are prime candidates for potential electronic transition chemical laser application, because of their high exothermicity, the availability of numerous low-lying electronically excited states and the observation in these reactions of visible chemiluminescence.

A study has been made of optical emissions from low pressure (~ 1 torr) dilute diffusion flames of Ca and Mg vapor with O_2 , N_2O and mixtures of CCl_4 and O_2 . The Ca flames with O_2 and N_2O revealed high vibrational excitation of the product CaO molecule (up to $v=30$). The flames with CCl_4 revealed extreme non-equilibrium metal atom electronic excitation, up to the metal atom ionization limit (6.1 eV for Ca, 7.6 eV for Mg). The metal atom excited electronic state populations did not follow a Boltzmann distribution, but the excitation rates ("pumping rate") were found to obey an Arrhenius-type expression, with the electronic excitation energy playing the role of activation energy and a "temperature" of about $5000^\circ K$ for triplet excited states and $2500^\circ K$ for singlets (vs. $\sim 500^\circ K$ translational temperature). Evidence is presented for a proposed excitation mechanism $C+MO^V \rightarrow CO+M^*$.

The observed distribution of pumping rate with excited state energy, plus tabulated transition probabilities, would lead one to predict a number of population inversions, and some of these have been observed but at inversion densities too low for oscillation. Much higher excited state populations were observed for the metastable $M^*(^3P)$ state, and a possible method for producing laser action by collisional transfer from $M^*(^3P)$ to another atomic species is discussed.

ACKNOWLEDGMENTS

The author wishes to express his sincere appreciation to his thesis advisor, Professor Irvin Glassman, and to acknowledge, with deepest thanks, the guidance, encouragement, and understanding provided by Professor Glassman throughout the author's graduate studies at Princeton.

Special thanks are due also to Dr. David W. Naegeli for many hours of discussion of spectroscopy, reaction mechanisms, and experimental technique, and for much valuable constructive criticism.

Helpful discussions were held, as well, with Dr. Frederick L. Dryer and with fellow-students Richard Cohen, Meredith Colket, Michael Campbell, and Daniel Aronowitz.

The author wishes to acknowledge the valuable assistance of Mr. Thomas M. Shelton who provided information and advice regarding electronic instrumentation, photodetectors, and synchronous detection.

Mr. Joseph Sivo deserves special thanks for his heroic efforts in the fabrication, assembly, and maintenance of the experimental apparatus. The able assistance of Mr. Donald Peoples and the welding wizardry of Mr. Zigmond Lakacauskis are also acknowledged.

The author wishes to thank Mr. Toni Poli and his Design Group for their assistance in the design of the apparatus.

Mr. Michael Freeman for drawing the figures, and Mr. Donald Neiler for preparing the photographs in this report.

The manuscript was patiently typed by Mrs. Natalie Mendelson and the revisions completed by Ms. Peggy Werts, both of whom the author wishes to thank.

Last, but far from least, the author offers his heartfelt thanks to his wife, Myrna, and his parents for their understanding, patience, and encouragement which have sustained him throughout his studies.

Financial support as an Air Reduction Company Fellow and as a National Science Foundation Fellow is gratefully acknowledged.

This research was made possible by the National Aeronautics and Space Administration under NASA Grants ^{NGR} 31-001-129 and ^{NGR} 31-001-312.

This thesis bears the number 1214-T in the records of the Department of Aerospace and Mechanical Sciences.

TABLE OF CONTENTS

	<u>Page</u>
Title Page	i
Abstract	ii
Acknowledgements	iv
Table of Contents	vi
List of Tables	ix
List of Symbols	xi
Chapter I: INTRODUCTION, Chemical Laser Theory and Principles of Experimental Technique	1
1. Introduction	1
2. Laser Action	5
3. Chemical Lasers	10
A. Historical Considerations	10
B. Alkali and Alkaline Earth Metal Reactions: Rates, Cross-Sections and "Harpooning"	13
C. Thermochemical Calculations	15
D. Observations of Electronic Chemi- luminescence	19
E. Depletion of the Lower Electronic State and Lasing	23
F. Spin Conservation	26
4. Discussions, Conclusions and Selection of Systems for Study	27
5. Discussion of Experimental Technique	30
a. Low Pressure Diffusion Flame Technique	30
b. Determination of Excitation Rates, Quantum Yields and Excited State Population Densities.	34

	<u>Page</u>
c. Detection of Self-Absorption or Stimulated Emission, and Calculation of Lower State Population Density or Inversion Density.	41
Chapter II: Experimental Apparatus and Procedure	50
1. Materials	51
a. Metal Samples	51
b. Gases	52
c. Photographic Materials and Processing	56
2. Apparatus	57
a. Vacuum Chamber	58
b. Multiple-Reflection (White) Cell	58
c. Metal Vapor Furnace	65
d. Vacuum System	72
e. Pressure Measurement and Gas Flow Control System	72
f. Spectrographic Instrumentation	74
g. Electronic Instrumentation	76
h. Photomultiplier/Spectrometer Calibrations	80
i. Auxilliary Equipment	83
3. Procedure	84
Chapter III: Experimental Results and Discussion of Results.	89
a. Types of Flames Studied and Range of Experimental Parameters.	89
b. General Appearance of Metal Vapor Flames	92
c. Chemiluminescent Origin of the Emitted Radiation.	98
d. Estimation of Metal Atom Flux and Mole Fraction.	100
e. Mg/O ₂ and Mg/N ₂ O Flames	106
f. Ca/O ₂ and Ca/N ₂ O Flames	117

	<u>Page</u>
g. Mg/CCl ₄ /O ₂ and Ca/CCl ₄ /O ₂ Flames	146
(1) Flame Spectra	146
(2) Molecular Excitation	155
(3) Atomic Line Emission and Excitation Temperatures.	158
(4) Effect of Experimental Parameters on Flame Size, Intensity and Excitation Temperature.	170
(a) Flame Diameter	170
(b) Flame Intensity	175
(i) Variation with Pressure	175
(ii) Variation with Oxidizer Concentration.	178
(iii) Variation with CCl ₄ Concentration.	183
(c) Excitation Temperatures	187
(5) Quenching Experiments	195
(a) Nitric Oxide Quenching	197
(b) N ₂ Quenching	214
(c) Quenching by O ₂ and CCl ₄	219
(6) Excitation Mechanisms	235
(7) Ground and Excited State Population Densities and Quantum Yields.	267
(8) Population Inversions, Predicted and Observed.	280
(9) Mg*(3P) - K Collisional Transfer Laser	290
Chapter IV: Conclusions	295
References	306
Figures	323

List of TablesChapter I

- I. Energy release and minimum electronic excitation energy
- II. Energy release and minimum excitation energy

Chapter II

- I. Purity of gases used
- II. Melting and boiling points of alkaline earth metals
- III. Condensed specifications of PAR 128A lock-in-amplifier

Chapter III

- I. Range of experimental parameters
- II. Minimum flame zone thickness
- III. A. Estimated thermocouple error
B. Temperature difference with and without oxidizer
- IV. Estimation of metal vapor flux
- V. Excitation energies of MgO electronically excited states
- VI. Visible bands observed in Ca + O₂ flame spectra
- VII. Visible bands observed in Ca + N₂O flame spectra
- VIII. Photoelectrically observed bands and assignments, Ca/O₂ and Ca/N₂O flames
- IX. Wavelengths and vibrational assignments of Ca/N₂O flame bands
- X. Wavelengths and vibrational assignments of Ca/O₂ flame bands
- XI. Calculation of vibrational energy
- XII. Available exothermicity and required excitation energy of observed CaO band systems

- XIII. Molecular bands observed in $\text{Ca/CCl}_4/\text{O}_2$, $\text{Mg/CCl}_4/\text{O}_2$ and $\text{Mg/CCl}_4/\text{N}_2\text{O}$ flames
- XIV. Minimum excitation energies of highest observed molecular energy levels
- XV. Peak intensity and oxidant/ CCl_4 ratio
- XVI. Excitation temperature, T_{ex} , and experimental conditions
- XVII. Effect of N_2 addition on T_{ex}
- XVIII. Comparison of Mg and Ca triplet and singlet excitation temperatures
- XIX. Carbon atom reaction rate constants
- XX. Values used in estimating \bar{t} and \bar{X}
- XXI. N_2 quenching of Ca and Mg singlets and triplets
- XXII. Rate constants calculated from I vs. $[\text{O}_2]$ and $[\text{CCl}_4]$ curves by different methods
- XXIII. Literature rate constant values for reactions of C, CCl_4 and related molecules
- XXIV. Ground and metastable state population densities from absorption and emission data
- XXV. Maximum observed excited state population densities
- XXVI. Quantum yields
- XXVII. Observed population inversion ratios and upper state densities
- XXVIII. Threshold inversion densities
- XXIX. Calculated inversion ratios for potassium

List of Symbols

a	CCl_4 concentration
A	First excited molecular electronic state; Stern-Volmer constant
A_{ul}	Einstein coefficient for spontaneous emission from upper state "u" to lower state "l"
A_{21}	Einstein coefficient for spontaneous emission from state 2 to state 1 (transition probability)
b	Oxygen concentration
B	Second excited molecular electronic state; Source brightness; a constant.
c	a constant; speed of light
C	Third excited molecular electronic state; Concentration; a constant
C_p	Specific heat capacity at constant pressure
D	Diffusion coefficient; Diameter; Dissociation energy
e	Electronic charge; Base of natural logarithms
E_a	Activation energy
E_u	Energy of upper state
E_v	Vertical electron affinity
E_1, E_2	Energy of state 1, 2
f	Electron oscillator strength
F	Total photon emission rate
$F(T)$	Partition function
ΔG	Vibrational spacing (In Deslandres table)
G_o	Laser gain per unit length at center of line
h	Planck's constant
H	Enthalpy

ΔH_r	Heat of reaction
I	Radiative intensity; Ionization potential
j	Rotational quantum number
J	Emission coefficient; Total angular momentum quantum number of an atom
k	Kinetic rate constant; Boltzmann constant; ratio of specific heats.
K, K'	Constants; Effective absorption coefficient
Kn	Knudsen number
K_0	Zero order Bessel function of the second kind
l	Lower state
L	Mean free path
m	Molecular mass; Effective number of optical passes through White cell
m'	Reactant input rate
M	Metal atom
MO	Metal oxide molecule
MX	Metal halide molecule
n	Number density
n'	Rate of excitation
N	Number of data points; Number of spectral lines
\bar{N}	Effective number of spectral lines
N_1, N_2	Population of state 1, 2
P_A, P_B	Partial pressure of components A, B
P_m, P_M	Metal vapor partial pressure
P	Pressure; Statistical probability
$p_{m,m}^{n,n-1}$	Vibrational transition probability of $A(v=n) \rightarrow A(v=m) \rightarrow A(v=n-1) \rightarrow A(v=m+1)$
q	Volumetric flow rate

$q_{v',v''}$	Franck-Condon factor for $v' \rightarrow v''$ band
Q_r	Reactive collision cross section
r	Radial coordinate; recovery factor; flame radius;
r_c	Crossing radius
R	Gas constant per unit mass; Radius of field of view of optical system
Ratio	Flame intensity at visible edge/Flame intensity at center
S	Geometric path length; Total spin quantum number of an atom
S_{ul}	Line strength of transition $u \rightarrow l$
t	Time; Residence time
\bar{t}	Mean residence time
T	Absolute temperature, Third body
T_e	Electronic term value (Electronic energy of potential curve minimum)
u	Upper state
U	Velocity
v	Vibrational quantum number
V	Volume; Velocity
\vec{V}	Velocity
X	Geometric path length; Ground molecular electronic state; Mole fraction; $KS/\Delta v$
Y	Rate of excitation per sublevel $= R_u/g_u = I\lambda/g_u$; Normalized intensity as function of reactant concentration

Greek Symbols

ν	Frequency
ρ	Density
ρ_ν	Radiation density at frequency ν
σ	Collision radius ($\pi\sigma^2$ =cross section); Standard deviation
τ	Lifetime; Space-time in a chemical reactor = volume/flow rate
τ_u	Radiative lifetime of state "u"
ω_e	First molecular vibrational constant (Zero amplitude vibrational frequency)
ϕ	Measured ratio of multipass to single-pass in- tensities
ϕ	Measured ratio of multiplet component intensities
ψ	Wave function; Theoretical ratio of multiplet component intensities

Subscripts:

av	average
A	Argon
c	Collisional; Crossing
D	Doppler-broadened
e	Electron
eff	Effective
ex	Excitation
H	Upper limit of energy interval

j	Thermocouple junction
L	Lower limit of energy interval
M, m	Metal
max	Value at edge of flame; Value at peak of Intensity vs. concentration curve
o	Ground state; Initial value; Stagnation value; Value with no quenching
obs	Observed
p	Production
r, rad	Radiative
s	Standard conditions; Static value
trans	Translational
1/2	Value of independent variable for which dependent variable has 1/2 its initial value

Superscripts:

- Average
- ' Upper State
- " Lower State
- * Electronically excited (or any other excitation if not specified)
- v Vibrationally excited

Other Symbols:

[X] Concentration of X

Spectroscopic Notation:

$1s, 1p, 1d, 1f$ are singlet atomic states

$1\Sigma, 1\Pi$ are singlet molecular states

$3s, 3p, 3d, 3f$ are triplet atomic states

$3\Sigma, 3\Delta$ are triplet molecular states

$2p, 2\Sigma$ are doublet atomic and molecular states respectively

See Herzberg (1944, 1950) for detailed explanation of notation.

R, V, denote bands shaded to red, violet ends of spectrum.
M denotes a band with no preferred direction of shading (i.e. a maximum).

L denotes an atomic line.

Chapter I - Introduction,

Chemical Laser Theory and Principles of Experimental Technique

1. Introduction

The chemiluminescent reactions of alkali metals with halogens and halogen compounds have received great attention over the past 50 years (von Haber and Zisch, 1922, Heller and Polanyi, 1936, Beutler and Polanyi, 1928, Polanyi and Schay, 1928, Glasstone, Laidler and Eyring, 1941, Miller and Palmer, 1963, Naegeli, 1967). Until very recently, very little attention had been given to another class of highly exothermic chemical systems in which the observation of chemiluminescence has indicated the presence of electronically excited products -- the reactions of the alkaline earth metals with oxygen, halogens, halogen compounds and other oxidants. Thermochemical calculations performed on many of these systems show that the energy release of many is more than adequate for electronic excitation, not only to the first electronically excited state, but in some cases to higher electronic states as well.

All successful chemical lasers, to date, have utilized vibrational-rotational transitions of excited product molecules (either directly or via energy transfer to another molecule). Consideration of the relative magnitudes of radiative lifetimes, chemical reaction rates and collisional de-excitation rates, indicates that population inversion and chemical laser action

based on electronically excited product molecules or atoms produced in alkaline earth metal reactions may be possible. In order to put this system in the proper perspective, a detailed and critical review of the literature with respect to pertinent points is given. Because of the potential seen the present experimental investigation was begun. A discussion is included of several other interesting chemical systems and the possibility of "more conventional" vibrational-rotational population inversion in the above systems.

Chemical Lasers

It is deemed appropriate to begin with a discussion of what constitutes a chemical laser. The various types of so-called gas dynamic lasers, (Gerry 1971), in which the products of combustion are expanded rapidly through a nozzle cannot be considered true chemical lasers, even though the source of the energy may be a chemical reaction. Here the chemical reaction merely provides thermal pumping (which could equally be provided by a non-chemical heat source), and produces an equilibrium distribution of energy states at high temperature. Disequilibrium and population inversion in the gas dynamic laser are the result of differential rates of vibrational relaxation during the expansion process. A non-equilibrium distribution of energy states is a necessary (but not sufficient) condition for laser action. An inverted population (i.e., the excited state population higher than the lower state population) must be obtained if the stimulated

emission process is to result in amplification. A point of interest is that while all existing gas dynamic lasers utilize vibrational-rotational population inversion, early proposals of Hurle and Hertzberg (1965) dealt with electronic transitions.

Also excluded from consideration as chemical lasers are systems where chemically powered light sources (e.g., flames, shock-excited gases) are used to optically pump a laser system, (Conger and Johnson, 1966, Stokes, 1970, Wieder, 1970), and systems where molecular systems are pumped by optical (Hajdu, 1963, Gorog, 1961, Askar'ian, Gol'ts and Rabinovich, 1966, Ewing, Milstein and Berry, 1970, Bennett, 1965), gas dynamic shock or electrical discharge methods. A particular case of non-chemical excitation is the metal vapor laser in which electronically excited atoms are produced by electrical discharge or optical pumping, (Bennett, 1965, Mishakov, Tibolov and Shukhtin, 1971, Sorokin and Lankard, 1971), but in which chemical reactions play no part at all.

There has been much interest in explosion or detonation wave chemical lasers (Cool, 1971, Corneil and Pimentel, 1968, Marchenko and Prokhorov, 1971, Bowen and Overholser, 1969, Cohen, Wilkins and Jacobs, 1970, Corneil and Kasper, 1970, Graham, 1971), both pulsed and c.w., because of the possibility of premixing reactants before initiating chemical reaction. These devices would constitute true chemical lasers, as the chemical production of excited species underlies their operation. Because, as will be shown below, ordinary combustion reactions in the

alkaline earth/oxidizer chemical systems proposed have not yet been thoroughly investigated, it did not seem justified to incur the experimental and operational difficulties of explosion systems, stabilized detonation waves, supersonic flows, etc., before the simpler combustion systems have been studied. For this reason, detonation chemical lasers were not considered further.

There now remain for discussion the "pure" chemical lasers in which population inversion is produced by the simple mixing of chemical reactants. Variants of this scheme, which some exclude from the class of "pure" chemical lasers, are those where energy is added to one reactant (e.g., via an electric discharge) to produce ground state or excited atoms from a molecular reactant. These atoms then are mixed with a second reactant to form the excited products which support laser action. Most of the systems to be considered are of the first type, with no external energy input (except heating required to vaporize the metal). However, some reactions of particular interest involving excited reagents will also be discussed.

Because the chemical laser literature has mushroomed so in the past few years, only those references of particular relevance to the discussion will be cited. Excellent review articles have been presented by Cool (1969,1971), Peyron (1971), Pimentel (1966), Chester (1971) and Arnold and Rojeska (1973).

Nieuwpoort and Bleekrode (1965) have presented a very good theoretical analysis of the relationship of flow rates, reaction times and radiative lifetimes to the possibility of obtaining laser action, and this is all the more interesting since it was written before anyone had built a chemical laser. There are many useful articles on the theoretical foundations of chemical lasers in the Applied Optics (1965) supplement on chemical lasers, (also written before the first operational chemical laser). Carrington and Garvin (1969) give an excellent review of the chemical production of excited states, and a brief review of chemical lasers, and Callear and Lambert (1969) discuss the processes by which energy is transferred between internal modes. Kikuchi and Broida (1965) give a mathematical analysis of a 3-electronic level laser based on inversion involving the A,B and X levels. As will be shown below, this has possible application to the MgO and CaO systems, as well as a number of other alkaline earth oxides and halides. The present author has reviewed the chemical laser literature elsewhere (Zwillenberg, Naegeli and Glassman, 1974; Zwillenberg, 1975) from the standpoint of the present work.

2. Laser Action

A number of points regarding requirements for chemical lasers which have been discussed at length elsewhere (Zwillenberg,

Naegeli and Glassman, 1974, Zwillenberg, 1975) will be summarized here and relevant results quoted.

Let N_2 and N_1 be the populations of two states connected by a radiative transition with $E_2 > E_1$ and statistical weights g_2 and g_1 respectively. It can then be shown (Carrington and Garvin, 1969, Polanyi, 1965, Spinnler and Kittle, 1970) that the optical absorption coefficient for the transition is:

$$\bar{k} = - \frac{1}{I} \frac{dI}{dx} \sim \left(\frac{N_1}{g_1} - \frac{N_2}{g_2} \right) \quad (1)$$

For $N_2/g_2 > N_1/g_1$, negative absorption (gain) results and a population inversion is said to exist. Note that what must be inverted is N/g , not N . Thus a population inversion and laser action can exist for $N_2 < N_1$, as long as $N_2 > \frac{g_2}{g_1} N_1$. The improvement obtained in this manner is limited by the optical selection rules $\Delta S=0$, $\Delta l=\pm 1$, $\Delta J=0, \pm 1$. Taking $g=2J+1$, the maximum change of statistical weight in an optically allowed transition is 2 and the maximum improvement (smallest g_2/g_1) obtainable is:

$$\frac{g_2}{g_1} = \frac{g_2(J=0)}{g_1(J=1)} = \frac{1}{3}$$

Unfortunately, the ground states of the alkaline earth metals and metal oxides are 1S and $^1\Sigma$ states respectively, ($g_1 = 1$), providing no reduction in the difficulty of lasing on a transition terminating in the ground state. However, this statistical weight effect might help in transitions between two excited states (analogous to the usual "four-level laser"). Thus, a $^3P_0 \rightarrow ^3D_1$ transition would have $g_2/g_1 = 1/3$.

For laser action, there must be not only a population inversion but also a minimum inversion density $N_2/g_2 - N_1/g_1$, so the negative absorption calculated from Equation (1) can overcome the inevitable losses in any practical laser system (e.g. window losses, mirror absorption diffraction losses). Thus, for a given cavity configuration, even in the most favorable case where the lower state is empty, there is a minimum concentration of excited atoms or molecules for which oscillation can occur.

Several relevant characteristic times (whose relative magnitudes determine the possibility of chemical laser action in a given system) will now be defined. The radiative lifetime, τ_r , is the reciprocal of the spontaneous radiative transition probability (Einstein A-coefficient) for the upper level. The lifetime for collisional deactivation, τ_c , is defined by $\tau_c = \frac{1}{k_{col} [M]}$, where k_{col} is the bimolecular rate constant for quenching of the excited species by M.

Consider the reaction of A and B to form excited species C^* , with bimolecular rate constant k_{AB} . The reaction rate per A molecule is $k_{AB} n_B$, where n_B is the concentration of B. Assume that $n_A \ll n_B \approx n$, the total concentration. The mean time for an A molecule to react and form C^* , which we will call

(Niewpoort and Bleekrode, 1965) the "production time", τ_p , is thus:

$$\tau_p = \frac{1}{k_{AB}n}$$

For efficient utilization of the excited species to attain threshold, they must radiate before they are collisionally deactivated and hence we must have $\tau_r < \tau_c$. To maintain a supply of excited atoms or molecules as they decay, $\tau_p \ll (1/\tau_r + 1/\tau_c)^{-1} \approx \tau_r$ is required.

Numerical estimates have been made of these three characteristic times. Parrish and Herm (1969) give $Qr=86\text{\AA}^2$ for the reactive cross section for the $\text{Li}+\text{Cl}_2$ reaction, which leads to a value of $\tau_p=6 \times 10^{-6}$ sec. Similarly large cross-sections are estimated for alkaline earth reactions using the methods given by Parrish and Herm (1969) and Polyani (1965) for electron-jump reaction mechanisms. Johnson (1971) measured values of τ_r in the range 10^{-7} - 10^{-6} sec in his laser-excited fluorescence studies of BaO, AlO, BeO, PbO, and FeO. Johnson (1971) also gave a collisional deactivation rate for $\text{BaO}(A^1\Sigma)$ by helium of $K \sim 10^{-11} \text{ cm}^3 \text{ sec}^{-1} \text{ molecule}^{-1}$. At 10^{-3} atmosphere, 500°K (typical conditions for a low pressure metal vapor flame) this corresponds to $\tau_c=10^{-5}$ sec.

Sakurai, Johnson and Broida (1970) reported similar magnitudes of electronic quenching of BaO by He, Ar and N_2 , but greater quenching by O_2 . However, Johnson reported that when his Ba/ O_2 flame was adjusted for maximum signal, no increase in apparent BaO lifetime resulted from a decrease in added O_2 . He interpreted this as indicating that under these conditions all the added O_2 was consumed in forming BaO, and little or no O_2 remained for quenching.

The typical values of the various characteristic times estimated above are thus $\tau_r \sim 10^{-7}$ - 10^{-6} sec, $\tau_p \sim 6 \times 10^{-8}$ sec and $\tau_c \sim 10^{-5}$ sec,

the inequalities given above are satisfied and laser action is a possibility. Alkaline earth oxides have radiative lifetimes 1 to 2 orders of magnitude longer than the 10^{-8} sec characteristic of atoms (Wiese et. al., 1966, 1969) and many other molecules (Laidler, 1955, Smith, 1969). These metals, like the alkali metals, react with oxidants by an electron-jump mechanism resulting in reactive collision cross-sections more than an order of magnitude higher than hard-sphere gas kinetic values. All these differences are in the direction tending to make laser action more feasible.

It has been suggested (Shuler, Carrington and Light; 1965) that inversions on molecular transitions might be more difficult to attain than in the atomic case, because of the division of each molecular transition into a multitude of vibrational-rotational transitions. However it has been shown (Tewarson, Naegeli and Palmer, 1969, Jones and Broida, 1973) that there is a tendency to form electronically excited product molecules in one or a few vibrational states. The Franck-Condon principle would cause a relatively few $v'-v''$ transitions to be much more intense than the others. The excitation energy would thus be divided among only a few transitions, making the attainment of inversion only slightly more difficult than in the case of atoms.

Redistribution of energy among vibrational states, even by extremely efficient collisional processes, can be shown to be unimportant. The mean time between collisions for

MgO molecules at 300°K and 10^{-3} atm. (using hard-sphere collision cross sections) is 5×10^{-7} sec. In a dilute flame where (for example) 99% of the molecules are rare gas, the mean time between potentially relaxing collisions thus becomes 5×10^{-5} sec since vibrational-translational relaxation is much less efficient than vibrational-vibrational relaxation (Stratton, 1969). This is much longer than the radiative lifetime for electronic transitions (Johnson, 1971) and the molecules thus radiate before they can be vibrationally relaxed. In the case of rotation, relaxation by collision with rare gas molecules is effective and the mean time between potentially relaxing collisions is 5×10^{-7} sec. Since the electronic radiative lifetime of the excited molecules is of this order or larger the rotational levels will be at least partially equilibrated. Thus the transition $A(v', j') \rightarrow X(v'', j'')$ has available to it the excitation present in all the rotational levels of the state $A(v')$ and similarly, equilibration in the lower state will deplete $X(v'', j'')$. (Shuler et.al., 1965).

3. Chemical Lasers

A. Historical Considerations

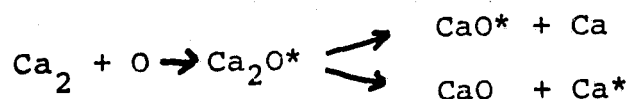
The early history of chemical laser research has been described at length in the review articles cited earlier and will not be repeated here. To date, all successful chemical lasers have followed Polanyi's early proposal (1961) for a laser based on vibrational-rotational rather than electronic transitions. Polanyi himself acknowledged

(1961) that electronic transitions have certain advantages for laser application. These include higher radiative transition probabilities (and consequent lower threshold inversion density), less serious quenching problems and the practical and experimental advantages of visible and ultraviolet (rather than infrared) emission (Zwillenberg, Naegeli and Glassman, 1974, Zwillenberg, 1975).

A large number of lasers have been reported utilizing vibrational transitions of excited HF, DF, CO, CO₂, HCl and HBr. In electrical discharges, laser action has been reported on vibrational transitions of SO₂, H₂S, H₂O and other gases (IEEE, 1970). Population inversions have been reported in electronic states of metal atoms formed by shock-dissociated alkali halides (Ewing, Milstein and Berry, 1970). Laser action has been produced in electric discharge excitation of alkali metal atoms (Bennett, 1965 Mishakov, Tibolov and Shukhtin, 1971 and Sorokin and Lankard, 1971). However, no investigations have been reported until recently of possible population inversion in either vibrational or electronic states of reaction products of the alkaline earth metals with oxygen, halogens, halogen compounds or other oxidants, or in the electronic states of metal atoms excited in such reactions. Recently, Rice and Jenson (1973) and Rice and Beattie (1973) have reported pulsed far infrared laser emission on vibrational

transitions from aluminum wires exploded in fluorine, (Rice and Jensen, 1973), and from the explosion of metallic wires, films and graphite smears into various oxidants, (Rice and Beattie, 1973). The combinations reported were: (Li, C, Mg, Al, Ti, Fe, Ni, Cu, Pt, Au, U) + F₂, (C, Ti, U) + O₂ and Ti + NF₃, and in all cases the wavelength was longer than 8.8 microns. However, no chemically produced electronic population inversions have been reported. Zhitkevich et al.(1963a,b) and Padley and Sugden (1960) have reported anomalous excitation of metal atoms in the inner cone of C₂H₂-air and H₂/O₂/N₂ flames respectively. Zhitkevich et al.(1963a) have also reported similar excitation and chemiluminescence in the reactions of the vapors of many metals (including alkaline earths) with alkyl halides. These studies, however were not concerned with chemical laser possibilities, and no laser action has been reported in any of these systems. Polanyi (1965) has suggested a vibrational-rotational laser based on the production of excited NaCl in the Cl + Na₂ reaction. Naegeli (1967) and Tewarson, Naegeli and Palmer (1969) have reported vibrational population inversion in the electronically excited products of reaction of alkali metals with halogen compounds. No laser action, however, has been reported. Early work, (Hansel, Mellor and Sullivan, 1967) in this laboratory attempted to explain certain observations in low pressure (~1 torr) calcium -O₂ flames in terms of chemiluminescence

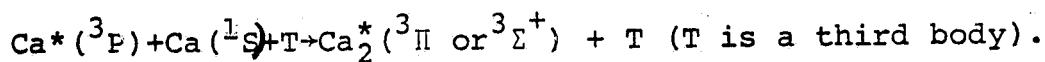
due to electronically excited CaO and Ca produced by the reactions:



It was also proposed that the exchange reaction



was a possible candidate for population inversion and laser action, but the possibility was not pursued further. Another possible mechanism (Zwillenberg, Naegeli and Glassman, 1974, Zwillenberg, 1975) is:



Here the excited state might be more stable than the ground state molecule (as it is in Mg_2 , Balfour and Douglas, 1970), and the ground state might thus be rapidly depleted by dissociation. Ground state Mg_2 (Balfour and Douglas, 1970) and Ca_2 (Balfour and Whitlock, 1971) have been reported in absorption in a King furnace at ~ 30 torr metal partial pressure. However, as described later, no evidence of electronically excited dimers was found in the present emission studies of flames at lower pressures.

B. Alkali and Alkaline Earth Metal Reactions: Rates, Cross-Sections and "Harpooning"

One feature which makes the alkali and alkaline earth metal reactions particularly attractive for chemical laser use is their extremely fast reaction rate, reflected in a reactive collision cross section ~100Å, 1-2 orders of magnitude greater than the hard-sphere gas kinetic value.

(Parrish and Herm, 1969, Birely et.al., 1969, Kwei and Herschback, 1969). This phenomenon has been described (Parrish and Herm, 1969, Polanyi, 1965) in terms of an electron jump process called "harpooning". This involves a crossing from a covalent to an ionic potential curve at a radius, r_c , given by:

$$e^2/r_c = I - E_v$$

Here e is the electronic charge, I the metal ionization potential and E_v the vertical electron affinity of the molecule. The two ions then fall toward each other under electrostatic attraction, rebounding from the inner portion of the potential curve, which can result in vibrational excitation of the product (Polanyi, 1961, 1959, Evans and Polanyi, 1939, Polanyi and Cashion, 1960). The "harpoon" mechanism and possible vibrational excitation are discussed at length elsewhere (Zwillenberg et.al., 1974, Zwillenberg, 1975). Vibrational transitions of alkaline earth oxides and halides are at wavelengths greater than 5 microns and were outside the scope of the present work which is concerned with electronic transitions in the visible, ultraviolet and near-infrared. As noted earlier, however, pulsed IR laser emission on some of these vibrational transitions has been reported by Rice and co-workers (1973).

C. Thermochemical Calculations

Thermochemical calculations were performed on 26 chemical systems of interest, and include both alkali and alkaline earth metals. (Zwillenberg et. al., 1974, Zwillenberg; 1975). JANAF (1960-1964) thermochemical data were used when available and bond energies were taken from Sullivan (1969) and Herzberg (1950). The list of systems for which calculations were performed is not exhaustive. It soon became apparent that the number of systems with adequate energy for electronic excitation was enormous and that additional considerations would determine which were to be investigated experimentally.

TABLE I

Energy Release and Minimum Electronic
Excitation Energy

Energy Release, Electron Volts

<u>System</u>	<u>M_2+X MX^*-M</u>	<u>$M+X_2$ MX^*+X</u>	<u>M_2+X_2 MX^*+MX</u>	<u>Minimum Electronic Excitation Energy</u>
Mg-O	3.64	N	2.59	2.48
Mg-N ₂ O	2.08	2.20 (Mg+N ₂ O)	--	2.48
Mg-Cl	2.66	0.23	2.88	3.29
Mg-F	4.56	3.02	7.56	3.46
Ca-O	4.26	N	3.48	1.43
Ca-N ₂ O	2.48	2.64 (Ca+N ₂ O)	--	1.43
Ca-Cl	4.24	2.08	6.33	1.99
Na-Cl	3.47	1.77	5.24	2.23-4.09 (diffuse)
K-Cl	3.86	1.89	5.74	4.47
Na-I	2.30	1.50	3.80	3.14
Na-Br	2.96	1.45	4.40	3.78
K-F	4.57	3.48	8.06	4.84 (continuum)
K-Br	3.30	1.70	4.98	3.83 (diffuse)
Ba-O	5.46	0.65	6.11	2.06
Ba-Cl	4.68	2.51	7.19	2.06

(Note: N=endothermic reaction)

Another class of reactions worthy of consideration is that in which energy released in an exothermic chemical reaction is transferred to a metal atom, exciting it electronically. Such excitation has been described by Padley and Sugden (1960) and Zhitkevich et al. (1963a), and discussed by Mavrodineanu and

and Boiteux, (1965). One mechanism suggested (Mavrodineanu and Boiteux, 1965) to explain the anomalous atomic excitation has invoked the considerable energy (≈ 11 .eV.) made available when the C-O bond is formed, in a reaction such as:



Other similar mechanisms are possible, and this one will be used merely to estimate the energy available for excitation of M^* . The following table shows this energy release for the alkaline earth metals (except beryllium), calculated from energy data given by Gaydon (1968). It should be noted that sufficient energy is available to excite any electronic state (since the ionization energy is exceeded), in all cases but Mg, where 0.64 eV. of vibrational energy in MgO must be assumed to supply the discrepancy. The possibility should also be noted of spatially separating the generation of C atoms from that of MO. These two species could then be brought together in a region containing no initial ground state metal atoms, which would facilitate production of a population inversion.

The energy level diagrams of Mg and Ca, as given by Kuhn (1962) are shown in Figs. (I-1) and I-2).

Table II

Energy Release and Minimum Excitation Energy

$C+MO \rightarrow CO+M^*$ (Both C and MO in ground state)

<u>Metal</u>	<u>MO bond energy eV. *</u>	<u>Energy Release, eV.</u>	<u>Lowest electroni- cally excited state of M, eV. *</u>	<u>ionization potential of M, eV. *</u>
Mg	4.1	7.0	2.71	7.64
Ca	4.3	6.8	1.88	6.11
Sr	4.2	6.9	1.78	5.69
Ba	5.75	5.3	1.12	5.21

*Gaydon (1968)

D. Observations of Electronic Chemiluminescence

A few words will be said here about chemical systems in which chemiluminescence due to electronically excited product species has been observed. Such systems would be prime candidates for investigation for potential laser application. The early and more recent studies in alkali metal systems, (von Haber and Zisch, 1922, Heller and Polanyi, 1936, Beutler and Polanyi, 1928, Polanyi and Schay, 1928, Glasston Laidler and Eyring, 1941, Miller and Palmer, 1963, Naegeli, 1967, Tewarson, Naegeli and Palmer, 1969) have been mentioned already. Here, however, the chemiluminescence seems due either to hydrocarbon fragments or to excitation of ground state metal atoms (of which there is an excess) to the resonance state, from which they can decay only to the ground state. At the time the present investigation was begun, very little published work existed on chemiluminescence in alkaline earth metal systems. Sakurai, Johnson and Broida (1970) and Johnson (1971) had reported chemiluminescence (with identification of molecular band spectra) in the low pressure formation of BaO, BeO and SnO (incidental to a study of laser-excited fluorescence). Crossed molecular beam studies of chemiluminescence at 10^{-5} - 10^{-3} torr pressure had been reported for the Ba+Cl₂ system (Jonah and Zare, 1971) and for the reactions of Ba, Ca and Sr with NO₂ and N₂O, (Ottinger and Zare, 1970, Jonah, Zare and Ottinger, 1972). Hansel, Mellor and Sullivan (1967)

had observed possible chemiluminescence in the Ca-O_2 system at ~ 1 .torr. Zhitkevich et al.(1963a) had observed chemiluminescence of MgCl in the cold luminescence of Mg vapor with CCl_4 and CHCl_3 , and of CaCl with Ca vapor and CCl_4 vapor, as well as numerous atomic metal lines with excitation energies up to ~ 7.5 eV. These latter systems are particularly interesting since the Mg-CCl_4 reaction lacks sufficient energy release to electronically excite MgCl or many of the atomic lines seen. The observation of Zhitkevich et al.(1963a) that the chemiluminescence was dependent on the presence of traces of oxygen, plus their observation of atomic C and molecular C_2 emission, suggest that the excitation may be due to a mechanism involving the formation of the C-O bond, such as the $\text{C+MO} \rightarrow \text{CO+M}^*$ reaction discussed earlier. Markstein (1963) had reported spectroscopic studies of a dilute Mg-O_2 diffusion flame, and attributed his results to heterogeneous reaction.

As recently as mid-1972, the above constituted the scant literature on alkaline earth chemiluminescence. To this might be added the paper by Batalli-Cosmovici and Michel, (1971) on molecular beam scattering of O_2 and Ba , but this did not deal with chemiluminescence.

However, starting in late 1972 and continuing unabated to the present, this area has become a field of intense activity. One cause for this sudden surge of activity may be a meeting in September 1972, resulting in a report published

in May 1973 (Wilson et al., 1973), which proclaimed the desirability and possibility of producing an electronic-transition chemical laser operating in the visible, and placed the alkaline earth oxides and halides high on the list of candidate systems. Since then, a flood of papers have appeared. Obenhaus, Hsu and Palmer (1972a, 1972b, 1973a, 1973b) reported studies of the reactions of Ba with O_2 , N_2O , NO_2 and $ONCl$. Gole and Zare (1972) and Gole (1973) have studied $(Mg, Ca, Sr, Ba) + (F_2, Cl_2, Br_2, I_2, ICl, IBr \text{ and } ClF)$ (Gole 1973) and $Al + O_3$ (Gole and Zare 1972). Menzinger and Wren (1973) and Wren and Menzinger (1973) have examined chemiluminescence in the $Ba-Cl_2$ system and reported branching ratios for the production of excited vs. ground state products. Eckstrom, Edelstein and Benson (1974) have measured quantum yields in the systems $(Mg, Ca, Sr, Ba) + F_2$ and $Ba + (Cl_2, NOCl, N_2O)$, and Black Luria, Eckstrom, Edelstein and Benson (1974) have reported (extremely small) quantum yields in the reactions of metal alkyls and carbonyls and hydrocarbons with F_2 . Jones and Broida (1973, 1974a, 1974b) and Field, Jones and Broida (1974) have measured quantum yields vs. pressure in the $Ba + N_2O$ system, Capelle, Bradford and Broida (1973) have reported spectra of $(Ba, Bi, Cu, Pb) + (Br_2, Cl_2)$, and Field, Capelle and Jones (1974) have reported spectroscopic observations of $Ca + N_2O$. Shultz and Zare (1974) have compared spectra of $Ba + O_3$ and $Ba + N_2O$, and Hsu, Krugh and Palmer (1974)

have studied $\text{Ba} + \text{N}_2\text{O}$ and NO_2 . To this must be added the molecular beam (non-chemiluminescence) studies mentioned earlier of Lin, Mims and Herm (1973a, 1972, 1973b) on $(\text{Ca}, \text{Sr}, \text{Ba}) + \text{HI}$ (Mims, Lin and Herm, 1972), $(\text{Ba}, \text{Sr}, \text{Ca}, \text{Mg}) + (\text{Cl}_2, \text{Br}_2)$ [Lin, Mims and Herm, 1973] and $(\text{Ba}, \text{Sr}, \text{Ca}, \text{Mg}) + \text{ICl}$ and $\text{Ba} + \text{BrCN}$ (Mims, Lin and Herm, 1973).

It should be noted that at the time the course of the present investigation was planned, and the systems to be studied were selected, none of the above work had yet been reported, and much of it has appeared since the completion of the experimental phase of the present investigation. The distributions of atomic excited state populations and excitation rates were not measured by other workers, and hence no electronic population inversions were observed by them. In the present study however, both populations and excitation rates were measured and population inversions were detected. (See Chapter III for a detailed discussion). Because of the differing excitation conditions (chemiluminescent vs. thermal) the Ca/O_2 flames observed in the present study were very different from those observed by previous workers (Sullivan, 1969). Because of the vast, hitherto unexplored area represented by the alkaline earth reactions, there has been no overlap between the present investigation and any of the studies cited above, with the exception of some observations on the $\text{Ca}/\text{N}_2\text{O}$ flame

(Field, Capelle and Jones, 1974).

The studies under molecular beam (single collision) conditions provide useful information on rates of elementary reactions. However, they are not directly relevant to flames at higher pressures (~ 1 torr) where secondary reactions have been shown to be very important, (this work and Jones and Broida (1973)).

E. Depletion of the Lower Electronic State and Lasing

Production of electronically excited product molecules or atoms is not sufficient alone to produce population inversion. A large ground or lower state population of the same atom or molecule can prevent attainment of inversion. Even if the product is not initially present (e.g., MgO in the Mg-O₂ system), unless there is an efficient process for removing product molecules from the lower lasing state, population inversion will last only long enough to populate this state and then cease. Bennett (1965) noted that even without removing ground (or lower) state product, a pulsed or momentary inversion could be maintained for a time $T \lesssim \frac{1}{2A_{21}}$ where A_{21} is the Einstein A-coefficient for the laser transition. However, the excitation rise time must be small relative to T for efficiency. As T is of the order of the radiative lifetime, 10^{-6} - 10^{-7} sec., the slowness of mixing processes makes the

production of a chemical laser in this manner unlikely. (This does not, however, preclude a flash-photolysis or discharge pumped pulsed laser of this type. The exploding-wire type of pulsed chemical laser reported by Rice and co-workers (1973a, 1973b) operates in the infrared, on vibrational transitions, and hence, with a radiative lifetime $\sim 10^{-3}$ sec., does not face as severe mixing time requirements.

Of course a transition in which the lower state is not the ground state would be more favorable for laser applications. Consider a molecule with three electronic energy levels, X (the ground state), A and B in order of increasing energy. Assume that a chemical reaction preferentially forms molecules in state B and that $B \rightarrow A$ is the lasing transition. If the rate of the $A \rightarrow X$ transition is sufficiently greater than that of $B \rightarrow A$, the population of A will be kept low and inversion on $B \rightarrow A$ can be maintained continuously. The alkaline earth oxides and halides have numerous energetically accessible low-lying excited states which might be suitable for such three-level laser action (Sullivan, 1969, Herzberg, 1950, Zwillenberg, et. al., 1974).

However, there are a number of stratagems by which lasing might be possible even on a resonance transition. One such method is fluid flow. Consider a reaction at a point in a gas stream forming excited products only, which decay with lifetime τ . If N_2 and N_1 are the upper and lower state populations respectively, it may be shown (Zwillenberg

et. al., 1974, Zwillenberg, 1975) that

$$N_2/N_1 = \frac{1}{\exp(t/\tau) - 1}$$

and that inversion ($N_2/N_1 > 1$, assuming equal statistical weights) will exist for flow time $t > \tau \ln 2$.

Large ground state populations can also be depleted by chemical reaction or condensation. The latter is often thought to be a serious problem in a chemical laser due to large scattering losses from condensed particles. However there is a large range between molecular dimensions ($\sim 2-5\text{\AA}$) and the wavelength of light ($\sim 5000\text{\AA}$) and the Rayleigh scattering cross section varies as r^6 . Thus there is a wide range of molecular agglomerates, e.g., $(\text{CaO}_2)_2$, $(\text{CaO}_2)_3$, ... $(\text{CaO}_2)_n$, which have negligible scattering coefficient, yet which have different optical absorption frequencies than the monomer CaO (or other product molecule). Thus, as far as population inversion is concerned, ground state molecules which have condensed into such agglomerates are effectively removed from the system.

Another possibility is formation of a molecular product in a vibrational level v' of electronic excited state A, such that the Franck-Condon factor for the radiative transition $A(v') \rightarrow X(v'')$ is large and v'' is a high vibrational level. Since v'' will not be thermally populated, lasing might

be possible on this transition even if the total population of state X is larger than that of A. There would however be a tendency for the lower state X(v") to fill up since electronic radiative decay into it is much faster than vibrational relaxation out of v".

F. Spin Conservation

In the discussion of reaction mechanisms, use will be made of the Wigner-Witmer spin correlation rule or "spin conservation" (Laidler, 1955). This rule states that if S_1 and S_2 are the spins of reactant atoms and molecules and S_3 and S_4 the spins of the products, then the series

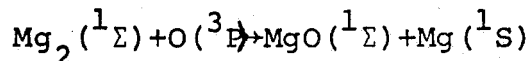
$$S_1+S_2, S_1+S_2-1, S_1+S_2-2, \dots, |S_1-S_2|$$

and

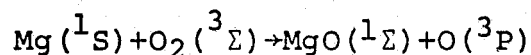
$$S_3+S_4, S_3+S_4-1, S_3+S_4-2, \dots, |S_3-S_4|$$

must have at least one term in common for the reaction to be "spin-allowed" and have a high rate. (This is equivalent to stating that at least one possible vector sum of S_1 and S_2 must equal one possible vector sum of S_3 and S_4).

For example, the reaction



is spin forbidden, while the endothermic reaction



is spin allowed.

It should be noted that examples exist of reactions which are spin-forbidden, yet which occur with rapid rates. Thus, Massey et al. (1970) describe the ionic reaction: $O^+(^4S) + CO_2(^1\Sigma) \rightarrow O_2^+(^2\Pi) + CO(^1\Sigma) + 1.5\text{eV}$ which occurs with a cross section of 180\AA^2 , far greater than the hard-sphere value. Benson (1960) considers the spin conservation rule "...of questionable validity for any species containing atoms of atomic number in excess of 10..", due to the breakdown of L-S coupling. (Note that the atomic numbers of Mg and Ca are 12 and 20, respectively.) Tully (1974) has explained the high rate of the spin forbidden quenching reaction



as due to the formation of a long-lived collision complex, and Mavrodineanu and Boiteux (1965) have stated that such complexes may undergo radiationless transitions not subject to the rule $\Delta S=0$. As noted earlier, Field, Jones and Broida (1974) have invoked a mechanism violating spin conservation in their explanation of the Ba-N₂O reaction. It thus appears that the spin conservation rule, while sometimes helpful, is far from an infallible guide.

4. Discussions, Conclusions and Selection of Systems for Study

It is recognized that in the foregoing discussion, many assumptions have been made regarding chemical reaction rates, condensation rates, relative rates of excitation and decay of various energy levels and modes, inter-mode transfer processes

and chemical reaction mechanisms. The fact is that a detailed search of the literature has revealed that very little is known in these areas. Molecular and chemical laser research has hitherto concentrated on vibrational-rotational transitions rather than electronic transitions. Much work has been done on alkali metal-halogen systems, and until very recently, almost none on alkaline-earth metal/halogen, oxygen and halide systems. This was particularly so when the present investigation was begun. This area of study appeared as one which had been neglected and which should be investigated, if only to remedy the lack of information.

Because of the multitude of candidate exothermic chemical systems described above, it was obviously necessary to make some selection as to which systems were to be studied first. In view of the earlier work in this laboratory on the Ca and Mg + O₂ systems (Hansel, Mellor and Sullivan 1967, Sullivan 1969), as well as observations in this laboratory of Ca-O₂ chemiluminescence (Hansel, Mellor and Sullivan 1967), these systems were selected as two of the systems to be studied. Since the $\text{Ca} + \text{O}_2 \rightarrow \text{CaO} + \text{O}$ and $\text{Mg} + \text{O}_2 \rightarrow \text{MgO} + \text{O}$ reactions are endothermic, the exothermic $\text{Ca} + \text{N}_2\text{O}$ and $\text{Mg} + \text{N}_2\text{O}$ systems were added. The observation by Zhitkevich et al. (1963a) of chemiluminescence at atmospheric pressure in the Ca/CCl₄/trace O₂ systems, with excitation of atomic and molecular emissions to 7.5 eV. (including some transitions not terminating in the ground state) suggested that these systems warranted further study. It was considered that

operation at lower pressures would improve the performance of these systems by reducing collisional quenching and relaxation effects. Atomic excited state populations could readily be calculated from emitted intensities because of the availability of atomic transition probability data (Wiese et al., 1969). Similar calculations for metal oxide excited states are not possible since electronic transition probabilities and Franck-Condon factors for MgO and many CaO bands are not available. For many bands, even vibrational assignments are lacking.

Atomic systems are preferable to molecular systems for laser application (Wilson et al., 1973) because of the smaller number of states among which excitation is divided. The observed metal oxide bands terminate in the ground electronic state (making inversions difficult to achieve) while many of the atomic lines excited in the Mg/CCl₄/O₂ and Ca/CCl₄/O₂ flames do not terminate in the ground state. Preliminary experiments on the Mg/CCl₄/O₂ flames showed clear evidence of strong, non-equilibrium metal atom excitation and the possibility of electronic population inversions produced by chemical means. As a result of all the above reasons, most of the experimental effort was concentrated on the Mg/CCl₄/O₂ and Ca/CCl₄/O₂ systems.

5. Discussion of Experimental Technique

A. Low Pressure Diffusion Flame

The low pressure dilute diffusion flame technique was originally devised by M. Polanyi and co-workers (1930, 1932, 1936) as a means of determining reaction rate constants of rapid alkali metal-halogen (or halide) reactions. In this method, an inert carrier gas flowed through a heated chamber containing the metal, and carried the metal vapor, through a nozzle, into a chamber where it reacted with a dilute atmosphere of halogen or halide in inert diluent. The reaction rate constant was determined from the measured diameter of the flame, assuming a carrier gas flow rate low enough that one could neglect the convective term in the steady-state continuity equation

$$D \nabla^2 p_m - \underbrace{\nabla \cdot (p_m \vec{V})}_{\text{convection}} - \underbrace{k p_m p_A}_{\text{reaction}} = 0$$

diffusion

and the flow could be considered completely diffusive. In the above equation, p_m and p_A are the partial pressures of the metal and atmospheric reactant respectively, V is the convective velocity, k the reaction rate constant, and D the diffusion coefficient of the metal vapor through the inert gas. The flame diameter was interpreted in terms of a minimum metal concentration which could be detected by resonance fluorescence.

The metal vapor partial pressure at the nozzle was assumed to be the equilibrium vapor pressure at the furnace temperature, P_A was assumed uniform in space, and the continuity equation could be solved, yielding reaction rate constant k in terms of measured flame diameter.

Heller (1937) examined the validity of the basic assumptions of this technique and recommended that the ratio V/D of convective velocity to diffusion coefficient be restricted to the range $5-12 \text{ cm}^{-1}$ to prevent reaction inside the nozzle at the lower extreme, and to avoid sweeping away the atmospheric reactant, as well as the onset of turbulence at the higher limit. Garvin and Kistiakowsky (1952) extended the technique to non-luminescent exothermic reactions by measuring temperature profiles through the flame with fine-wire thermocouples, and Smith (1954) gave an analytical solution of the continuity equation, including the effect of atmospheric reactant depletion, for the case of purely diffusive flow. Reed and Rabinovitch (1955) considered theoretically the quantitative effects of halide back diffusion into the nozzle, atmospheric depletion and the displacement of the flame by convective flow, subject to the simplifying assumption of constant unidirectional convective velocity. They concluded that Heller's (1937) limits on V/D might be successfully exceeded in some cases, and applied their theoretical treatment to an experimental determination of the rates of reaction of sodium

vapor with fluorinated methyl chlorides (Reed and Rabinovitch 1957). Kaufman and Reed (1963) used a similar method, with the definition of the flame diameter in terms of a minimum detectable light flux (taking into account length of the line of sight through the flame) instead of a minimum Na concentration, as had been done by earlier workers (Polanyi, 1932, Heller and Polanyi, 1936, von Hartel and Polanyi, 1936, Heller, 1937). Rapp and Johnston, (1960) successfully used a photographic measurement technique in studies of the kinetics of the NO-F_2 reaction at V/D ratios up to 90, far outside Heller's (1937) upper limit.

All the above investigators used the low pressure metal vapor flame as a means of precisely determining reaction rate constants based on measurement of flame diameter or temperature profile. The accuracy of their measurements thus depended on the accuracy of the assumptions (of atmospheric reactant concentration and back-diffusion, convective vs. diffusive flow, etc.) used in the solution of the differential equations relating their experimental measurements to the desired reaction rate constant. In the present investigation, the low pressure dilute diffusion flame is used simply as a combined chemical reactor and spectroscopic light source, and flow velocities are not limited to the low velocity diffusive flow regime. It is simply a means of rapidly bringing together the metal vapor and other reactant(s) and maintaining the

reaction in a quasi-steady manner for the long periods of time needed for detailed spectroscopic studies. Markstein (1963) has used this technique in a spectroscopic study of the Mg-O_2 flame, as have Sakurai, Johnson and Broida (1970) and Johnson (1971) as a source of metal oxide in their laser-excited fluorescence studies. It is thus possible to use higher flow velocities than in previous studies, up to 10,000 cm/sec, with consequent advantages in preventing nozzle clogging and facilitating production of long duration and steady flames. Indeed, turbulence, which was feared by Heller (1937) would here be an advantage by promoting rapid mixing of reactants. Although knowledge of the distribution within the flame of the various excited species could be useful (particularly in attempts to separate upper and lower laser states physically by fluid flow, as discussed earlier,) it was considered that such detailed studies of spatial distribution would be premature in a state of almost complete ignorance regarding the identity and state of excitation of the emitting species. For this reason the present study has concerned itself with the overall radiation from the flame as a whole. This has permitted the use of a multiple reflection cell to average emissions from all parts of the flame, provide longer path length (and allow the study of the effects of path length changes) as well as a number of other advantages discussed in detail in the follow-

ing chapter on experimental apparatus. Tewarson, Naegeli and Palmer (1969) and Naegeli (1967) have utilized an inverted alkali metal diffusion flame technique in which the halogen or halide is introduced into a chamber filled with metal vapor, and burns in an excess of metal vapor. This technique has the advantage that the metal vapor concentration is clearly the equilibrium vapor pressure, and that flows of (gaseous) oxidants are easier to measure than metal vapor flow rates. In the present study however, the required furnace temperatures for alkaline earth metals are considerably higher than required for alkali metals, $\approx 1000^{\circ}\text{C}$ compared with $\approx 400^{\circ}\text{C}$, and the use of the inverted diffusion flame technique would require that the entire walls of the apparatus (and the multiple reflection cell mirrors!!) be at these high temperatures, to avoid condensation of metal. The size of the apparatus, the enormous heating power which would be required and the probable near impossibility of preventing condensation of metal vapor on the mirrors resulted in the decision to use the normal Polanyi diffusion flame arrangement, with metal vapor entering an atmosphere of oxidant, and only a small furnace tube and heating element at high temperature.

B. Determination of Excitation Rates, Quantum Yields and Excited State Population Densities.

The intensity, I , as measured by a detector, of an

atomic or molecular radiative transition may be expressed as

$$I = Kh\nu n'$$

where h is Planck's constant, ν is the frequency of radiation emitted, n' is the rate of photon emission in quanta/sec, and K is a constant. For a steady state, with short enough radiative lifetime τ_{rad} that collisional de-excitation is negligible compared to radiative decay, the rate of excitation of the upper state of the transition is equal to its rate of radiative decay, and n is also the rate of excitation of the upper state. Thus, the rate of excitation is given by

$$n' = \frac{I}{Kh\nu} = \frac{I\lambda}{Khc} = K'I\lambda$$

where K' is a calibration constant and c is the speed of light in vacuo. (Note that the above discussion assumes that each upper state decays through only one transition, and in practice, often one transition will be much stronger than the others, or only one will be within the spectral range covered by the detector. If more than one transition is observed originating from the same upper state, $\sum I\lambda$ should be substituted for $I\lambda$ above, and in the discussion which follows).

If the upper state is divided among g_u sublevels, (where g_u is the statistical weight of the upper state) then the rate of excitation, per sublevel is:

$$\frac{n'}{g_u} = K' \frac{I\lambda}{g_u}$$

If m' is the rate of input of a reagent B (metal atoms, oxidizer, etc.), then the quantum yield in quanta per atom or molecule of B is:

$$\frac{n'}{m'} = \frac{K' I \lambda}{m'}$$

Note that no knowledge of transition probabilities is needed in either of the above calculations.

The intensity of an electronic transition may be expressed (Mavrodineanu and Boiteux, 1965) as

$$I = K A_{ul} h \nu N_u$$

where K is the same instrumental constant as previously, A_{ul} is the Einstein coefficient for spontaneous emission from upper level "u" to lower level "l" (also called the transition probability) and N_u is the number of atoms or molecules in the upper state. Then:

$$N_u = \frac{I}{K A_{ul} h \nu} = \frac{I \lambda}{K h c A_{ul}} = \frac{K' I \lambda}{A_{ul}}$$

and the number per sublevel, N_u/g_u (which is the quantity which must have an inverted population for laser action to occur) is:

$$N_u/g_u = K' \frac{I \lambda}{g_u A_{ul}}$$

If the volume, V, of the region containing these excited species (i.e. the flame) is known, or can be estimated, then the population density can be calculated:

$$\frac{N_u/g_u}{V} = \frac{K'}{V} \cdot \frac{I\lambda}{g_u A_{ul}}$$

The above discussion applies both to atomic and to molecular electronic transitions, if I refers to the total emission due to the electronic transition from one electronic state to another. However, in molecular transitions, due to the rotational and vibrational fine structure superimposed upon the electronic energy levels, the emission due to a single electronic transition is spread into systems of bands extending over a wide portion of the spectrum. Herzberg (1950) gives the following expression for the integrated emitted intensity (i.e. integrating over the rotational structure) of a band, $B(v')$ \rightarrow $A(v'')$, where B and A are two electronic states, and v' and v'' are the vibrational quantum numbers in the two states:

$$I^{v';v''} = \frac{64}{3} \pi^4 c N_{v'} \nu^4 \bar{R}_e^2 \left[\int \psi_{v'} \psi_{v''} dr \right]^2$$

where $N_{v'}$ is the population of the v' vibrational level of the upper electronic state, ν is the average wavenumber of the $v'-v''$ band, \bar{R}_e is the average value of the electronic transition moment (assumed to vary slowly with radial coordinate r) and $\psi_{v'}$ and $\psi_{v''}$ are the vibrational wave functions for the two states. In deriving this expression, the Born-Oppenheimer approximation of separable electronic, vibrational

and rotational wave functions (i.e. that the electronic, vibrational and rotational energies can be treated separately) has been made.

Defining:

$$[\int \psi_{v'} \psi_{v''} dr]^2 \equiv q_{v',v''} = \text{Franck-Condon Factor}$$

and assuming \bar{R}_e constant for all bands of a given electronic transition:

$$I^{v',v''} = \text{const.} \cdot Z^{v'} N_{v'} q_{v',v''}$$

Thus, to calculate level populations from molecular band intensities requires a spectrum in which the vibrational assignments (i.e. the v', v'' values corresponding to a given band), the Franck-Condon factors and the electronic transition probabilities (or radiative lifetimes) are known, conditions which are not met for many of the molecules and bands considered (Pressman, Wentink and Schuler, 1967, Ortenberg and Antropov, 1967, Klemsdal, 1973). If the only data lacking were the electronic transition probabilities, relative vibrational populations could be calculated from:

$$\frac{N_{v'}}{N_{v=0}} = \frac{I^{v',v''}}{I^{0,v''}} \left(\frac{Z_{0,v''}}{Z_{v',v''}} \right)^4 \frac{q_{0,v''}}{q_{v',v''}}$$

as was done by Naegeli (1967). However, Franck-Condon factor data are scarce also (Pressman, Wentink and Schuler, 1967, Ortenberg and Antropov, 1967) and for some of the more interesting bands of the CaO and MgO spectra even vibrational assignments are lacking (Pearse and Gaydon, 1963).

For atomic transitions, however, the excellent critical compilation of Wiese et al. (1966, 1969) is available, for elements up to calcium. As noted by Wiese et al., (1969) the earlier compilation of Corliss and Bozman (1962) is inaccurate because of inhomogeneities and demixing in the arc source used and non-existence of local thermodynamic equilibrium.

For atomic state populations obeying a Boltzmann distribution (not necessarily in thermal equilibrium) one may write (Mavrodineanu and Boiteux, 1965)

$$I = KA_{ul} N h \nu \cdot \frac{g_u \exp(-E_u/kT)}{F(T)}$$

where k is the Boltzmann constant and $F(T)$ is the partition function,

$$F(T) = \sum_j g_j \exp(-E_j/kT)$$

If, as is often the case, the lowest excited states are far enough above the ground state that the exponential term becomes negligible, then $F(T)$ may be approximated by g_0 , the statistical weight of the ground state.

$$\therefore \frac{I}{KA_{ul} h \nu} = \frac{K' I \lambda}{g_u A_{ul}} = \frac{\exp(-E_u/kT)}{g_0}$$

Thus a plot of $\log (I \lambda / g_u A_{ul})$ vs. E_u (if a Boltzmann distribution exists) should be a straight line of slope

$-1/kT$, where T is the electronic excitation temperature (which in flames may differ from the translational temperature of the gas) (Mavrodineanu and Boiteux, 1965, Gaydon and Wolfhard, 1960).

A different type of situation is possible, however. The rate of excitation defined earlier may be governed by a reaction rate constant obeying an Arrhenius expression. Identifying the excitation energy of the excited state with the activation energy of the (endothermic) $M \rightarrow M^*$ process, one may derive:

$$K' \frac{I\lambda}{g_u} = \frac{n'}{g_u} \sim e^{-E_u/kT}$$

and a plot of $\log \left(\frac{I\lambda}{g_u} \right)$ vs. E_u should be a straight line of slope $-\frac{1}{kT}$, which determines a different excitation temperature which one may call the chemical kinetic excitation temperature.

Obviously, both of the above mathematical expressions cannot hold at once, since A_{ul} varies from atomic state to state (Wiese, Smith and Glennon, 1966, Wiese, Smith and Miles, 1969). As shown later, in the discussion of experimental results, only one of them, the second, is followed.

A point should be noted here, which is of considerable importance in comparing spectrometric measurements made at different spectrometer slit widths and in comparing line and band intensities. Considering a spectrometer with identical

entrance and exit slits, and a slit image width corresponding to a wavelength range $\Delta\lambda$, the signal, I , corresponding to a given source brightness B is given (Turner, 1965) by:

$$I \sim B \cdot (\Delta\lambda)^2 \quad (\text{continuum or unresolved band})$$

$$I \sim B \cdot \Delta\lambda \quad (\text{line much narrower than } \Delta\lambda)$$

and these factors must be used in comparing readings taken at different slit widths. Similarly, the signals corresponding to a line and a band of identical total photon emission rate will not be equal, but will be in the ratio

$$\frac{\int_{\text{band}} I_{\text{band}} d\lambda}{I_{\text{line}}} = \Delta\lambda$$

and a correction for this factor must be made in calculating and comparing quantum yields for lines and bands.

C. Detection of Self-Absorption or Stimulated Emission, and Calculation of Lower State Population Density or Inversion Density.

In an optically thin flame, the intensity of emission at a given wavelength is proportional to the optical path length, and the intensities of the components of a multiplet have their theoretical ratio. Deviation from such behavior indicates the presence of either self-absorption or stimulated emission, with the direction of the deviation indicating which. (In general, self-absorption causes lower intensity than expected, and stimulated emission, more.) Thus, the

ratio of the intensities observed with two different optical path lengths (whose ratio is known), or the ratio of the intensities of the components of a multiplet for which the line strength factors (Wiese, Smith and Miles, 1969, Wiese, Smith and Glennon, 1966) are known, allows the determination of the lower state population density, n_1 , in the case of self-absorption, and the inversion density ($n_2 - \frac{g_2 n_1}{g_1}$) in the case of stimulated emission.

In comparing experimentally measured absorption or emission data with tabulated Einstein coefficients, one should note that different authors define them in different ways. Some (Mavrodineanu and Boiteux, 1965, Herzberg, 1944, Kuhn, 1962) define the absorption coefficient B_{12} to make the energy absorbed proportional to the radiation density, S_ν , while others (Herzberg, 1950, Bauman, 1962, Chandrasekhar, 1960) define B_{12} to make the energy absorbed proportional to the radiation intensity, I_ν . Since $S_\nu c = I_\nu$ (where c is the speed of light), this can introduce a difference of a factor of c in the ratio A_{21}/B_{12} .

Following Chandrasekhar (1960), using the second definition above, the ratio of the Einstein coefficients for spontaneous emission and absorption is:

$$\frac{A_{21}}{B_{12}} = \frac{2h\nu^3}{c^2} \frac{g_1}{g_2}$$

where 1 and 2 denote lower and upper states respectively, ν is the frequency of the radiation emitted or absorbed, h is Planck's constant and g_1 and g_2 are the statistical weights of the two states. The equation of radiative transfer is then (Chandrasekhar 1960):

$$\Delta\nu \frac{dI_\nu}{ds} = [n_2 A_{21} + n_2 B_{21} I_\nu - n_1 B_{12} I_\nu] \frac{h\nu}{4\pi}$$

where I_ν is the spectral specific intensity, and has the units $[\frac{\text{energy/solid angle}}{\text{area-time-frequency interval}}]$, n_1 and n_2 are lower and upper state population densities, ds is an element of distance along the line of sight and $\Delta\nu$ is the linewidth in frequency units. A_{21} is the spontaneous emission coefficient, B_{21} the stimulated emission coefficient, and B_{12} the absorption coefficient. Marr (1968) discusses the calculation of the width of spectral lines subject to natural broadening (due to the finite lifetimes of excited states), Doppler broadening, pressure or collision broadening, Stark (electric field) broadening, and several combinations of these. At the low densities being studied, the mean time between collisions is about 10^{-6} seconds, while the radiative lifetimes of most atomic lines are about 10^{-8} seconds, and the linewidth can be calculated from pure Doppler broadening:

$$\Delta\nu_D = \frac{2\nu}{c} \sqrt{\frac{2kT \ln 2}{M}}$$

where k is the Boltzmann constant, $\Delta\nu_D$ is the Doppler linewidth and M is the atomic mass. (For metastable lines with long radiative lifetimes, collision broadening could become important.)

The three Einstein coefficients are not independent but are related by $B_{21} = B_{12} g_1/g_2$ and the relation between A_{21} and B_{12} given earlier. Substituting these relations into the equation of transfer, one may obtain:

$$\Delta\nu \frac{dI_\nu}{ds} = \left[n_2 + \left(n_2 - \frac{g_2}{g_1} n_1 \right) \frac{c^2}{2h\nu^3} I_\nu \right] A_{21} \frac{h\nu}{4\pi}$$

Defining:

$$J \equiv A_{21} n_2 \frac{h\nu}{4\pi} = \text{emission coefficient}$$

$$K \equiv A_{21} \left(\frac{g_2}{g_1} n_1 - n_2 \right) \frac{c^2}{8\pi\nu^2} = \text{effective absorption coefficient}$$

the equation of transfer becomes:

$$\Delta\nu \frac{dI_\nu}{ds} = J - K I_\nu$$

which is easily integrated to yield:

$$\ln \left(\frac{I_\nu - \frac{J}{K}}{I_\nu^0 - \frac{J}{K}} \right) = -KS/\Delta\nu$$

If $I_\nu^0 \equiv I_\nu(S=0) = 0$, (zero incident radiation at $S=0$), this becomes:

$$I_\nu = \frac{J}{K} (1 - e^{-KS/\Delta\nu})$$

where S is the optical path length (through the flame). It will now be shown how this equation may be used to determine K from experimental measurements. Note that for positive ab-

sorption, with $\frac{g_2}{g_1} n_1 \gg n_2$, $K \approx A_{21} n_1 \frac{c^2}{8\pi\nu^2}$, and a measurement of K gives n_1 . For negative absorption (stimulated emission) $\frac{g_2}{g_1} n_1 < n_2$ and measurement of K gives $(\frac{g_2}{g_1} n_1 - n_2)$, the (negative of) the inversion density. Note that a value of K near zero need not mean low n_1 . It could mean a nearly inverted population (i.e. $\frac{g_2}{g_1} n_1 \approx n_2$). An independent determination of n_2 (e.g. by an absolute intensity measurement) can resolve the ambiguity.

Let m be the effective number of optical passes through the flame in a multiple reflection cell (described later in the section on experimental apparatus). If $I_\nu(m\text{-pass})$ and $I_\nu(1\text{-pass})$ are the respective measured intensities with m and one pass through the flame, then (from the above equation for I_ν):

$$\frac{I_\nu(m\text{-pass})}{I_\nu(1\text{-pass})} = \frac{1 - e^{-mKS/\Delta\nu}}{1 - e^{-KS/\Delta\nu}}$$

For the optically thin case:

$$e^{-KS/\Delta\nu} \approx 1 - \frac{KS}{\Delta\nu}$$

$$e^{-mKS/\Delta\nu} \approx 1 - \frac{mKS}{\Delta\nu}$$

$$\therefore \frac{I_\nu(m\text{-pass})}{I_\nu(1\text{-pass})} = \frac{mKS/\Delta\nu}{KS/\Delta\nu} = m$$

Thus, the effective number of passes can be determined by

measuring the ratio of single and multipass intensities of an optically thin line (e.g. a metastable or non-resonance line).

For the optically thick case, $KS/\Delta\nu$ can be found using the experimentally measured ratio $\phi \equiv \frac{I_{\nu}(m-pass)}{I_{\nu}(1-pass)}$ and a family of universal curves of $(1-e^{-mx})/(1-e^{-x})$, using the value of m determined above, and defining $X = KS/\Delta\nu$. Such a family of curves is shown in Fig. (I-3) for positive values of X and in Fig. (I-4) for both positive and negative values of X . (Note that both positive and negative values of X can be determined from measurements of ϕ .) In Figs. (I-3) and (I-4), the ordinate of each curve is divided by m to fit all curves on the same scale.

The procedure to be followed is thus:

- (1) Determine m from multipath vs. single path measurement of an optically thin line.
- (2) Measure ϕ = ratio of multipath to single path intensity for line under study.
- (3) Get X from curve for measured values of m , ϕ/m .
- (4) If $X < 0$, calculate $-\left(\frac{g_2}{g_1} n_1 - n_2\right)$ = inversion density.
- (5) If $X > 0$, calculate $\left(\frac{g_2}{g_1} n_1 - n_2\right)$.

Using n_2 from absolute intensity measurement, calculate n_1 .

Similar results can be obtained using the ratio of multiplet (triplet in the case of alkaline earths) component intensities and comparing it with the theoretical ratio. Let ϕ be the observed ratio of the intensity of a stronger to a weaker component of a multiplet, and let ψ be the theoretical ratio of their intensities.

$$\phi = \frac{I'_v}{I_v} = \frac{\frac{J'}{K'} (1 - e^{-K'S/\Delta\nu})}{\frac{J}{K} (1 - e^{-KS/\Delta\nu})}$$

where the primed quantities refer to the stronger component. Neglecting stimulated emission so the "effective absorption coefficient" is given by

$$K = A_{21} n_1 \frac{g_2}{g_1} \frac{n_2}{c} \frac{1}{8\pi\nu^2}$$

and using the previously given expression for J,

$$\begin{aligned} J/K &= 2 \frac{n_2}{n_1} \frac{g_1}{g_2} \frac{h\nu^3}{c^2} \\ \frac{J'/K'}{J/K} &= \frac{\frac{n'_2}{g'_2} \cdot \frac{n_1}{g_1} \nu'^3}{\frac{n_2}{g_2} \cdot \frac{n'_1}{g'_1} \nu^3} \end{aligned}$$

If the frequency difference between components is neglected, then

$$\frac{J'/K'}{J/K} = \frac{\frac{n'_2}{g'_2} \cdot \frac{n_1}{g_1}}{\frac{n_2}{g_2} \cdot \frac{n'_1}{g'_1}}$$

Assuming that all sublevels of the upper state are equally filled, so $n_2/g_2 = n'_2/g'_2$, and a similar situation for the lower state so $n_1/g_1 = n'_1/g'_1$, the ratio $(J'/K') \div (J/K) = 1$. From the definition of K, neglecting the frequency difference between components and using the above assumption that $n_1/g_1 = n'_1/g'_1$ yields:

$$\frac{K'}{K} = \frac{A_{21}' g'_2}{A_{21} g_2}$$

but the tabulated line strength factors (Wiese et. al., 1966, 1969) $S_{ul} \sim A_{ul} g_u \lambda^3$ (and the wavelength difference between components has already been neglected). Thus $\frac{K'}{K} = \frac{S_{ul}'}{S_{ul}} \equiv \psi$ defined earlier:

Then $K' = \psi K$ and

$$\frac{\phi}{\psi} = \frac{1}{\psi} \cdot \frac{1 - e^{-\psi K S / \Delta \nu}}{1 - e^{-K S / \Delta \nu}}$$

But this is the same equation derived earlier for the multipass case, with ψ substituted for m and ϕ for ϕ . It can be solved for K in the same manner, using the curves (Figs. **I3**, **I4**). ψ , (the theoretical intensity ratio of strongest to any other component) is simply used in place of m (the effective number of optical passes) and ϕ (the measured ratio of intensities of the two components) in place of ϕ (the ratio of multipass to single pass intensity). The two methods could both be

used, as a check on one another (although only the multipath method can be used for singlets, and the multiplet component ratio method should not be used where there is reason to suspect non-uniform population of the sublevels of either upper or lower states).

CHAPTER II

EXPERIMENTAL APPARATUS AND PROCEDURE

The experimental investigations were performed in a low-pressure metal vapor combustion apparatus specifically designed to allow optical and spectroscopic measurements on metal vapor flames under reasonably steady conditions for prolonged periods. (Up to 5 hours in some experiments; 3 hours are more typical). In these experiments, pressure ranged from 0.5 to 10. torr., with most experiments performed in the vicinity of 1.5 torr.

The experiments performed divide themselves naturally into two groups: The first consists of studies of the flames of magnesium and calcium vapors burning in oxygen and nitrous oxide, in which molecular emission predominated. The second consists of studies of the flames of magnesium and calcium burning in carbon tetrachloride vapor, with and without additives such as O_2 and N_2O . In these flames, intense atomic line emission with excitation energies as high as 7.5 eV. was seen, in addition to molecular band emission. Detailed quantitative measurements were made of the non-equilibrium electronic excitation and excited state populations present in this latter group of flames.

The first portion of this chapter will describe the materials (metal samples, gases, reagents) used in these

experiments. The second portion will describe the experimental apparatus and the experimental procedure.

1. Materials

a. Metal Samples

Magnesium was obtained from A. D. MacKay, Inc. in the form of a 1/8 inch diameter wire of 99.9% purity. Typical sample size was a 9 inch length of this wire, weighing approximately 1.2 grams. The surface of the sample was cleaned with fine emery paper, wiped clean with a paper towel, cut into 3 parts to fit in a ceramic combustion boat (Sargent-Welsh Scientific Co., single-use combustion boat S-21820-A, dimensions: 80x6 mm. inside, 95x12 mm. outside) and placed in the furnace tube (which was then evacuated).

Calcium was obtained from A. D. MacKay, Inc. in the form of 0.035 inch thick sheet packed under heavy mineral oil. The purity of the calcium was 99.% with the balance mostly CaCl_2 . The calcium was cut into 2.75"x0.33"x.035" strips, rinsed in cyclohexane to remove the mineral oil, and stored under cyclohexane until use. A typical sample consisted of two such strips, weighing a total of approximately 0.6 grams. As received, the calcium sheet had an adherent brown-gray coating (probably oxide, nitride and hydroxide). If this was not removed before placing the sample in the oven, it was found to prevent the escape of calcium vapor. This differs from the experience of Mellor (1967) who found no effect of this coating on ignition. However, the ex-

planation is probably that the oven temperatures in the present study (chosen to give metal vapor pressure about 1 torr.) are far below the melting point or transition temperature of the metal oxide, or the ignition temperatures studied by Mellor (1967). Therefore, before each experiment with calcium, the calcium strips to be used were removed from the container of cyclohexane and the surface film removed with fine emery paper (holding the calcium with tweezers to avoid reaction with moisture on the hands). The calcium strips were then cut further into pieces about 0.33 inch x 1 mm. and dropped, as cut into a ceramic combustion boat filled with cyclohexane (to prevent reaction with the air), and rinsed further with cyclohexane. The liquid was then poured out of the boat, and the sample placed immediately into the furnace tube, which was then evacuated, evaporating the remaining cyclohexane.

b. Gases

In most of the experiments performed, argon was used as inert diluent and metal vapor carrier gas. In several experiments, nitrogen was substituted for argon to study possible quenching effects of molecular N_2 on vibrationally excited species. Both gases were initially obtained in commercial purity grade (99.998% and 99.95% nominal, respectively) from Liquid Carbonic Corp.

When the sensitivity of the metal vapor flames to small O_2 impurities in these gases was noted, gases of higher purity were substituted. UHP grade argon (99.999%) and "oxygen-free" nitrogen (99.998% N_2 , less than 5 ppm. O_2) were obtained from Matheson Gas Products. An attempt had been made to use nitrogen from the vapor space in a liquid nitrogen tank. However this was found gas chromatographically to contain excessive O_2 (≈ 550 ppm.).

Oxygen was obtained from Liquid Carbonic Corp. in commercial purity (99.5%). Nitrous oxide was obtained from Matheson in the only grade available, 98.0% minimum. Nitric oxide, used in chemiluminescence quenching tests, was obtained from Matheson in C.P. grade (99.0% minimum). A mixture of approximately 4% NO in UHP argon was prepared by evacuating a metal lecture bottle, filling it with NO to about 20 psia and then filling it with UHP argon to total pressure of 500 psia. A 1.56% mixture of O_2 (UHP grade, 99.99%) in helium (HP grade, 99.995%) was obtained from Matheson for use in accurately metering small flows of O_2 to the flames. Helium was used instead of argon in this mixture to enable gas chromatographic verification of the O_2 content. (It is difficult to determine small amounts of O_2 in Ar chromatographically as their retention times are very close together).

The sources and purity of all the gases used are

shown in Table I. Gases were dried before use using Matheson model 450 purifiers with type A cartridges, capable of attaining a dew point of -100°F .

The carbon tetrachloride whose vapor was used in studies of the Mg/CCl_4 and Ca/CCl_4 flames was obtained from Matheson Coleman and Bell, and is of A.C.S. Analyzed Reagent grade, "suitable for spectrophotometry". It contains less than 0.003% H_2O . Because CCl_4 is more volatile than H_2O , the vapor should contain even less H_2O .

Table I
Purity of Gases Used

<u>Gas</u>	<u>Supplier</u>	<u>Purity Grade</u>	<u>Manufacturer's claimed Purity %</u>	<u>Impurities Noted</u>
<u>Argon</u>	Liquid Carbonic Matheson	commercial UHP	99.998% <10 ppm O ₂ (5ppm typical) <10 ppm N ₂ <5 ppm H ₂ O 99.99%	visible luminescence with Ca vapor ---
<u>Oxygen</u>	Liquid Carbonic	commercial	99.5% min. <0.5% (N ₂ +Ar) <11 ppm H ₂ O	---
<u>Nitrogen</u>	Liquid Carbonic	commercial	99.95% min <0.05% O ₂ <11 ppm H ₂ O	~0.3% O ₂ measured by gas chromatography
	Matheson	oxygen free	99.998% <5 ppm O ₂	~150 ppm O ₂ measured by Gas Chromatograph
	vapor above liquid N ₂ tank	---	---	550 ppm O ₂ measured by G.C.
<u>Nitrous Oxide</u>	Matheson	(only grade available)	98.0% min.	---
<u>Nitric Oxide</u>	Matheson	C.P.	99.0% min.	---
<u>He/O₂ mixture</u>	Matheson	O ₂ -UHP (99.99%)	1.56% O ₂	O ₂ analysis verified by G.C.
		He-HP (99.995%)	Bal. He	

c. Photographic Materials and Processing

Polaroid self-processing photographic materials were used for initial, preliminary flame spectra and photographs. Polaroid types 57 (ASA 3000) and P/N 55 (ASA 50, but finer grain and longer wavelength response than type 57) films were used for spectra, and a Graflex 4x5" view camera with Polacolor type 58 film (ASA 75) was used for flame photographs. However the long wavelength cutoff (6400\AA) and grain of the Polaroid materials limited their usefulness, except for quickly checking if the apparatus was working. Therefore, all subsequent spectra were taken on Kodak 2x4" glass photographic plates. As the McPherson spectrograph/monochromator (described below) covers only a 1700\AA span at each setting, the spectral response of the plates used was matched to the spectral region being observed, so the plate of highest sensitivity in that region could be used. Thus, Kodak 103a-O plates were used in the ultraviolet, 103a-F plates the visible and 1-N plates in the far red and near infrared (to 8900\AA).

Kodak recommends processing these plates in D-19 developer for 4 minutes at 68°F . However, it was found that use of D-76 developer for 12 minutes gave comparable sensitivity with decreased contrast, which was found preferable because of the wide range of intensities of the

lines and bands in the spectra being recorded.

Flame photographs were taken with a Beseler Topcon Super D 33 mm. single-lens-reflex camera using Kodak High-Speed Ektachrome film, using both the manufacturers recommended processing (ASA 160) and prolonged processing for higher film speed (ASA 400) at the cost of increased graininess.

2. Apparatus

In order to maintain the low-pressure metal vapor flames under essentially steady conditions for long periods of time (up to 5 hrs.), the apparatus was designed as a continuous flow system, in which fuel, oxidant, additive and diluent gases are continuously flowing into the vacuum chamber and reaction products continuously being pumped out, the flow rates and pumping rate being adjusted to maintain the desired ambient pressure.

The experimental arrangement shown in Figs. (II-1 and II-2) consists essentially of the vacuum chamber in which the low pressure flame burns, the vacuum system to measure and maintain the desired low pressure, an oven to produce the metal vapor, a gas mixing and flow control system to meter fuel, oxidant, additives and diluents into the chamber, a spectrometer (with condensing optics, chopper,

photomultiplier and lock-in amplifier) to analyze and detect the light emitted by the flame, plus instruments for measuring and controlling temperatures, pressures and flow rates. Each of these components will now be described in detail.

a. Vacuum Chamber

The cross-shaped vacuum chamber consists of a stainless steel tube 6 inches in diameter x 52 inches long (whose centerline is the optical axis of the system) bisected perpendicularly by an 8 inch diameter stainless steel tube (the seam being Heliarc welded). One of the 8 inch diameter sidearms so formed contains the electrically heated furnace in which the metal is vaporized. The other contains the vacuum pumping port, a window for visual observation of the flame and a 1/16 inch diameter, stainless steel sheathed, chromel/alumel thermocouple probe (movable axially and rotatable through a double "O"-ring seal fitting mounted on the window). The probe is angled in such a way (Fig. II-3) that rotating it sweeps the junction through the flame, from the centerline to the outer edge. Another window assembly, containing a port for sampling chamber gas composition, may be substituted for the window containing the thermocouple probe.

b. Multiple-reflection (white) Cell

The 6 inch diameter tube contains the mirrors of

a multiple reflection cell of the type first described by White (1942) and later modified by Welsh, Cumming and Stansbury (1951) and by Welsh, Stansbury, Romanko and Feldman (1955) and described by Charters and Polanyi (1960). For brevity (and because the nomenclature is common in the literature) such a cell will be referred to as a White cell. Some construction features were adapted from the design described by McKubbin and Grosso (1963).

The cell consists of two identical concave spherical mirrors, 5 inches in diameter, aluminized and silicon monoxide overcoated (to protect the reflective coating), separated by their mutual radius of curvature of 40 inches. The mirror dimensions were chosen to make the cone of light leaving the cell ($f/8$) match the acceptance angle of the spectrometer ($f/8.7$). The mirrors are each split along a diameter, and each half-mirror is independently mounted in a three-point suspension allowing tilting about two orthogonal axes and about one inch of axial adjustment (Fig.II-4). The two mirrors at the end of the cell away from the spectrometer are tilted so their centers of curvature lie on opposite edges of the slot between the other two mirrors, in a "crossed" configuration. The optical alignment procedure is similar to that of Welsh et. al. (1955) and is described in detail elsewhere (Zwillenberg, 1975).

The multiple reflection cell has a number of very important functions in these experiments:

1. By increasing the path length (and hence intensity of weak chemiluminescence) the required length of photographic exposure (or detector sensitivity) is reduced.
2. By collecting light from all parts of the flame, effects of changes in flame size or position are alleviated. In addition, one is not forced to forego the great advantage in sensitivity afforded by use of a condensing lens to measure absolute intensities and quantum yields, as were Gaydon and Wolfhard (1950) and Jones and Broida (1973). Clough and Thrush (1967) used a multiple reflection cell with condensing optics in their determination of the absolute intensity of the chemiluminescent emission from the $\text{NO} + \text{O}_3$ reaction.
3. By covering and uncovering the rear set of White cell mirrors and observing the relative changes of intensity of different emissions, the effect of path length can be determined, and either self-absorption or stimulated emission detected.

4. The ratio of intensities with and without multiple reflections of an optically thin line or band, can be used to monitor any deterioration in reflectance of the White cell mirrors.
5. By a slight readjustment of the mirrors, the cell becomes a confocal resonator in which laser action of systems producing adequate negative absorption to overcome losses, could be observed. (since high enough inversion densities were not observed, this was not done).

A shutter, operated through the same "o"-ring seal as the thermocouple probe described above (Fig.II-3) permits blocking and uncovering of the White cell rear mirrors during an experiment (while the chamber is under vacuum), as required in items 3 and 4 above.

Aluminized mirrors were used despite their relatively low reflectance (≈ 0.9) for laser applications, because of the wide range of wavelengths being examined, from the ultraviolet to the near infrared ($\approx 2500-9000\text{\AA}$). High reflectance multilayer interference coatings show maximum reflectance over narrower wavelength ranges (Oriel Corporation has one with 99.5% reflectance over the range $4500-6500\text{\AA}$),

and of course the gold mirrors used in much infrared laser work are not good reflectors in the ultraviolet and visible. However, extremely high mirror reflectance is not essential to measurements of excitation and excited state populations, where its only effect is increased sensitivity. It is critical only in attempts to lase a system once population inversion has been detected. In such a case, high reflectance mirrors could be obtained for the specific prospective laser wavelength.

Jesson and Gaydon (1967) have proposed another type of multiple reflection cell, where the mirrors are spaced at twice their radius of curvature, with the flame at their mutual center of curvature. They claim superior spatial resolution for this system in absorption studies. The present study, however, deals with diffuse low pressure flames, where spatial resolution is not needed, certainly not when emissions from the flame as a whole have yet to be characterized. Geometrical ray-tracing calculations have been performed which show a tendency for off-axis rays to "walk" off the mirrors when Jesson and Gaydon's (1967) system is used for emission studies. Hill and Hartley (1974) have described a multiple-reflection light-trapping cell utilizing a combination of ellipsoidal, spherical and flat mirrors for laser-excited Raman spectroscopy. However, their system depends critically for its operation upon the incident

laser beam passing exactly through one focus of the ellipsoidal mirror, and is thus unsuitable for use with an extended, diffuse low pressure metal vapor flame.

A spherical cavity, as suggested by Gebbie and Bohlander (1972) or an ellipsoidal cavity (with the flame at one focus) completely surrounding the flame would of course, by completely surrounding the flame, in principle, collect a greater fraction of the light emitted by the flame than the White cell system described above. In practice, however, in addition to being more difficult to fabricate, and to having unavoidable losses due to the necessity of piercing the reflecting surface with fuel and oxidizer inlets and a vacuum port, the very fact that such cavities completely enclose the flame make it nearly impossible to prevent deposition of condensed reaction products on the reflecting surface, with consequent severe degradation of performance. Determining the effects of changes in path length, as described earlier, would also be more difficult with such cavity reflectors.

In the White cell system used in this investigation, the mirrors and windows were protected from deposited condensed reaction products (and oxidant if corrosive oxidants were to be used) by a flow of argon through inlets at the ends of the cross arms containing the mirrors. The effectiveness of this protection was good, but not perfect, and removal of the

mirrors for cleaning was required about once every six months. When necessary, the mirrors were cleaned by blowing off loose deposit with dry nitrogen, flowing distilled water over the surface, and then removing any additional deposit carefully with lens tissue or clean cotton swabs and Kodak lens-cleaning fluid. The mirrors were then rinsed with distilled water, then 50/50 methanol/water, then pure methanol, and allowed to air-dry while protected from dust. The mirrors were then replaced in the chamber, and realigned if necessary. (As the entire mirror mounting plate was removed, without disturbing the mirror mount adjustments, only minor realignment was usually necessary after cleaning).

Light exiting the slot between the front White cell mirrors passes through a window and is focused by a condensing lens on the slit of a McPherson 0.5 meter, $f/8.7$ spectrograph/scanning monochromator, which will be described below. In early experiments, before installation of the White cell, an image rotating device (dove prism, or its mirror analogue) described by Sullivan (1969) was used to place the long dimension of the flame image along the length of the spectrograph slit. This device is shown in place in Fig. II-1. Once the White cell was installed, the image rotator was no longer needed as the (vertical) exit slot of the White

cell was then imaged on the (vertical) spectrograph entrance slit.

In preliminary experiments in the visible, a plexiglass chamber window and glass condensing optics were used. These were replaced later by quartz optics, when observations were extended to the ultraviolet. For nearly all the quantitative measurements to be described, the condensing system was a quartz plano-convex lens of 2 inch diameter and 8 inch focal length, located 12 inches from the spectrograph entrance slit and about 24 inches from the exit slot between the front White cell mirrors (measured to the mirror surface). The free aperture of the 1/4 inch thick quartz window was 2 inches in diameter.

A telecentric (Hardy and Perrin, 1932) optical system consisting of a lens placed at its focal length from the exit slot of the White cell, permitted photography of the entire flame through the narrow slot without the necessity of removing the mirrors or otherwise disturbing their alignment. This lens, an 8 inch focal length $f/4.5$ anastigmat copy lens (Edmund Scientific Co. #41432), forms a real image of the flame which is in turn photographed using a 35 mm. single-lens-reflex camera with extension tubes to allow close-focusing. The optics of this interesting method of photographing through keyholes has been described in detail (Zwillenberg, 1975).

C. Metal Vapor Furnace

The furnace for vaporizing the metal consists of a

1 inch o.d. stainless steel tube surrounded by a Kanthal-A heating element (maximum temperature 1260°C) and a 1 inch layer of Kaylo-20 insulation (a calcium silicate based refractory). The heating element consisted of two hemi-cylindrical commercial units (Electro-Applications Inc., Type Y-3, 6 inches long x 1.25 inch i.d., 2.062 inch o.d.), each rated at a maximum power input of 335 watts at 57.5 volts, and connected in series for 115 volt operation. The furnace tube is sealed to the vacuum chamber by "O"-ring seals, and is easily removed for cleaning or modification. The furnace temperature was controlled by adjusting the a.c. voltage applied with a variable transformer. Furnace temperature was monitored by a chromel/alumel thermocouple, electrically insulated by a ceramic tube, and inserted longitudinally through one of the coils of the heating element. It was found that increased conductivity of the ceramic tube at high temperatures allowed some electrical leakage from the heating element to the thermocouple. After unsuccessful attempts to filter out the a.c. interference with a capacitative filter, the problem was sidestepped by momentarily turning off heater power when measuring furnace temperature. The metal sample is contained in a refractory combustion boat placed inside the furnace tube. The furnace has proven successful for prolonged operation at 900°C. It could be operated at

temperatures in excess of 1000°C by replacing the stainless steel tube and orifice by an alumina tube and orifice. Examination of Table II, which contains alkaline earth metal melting and boiling points (Sullivan 1969), plus the consideration that a metal vapor pressure of only around 1 torr or less is needed (the remainder being argon carrier gas), shows that the furnace is suitable for experiments with all the alkaline earth metals except beryllium. Beryllium was never considered, due to its extreme toxicity.

Table II

Melting and Boiling Points of Alkaline Earth Metals

<u>Metal</u>	<u>Melting Point, °C</u>	<u>Boiling Point(1 atm.), °C</u>
Be	1283	2484
Mg	649	1105
Ca	848	1240
Sr	774	1366
Ba	850	1587

Fig. II-5 gives vapor pressure data (Perry 1950) for all the alkaline earth metals (except beryllium).

Refractory insulation and the vacuum conditions reduce heat losses from the furnace to the point where a

power input of about 200 watts is sufficient to maintain the furnace at 900°C. After 3 hours of operating, the vacuum chamber wall nearest the furnace has reached a temperature of only about 70°C.

It should be emphasized that the apparatus developed is capable of studies not only of the alkaline earth reactions, but can be used with any fuel having a vapor pressure of the order of 1 torr or more at 1200°C (or below), and with a variety of oxidizers including oxygen, halogens, alkyl and other halides, nitrogen oxides and even (with the addition of a discharge tube source) atomic species.

A stream of argon flows through the furnace tube, over the ceramic boat containing the metal sample, and carries the metal vapor through an orifice into the vacuum chamber where it reacts with oxidizer introduced through a separate inlet. Initially, clogging of this orifice by metal and condensed combustion products severely limited the duration the flame could be maintained. Changes in orifice design were made in an attempt to attain both longer optical path length and longer flame duration.

The longest flame duration obtained with the nozzle of Figure II-6a was about 20 minutes, after which the nozzle

clogged, apparently with calcium oxide. Figure II-6g illustrates the mechanism by which it is thought that oxygen may reach the nozzle and cause the deposit of oxide. A number of different nozzle configurations were tried (Figure II-6) and those shown in Figures II-6e and II-6f were found to give the best results. These consist of a small circular or slit-shaped orifice with a larger, similarly spaced orifice spaced about 1/2 inch in front of it. The space between the two orifices is filled with metal vapor and inert carrier gas. Any oxidizer diffusing into this space is promptly swept out by the carrier gas jet. Because no oxidizer can reach the inner orifice, no reaction product deposits can form there. Products do deposit on the outer orifice, but, since it is much larger, it takes much longer to clog. Runs of up to 5 hours in length have been achieved with these nozzles, and seem limited more by exhaustion of the metal sample than by clogging of the orifice. In addition, the width of the flame seems to be determined by the dimension of the outer, larger orifice. Thus a much wider flame is produced and hence there is a longer optical path length. Of the two, orifice 6f provides a longer optical path than orifice 6e, but requires higher carrier gas flow (and hence higher vacuum pumping capacity) for the same flame length. Because this pumping capacity was available, orifice 6f was adopted for use in all subsequent experiments. A more detailed view of the furnace tube with this orifice

is shown in Fig.II-7. The copper section conducts heat from the hot zone of the furnace, keeping the orifice hot and reducing condensation of metal vapor on the orifice.

Because the ratio of furnace pressure (~ 25 . torr) to vacuum chamber pressure (~ 1.5 torr) exceeds the sonic ratio, it was originally thought that the flow is supersonic, with the narrow slit orifice serving as the throat of an inefficient de Laval nozzle. A number of sources soon made it evident that the flow, at least outside the $3/8$ inch x $3/4$ inch shield slit, was subsonic. First, calculations using measured furnace carrier gas flow rates and temperatures, the measured chamber pressure and the area of the shield slit, predicted Mach numbers in the range 0.1 to 0.3. Secondly, no shock phenomena were visible when a probe was introduced into the flame, although one might expect the resultant temperature and pressure variations to affect the intensity of chemiluminescence. Thirdly and most conclusively, a series of cold argon flow tests were performed, with furnace pressure in the range 5-80 torr, chamber pressure in the range 0.8-6. torr and pressure ratio from 6:1 to 40:1. Thermocouple probing of the flow field revealed no variation of measured junction temperature from room temperature (i.e. the stagnation temperature of the flow). Calculations (Zwillenberg, 1975) using the recovery factor data of Bundy and Strong (1954) indicate the flow Mach number must be less than 0.3.

It thus seems clear that while the gas flow through the 0.020 inch inner furnace orifice might be sonic, dissipative processes in the region between the orifice and shield slit cause the flow leaving the shield slit to be subsonic.

It was originally intended to estimate metal vapor flow rate using the vapor pressure of the metal, P_v , the furnace pressure, P_F , and the measured argon carrier gas flow rate, q_A , to calculate metal vapor volumetric flow rate, q_m , by:

$$q_m = q_A \times \frac{P_v}{P_F - P_v} \quad \text{Eqn. (II-1)}$$

However, it was found that the shield plate is several hundred degrees cooler than the furnace and condensation of metal on its inner surface often occurs. Instead, average metal vapor flow rate is estimated by using the metal sample weight, the flame duration, and a rough estimate of the fraction of the sample remaining (in the ceramic boat and deposited inside the shield plate). As further checks, the use of Eqn. (II-1) at the furnace temperature and at the (measured) shield plate temperature provide upper and lower bounds on q_m . Because of the approximate nature of all such estimates, when quantum yields are calculated, they are expressed in terms of quanta per oxidizer molecule (O_2, N_2O or CCl_4), since these are much more accurately determined.

d. Vacuum System

Leakage and outgassing rates in the system are low enough so that a two-stage mechanical vacuum pump (Welch Scientific Co., Model 1397) with a nominal pumping speed of 500 liters/minute can hold the chamber at a pressure of 3. millitorr. Pressures of less than 1.5 torr can be maintained with input gas flows of more than $800 \text{ cm}^3/\text{min}$ (STP). Initially, pressed-fiber and fine stainless steel mesh filters were used in the vacuum pump inlet line, to protect the pump from condensed reaction products. However, these filters severely limited the attainable vacuum, and the change in their flow resistance in the course of a single experiment made maintenance of constant chamber pressure difficult. Finally, it was found that the filters could be omitted, at the cost of changing the pump oil every few months. One pump developed an oil leak at a bearing seal after two years of constant use, which may be due to reaction products in the oil. Pump inlet filters of larger area might prevent this without undue limitations on pumping speed.

e. Pressure Measurement and Gas Flow Control System

Vacuum chamber pressure was measured by a Wallace & Tiernan bellows-type absolute pressure gauge (Model FA 160, 0.1-20. torr, absolute) and checked against a Stokes (McLeod-type) gauge (1.millitorr-5. torr). A Bendix GT-340A thermistor vacuum gauge (two ranges: 0-1 atm. with midscale at 0.5 torr, and 0-100 millitorr, with mid-scale at 40 millitorr) was used to continuously monitor the quality of vacuum attained and aid in detecting and

finding leaks. Furnace pressure was measured with a Wallace and Tiernan bellows-type differential gauge (Model FA-141, -10-0-+10 inches of mercury), reading the pressure difference between the furnace and the vacuum chamber.

A schematic diagram of the gas flow control system is given Fig. II-8. Gas supply pressures were reduced and controlled with two-stage pressure regulators. Flows were controlled with micrometer needle valves and measured with Brooks Sho-Rate ball-in-tube flowmeters. The flowmeters were calibrated using a soap-film flowmeter and stopwatch (measuring the time for a known volume of gas to flow) after the "typical" calibration curves supplied by the manufacturer were found to be inaccurate. Bourdon tube type pressure gauges were used to measure flowmeter exit pressure, to permit application of flowmeter pressure corrections. The oxidizer gas stream, before entering the chamber, was passed through a coil made of a 6 ft. length of 1/4 inch tubing to thoroughly mix it and bring it to room temperature.

In experiments with flames burning in CCl_4 vapor, the vapor was generated by flowing argon first through a flowmeter, then through an evaporator containing 100.ml. of reagent grade liquid CCl_4 . (In this manner only argon passed through the flowmeter). Originally, the

argon was bubbled through the liquid, but it was found that this allowed trapped pressure in the evaporator to force liquid CCl_4 back into the flowmeter when the supply pressure was reduced. To prevent this, the evaporator inlet was modified so it was just above the liquid surface, and the argon blew over the liquid surface. CCl_4 vapor flow rates were calculated by assuming saturation of the argon and taking the CCl_4 vapor flow as the quantity $q_A \frac{P_V}{P_E - P_V}$ where q_A is the volumetric argon flow through the evaporator (STP), P_V is the CCl_4 vapor pressure and P_E is the total pressure in the evaporator. As typical CCl_4 flow rates were of the order of 15 mg/min., the assumption of saturation was considered justified. The evaporator was supplied with a strap heater and thermocouple for use if low volatility oxidants (e.g. I_2) were to be used. However, since the vapor pressure of CCl_4 is about 100. torr at room temperature, the heater and thermocouple were not used. Since the heat of vaporization of CCl_4 is 46.4 Cal/g. [Hodgman, Weast and Selby 1958], the required heat to evaporate the CCl_4 is less than 1.5-Cal/min. The evaporative cooling effect is thus negligible, and the liquid is at room temperature which was read on a thermometer in contact with the evaporator.

f. Spectrographic Instrumentation

Spectroscopic studies were performed using a McPherson Model 216.5, 0.5 meter, f/8.7 combination

scanning monochromator and spectrograph. The instrument has a plane grating in a modified Czerny-Turner mount, and is usable from 1050\AA - $160,000\text{\AA}$ (16μ) by replacing the grating. (In the vacuum ultraviolet, 1700\AA can be reached by purging and 1050\AA by evacuating the instrument). In the current investigations, the instrument was equipped with a 1200 lines/mm grating blazed for 5000\AA , which provides a range of $1,050$ - $10,000\text{\AA}$, a reciprocal linear dispersion of $16.6\text{\AA}/\text{mm}$ and a resolution in first order (with $10\mu\times 4\text{ mm}$ slit) of 0.4\AA . Most experiments were performed with 50 micron slits (exit and entrance in monochromator mode) with experimentally determined resolution of about 1.5\AA . Wavelength coverage was limited on the short wavelength end, by the use of quartz optics to about 2000\AA , and by photomultiplier response to 2500\AA . On the long wavelength end, the spectral response was limited by both spectroscopic plates and photomultiplier to 8900\AA . A 600 line/mm grating was available, which would let the spectrometer reach $20,000\text{\AA}$, but without sensitive detectors for this region, this would have accomplished nothing. (Solid state detectors sensitive in this region are orders of magnitude less sensitive than photomultipliers).

The instrument accepts a plateholder for 2×4 inch

glass plates, a Polaroid adapter and up to 3 photomultipliers. In the present work, one photomultiplier was used at a time, with a single exit slit equal in width to the entrance slit. The photomultipliers used were an RCA 1P28 for the ultraviolet and most of the visible, and an RCA 7326 for the red and near infrared. The 1P28 has S-5 response, with extended ultraviolet response due to its SiO_2 envelope. The 7326 has S-20 response, and the particular specimen used had usable sensitivity to 8900\AA , about 500\AA further than predicted by the nominal S-20 response curve. The photomultipliers were powered by a regulated high voltage supply (Electron Research Associates, Inc. Model TH5K-15LM, 0-5 kV, 0-15 ma) set at the manufacturer's recommended voltage for each photomultiplier (1000 V. for the 1P28, 1800V. for the 7326).

g. Electronic Instrumentation

Initially, photomultiplier output signals were measured in a d.c. mode. The d. c. signal was filtered by an RC filter consisting of the 100,000 ohm load resistor paralleled by a 5. microfarad capacitor. The time constant of this combination is 0.5 seconds, which corresponds to a bandwidth ($1/4RC$) of 0.5 hz. The d.c. signal was then amplified by a d.c. amplifier set at a gain of 20, and recorded on a Bristol potentiometric chart recorder (0-50.mV. response, 0.5 sec. response).

The photomultiplier dark current signal was balanced out by connecting a Leeds and Northrup potentiometer, as a voltage source, to the differential input of the d.c. amplifier.

It was found, however, that the signal-to-noise ratio of this arrangement was too low, requiring excessively large slit widths (as wide as 2.mm for some flames) with consequent loss in resolution. Consequently, an a.c./synchronous detection mode of measurement was adopted. The input optical beam was chopped by a mechanical chopper disk with 16 holes, driven at 3600 rpm by a synchronous motor, giving a chopping frequency of 960 hz. The motor speed was checked against a.c. power line 60 hz frequency, using a General Radio Strobotach (stroboscopic tachometer). A light emitting diode and phototransistor mounted on the same chopper provided a 960 hz reference signal, which was amplified and filtered to remove noise at frequencies above 960 hz. The photomultiplier signal and reference signal were then fed into a Princeton Applied Research Corp. Model 128A lock-in amplifier. This instrument operates on the principle of synchronous detection, providing d.c. output only from signals coherent with the reference frequency. Noise at other frequencies provides only a.c. output, which may be filtered out by a suitable

output filter time constant. Effectively, the signal is translated from a frequency band centered about zero frequency, to one centered at the chopper frequency. Since many electronic components (transistors, some resistors, etc.) produce noise which varies inversely as the frequency ("1/f noise"), it is advantageous to translate the signal to higher frequencies. All types of noise not varying with light intensity will not be modulated at the chopper frequency, and will not be so translated. In addition, the use of long time constants in the output filter provides a narrow passband centered on the chopper frequency. Thus, a 30 second time constant in a 6dB/octave filter provides an equivalent bandwidth of 0.0083 Hz. A condensed set of specifications of the PAR 128A is given in Table III. The output of the lock-in amplifier was then recorded by the same Bristol recorder described earlier.

Table III

Condensed specifications of PAR 128A
Lock-in Amplifier

full-scale output	: 1. volt
non-coherent overload capability	: 1000x full scale
response to non-coherent signal	: 50. ppm.
output drift	: 0.1%/°C
gain stability	: 0.05%
overall gain accuracy	: 2.%
input impedance	: 100 M Ω shunted by less than 20 pf.
sensitivity ranges (input for l.v. out)	: 1. μ v-250 mv.
common mode rejection	: greater than 100 dB@1.Khz.
internal noise	: less than 10 nv/hz ^{1/2} @1.Khz.
filter time constants	: 1.ms-100.seconds (Plus additional 0.1 or 1. second) dc pre-filter
high pass filter	: <0.5 hz, 5 hz or 50 hz
low pass filter	: 100 hz, 10Khz or >100 Khz.

h. Photomultiplier/Spectrometer Calibrations

To compare the intensities of flame light emissions at different wavelengths, the relative response, as a function of wavelength, of the photomultiplier/spectrometer system must be obtained. This differs from the nominal photomultiplier spectral response curve provided by the manufacturer, because of such factors as variation of grating efficiency and dispersion with wavelength and the deviation of a particular photomultiplier from the nominal "type" spectral response. The 1P28 photomultiplier/McPherson spectrometer system was calibrated using a strip filament tungsten lamp with quartz window, powered by an NJE Corp. Model QR15-20C (0-15VDC, 0-20 ampere) regulated variable d.c. power supply set in current regulated mode. Lamp brightness temperature was measured with a Leeds & Northrop Model 8622-C optical pyrometer, sighting through the same quartz window used for the photomultiplier calibration. True filament temperature was calculated using tabulated tungsten emissivity values (Weast 1967), a 3.5% reflection loss at each quartz surface (calculated from the refractive index of quartz and the Fresnel formula for normal incidence) and Wien's Law. At 0.665μ wavelength, the error in Wien's law corresponds to less than 0.3°K at up to 3000°K (Forsythe 1937). Calibration was performed over the range 2500-7500 \AA ,

at a number of filament temperatures from 2015°K to 2879°K. Light scattered within the spectrometer was estimated from the (non-zero) signal at the upper and lower wavelength limits, where the measured value of $dI/d\lambda$ was zero (and detector response known to be zero), and corrected for. The system response was then calculated as the ratio of photomultiplier signal to computed emission (from Wien's law) and the relative response obtained by normalizing with respect to the peak value of response.

Because of the rapid falloff of lamp intensity toward the ultraviolet, correction for the second order spectrum was found unnecessary.

This relative spectral intensity calibration was converted to an absolute intensity calibration by making an absolute intensity measurement at 4300Å (the peak of the experimentally determined relative response curve). This was done by placing a small strip-filament tungsten lamp inside the vacuum chamber, at the flame position, and measuring the resulting photomultiplier signal. A lamp with a glass window was used in this calibration,

as the quartz-window lamp was too large to fit in the chamber, and at 4300\AA , there is no need for quartz. The filament temperature was determined using an optical pyrometer and Wien's law, as above. During this calibration, the rear White cell mirrors were covered to avoid errors due to light reflected from them. The total energy per unit time and solid angle within the 1.5\AA spectrometer passband (with 50μ slits) was then calculated using Wien's law and the measured filament dimensions ($2\text{mm} \times 19\text{mm}$), and the corresponding emission from a flame (into 4π times steradians) to give the same photomultiplier signal is 4π times this value. This calibration was performed at several filament temperatures, and the correspondence between the product, $I\lambda$ of photomultiplier signal and wavelength, and photon emission rate into 4π steradians was found to be:

$$1 \text{ millivolt} - \text{\AA} = (3.87 \pm 0.35) \times 10^{10} \frac{\text{quanta}}{\text{second}}$$

or about 4×10^{10} quanta/sec.

It should be noted that in comparing emission from a flame with this figure, the measured intensity must be divided by the White cell gain (the ratio of the signal with the White cell operative to that with the rear mirrors blocked).

It should also be noted that the condensing lens images the White cell exit slot, not the flame, on the spectrometer slit. In effect it is this slot which acts as the light source illuminating the spectrograph slit. As long as the distance from flame (or filament) to the White cell exit slot is large relative to flame (or filament) dimensions, the slot will be uniformly illuminated and there will be little effect of the difference in geometry between flame and lamp filament. Since typical flame dimensions are 2-4 inches, the filament length is 19mm. and the distance between the flame and exit slot is 20. inches, this condition is satisfied.

i. Auxilliary Equipment

A Sorenson Model ACR-1000 a.c. voltage regulator was used to minimize the effects of line voltage variations on electronic equipment. A University Laboratories Inc. Model L-240 Helium/Neon laser was used to align optics, as well as for an attempted laser-excited-fluorescence experiment described later. Helium, neon and mercury discharge tubes, excited by a tesla coil were used to provide calibration spectra. Spectrographic plates were read on a Gaertner Scientific Co. traveling microscope, and wavelengths calculated using a second degree least squares curve fitting computer program adapted from a program by Green (1968). An

Aerochem Research Labs. Model MB-4 chemiluminescence NO monitor was used to check for traces of NO in reagents and reaction products. O₂ analysis was performed with a model 7624A Hewlett-Packard gas chromatograph.

3. Procedure

The metal sample was prepared as described earlier, placed in a refractory combustion boat and placed in the heated zone of the furnace tube. The furnace tube was closed, the chamber pumped down, and argon flowed through the furnace to flush out air (and cyclohexane vapor in the case of calcium). The argon was then shut off, and the chamber pumped down to maximum attainable vacuum to complete outgassing of the system. A flow of argon was then begun, through the mirror/window purging inlets, sufficient to maintain the chamber at 1-2 torr pressure, while pumping continued. The furnace heating power was turned on and the furnace heated to the desired operating temperature (about 660°C for magnesium, 860°C for calcium), which typically took about one hour. The continuous flow of argon was to flush out any air leaking into the system, and prevent its reacting with the heated metal sample. The pressure was maintained at 1-2 torr, to retard diffusion of metal vapor out of the furnace. Argon was not flowed

through the furnace during the heating period to avoid sweeping metal out of the furnace and to avoid reaction of the metal sample with O_2 impurity in the argon. (O_2 in the argon introduced directly into the chamber would have to diffuse into the furnace through the narrow slit orifice to reach the metal sample). When the desired furnace operating temperature was reached, heater voltage was reduced until furnace temperature was steady. If spectrographic measurements were to be made, the plateholder was loaded and placed into the spectrograph, or the electronic instrumentation (D.C. or lock-in amplifier, photomultiplier power supply, etc.) was turned on and allowed to stabilize during the furnace heat-up period.

The predetermined metal vapor carrier, oxidizer, additive or diluent and mirror/window purge gas flows were then set, sometimes adjusting them slightly to adjust flame geometry and size. The flame would usually appear at once. Chamber pressure was set at the desired value by adjusting a Veeco vacuum valve in the vacuum pump inlet line, and by varying the mirror/window purge gas flow. When effects of pressure variation on the flame were being studied, pressure was varied solely by means of the

vacuum valve, keeping all flow rates (and input mole fractions) constant. The desired optical, thermocouple probe and spectrographic measurements were then made, as functions of the experimental parameters (flow, pressure, concentrations, etc.). Spectrographic measurements were made initially on photographic plates, to survey the entire flame spectrum and determine the emitters and excited states present. Quantitative intensity measurements were then made photoelectrically. These latter were made in 3 modes. Firstly, a continuous scan of an extended portion of the spectrum might be made, when a large number of features of similar intensity, or an extensive band system were to be measured. Secondly, the spectrometer might be set at the peak of a line or band. This was often done when the effects of oxidizer or additive flow rate or pressure upon emission intensity was to be measured. Thirdly, an individual line or band might be scanned. This was often done when background continuum existed in its vicinity, or where the peak of a weak spectral feature was otherwise difficult to locate. In all cases, an absolute zero intensity level was recorded by closing the spectrograph entrance shutter. When relative intensities of a number of different wavelengths (necessarily measured at different times) were to be compared, it was necessary to correct the intensities for variations in

overall flame intensity due to slow exhaustion of the metal sample or obstruction of the furnace outlet. This was done by measuring the intensity at some single wavelength (usually a strong, non-resonance line) at the beginning and end of the experiment and a number of times during the experiment. These intensities were then plotted vs. time (usually on a semilogarithmic plot, as decay tended to be exponential with time), and the resultant curve used to correct all measured intensities to time=0. (The assumption was here made that all emissions vary in the same manner with metal vapor input). Some justification of this method of correction is gained from the observation that similar results were obtained from experiments in which such corrections were made, and others in which flame intensity varied by less than a few percent over the duration of the experiment and no corrections were needed.

After completion of the experiment, all gas flows except the mirror/window purge were turned off, and the furnace heater turned off. When the furnace temperature had fallen about 200°C (so metal vapor pressure was negligible) the purge flow was turned off, and the furnace allowed to cool, usually overnight.

When the furnace was cool, the vacuum pump valve was closed and the chamber pressure raised to atmospheric. The furnace tube was then removed, emptied and cleaned. (First with water to remove remaining reactive metal, then with

dilute HCl to remove metal oxide and magnesium, then water rinses and a final methanol rinse to remove water, followed by air drying). The interior of the chamber was cleaned of reaction product deposits.

The furnace tube was then replaced within the heater and pumped down to the best attainable vacuum to outgas. Occasionally, gases adsorbed on the furnace tube and/or moisture adsorbed in the furnace insulation (while the chamber was open to the air) limited the lowest vacuum attainable to 50-100 millitorr. In these cases, the furnace was heated to over 800°C under vacuum and the chamber flushed periodically with inert gas, to drive off these adsorbed materials.

CHAPTER III: EXPERIMENTAL RESULTS AND DISCUSSION OF RESULTS

a. Types of Flames Studied and Range of Experimental Parameters.

The flames studied experimentally fall naturally into two groups. The first, in which the major optical emitters were molecular species, includes the flames of magnesium and calcium with oxygen and N_2O . The second group, in which intense metal atom line emission accompanies emission by molecular species, includes the flames of magnesium and calcium with CCl_4 , with and without the addition of oxygen, which was found to profoundly affect the nature and intensity of the emissions. A small number of experiments were performed on the $Mg/CCl_4/N_2O$ system to examine the effects of oxidant additives other than O_2 . The availability of accurate transition probability data (Wiese, et.al. 1969) for Ca and Mg allowed the calculation of relative excited state population densities for these atomic species. Measurement of spectral line self-absorption and absolute intensity then allowed the estimation of absolute ground and excited state population densities.

The range of experimental parameters over which the flames were studied is shown in Table I. Of course, all possible combinations of pressure, oxidizer concentration(s), flow rates, etc.- could not be studied. In addition, the time consumed by spectroscopic measurements (hours-long photographic exposures, or for photoelectric detection, long scans at $5\text{\AA}/\text{minute}$, or 100 second averaging time) limited each

experiment to either the measurement of many wavelengths at one or a few sets of experimental conditions, or a small number of wavelengths over a range of one or two experimental parameters. In general, most experiments were performed in the lower portion of the pressure and mole fraction ranges listed in Table I, to avoid problems with burner clogging, small flame size and collisional deactivation or quenching of excited species, and 1-2 torr pressure, 0.5% O_2 (in Ca or Mg + O_2 flames), 0-0.5% CCl_4 and 0-1% O_2 (in Ca or Mg/ CCl_4/O_2 flames) are more typical values, except in those experiments where the effect of varying pressure or oxidant concentration was being studied. Flame length and location were adjusted by varying metal vapor/carrier gas flow.

Table I

Range of Experimental Parameters

Flame Size: 3/4" - 4" diam.(spherical), 2" diam x 5" long
(elongated.)

Furnace Temperature: Mg:600-770°C; Ca:800-950°C.

Chamber Pressure: 0.1-10. torr

Oxidizer Mole Fractions (Based on total gas input flow rate):

Ca + O ₂ :	X _{C2}	=	0-15.5%
Ca + N ₂ O:	X _{N₂O}	=	0-3.%
Mg + O ₂ :	X _{O₂}	=	0-18.%
Mg + N ₂ O:	X _{N₂O}	=	0-16.8%
Ca/CCl ₄ /O ₂ :	X _{O₂}	=	0-4.%, X _{CCl₄} = 0-1.3%
Mg/CCl ₄ /O ₂ :	X _{O₂}	=	0-6.3%, X _{CCl₄} = 0-0.7%
Mg/CCl ₄ /N ₂ O:	X _{N₂O}	=	0-12.%, X _{CCl₄} = 0-0.3%

*one experimental point at 28.1% O₂

Estimated Metal Vapor Input Fluxes:

Ca: 2.2×10^{17} - 1.1×10^{18} atoms/sec = 0.5-2.5 std. cm³/min

Mg: 1.8×10^{18} - 3.6×10^{18} atoms/sec = 4.-8.1 std. cm³/min

Estimated Metal Vapor Input Mole Fractions (based on total input gas flow)

Ca: 0.06-1. %

Mg: 0.4 -3. %

b. General Appearance of Metal Vapor Flames

At pressures below several torr, the flame structure was diffuse, becoming more condensed as chamber pressure was raised. Flame shape varied from spherical to elongated as metal vapor/carrier gas flow was increased (ranging from 3/4-2 inches in diameter and 3/4-5 inches in length). The visual colors of the different flames are as follows:

Ca/O ₂	- orange core with reddish halo
Ca/N ₂ O	- yellow-orange, tinge of pink
Mg/O ₂	- bluish-green
Mg/N ₂ O	- bluish-white with green tinge
Ca/CCl ₄ with & w/o O ₂)	- pink-purple with thin blue-green halo
Mg/CCl ₄	- faint violet with reddish halo
Mg/CCl ₄ /O ₂	- intense emerald green with blue tinge
Mg/CCl ₄ /N ₂ O	- green core, yellow-orange halo, reddish purple near edges

In general, the flames decreased in size as chamber pressure was raised, growing more condensed and brighter. This is consistent with the description by Gaydon and Wolfhard (1960) of the inverse variation of luminous reaction zone thickness with pressure in low pressure flames. The size of the Ca vapor flame burning in O₂ or N₂O was found to decrease with increasing oxidizer flow, and the flames of

Ca and Mg vapor in CCl_4 vapor showed similar behavior with increased CCl_4 flow. These observations are in accord with the theory of the dilute diffusion flame described by Garvin and Kistiakowsky (1952) which describes the metal vapor concentration, C_M , in the case of purely diffusive flow by:

$$C_M \sim \frac{e^{-cr}}{r}$$

where $c = \frac{kC_A}{D}$, C_A is the concentration of atmosphere reactant, D the diffusion coefficient and k the reaction rate constant for the $A + M$ reaction. Reed and Rabinovitch (1955) showed that the effect of convective flow is to change the former spherical flame shape (and metal vapor distribution) to an oval one, and displace its center along the flow axis. The size of Mg/O_2 and $\text{Mg}/\text{N}_2\text{O}$ flames did not seem to vary appreciably with moderate increases in oxidizer concentration, which may be due to the relatively low reaction rate (small k in the equation above), which will be discussed further below. The $\text{Mg}/\text{CCl}_4/\text{O}_2$, $\text{Mg}/\text{CCl}_4/\text{N}_2\text{O}$ and $\text{Ca}/\text{CCl}_4/\text{O}_2$ flames decreased only slightly in size with moderate increases in O_2 or N_2O flow, indicating that the metal vapor - CCl_4 reaction is faster than the metal vapor - O_2 or N_2O reaction. With large increases in O_2 or N_2O flow, however, a point was reached where the region of metal atom and metal halide emission (green in Mg flames,

pink in Ca flames) began to contract into a small region near the metal vapor nozzle, while the main flame, now violet or greenish violet (C_2 emission) remained essentially unchanged in size. Similar contraction of the zone of metal emission (faster than contraction of overall flame) was observed with increases in CCl_4 mole fraction and chamber pressure. (Note that an increase in P at constant X_{CCl_4} is an increase in CCl_4 concentration, as $[CCl_4] \propto P X_{CCl_4}$.)

Photographs of some typical flames are shown in Figures (III-1) and (III-2), showing the Ca/O_2 and the $Mg/CCl_4/O_2$ flames respectively.

As pressure was reduced from 8 torr to about 2 torr, the Ca/O_2 flame was observed to change from a roughly conical, relatively sharp-edged shape (similar to an atmospheric pressure hydrocarbon diffusion flame) to a diffuse, spherical or oval form. This change has been explained (Fristrom and Westenberg, 1965, Zwillenberg, 1975) as a transition from diffusion flame to premixed flame, as the mixing rates become comparable with the chemical reaction rates. A similar transition has been reported (Fristrom and Westenberg, 1965, Gaydon and Wolfhard, 1960) in hydrocarbon flames at pressures about 20 times higher, suggesting that the rate of the Ca/O_2 reaction is higher than those in hydrocarbon flames by a similar factor.

It thus appears clear that in the range of pressures below about 5 torr, in which most of the present experiments were performed, light emission from the flame is a volume phenomenon, from all or nearly all of the flame volume, rather than from a thin shell as in the atmospheric pressure diffusion flame. As noted earlier, Gaydon and Wolfhard (1960) report an inverse variation of flame zone thickness with pressure. Their results for the C_2H_2 /air flame, extrapolated to 1. torr pressure, indicate a flame zone thickness of the order of 10. cm. Consideration of oxidizer concentrations, diffusion rates and gas velocities lead to similar conclusions regarding flame zone thickness. For the experimental conditions ($T \sim 500^\circ K$, $P \sim 1.$ torr), the collision frequency for a molecule (assuming molecular weight and cross section about those of argon) is about 10^6sec^{-1} , and the frequency of collisions with oxidizer molecules is thus $10^6 X_O$ where X_O is the oxidizer mol fraction. The mean time between collisions with an oxidizer molecule is thus $1/10^6 X_O$. Assume that for excitation (and subsequent luminescence) a metal atom must undergo at least one collision with an oxidizer molecule, which requires a time $t = 1/10^6 X_O$. (If the excitation process requires more than one collision, t will be longer in proportion to the number of collisions required.) If flow is diffusive, in this time the molecule travels a distance $X = \sqrt{Dt}$ where D is the diffusion coefficient. If flow is convective, in time t , the molecule travels

$X=Vt$, where V is the flow velocity. Using the diffusion coefficient $0.20 \text{ cm}^2 \text{ sec}^{-1}$ given by Fristrom and Westenberg (1965) for $D(\text{N}_2\text{-Ar})$ at 1 atm., 298°K , and correcting it to 500°K , 1 torr by $D \propto \frac{T^{3/2}}{P}$ (Yielding $D=3.3 \times 10^2 \text{ cm}^2 \text{ sec}^{-1}$), the following values of X are calculated, and can be considered lower bounds on flame zone thickness:

Table II

Minimum Flame Zone Thickness, cm.

Diffusive Flow, $X = \sqrt{Dt}$:

<u>X_O (oxidizer mol fraction)</u>	<u>X, cm.</u>
0.01 (1%)	0.18
0.001 (0.1%)	0.57

Convective Flow, $X=Vt$, $V=10^4 \text{ cm/sec}$.

<u>X_O (oxidizer mol fraction)</u>	<u>X, cm.</u>
0.01 (1%)	1.0
0.001 (0.1%)	10.

The theories of the low pressure dilute diffusion flame (Garvin and Kistiakowsky, 1952, Reed and Rabinovitch, 1955) upon which nearly 40 years of reaction rate measurements are based assume that reaction (and luminescence) occurs throughout the volume of the flame. If emission were restricted to a thin shell, this would be obvious visually, as a peak in the lateral brightness distribution of the flame. Yet in the flames reported here, no such thin luminous zone was visible. Visual observations of the $\text{Ca}/\text{CCl}_4/\text{O}_2$ flame through a narrow band (12\AA half-width) interference filter isolating the 4226\AA resonance line showed a bright central zone, with intensity falling off radially outside it, in a manner consistent with low pressure dilute diffusion flame theory (Garvin and Kistiakowsky, 1952, Reed and Rabinovitch, 1955). In the $\text{Mg}/\text{CCl}_4/\text{O}_2$ flame, when a thermocouple probe was inserted into the flame and observed along the flame axis, it appeared black against a bright flame background (indicating that light was being emitted by the portion of the flame behind the probe), until the probe approached within about $1/2$ inch of the metal vapor nozzle. It thus appears that, except for a small central region near the nozzle (probably a mixing region), luminosity is distributed throughout the volume of the flame.

c. Chemiluminescent Origin of the Emitted Radiation

The presence of chemiluminescence in low pressure, dilute, metal vapor diffusion flames has been noted since the early experiments of M. Polanyi and co-workers (1936). More recently, Zhitkevich et al. (1963a) have observed emissions which they concluded were chemiluminescent in origin in the reactions of organic compounds (including CCl_4) with metals (including Ca and Mg). However, it was desired, in the present work, to verify this for the flames studied, and eliminate at the outset any possibility of thermal excitation. For this reason, approximate measurements of flame temperature were made using a 1/16 in. diameter, stainless steel sheathed chromel/alumel thermocouple probe described earlier. It was not important, for this purpose, that a precise measurement of flame temperature be made, but only that an upper bound be placed on this temperature and that this be lower than that required for thermal excitation to be significant. The use of a relatively large jacketed thermocouple was required to avoid corrosion and short-circuiting of the junction by metal vapor and liquid, and to facilitate removal of condensed deposits without damage to the junction. Possible thermocouple error from various sources were estimated, and discussed in detail (Zwillenberg, 1975). Errors due to radiation losses and to radiative heating of the thermocouple by the furnace were calculated by the method described by Fristrom and Westenberg (1965) (slightly modified for the heating calculations). Axial

conductive losses were calculated as described by Chapman (1967) and heating by condensation of metal vapor or metal oxide was estimated using the assumption of similarity of heat and mass transfer (Lewis number = 1). The results of these calculations are shown in Table IIIA. Some of the corrections partially cancel, and in all cases, the measured temperature is higher than the true gas temperature, and represents an upper limit on it. Typical measured flame temperatures ranged from 200-300°C, and in calculations of density and other gas properties, a gas temperature of 500°K was used.

Using this temperature, the chemiluminescent nature of the flame emissions is easily proven. Consider an atomic line whose upper state has an excitation energy of 5 eV. = 115.3 kcal/mol. Many of the intense lines seen in the Ca and Mg flames with CCl_4 have excitation energies of this magnitude. Assuming that most atoms are in the ground state, and assuming equal statistical weights of ground and excited states, the fraction of excited atoms due to thermal excitation would be, at a gas temperature of 500°K, $e^{-E_u/kT} = \exp\left(-\frac{115.3 \times 10^3}{1.987 \times 500}\right) = e^{-116} = 4.2 \times 10^{-50}$. As the total gas density under the experimental conditions is $\sim 10^{16} \text{ cm}^{-3}$ (and only a small fraction are metal atoms) it is clear that thermal excitation is totally insignificant at this temperature. Even at the much higher furnace temperature (up to 1200°K) the fraction of atoms in the excited state would still be only $e^{-48.4} = 1. \times 10^{-21}$, still negligible.

It should be noted that although the term "flame temperature" was used above, the measured temperature has very little to do with the exothermicity of the chemical reaction, as do "adiabatic flame temperatures". Due to the extreme dilution with inert gas, the temperature measured is almost entirely a function of the heating of the carrier gas in the furnace and its subsequent cooling by passage through the (radiatively cooled) nozzle and mixing with cooler ambient gas. The large excess of inert carrier gas (>99%) serves as a thermal sponge which soaks up the energy release with little temperature rise. The small temperature rise produced by reaction is an even further proof of chemiluminescence, and is independent of the thermocouple corrections described earlier. (Table IIIB).

d. Estimation of Metal Atom Flux and Mole Fraction

As described earlier (in the section on experimental apparatus) it was originally intended to calculate the rate of metal vapor input to the flame using the equilibrium vapor pressure of the metal at the furnace temperature, the (measured) total furnace pressure and the measured carrier gas flow rate. It was found, however, that the slotted shield plate (which protects the inner 0.020" slot orifice), being outside the heated zone of the furnace, is 100-300°C cooler than the furnace, and condensation of metal occurs on its inner surface. Calculations of metal vapor flux using the metal vapor pressure at the furnace temperature yielded unreasonably high values (e.g. metal mole

Table IIIA
Estimated Thermocouple Error
Error, Centigrade degrees

<u>Cause</u>	<u>1 in. from oven</u>		<u>4 in. from oven</u>
Radiative losses	-74.		-74.
Radiative heating (by oven)	+140.	(from $\frac{1}{r^2}$)	8.
Axial conductive loss	-17.		-17.
Oxide condensation	+136		+136.*
Net	+185		+53

*possibly lower due to dilution by ambient gas

Table IIIB
"Flame Temperature" difference with and without oxidizer.

<u>Flame</u>	<u>Temperature, °C</u>	<u>Change</u>	<u>Δt, °C</u>
Ca+N ₂ O	290°C	N ₂ O turned on	+20°
Ca+CCl ₄ /O ₂	280°C	CCl ₄ turned on	<+5°
Mg+CCl ₄ /O ₂	205°C	O ₂ turned off	} no noticeable change
" "	"	CCl ₄ turned off	

fractions 2-3 orders of magnitude higher than the oxidizer mole fraction, in which case the flame should stand at the oxidizer inlet, not the metal vapor inlet, contrary to observation), while using the partial pressure at the shield temperature led to unbelievably low metal vapor fluxes. The true value is somewhere between these two extremes, but since they differ by several orders of magnitude, an arithmetic average of the partial pressures would be meaningless.

However, brief consideration of the vapor pressure - temperature relation, as given by the integrated form of the Clausius-Clapyron equation (Glasstone and Lewis, 1960), shows that the proper average to use is the geometric mean of the vapor pressures at the two temperatures. The use of the geometric mean vapor pressure is approximately equivalent to assuming equilibrium at the average between the furnace and shield temperature. This seems plausible since due to the high velocity with which the gas exits the shield, the gas is unlikely to equilibrate with it, and only partial condensation is likely.

The results of these calculations, based on experiments in which the movable thermocouple probe normally used for flame temperature measurements was inserted into the slot in the shield, so it was in contact with the deposit of condensing metal, are presented in Table IV. Results are also presented of estimates of metal flux by two other methods. Firstly, the known weight of the metal samples used,

an average length of run of about 3 hours and a rough estimate (by eye) that about 1/2 of the metal sample condenses on the shield or remains in the furnace, allows an estimate for average metal vapor flux. Secondly, the observation that, in the Ca/N₂O flame, a 20°C rise in gas temperature occurs when the oxidizer flow is started, plus a calculated heat of reaction (gas phase products and reactants) of 60.9 kcal/mol for $\text{Ca} + \text{N}_2\text{O} \rightarrow \text{CaO} + \text{N}_2$, allows an estimate for the mole fraction of calcium, and hence (since the other gas flows are known) of the metal vapor flow. If C_p is the specific heat at constant pressure of argon ($\approx 5 \text{ cal/mol}^\circ\text{K}$), ΔT the temperature rise, ΔH_r the heat of reaction, and X_m the metal mole fraction, then:

$$X_m \Delta H_r \approx C_p \Delta T$$

$$X_m = \frac{C_p \Delta T}{\Delta H_r}$$

The results of these various calculations, shown in Table IV are in reasonably good agreement. The value for Ca estimated from sample size and run length seems somewhat high, possibly due to deviation from the "average" run length of 3 hours and to error in the "eyeball estimate" that 1/2 the sample remains in the furnace and shield. Based on the spread of results, it is estimated that metal vapor flow is known within less than a factor of 2, and metal vapor mole fraction within about a factor of 3. Because of this uncertainty, quantum yields, when calculated, are given in quanta per oxidizer molecule, as oxidizer flows are more accurately known.

It is recognized that more accurate determination of metal vapor flow is desirable, and should be attempted in future experiments. Heating of the nozzle shield to a higher temperature than the furnace should eliminate the problem of metal condensation. Weighing the furnace before and after each run, as done by Jones and Broida (1974) would determine metal consumption more accurately than an estimate by eye, but would still yield only an average flow over the length of the experiment. Trapping the metal jet on a probe for a known time, as done by Eckstrom et. al. (1974) with subsequent analysis of the deposit is subject to uncertainty as to whether all the metal is trapped from the jet, and whether deposition on the probe occurs due to drift of condensed reaction products out of the flame proper. Significant drift of fine particles, even at 1. torr pressure, has been observed (Johnson, 1971 and this work). In addition, only one measured value is obtained per run, while metal flux may vary during a run. Perhaps a semi-continuous method using atomic absorption or resonance fluorescence with measurement of self absorption (by varying path length with White cell) could yield more accurate values.

TABLE IV

ESTIMATION OF METAL VAPOR FLUX

Run Number	Temp., °C	Equilibrium Metal Vapor Pressure, Torr	Metal Vapor Flux, Std. Cm ³ /Min	Average (A) or Geometric Mean Flux Std. Cm ³ /Min	Mole Fraction Metal Vapor (Based on Total Chamber Flow)
<u>Magnesium:</u>					
MG-4-3-74-1	Furnace 685 Shield 480	3.7 3.05X10 ⁻²	50.6 0.317	4.0	0.43-0.68%
MG-4-5-74-1	Furnace 680 Shield 550	3.3 0.215	43.7 2.27	9.9	1.60-1.67%
Calculated From 1/2 Metal Sample Size, Average Run Length (3 Hr.) and Range of Total Gas Flows (~250-1000 Std.Cm ³ /Min)				8.1 (A)	0.8-3.8
<u>Calcium</u>					
CA-3-26-74-1	Furnace 850 Shield 560	1.68 4.8X10 ⁻³	23.7 6.29X10 ⁻²	1.2	0.17-0.20%
CA-3-28-74-1	Furnace 850 Shield 503	1.68 0.94X10 ⁻³	23.1 1.20X10 ⁻²	0.53	0.061-0.089%
CA-4-2-74-1	Furnace 850 Shield 545	1.68 3.3X10 ⁻³	19.8 3.6X10 ⁻²	0.85	0.14%
CA-6-20-73-1	Calculated from 20° Temperature Rise When N ₂ O Oxidant Turned on, and Known Heat of Reaction			0.51 (A)	0.14%
Calculated From 1/2 Metal Sample Size Average Run Length (3 hr.) and Range of Total Gas Flows (~250-1000 Std.Cm ³ /Min)				2.5 (A)	0.25-1.8

-105-

e. Mg/O₂ and Mg/N₂O Flames

The spectra of the Mg/O₂ and Mg/N₂O flames were nearly identical, and completely different from the discrete band spectra described below, produced in the flames of calcium vapor with these same two oxidizers. The magnesium flame spectra consisted of a broad continuum extending from 8500 Å to a sharp cutoff at 3800 Å with a broad maximum at 5400 - 5500 Å. An unidentified weak line or band at 3860 Å was observed, as well as the resonance lines of sodium and potassium impurities. The 4571 Å $^3P_1 \rightarrow ^1S_0$ "forbidden" line of Mg was seen, strongly in the Mg/N₂O flame, weakly or not at all in the Mg/O₂ flame. Emitted intensity increased with increasing oxidizer concentration and total pressure, and was greater in the flames with N₂O than in those with O₂. Flame diameter decreased much more slowly with increasing oxidizer concentration than in the corresponding flames with calcium vapor (hardly any decrease with O₂, noticeable decrease only with N₂O mole fractions as high as 10%), and suggests a much lower reaction rate for magnesium than calcium. This is also supported by the lower luminosity of the magnesium flames, and by the coating of the interior of the vacuum chamber with finely divided magnesium powder (fine enough to be pyrophoric upon exposure to air), indicating that much of the magnesium vapor was unreacted. On rare occasions, submicron

sized particles of magnesium were observed, when the apparatus was operated without oxidizer flow. (Particles were detected by observing light scattering when a light beam was passed through the chamber. Particle size was estimated from Tyndall scattering colors (Ladenburg, et.al. 1954), from the observation that the particles followed gas streamlines into the vacuum port and from particle settling time calculations). When oxidizer flow was turned on, the particles vanished, probably due to the reduction in Mg vapor concentration. An interesting transient effect was observed in the Mg/O_2 flame, when chamber pressure was raised (by increasing inert gas flow) and then suddenly dropped (by cutting the inert gas flow. Under these conditions, the flame was observed to appear momentarily much more intensely green and brighter. Despite attempts by varying pressure and metal vapor and oxidizer flows, it was not possible to maintain this condition in a steady state, and consequently it was not possible to record a spectrum of it, to determine if it differs from the normal Mg/O_2 flame spectrum. A possible mechanism for this effect will be discussed below.

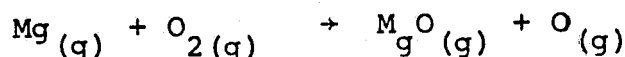
Figures III-3 and III-4 show photoelectric scans of the $\text{Mg}/\text{N}_2\text{O}$ and Mg/O_2 flame spectra. Relatively large slit

widths were required because of the low flame intensity and the fact that these spectra were taken before acquisition of the PAR lock-in amplifier (and hence have a much lower signal/noise ratio). However, photographic spectra of the $\text{Mg}/\text{N}_2\text{O}$ flame at 50μ slit width (nominal resolution 0.8\AA) shows the same unresolved continuum as observed photoelectrically.

An extended continuum, such as that observed in the Mg/O_2 and $\text{Mg}/\text{N}_2\text{O}$ flames, can be caused by a number of different phenomena, including emission from solid particles, from a polyatomic molecular emitter (either a closely spaced, unresolved discrete emission, or a genuinely continuous state) or from a diatomic emitter in which either the initial or final state is weakly bound or repulsive (Gaydon 1957).

A heterogeneous reaction, with accompanying surface luminescence was first suggested by Markstein (1963, 1967), who reported an Mg/O_2 flame spectrum consisting of a continuum with a broad maximum at 4500\AA and narrower maxima at 3900, 6000, 6500 and 6900\AA , and luminescence peaking at 4300\AA when the flame impinged on a solid surface. This latter effect has been observed in the present experiments. Fukuda et al (1965) have observed luminescence peaking at 4050\AA in solid MgO exposed to an O_2 gas discharge. Johnson (1971) has observed the emission of a broad continuum extending from 3700 to 6000\AA in the reaction of Mg vapor

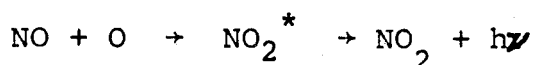
with molecular O_2 , with a peak at 3850A, similar to observations in the present investigation. (The difference in long wavelength limit may reflect a difference in photomultiplier spectral response.) With atomic oxygen, Johnson observed the $B^1\Sigma^+-X^1\Sigma^+$ (green) band system of MgO . It seems likely that the reaction



proceeds slowly if at all in low pressure flames (and being endothermic, cannot produce electronically excited species). At higher pressures (and temperatures) the exothermic condensation of MgO provides the energy needed to dissociate O_2 molecules, and excitation of the MgO green system by the $Mg+O$ reaction observed by Johnson (1971), as well as by direct thermal excitation of MgO , is possible. The conclusion of Sullivan (1969), that the MgO green system emission in Mg/O_2 flames at higher pressure is thermal in origin, seems verified by the absence of these bands in the low pressure Mg/O_2 dilute diffusion flame. Markstein (1963, 1967) suggested that the continuum luminescence observed in this flame is due to heterogeneous reaction on the surface of minute Mg or MgO particles, (Such particles were observed by Johnson [1971]). However, in nearly all of the present experiments, no such particles were seen, though they were sought by shining flashlight and He/Ne laser beams through the flame, in an effort to detect particles by scattered light. It thus appears that

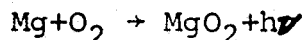
an alternative explanation of the observed continuum emission must be sought.

Continua similar to the one observed in the present work have been observed in other situations and attributed to polyatomic emitters. The air afterglow reaction (Gaydon 1957, Kaufman, 1958, Ottinger and Zare 1970).

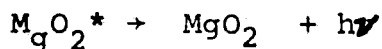
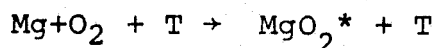


is a well known example. Ottinger and Zare (1970) suggested a polyatomic emitter for the apparent continuum they observed in the $\text{Ca} + \text{NO}_2$ system. Gole and Zare (1972) attribute a broad continuum (4000-8500Å) observed in the $\text{Al} + \text{O}_3$ system to AlO_2^* , and Wren and Menzinger (1973) attribute a continuum in the $\text{Ba} + \text{Cl}_2$ system to BaCl_2^* .

An obvious candidate polyatomic emitter in the Mg/O_2 system is MgO_2 , either in the radiative association process:



or the three-body recombination:



where T is a third body and * denotes electronic excitation. However, these reactions are insufficiently exothermic to account for the 75.2 kcal/mol excitation energy corresponding to the 3800Å short wavelength limit of the Mg/O_2 continuum. They also cannot explain the emission of the same continuum (presum-

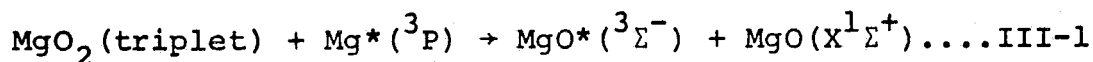
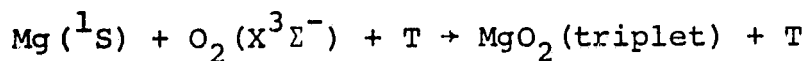
ably by the same emitter) in the $\text{Mg}/\text{N}_2\text{O}$ flame where a simple one-step reaction forming MgO_2 is not possible. One could answer the first of these objections by invoking reaction of O_2 with $\text{Mg}^*(^3\text{P})$, but the second objection would still remain. Two-step mechanisms forming MgO_2 in the $\text{Mg}/\text{N}_2\text{O}$ flame can be constructed, but they are unconvincing and appear ad hoc hypotheses, especially in the absence of any information on the energy levels, spectroscopic properties or even existence (Sullivan, 1969) of MgO_2 . They also do not explain why nearly identical continua are produced by reactions of differing exothermicities.

A more plausible explanation of the continuum observed in the low pressure Mg/O_2 and $\text{Mg}/\text{N}_2\text{O}$ diffusion flames is that it results from a transition between two of the triplet states of the diatomic MgO molecule for which potential curves have been calculated quantum - mechanically by Schamps and Lefebvre-Brion(1972). Their results are shown in Fig. (III-5). They show a weakly bound (or possibly repulsive) $^3\Sigma^-$ state with potential minimum at 30060 cm^{-1} above the ground state ($X^1\Sigma^+$) and a strongly bound $^3\Pi$ state at 2360 cm^{-1} above the ground state. Schamps and Lefebvre-Brion (1972) predict a wavelength of $3600 \pm 100\text{ \AA}$ for the (0,0) band of the $\text{MgO } ^3\Sigma^- \rightarrow ^3\Pi$ transition, which is in very good agreement with the observed continuum short wavelength limit of 3800 \AA . The weak, sharper feature observed at 3860 \AA may be due to a contribution by the more strongly

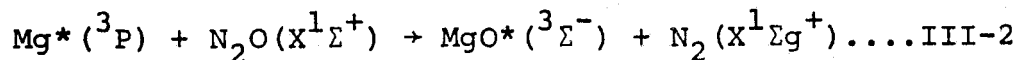
bound $^3\Sigma^+$ or $^3\Delta$ states at 28050 and 28980 cm^{-1} respectively. Schamps and Lefebvre-Brion (1972) predict wavelengths of $3900 \pm 300 \text{\AA}$ and $3750 \pm 100 \text{\AA}$ respectively for the (0,0) bands of the $^3\Sigma^+ \rightarrow ^3\Pi$ and $^3\Delta \rightarrow ^3\Pi$ transitions. They are undecided as to whether the $^3\Sigma^-$ state is weakly bound or repulsive. The observation in the present work of the same, definite, short wavelength limit in both the Mg/O_2 and $\text{Mg}/\text{N}_2\text{O}$ flames (whose energy releases are bound to differ) suggests that the $^3\Sigma^-$ state is weakly bound. Gaydon (1957) has noted this relationship between a definite short wavelength limit and a weakly bound (as opposed to repulsive) upper state.

The mechanism supplying the energy for the excitation of the $^3\Sigma^-$ upper state ($30060 \text{ cm}^{-1} = 85.9 \text{ kcal/mole}$) must now be explained. The reaction $\text{Mg} + \text{O}_2 \rightarrow \text{MgO} + \text{O}$ is endothermic, and $\text{Mg} + \text{N}_2\text{O} \rightarrow \text{MgO} + \text{N}_2$ lacks 35 kcal/mole of the required energy. The reaction of Mg and O_2 to form MgO_2 , followed by $\text{MgO}_2 + \text{Mg} \rightarrow \text{MgO}^* + \text{MgO}$ falls short energetically by over 20 kcal/mole. $\text{Mg}^*(^3\text{P})$ metastable is known to be present in the flames since the $\text{Mg}(^3\text{P}_1 \rightarrow ^1\text{S}_0)$ line is observed. The very low intensity of the continuum emitted by these flames makes a mechanism involving a minor flame constituent seem plausible. Possible mechanisms for the excitation of $\text{MgO}^*(^3\Sigma^-)$ thus appear to be:

Mg/O₂ flame:



Mg/N₂O flame:



Reactions (III-1) and (III-2) obey spin conservation and have 124.7 and 113.1 kcal/mole respectively available for the excitation of $\text{MgO}^*(^3\Sigma^-)$, considerably more than the required 85.9 kcal/mole, even after generous allowances for energy carried off in vibration and translation of various species.

A comparison of the energies evolved in the foregoing reactions with the excitation energies of other known band systems of MgO (which are not observed in the low pressure Mg/O₂ and Mg/N₂O and Mg/N₂O flames) is of interest:

Table V

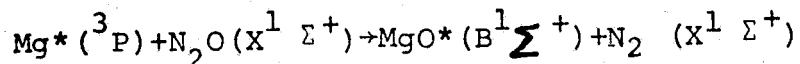
Excitation Energies of MgO Electronically Excited States

<u>State</u>	<u>Excitation Energy, eV.</u>	<u>Excitation Energy, kcal/mol.</u>
C ¹ Σ ⁻	3.74	86.2
D ¹ Δ	3.70	85.3
B ¹ Σ ⁺	2.48	57.2
A ¹ Π	0.45	10.4
X ¹ Σ ⁺	0	0

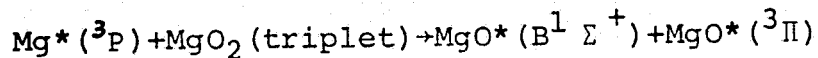
First, it is obvious that any of the exothermic reactions

considered is capable of exciting the $A^1\Pi$ state of MgO. However, the $A^1\Pi \rightarrow X^1\Sigma$ transition would be in the infrared ($\approx 2.8\mu$) and would hence not be observed. The $Mg(^1S) + N_2O$ reaction with an exothermicity of 50.6 kcal/mol cannot excite the MgO "green system" ($B^1\Sigma^+ \rightarrow X^1\Sigma^+$), and the exothermicity of the $2Mg(^1S) + O_2$ reaction sequence (62.2 kcal/mol) is so close to the required excitation energy of $MgO(B^1\Sigma^+)$, that any loss of energy into vibration or translation (or a small error in heats of formation or bond energy values) could result in failure to excite the MgO "green system". None of the reactions involving only ground state $Mg(^1S)$ has anywhere near enough energy to excite the $C^1\Sigma^-$ and $D^1\Delta$ states.

The situation in the reaction schemes involving $Mg^*(^3P)$ is slightly more complicated. Given that the formation of $MgO^*(^3\Sigma^-)$ is favored, there does not remain enough additional exothermicity in either reaction III-1 or III-2 to excite $MgO^*(B^1\Sigma^+)$ (the "green system") as well as $MgO^*(^3\Sigma^-)$. In the Mg/N_2O system, the reaction



is energetically possible, but spin-forbidden. However, the reaction

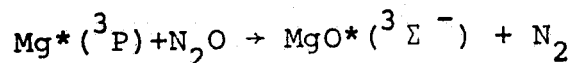


would be both energetically and spin-allowed, as would the corresponding reactions in the Mg/O_2 system. It is difficult,

in the absence of detailed trajectory calculations, using accurately known potential energy surfaces for all the relevant electronic states, to explain why certain energetically and spin-allowed processes occur and others do not. These data simply do not exist for the complex $\text{Mg}^*-\text{N}_2\text{O}$ and MgO_2-Mg^* systems, both involving four atoms. Fig. (III-5) shows the complexity of a cross-section of such a surface, restricted to only two atoms. For the present, the most that can be said is that in the $\text{Mg}/\text{N}_2\text{O}$ and Mg/O_2 systems, the formation of $\text{MgO}^*(^3\Sigma^-)$ seems to be favored, and this does not leave sufficient energy for the excitation of any other observable excited state of MgO .

The mechanisms suggested above to explain the formation of $\text{MgO}^*(^3\Sigma^-)$ and the subsequent continuum emission also explain an additional observed feature of the Mg/O_2 and $\text{Mg}/\text{N}_2\text{O}$ flames. The observed transient increase in brightness and green coloration in the Mg/O_2 flame when chamber pressure is first raised and then suddenly dropped by changing inert gas flow may be explained as follows: The concentration of MgO_2 is likely to be greatest in the outer region of the flame, and that of Mg atoms greatest in the interior. The $\text{MgO}_2 + \text{Mg}^*(^3\text{P}) \rightarrow \text{MgO}^*(^3\Sigma^-) + \text{MgO}(^1\Sigma)$ reaction is thus dependent on diffusion of MgO_2 back into the interior of the flame (or of Mg from the interior to the region of high MgO_2 concentration). When

chamber pressure is raised by raising inert gas flow, the formation rate of MgO_2 (by the three-body reaction $\text{Mg} + \text{O}_2 + \text{T} \rightarrow \text{MgO}_2 + \text{T}$) is increased at the same time that the rate at which Mg and MgO_2 can diffuse together is decreased (since $D \propto \frac{1}{p}$). When the pressure is suddenly dropped, this excess of MgO_2 can react quickly with Mg , causing a burst of luminescence. It is green, since the peak of the continuum emitted is in the green, as is the peak of sensitivity curve of the human eye. The flame is normally of such low intensity that it may be near the boundary between "night" vision (rod cells, no color discrimination) and "day" vision (cone cells, color vision) so any increase in intensity might be sensed as an increase in color as well. If the luminescence in the $\text{Mg}/\text{N}_2\text{O}$ flame is excited by the one-step process



it would not be dependent on the diffusion together of a reaction product and Mg , and such a "green flash" phenomenon would not be expected, and indeed, none is seen.

None of the three hypotheses advanced above, to explain the continuum emission in the low pressure Mg/O_2 and $\text{Mg}/\text{N}_2\text{O}$ flames, is favorable to the possibility of producing laser action in these systems. If the flames are supported by heterogeneous reaction, scattering losses caused by particles and the absence of electronically excited atoms or molecules

would seem to preclude laser action. A polyatomic emitter (e.g. MgO_2) would be unfavorable because of its high density of closely spaced energy levels, as well as possible level broadening by perturbations and predissociation, as noted by Wilson et al. (1973) which "... impedes our ability to retrieve the energy of chemical reaction in the form of laser emission", (Wilson et al. 1973). A transition between a strongly and a weakly bound state of a diatomic emitter might be favorable for laser applications if it were the lower state which were weakly bound, through the possibility of depleting the lower state by dissociation. However, in MgO the reverse situation seems to be found, with the upper state weakly bound or repulsive, making the attainment of high upper state population density difficult.

f. Ca/O_2 and $\text{Ca/N}_2\text{O}$ Flames

One would expect the Ca/O_2 and $\text{Ca/N}_2\text{O}$ flame spectra to be quite similar, since the emitter seems likely to be CaO in both cases. In actuality, the spectra are markedly different, as was found early in the present investigation (Zwillenberg, Naegeli and Glassman 1973). (Figures III-6 and III-7, both 5500-6900Å). The Ca/O_2 spectrum contains a large number of orange bands, somewhat diffuse and most shaded toward the violet, with spacings about 30 cm^{-1} , suggesting a heavy, loosely

bound diatomic or polyatomic emitter (Table VI). An intense head at 6400 Å is also seen (Fig. III-6). The Ca/N₂O spectrum contains an extensive system of sharper, more widely spaced bands, shaded toward the red, with spacings about 200 cm⁻¹, and suggests a more strongly bound diatomic emitter (Table VIII). Neither of these spacings agrees with the vibrational spacing of CaO (~700 cm⁻¹, [Herzberg 1950]), nor do the wavelengths of these bands agree well with tabulated values for CaO, CaOH or "calcium oxide" (Pearse and Gaydon 1963). The bands seen in the Ca/O₂ and Ca/N₂O flames suggest two different emitters, or at least two extremely different states of excitation.

Superimposed over these discrete bands, in both flames, are broad, diffuse bands with maxima at about 6037, 6150 and 6250 Å. The relative intensity of these bands varies with pressure and gas flow rates, indicating non-equilibrium excitation. Only these diffuse bands appear in the Ca/O₂ flame at extremely low O₂ concentration (~200 ppm) in the presence of ~7.5 N₂ (see Fig. III-8). In both Ca/O₂ and Ca/N₂O flames (but more intensely in the latter) the ³P₁ + ¹S₀ 6573 Å "forbidden line of Ca is clearly seen, indicating a sizable population of the metastable ³P₁ state of calcium. The present spectra differ completely from those reported by Zare and co-workers (1970) using a crossed molecular beam technique at pressures 3

TABLE VI

Visible Bands Observed in Ca + O₂ Flame Spectra

$\lambda, \text{\AA}$	Direction of Shading	ν, cm^{-1}	$\Delta\nu, \text{cm}^{-1}$
6462.4	?	15474	31
6449.4	?	15505	28
6438.0	R?	15533	35
6423.3	?	15568	34
6409.4	R?	15602	23
6400.0	V?	15625	7
6397.1	R?	15632	10
6393.2	M	15642	16
6386.6	M	15658	12
6381.5	V	15670	27
6370.6	R	15697	30
6358.4	R	15727	35
6344.5	M?	15762	17
6337.4	M	15779	19
6329.9	M	15798	24
6320.3	R	15822	23
6311.1	M	15845	27
6300.6	V	15872	55
6278.6	V	15927	68
6251.8	V	15995	297
6137.9	M, diffuse	16292	16
6132.0	V, diffuse	16308	31
6120.2	V, diffuse	16339	198
6046.9	M, broad, diffuse	16537	1144
5655.8	V	17681	201
5592.4	M, broad, diffuse	17882	

TABLE VII

Visible Bands Observed in Ca + N₂O Flame Spectra

$\lambda, \text{\AA}$	<u>Direction of Shading</u>	ν, cm^{-1}	$\Delta\nu, \text{cm}^{-1}$
6774.0	R	14762	236
6667.6	R	14998	248
6558.9	R	15246	222
6465.1	R	15468	252
6361.2	R	15720	176
6290.9	V?	15896	50
6271.2	V?	15946	25
6261.5	V?	15971	34
6247.9	R?	16005	59
6225.2	V?	16064	68
6198.7	R	16132	262
6099.8	R	16394	266
6002.3	R?	16660	172
5941.1	R?	16832	180
5878.4	R?	17012	294
5778.3	R	17306	135
5733.5	R	17441	569
5552.5	R?	18010	

} 236

*R = shaded to red
 V = " " " violet
 M = maximum
 L = line

TABLE VIII

Bands observed in Photoelectric scans of
Ca/O₂ and Ca/N₂O flames (wavelengths approximate),
and assignments, 400μ slits (~6Å resolution)

λ observed, A, Ca/O ₂	Direction of shading *	λ observed, A Ca/N ₂ O	Direction of shading *	Assignment: emitter system (v',v'')			wavelength of assigned feature Å
8652	R? weak	8647	R	CaO	A→X	(0,0), (4,4)	8652
		8429	L	Ca	resonance	2nd order	4226.7
8153	R	8162	R	CaO	A→X	$\Delta v = -1$ seq.	8167
8144	R	8150	R	CaO	A→X	(6,5)	8155
		7816	R	CaO	Field	(8,0)	7819
7707	R	7719	R	CaO	A→X	$\Delta v = -2$ seq.	7712
		7659	L?	K	resonance	—	7665
		7518	R	CaO	Field	(9,0)	7520.5
band obscured by electrical noise		7331	R	CaO	A→X	$\Delta v = -3$ seq.	7336
		7250	R	CaO	Field	(10,0)	7249.5
		7119	R?	CaO	Field	(12,1)	7117.5
		6997	R	CaO	Field	(11,0)	7001.0
6972	R, weak	6978	R	CaO	A-X	$\Delta v = -4$ seq.	6986
		6884	R	CaO	Field	(13,1)	6885.0
		6773	R	CaO	Field	(12,0)	6772.0
		6669	R	CaO	A→X	$\Delta v = -5$ seq.	6678 Also *Field 14,1) 6671
		6565	L	Ca	3p ₁ -1s ₀	-	6572.8
		6460	R	CaO	Field	(15,1)	6464.7
6360	V	6358	M, overlapped.	CaO	A→X	$\Delta v = -6$ seq.	6338
6238	V	6240	V, " "	Calcium oxide (Pearse & Gaydon)			6258.5, CaOH (Gaydon) 6230
6122	M	—	unresolved continuum	"	"	" "	6097
6028	M	6065	V	"	"	" "	6041; CaOH (Gaydon) 6038
600-5660	diffuse	—	—	"	"	" "	

Note: Field = A'¹Π-X¹Σ⁺ system reported by
 Field et. al. (1974).

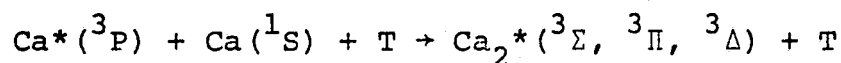
*Field = extrapolated from Deslandres table
 (Field, Capelle and Jones, 1974).

to 5 orders of magnitude smaller than in the present study. They reported a broad, unresolved continuum for the $\text{Ca}+\text{N}_2\text{O}$ reaction. (No results were reported for $\text{Ca}+\text{O}_2$). The difference in our results is probably attributable to sequential reactions, third body reactions or excitation transfer at higher pressures, which do not occur under molecular beam "single-collision" conditions.

Electronically excited CaO is definitely present in both flames, as the $(0,0)$, $(1,0)$, $(2,0)$, $(3,0)$ and $(4,0)$ sequences of the $\text{CaO } A^1\Sigma \rightarrow X^1\Sigma$ transition (at 8660, 8170, 7730, 7340 and 7010 Å respectively) are detected on photoelectric scans, (Fig. III-9, Table VIII). These bands as well as the $\text{Ca } ^3P_1 \rightarrow ^1S_0$ line are stronger in the $\text{Ca}/\text{N}_2\text{O}$ flame than in the Ca/O_2 flame, possibly due to the more labile O atom in N_2O (as compared with O_2). In the $\text{Ca}/\text{N}_2\text{O}$ flame, in addition to the $\text{Ca } ^3P_1 \rightarrow ^1S_0$ "forbidden" line, a number of other Ca lines were seen (Fig. III-13). All of them, except the resonance (4226.7Å) and "forbidden" (6572.8Å) lines were extremely weak. A continuum was also seen, extending from 3500Å and apparently merging into the discrete band spectra at about 5500Å , with a maximum at about 4500Å .

The band spacings of 200 cm^{-1} and 30 cm^{-1} noted above in the $\text{Ca}/\text{N}_2\text{O}$ and Ca/O_2 flames are interesting in light of

the similar vibrational spacings (ω_e) reported by Balfour and Douglas (1970) of 190.6 and 51.1 cm^{-1} respectively for the $A^1\Sigma$ and $X^1\Sigma$ states of magnesium dimer, Mg_2 . This suggested that the observed CaO_2 flame bands might involve an electronically excited calcium dimer, Ca_2 with $\omega_e \approx 200 \text{ cm}^{-1}$ and a ground state with $\omega_e \approx 30 \text{ cm}^{-1}$. This might be formed by a mechanism involving the metastable $\text{Ca}^*(^3\text{P})$ known to be present from observation of the $\text{Ca}(^3\text{P}_1 + ^1\text{S}_0)$ 6573Å line:



If this interpretation were correct, the greater stability of the excited state would result in preferential depletion of the ground state by dissociation, thus facilitating achievement of an inverted population. The literature regarding Ca_2 and the complex green and orange bands emitted in arcs, flames and furnaces containing Ca and O_2 have been reviewed in detail by Zwillenberg, Naegeli and Glassman (1973) and Zwillenberg (1975).

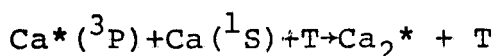
A brief attempt was made to detect the presence of Ca_2 by laser excited fluorescence of the upper state producing the orange bands, using the 6328Å line of a He-Ne laser for excitation. The laser beam was directed axially along the calcium vapor jet (with no oxidizer flow), and

spectrographic observations made in a perpendicular direction. No fluorescence was observed, only 6328⁰Å light scattered from the chamber walls (and present even in the absence of flow). This negative result may be due to low intensity of the exciting laser (~1 mw), low Ca₂ concentration, short optical path length, or to non-existence of ground state Ca₂. (Ca₂ might be formed in the flame in an excited state more stable than the ground state, and dissociate after radiating.)

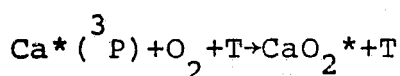
Another molecular species which was considered as a possible emitter for the bands observed in the Ca/O₂ flame was CaO₂. Obenauf, Hsu and Palmer (1972) have proposed BaO₂ as an intermediate in the production of excited BaO in the Ba/O₂ flame. Carabetta and Kaskan (1968) have shown that superoxides such as NaO₂ and KO₂ form readily in alkali-seeded H₂/O₂ flames. Thus, the formation of CaO₂ does not seem unreasonable. In addition, the Ca/O₂ spectrum in its diffuseness and apparent lack of definite sequences or simple progressions resembles the spectrum of a polyatomic rather than a diatomic emitter. The spectrum of Ca₂ might be expected to resemble in some ways that of CaCl (which has nearly the same reduced mass, and exhibits distinct sequences), except that the vibrational and rotational structure in Ca₂ would be compressed due to the weaker bonding (smaller force constant and larger interatomic distance, hence smaller vibrational and rotational constants). The direct reaction $\text{Ca} + \text{O}_2 + \text{T} \rightarrow \text{CaO}_2 + \text{T}$ is insufficiently exothermic to explain the excitation of bands extending to 6000⁰Å.

However, the energy might be supplied by substituting $\text{Ca}^*(^3\text{P})$ for $\text{Ca}(^1\text{S})$. Detailed consideration (Zwillenberg, 1975) of the potential curves for CaO presented by Field (1974) and possible potential surfaces in the triatomic Ca-O-O system suggests the possibility of an excited state of CaO_2 which would radiate in the region of the spectrum in which the Ca/O_2 flame bands are seen.

Further investigation has indicated, however, that the orange bands observed in the low pressure, chemiluminescent, calcium vapor flames studied are not emitted by Ca_2 or CaO_2 . Firstly, in the $\text{Ca/CCl}_4/\text{O}_2$ flames (discussed in a later section of this thesis), much higher concentrations of $\text{Ca}^*(^3\text{P})$ exist than do in either the Ca/O_2 or $\text{Ca/N}_2\text{O}$ flames (as indicated by the intensity of the $\text{Ca}^3\text{P}_1 \rightarrow ^1\text{S}_0$ line). If Ca_2^* or CaO_2^* were produced by the reactions:



or



one would expect the orange band system to be strongly excited in the $\text{Ca/CCl}_4/\text{O}_2$ flame. Instead, it is completely missing. Secondly, it has been found possible to account very well for the wavelengths of nearly all the observed bands in terms of transitions between high vibrational levels (not previously observed) of the $\text{CaO } A^1\Sigma^+$ and $X^1\Sigma^+$ states (in the Ca/O_2 and $\text{Ca/N}_2\text{O}$ flames) and the new $\text{CaO}(A'^1\Pi \rightarrow X^1\Sigma^+)$ transition ($\text{Ca/N}_2\text{O}$ flame) predicted recently by Field (1974), and

observed by Field, Capelle and Jones (1974).

The procedure for arranging the wavenumbers ($\nu=1/\lambda$) of molecular electronic band origins or bandheads in a Deslandres table has been described in detail by Herzberg (1967) and by Walker and Straw (1962). The differences, $\Delta G''(\nu+1/2)$, are approximately constant down each column, and represent the vibrational energy spacings in the lower electronic state, while the differences, $\Delta G'(\nu+1/2)$ are approximately constant across each row, and represent the vibrational energy spacings in the upper electronic state. (This constancy is more exact when band origins rather than bandheads are tabulated. However, when the rotational structure is incompletely resolved, only band head data may be available.) It may be seen that if $\Delta G'(\nu+1/2)$ and $\Delta G''(\nu+1/2)$ are known for every ν' up to some ν'_{\max} and every ν'' up to some ν''_{\max} , any missing values in the Deslandres table (in the region bounded by ν'_{\max} and ν''_{\max}) can be filled in, using the above-mentioned approximate constancy of $\Delta G'(\nu+1/2)$ across the rows and of $\Delta G''(\nu+1/2)$ down the columns of the table.

Missing entries in the Deslandres table for $\nu' > \nu'_{\max}$ and $\nu'' > \nu''_{\max}$ can also be estimated, as will now be shown, and in this manner, the wavenumbers of hitherto unobserved transitions between high vibrational states can be predicted. Following Herzberg (1950), the vibrational energy of a given level, ν , may be written as:

$$G(\nu) = \omega_e(\nu+1/2) - \omega_e x_e(\nu+1/2)^2 + \omega_e y_e(\nu+1/2)^3 + \dots$$

where ω_e , $\omega_e x_e$ and $\omega_e y_e$ are the first, second and third order vibrational constants of the molecule. (ω_e is the vibrational frequency in the simple harmonic case). Noting that:

$$\Delta G''(v+1/2) \equiv G(v''+1) - G(v'')$$

$$\Delta G'(v+1/2) \equiv G(v'+1) - G(v')$$

then

$$\Delta G''(v+1/2) = \omega_e'' - 2\omega_e'' x_e''(v'+1/2) + 3\omega_e'' y_e''(v'+1/2)^2 + \dots$$

$$\Delta G'(v+1/2) = \omega_e' - 2\omega_e' x_e'(v'+1/2) + 3\omega_e' y_e'(v'+1/2)^2 + \dots$$

where double and single primes refer to the lower and upper states, respectively. If, as is often the case (Herzberg 1950, Walker and Straw 1962), the higher order terms may be neglected, the graphs of $\Delta G''(v+1/2)$ vs. v'' and $\Delta G'(v+1/2)$ vs. v' become straight lines, and may then be extrapolated to higher values of v'' and v' , allowing the estimation of the wave-numbers of high $v'-v''$ transitions. Such a plot is shown for the $A^1\Sigma^+ \rightarrow X^1\Sigma^+$ transition of CaO, in Fig. (III-11). The points are experimental, from the data of Pearse and Gaydon (1963) and Hauge (1966). The figure is extended only to v', v'' of 20, but higher values are easily calculable, using the slopes of the lines. It should be noted that deviations from linearity in these ΔG plots will be less than in the similar Birge-Sponer extrapolation for determination of dissociation energies (Gaydon 1968), as in the present procedure the extrapolation is not extended to the vicinity of the dissociation limit, but is stopped at far lower energies.

Brewer and Hauge (1968) have reported an approximate value of 0.044 cm^{-1} for the third order vibrational constant, $\omega_e y_e$, of the $X^1\Sigma^+$ ground state of CaO. If correct, this would produce large deviations from linearity in the extrapolation described above. Brewer and Hauge (1968) themselves note that their value of $\omega_e y_e$ seems quite large and is subject to some uncertainty, as it depends critically upon extrapolated values of the rotational constant B_v . An examination of their plot of $\Delta G''(v+1/2)$ vs. v'' shows that a much better straight line can be drawn through their experimental points, requiring a much smaller value of $\omega_e y_e$ to account for deviations. Indeed, the excellent agreement of the wavenumbers calculated in the present extrapolation procedure (see below) with the experimentally observed bands, argues strongly that the true value of $\omega_e y_e$ is much smaller than that given by Brewer and Hauge (1968).

Tables IX and X list the wavelengths and wavenumbers of the bands observed in the Ca/N₂O and Ca/O₂ flames, the vibrational assignment and the wavenumbers of the assigned bands calculated by the extrapolation procedure described above. Vibrational assignments are listed in Table VIII for bands and sequences observed photoelectrically. Where more than one band falls within several cm^{-1} of an observed band, the various possibilities are listed. In the few cases where the difference between observed and calculated wavenumber is more than 5 cm^{-1} , the assignment is considered dubious, as indicated by "?" in the

table. The few bands in each table for which no assignment is given may represent cases where an accidental confluence of rotational lines was mistaken for a band head.

In the Ca/O_2 flame, bands belonging to the $\Delta v=0, -2, -5, -6$, and -7 sequences of the $\text{CaO } A^1\Sigma \rightarrow X^1\Sigma^+$ transition were seen, with many of them exhibiting extremely high vibrational excitation (up to $v = 30$). The sequence head of the $\Delta v=1$ and -4 sequences were also observed photoelectrically, but individual bands were not resolved. In the $\text{Ca/N}_2\text{O}$ flame, the $\Delta v=0$ through -6 sequences of the A-X transition were seen, along with members of the $v''=0, 1$ and 2 progressions of the $A'^1\Pi \rightarrow X^1\Sigma^+$ transition reported by Field, Capelle and Jones (1974), with vibrational excitation up to $v'=19$. Of interest is the fact that most of the $A^1\Sigma \rightarrow X^1\Sigma^+$ bands seen in the two flames are different due to differing degrees of vibrational excitation. There are only a few bands which are common to both flames. It is difficult to be certain of the highest vibrational level of $A^1\Sigma^+$ excited in the $\text{Ca/N}_2\text{O}$ flame because in a number of cases two or more bands have nearly the same wavenumber, and a number of bands of the $\Delta v=-6$ sequence with high v' show large ($\approx 10 \text{ cm}^{-1}$) discrepancies between experimental and calculated wavenumbers. It appears that the highest value of v'_{max} which can be confidently assigned lies between $v' = 15$ and 20 .

TABLE IX

Wavelengths, Wavenumbers and Vibrational Assignments of
Bands Observed in Low Pressure Ca/N₂O Flames

Note: A-X=CaO(A¹Σ⁺-X¹Σ⁺) Field=CaO(A¹Π-X¹Σ⁺) system reported by Field
λ and ν in air. et.al.(1974).
*Field=From extrapolation of Field's Deslandres
Table.

λ _{obs.} Å	ν _{obs.} = $\frac{1}{\lambda_{obs.}}$ cm ⁻¹	sequence	ASSIGNMENT		(v', v'')
			ν, cm ⁻¹	Transition	
552.5	18010		18013	Field*	(19,0)
733.6	17441				
778.3	17306		17294	Field	(19,1)?
878.2	17012		17026	" "	(20,2)?
941.1	16832		16845	" "	(18,1)?
1002.4	16660		16658	" "	(16,0)
1099.8	16394		16393	" "	(17,1)
1198.8	16132		16132	" "	(18,2)
1225.1	16064	Δv = -6	16051	A-X	(29,23)?
1248.0	16005		15992	A-X	(28,22)?
1261.3	15971				
1271.2	15946		15937	A-X	(27,21)?
1290.9	15896		15886	A-X	(26,20)?
1331.5	15794	Δv = -5	15796	A-X	(24,18)
1361.3	15720		15722	A-X	(22,16)
1365.8	15466		15720	Field	(14,0)
1359.1	15246		15469	"	(15,1)
1411.4	15057		15247	"	(13,0)
1452.5	15032		15054	A-X	(6,1)
1461.8	15011		15033	A-X	(7,2)
1457.6	14998		15009	A-X	(8,3)
1473.3	14985		15008	A-X	(17,12)
			14991	Field	(14,1)
			14994	A-X	(16,11)
			14982		(11,6)
			14983	A-X	(15,10)
1471.4	14765		14766	Field	(12,0)
1466.9	14648				
1460.4	14619				

ORIGINAL PAGE IS
OF QUALITY

TABLE IX (continued)

Ca/N₂O Flames

$\lambda_{\text{obs.}}$ Å	$\nu_{\text{obs.}} = \frac{1}{\lambda_{\text{obs.}}}$ cm ⁻¹	ASSIGNMENT			
		sequence	ν , cm ⁻¹	Transition	(ν' , ν'')
6852.1	14594				
6971.6	14344				
6977.4	14332	$\Delta\nu = -4$	14342	A-X	(6,2)
6979.3	14328		14330	A-X	(7,3)
6982.3	14322		14327	A-X	(13,9)
6985.2	14316		14320	A-X	(12,8)
			14316	A-X	(10,6) [Also: 14317 (11,7) 14315 (9,5) 14318 (8,4)]
6988.1	14310				
7001.8	14282		14284	Field	(11,0)
7010.6	14264				
7248.5	13796		13796	A-X	(17,14)
			13794	Field	(10,0)
7307.8	13684	$\Delta\nu = -3$	13684	A-X	(3,0)
7318.0	13665		13664	A-X	(4,1)
7324.9	13652		13650	A-X	(5,2)
			13651		
7328.7	13645				
7329.8	13643	$\Delta\nu = -2$	13641	A-X	(9,6)
7331.9	13639		13639	A-X	(6,3)
7333.5	13636		13635	A-X	(7,4)
7340.0	13629		13631	A-X	(8,5)
7342.1	13620				
7348.6	13608				
7354.6	13597				
7519.9	13298		13297	Field	(9,0)
7622.5	13119	$\Delta\nu = -2$	13122	A-X	(15,13)
7687.6	13008		13013	A-X	(11,9)
7691.1	13002		12995	A-X	(10,8)?
7711.9	12967		12966	A-X	(2,0)
7716.0	12960		12961		(3,1)
			12957	A-X	(8,6)
7741.1	12918				
7793.6	12831				

-132-
TABLE IX (continued)

Ca/N₂O Flames

$\lambda_{\text{obs.}}$ Å	$\nu_{\text{obs.}} = \frac{1}{\lambda_{\text{obs.}}}$ cm ⁻¹	ASSIGNMENT			
		sequence	ν, cm^{-1}	Transition	(ν', ν'')
7811.9	12801	$\Delta\nu = -1$ {	12802	A-X	(20,19)
7825.3	12779				
7852.4	12735	$\Delta\nu = 0$ {	12738	A-X	(19,18)
8652.0	11558		11554	A-X	(4,4)
			11558		(0,0)
8661.8	11545		11546	A-X	(3,3)
			11542		(1,1)
8669.3	11535		11531	A-X	(2,2)

TABLE X

Wavelengths, Wavenumbers and Vibrational Assignments of
Bands Observed in Low Pressure Ca/O₂ Flames

NOTE: A-X=CaO(A¹Σ⁺→X¹Σ⁺)

*=also observed in Ca/N₂O Flame

λ and ν in air

ASSIGNMENT

$\lambda_{\text{obs.}}$ Å	$\nu_{\text{obs.}} = \frac{1}{\lambda_{\text{obs.}}}$ cm ⁻¹	sequence	ν , cm ⁻¹	Transition	(v', v'')
5592.2	17882				
5655	17681				
6047.0	16537				
6120.3	16339	Δv=-7	16339	A-X	(11,4)
6132.0	16308		16314	A-X	(12,5)
6138.0	16292		16295	A-X	(13,6)
6252.0	15995	*	15992	A-X	(28,22) or "calcium oxide" (Pearse&Gaydon 1963)
6278.6	15927		15937	A-X	(27,21)? " " "
6300.4	15872		15886	A-X	(26,20)?
6311.1	15845		15839	A-X	(25,19)
6320.3	15822				"calcium oxide"
6329.9	15798	Δv=-6	15796	A-X	(24,18)
6337.5	15779		15777	A-X	(6,0)
6344.4	15762		15757	A-X	(23,17) or "calcium oxide"
6358.5	15727		15722	A-X	(22,16) " " "
6370.6	15697		15693	A-X	(9,3)
			15691		(21,15)
6381.6	15670		15673	A-X	(10,4)
			15669		(20,14)
6386.5	15658		15656	A-X	(11,5)
			15651		(19,13)

TABLE X (continued)

$\lambda_{\text{obs.}}$ Å	$\nu_{\text{obs.}} = \frac{1}{\lambda_{\text{obs.}}}$ cm ⁻¹	ASSIGNMENT			
		sequence	ν , cm ⁻¹	Transition	(ν' , ν'')
6393.0	15642	{	15640	A-X	(12,6)
			15638		(17,11)
6400.0	15625		15623	A-X	(14,8)
			15622		(16,10)
			15620		(15,9)
6409.4	15602				
6423.4	15568	{	15567	A-X	(30,25)
6437.9	15533				
6449.5	15505		15500	A-X	(29,24)
6462.0	15475				
7697.0	12992	*	12995	A-X	(10,8)
7712.5	12966	*	12966	A-X	(2,0)
7715.5	12961	*	12961		(3,1)
			12957		(8,6)
7741.7	12917	*			
8655.0	11554	*	11554	A-X	(4,4)
			11558		(0,0)

Fig. III-12 shows the A-X ($v'-v''$) sequences seen in the two flames. In cases where a given observed band could be given two assignments, both are shown, but the band of higher v' is indicated by a "?".

The complexity of the observed CaO $A^1\Sigma^+ \rightarrow X^1\Sigma^+$ bands may be explained by the closeness in value of the vibrational spacings $\Delta G'(v+1/2)$ and $\Delta G''(v+1/2)$ in the upper and lower electronic states, with a crossing of the $\Delta G'$ and $\Delta G''$ curves (Fig. III-11) at about $v=1$. This leads to the formation of sequence heads (what Herzberg [1950] calls a head of heads) in which entire band heads form a pattern similar to that of rotational lines in an ordinary band head. This is shown schematically for the $\Delta v=0$ through $\Delta v=-8$ sequences of the CaO A-X transition, in Fig. (III-13). All these sequence heads are not actually seen, as only in some sequences are the v' states in the vicinity of the turning point (sequence head) excited. Note that the piling up of numerous bandheads, each with its own rotational structure, in an interval of several cm^{-1} can easily produce the appearance of diffuse bands, broad "lines", etc. which were thought to indicate a polyatomic emitter in the Ca/O₂ flame. In the Ca/N₂O flame, the strong, clearly diatomic $A'^1\Pi \rightarrow X^1\Sigma^+$ bands were dominant.

This explanation of the bands observed in the Ca/O₂ flame spectrum and some of the bands observed in the Ca/N₂O flame

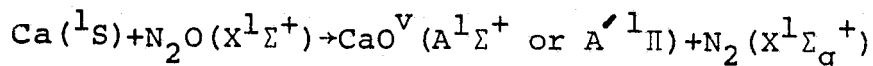
spectrum in terms of transitions between high vibrational levels of the $\text{CaO } A^1\Sigma^+$ and $X^1\Sigma^+$ states explains many features of the observed spectra. As noted above, the wavelengths (and wavenumbers) calculated under this hypothesis are in excellent agreement with the observed values. The apparent diffuseness of the bands is explained by the close spacing of unresolved band heads near the turning point of a sequence, as explained above. The sharp head observed at 6400\AA in the Ca/O_2 flame spectrum coincides in wavelength with the turning point of the $\Delta v = -6$ sequence (Fig. III-13) and thus is the head of that sequence. The disappearance of the discrete Ca/O_2 bands in the presence of N_2 can be explained by vibrational relaxation of the highly vibrationally excited $\text{CaO}(A^1\Sigma^+)$ molecules to low v' levels. The bands disappear because the low v' bands of the A-X transition are in the infrared, and the spectral region observed in the N_2 experiment extended only from $5700\text{--}6900\text{\AA}$. The remaining diffuse bands (with maxima near 6037 and 6250\AA) may be due to CaOH or a polyatomic emitter. Pearse and Gaydon (1963) describe diffuse bands with maxima near 6038 and 6230\AA , which they attribute to CaOH .

Many of the bands attributed here to high vibrational levels of $\text{CaO}(A^1\Sigma^+)$ are shaded to the violet, while most reported $\text{CaO}(A^1\Sigma^+ \rightarrow X^1\Sigma^+)$ bands are shaded to the red (Pearse and Gaydon 1963). This is consistent with the reversal of shading to be expected

in tail bands (bands from vibrational states past the turning point of a sequence)- as described by Herzberg (1967).

The conclusion of Lagerqvist and Huldt (1954) that the lower state of the orange band system lies about 2.eV. above the ground state is explicable in terms of high vibrational excitation of the lower $X^1\Sigma^+$ state of CaO. Consider, for example, the (30, 24) band of the CaO A-X transition. The average vibrational spacing of the lower electronic state over the range $0 \leq v \leq 24$ is 615 cm^{-1} , and the vibrational energy of the $v = 24$ level is thus $615 \times 24 = 15,375 \text{ cm}^{-1} = 1.91 \text{ eV.}$, in very good agreement with the 2.0 eV. excitation noted by Lagerqvist and Huldt (1954).

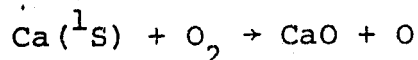
It now remains to demonstrate that there exist plausible mechanisms in the Ca/N₂O and Ca/O₂ flames to supply the excitation energies required by the band assignments given above (see Tables XI and XII). In the case of the Ca/N₂O flame, an obvious choice is:



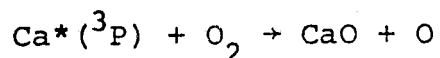
which also obeys spin conservation. Using Gaydon's (1968) value of $100 \text{ kcal/mol} \pm 0.7 \text{ eV.}$ (16.1 kcal/mole) for the bond dissociation energy of CaO, the energy available for excitation is calculated to be $61.3 \pm 16.1 \text{ kcal/mole}$. This is in excellent agreement with the values shown in Table XII for the observed bands (62.0 and 70.9 kcal/mol for the $A^1\Sigma^+ \rightarrow X^1\Sigma^+$ system depending on whether v'_{max} is taken as 15 or 20; 51.4 kcal/mole for the

$A^1\Pi \rightarrow X^1\Sigma^+$ system with $v'_{\max} = 19$).

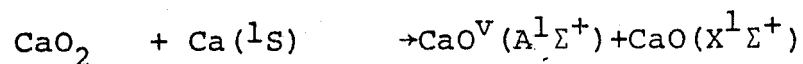
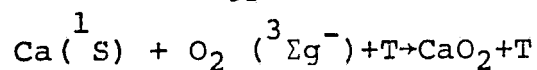
In the case of the Ca/O₂ flame, the situation is slightly more complicated. The obvious candidate:



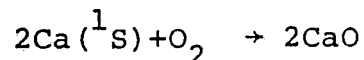
is eliminated, as it is endothermic. Even



is only 24.3 kcal/mol exothermic and cannot provide the required excitation energy. However, the sequence of reactions:



is thermochemically equivalent to:



and has 80.9 ± 32.3 kcal/mol available for excitation. (Since two CaO molecules are formed, the calculated energy release is uncertain by twice the uncertainty in the Ca-O bond energy.) This is in very good agreement with 87.7 kcal/mol required by the assigned $v'_{\max} = 30$ (see Table XII).

Table XI

Calculation of Vibrational Energy

<u>State</u>	<u>v' max</u>	<u>Average vibrational spacing, cm⁻¹*</u>	<u>Evib, vibrational energy, cm⁻¹**</u>	<u>Evib, vibrational energy, kcal/mole</u>
A ¹ Σ ⁺	15	676	10140	29.0
"	20	663	13260	37.9
"	30	638	19140	54.7
A ¹ Π	19	496	9424	26.9

$$* = \frac{1}{2} [\Delta G' (1/2) + \Delta G' (v'_{\max} - 1 + 1/2)]$$

$$** = \frac{v'_{\max}}{2} [\Delta G' (1/2) + \Delta G' (v'_{\max} - 1 + 1/2)]$$

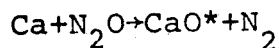
TABLE XII

Available Exothermicity and Required Excitation
Energy of Observed Band Systems of CaO

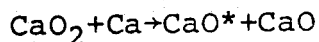
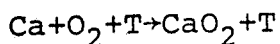
<u>Band System</u>	<u>v'_{\max}</u>	<u>v_{∞} kcal/mole</u>	<u>Evib, kcal/mole</u>	<u>Total Excitation Energy Evib+v_{∞}, kcal/mole</u>	<u>Available from Ca+N₂O**</u>	<u>Available from 2Ca+O₂**</u>
A $^1\Sigma^+ \rightarrow X^1\Sigma^+$	15	33.0	29.0	62.0	61.3 \pm 16.1	—
" "	20	33.0	37.9	70.9	61.3 \pm 16.1	—
" "	30	33.0	54.7	87.7	—	80.9 \pm 32.3
A $^1\Pi \rightarrow X^1\Sigma^+$	19	24.5	26.9	51.4	61.3 \pm 16.1	—

Notes:

*The full reactions are:



and



The uncertainties are due to use of Gaydon's (1968) value of 4.3 \pm 0.7 eV for the bond energy of CaO. Since two CaO molecules are formed in the Ca+O reaction sequence, this uncertainty is doubled.

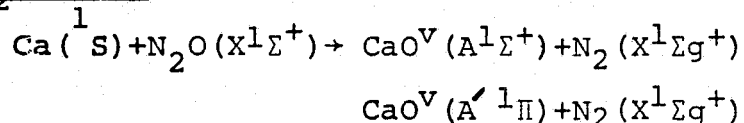
ORIGINAL PAGE IS
OF POOR QUALITY

It should be noted that in the $\text{Ca}(^1\text{S}) + \text{O}_2(^3\Sigma_g^-) + \text{T}$ reaction, spin conservation would require that CaO_2 be formed in a triplet state, and the reaction of $\text{CaO}_2 + \text{Ca}(^1\text{S})$ to form all singlet products would then be spin-forbidden. (Assuming that the third body T is an inert gas atom which remains in its singlet ground state). However, the relatively high atomic weight of Ca makes deviations from Russell-Saunders coupling likely, with consequent deviations from strict spin conservation. Obenauf, Hsu and Palmer (1972) use exactly the same mechanism as proposed above to explain the production of excited $\text{BaO}(^1\Sigma^+)$ in the $\text{Ba} + \text{O}_2$ system, without being troubled by the violation of spin conservation. Also, the possibility exists that the third body, T, might be another O_2 molecule, and the reaction:

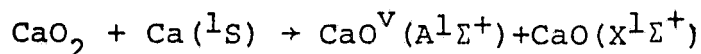
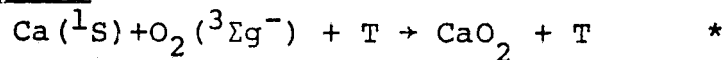
$\text{Ca}(^1\text{S}) + \text{O}_2(^3\Sigma_g^-) + \text{O}_2(^3\Sigma_g^-) \rightarrow \text{CaO}_2(\text{singlet}) + \text{O}_2(^3\Sigma_g^-)$
is clearly spin allowed. The subsequent $\text{CaO}_2(\text{singlet}) + \text{Ca}(^1\text{S})$ reaction could then clearly produce all singlet products.

It thus appears that from the spectroscopic, energetic and spin conservation standpoints, the observed $\text{Ca}/\text{N}_2\text{O}$ and Ca/O_2 spectra can be explained by:

$\text{Ca}/\text{N}_2\text{O}$ flame:



Ca/O₂ Flame:



(*spin-allowed only if $\text{T}=\text{O}_2(^3\Sigma\text{g}^-)$ or another triplet)

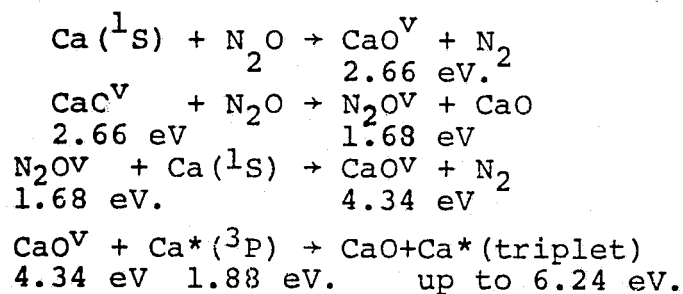
The blue ($\text{B}^1\Pi \rightarrow \text{X}^1\Sigma^+$) and ultraviolet ($\text{C}^1\Sigma^+ \rightarrow \text{X}^1\Sigma^+$) systems of CaO were not seen in the Ca/O₂ and Ca/N₂O flames. These systems have excitation energies (for zero vibrational excitation) of 3.22 eV. (74.2 kcal/mole) and 3.57 eV. (74.2 kcal/mole) and 3.57 eV. (82.3 kcal/mole respectively). Polanyi (1965) has noted that when a chemical reaction releases its exothermicity primarily during the formation of a new bond (on an attractive portion of the potential surface), a large portion of the exothermicity will be taken up in vibrational excitation of the new bond. This seems likely to be the case in the formation of the Ca-O bond, because of its ionic character and the electron-jump mechanism discussed earlier. Only a small amount of exothermicity need be taken up in vibration to make the excitation of the B-X and C-X band systems energetically impossible. (In the case of the Ca/N₂O flame, the excitation of the C-X system is already energetically impossible for $v'=0$, and only two or three quanta of vibrational excitation would suffice to make the excitation of the B-X transition energetically impossible).

The only spectral features remaining to be explained are the ultraviolet-blue continuum and the weak atomic lines (Fig. III-10) observed in the $\text{Ca}/\text{N}_2\text{O}$ flame. As for the first, the identification of a featureless continuum is always difficult, but a transition from a weakly bound or repulsive upper state (similar to that calculated by Schamps and Lefebvre-Brion (1972) in the case of MgO) seems a definite possibility. It should be noted that Field (1974) calculated only the very lowest states of CaO , with potential curve minima up to about $12,000 \text{ cm}^{-1}$, and hence did not exclude the existence of unidentified states higher than this. The lack of a sharp short wavelength cutoff in this continuum suggests that the upper state may be repulsive rather than weakly bound. The short wavelength limit, ($\sim 3500\text{\AA}$), requires an excitation energy of 81.7 kcal/mole , more than can be supplied by $\text{Ca}(^1\text{S}) + \text{N}_2\text{O} \rightarrow \text{CaO} + \text{N}_2$, but reaction of N_2O with $\text{Ca}^*(^3\text{P})$ can easily supply the required energy.

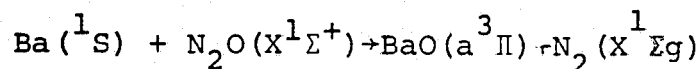
It would seem that the excitation of the observed atomic lines, requiring energies up to 5.7 eV . (131.4 kcal/mol) would present more of a problem from the energetic standpoint, since the $\text{Ca}(^1\text{S}) + \text{N}_2\text{O}$ reaction releases only 2.66 eV . However the extreme weakness of these lines makes reaction sequences of relatively low probability acceptable as explanations. Possible mechanisms include vibrational energy transfer from CaO to N_2O (producing "hot" N_2O which then reacts with Ca) and processes involving

Ca*(³P) and the CaO*(a³Π) state calculated by Field (1974). In the following discussion, the maximum vibrational energy of N₂O^V will be assumed limited by the N₂-O dissociation energy (38.7 kcal/mol=1.88 eV) and that of CaO by the Ca-O bond dissociation energy (100 kcal/mol=4.34 eV). The sum of the vibrational and electronic excitation energies of CaO(a³Π) is also limited to 4.34 eV, as it dissociates to ground state Ca and O (Field 1974). In the following equations, the vibrational or electronic energy of each species (relative to the ground state) will be indicated below its symbol. Three possible mechanisms for the excitation of the observed atomic lines are thus:

(1)



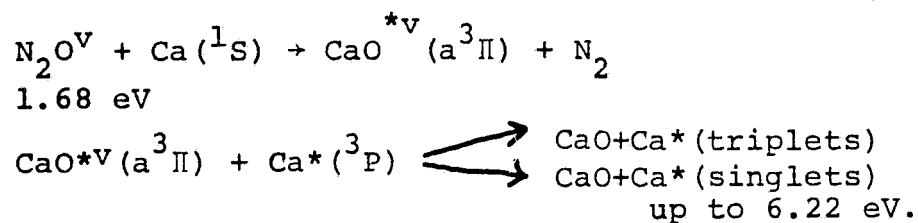
In the above reactions, CaO and N₂O are singlets, and spin is conserved. Field, Jones and Broida (1974) have proposed the reaction:



in the Ba/N₂O system, justifying it on the basis of a mixture of the (a³Π) and (A¹Π) states, giving both states both singlet and triplet character. If such a mechanism is admissible in

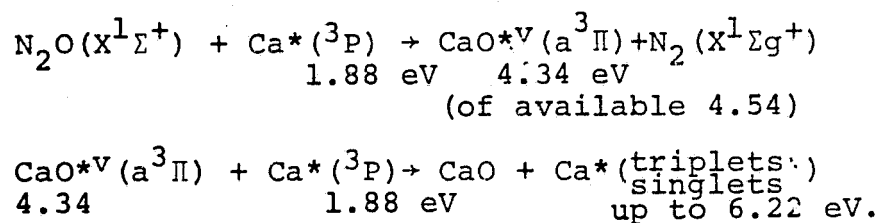
the analogous Ca/N₂O reaction, then the following sequence might be considered:

(2)



Another possibility, which strictly obeys spin conservation is:

(3)



There thus appears to be no shortage of possible mechanisms to account for the very weak excitation of atomic lines of high excitation energy in the Ca/N₂O flame.

g. Mg/CCl₄/O₂ and Ca/CCl₄/O₂ Flames

(1) Flame Spectra

The spectra of the Mg/CCl₄/O₂ and Ca/CCl₄/O₂ low pressure dilute diffusion flames are completely different in appearance from the corresponding M+O₂ flame spectra. Whereas the latter exhibit mostly molecular emission, plus resonance lines of low excitation energy, the Mg/CCl₄/O₂ and Ca/CCl₄/O₂ flames show numerous strong metal atom emission lines with excitation energies within several hundred cm⁻¹ of the ionization energy (6.08 eV. for Ca, 7.61 eV. for Mg) as well as many intense molecular band systems. Naegeli (1967) reported atomic excitation in the Na and K/CCl₄ flames to nearly the ionization limits of these metals (5.12 and 4.32 eV. respectively). In the present work however, excitations as high as 7.5 eV. were observed. Figures (III-14) and (III-15) show spectra of the Mg/CCl₄/O₂ and Ca/CCl₄/O₂ flames, respectively. The molecular bands observed are listed in Table XIII, and the atomic lines observed are shown on energy level diagrams in Figs. (III-16) (Mg) and (III-17) (Ca), respectively. Because of the large numbers of Ca lines, for clarity the wavelengths are omitted in Fig. (III-17). A vertical line along a series of upper states in the figure indicates that all members of the series, between the limits shown were observed. Although, as noted above, numerous atomic lines

of neutral Ca and Mg were observed, corresponding to excitation energies extending nearly to their respective ionization limits, no lines of ionized Ca or Mg were observed. In particular, the absence of the resonance doublets of Ca^+ (3968.5 \AA 3933.7 \AA ; $4p^2P_{1/2,3/2}^{\circ} \rightarrow 4s^2S_{1/2}$) and Mg^+ (2802.7 \AA , 2795.5 \AA ; $3p^2P_{1/2,3/2}^{\circ} \rightarrow 3s^2S_{1/2}$) was significant in that these ionic lines have high transition probabilities, and excitation energies of 35730 and 25340 cm^{-1} relative to the ion ground state. These are much lower than the excitation energies of many of the neutral Ca and Mg lines seen. If any sizeable degree of ionization existed, one would expect to see the ionic resonance lines since the same processes that excite neutrals should be effective on ground state ions also. Their absence suggests that little ionization exists, and this is discussed further later in the section on excitation mechanisms.

In all the flames in CCl_4 vapor studied, the $\Delta v = -1$ sequence of the C_2 Swan bands ($A^3\Pi_g - X^3\Pi_u$) up to $v' = 5$ and the (6,4) and (6,5) C_2 "High Pressure" bands ($A^3\Pi_g - X^3\Pi_u$) were seen.

In the $\text{Ca}/\text{CCl}_4/\text{O}_2$ flame, the $\Delta v = -1, 0$ and $+1$ sequences of the $A^2\Pi - X^2\Sigma$ and $C^2\Pi - X^2\Sigma$ transitions and the $\Delta v = -1$ and 0 sequences of the $B^2\Sigma - X^2\Sigma$ transition of CaCl were seen. The $\Delta v = 0$ sequences of the A-X and B-X systems were stronger than the

other sequences, with the A-X somewhat stronger than the B-X. The C-X band systems were weakest of all the CaCl bands. Because of their close spacing, individual bands within the CaCl sequences were not resolved. Some weak bands which may be the (0,0) and (0,1) bands of the CuCl $B^1\Pi-X^1\Sigma$ system (from CuCl impurity) and the (4,0) band of the CO triplet ($d^3\Delta-a^3\Pi$) system were also seen. CuCl may be formed from traces of copper vapor (from the copper portion of the furnace tube) reacting with CCl_4 or by volatilization of CuCl residue remaining from the cleaning of the furnace tube with HCl. These bands were not observed in the Mg flames where the furnace temperature is lower.

In the Mg/ CCl_4/O_2 flames, the $\Delta v = -1, 0$ and $+1$ sequences of the MgCl $A^2\Pi-X^2\Sigma$ transition were observed. The $\Delta v = 0$ sequence was the strongest, and in a photoelectric scan of the spectrum, individual band heads up to $v = 7$ were identified. In addition to the C_2 Swan and "High Pressure" bands mentioned earlier, weak bands which may be the (0,0) and (1,1) bands of the C_2 Deslandres-D'Azambuja ($c^1\Pi_g-b^1\Pi_u$) system were also seen. In some experiments, the (0,0) and (0,1) bands of the CH $A^2\Delta-X^2\Pi$ system were seen. They are probably due to traces of moisture in some of the gases used or adsorbed on the chamber walls. In experiments in which N_2O was substituted for O_2 (i.e. an

TABLE XIII

Molecular Bands Observed in Ca/CCl₄/O₂, Mg/CCl₄O₂ and Mg/CCl₄/N₂O Flames

Flame	Emitter	Band System	Transition	(v', v'')	Approximate $\lambda, \text{\AA}$
<u>ALL:</u>	C ₂	Swan	A ³ Π -X ³ Π_u	$\Delta v = -1$ seq., v' = 1-5	4737-4679
	C ₂	High Pressure	" "	(6, 5)	4680, 4663
				(6, 4)	4369, 4353
<u>Ca/CCl₄/O₂:</u>	CaCl	Ultraviolet	C ² Π -X ² Σ	$\Delta v = -1$ seq.	3730
				$\Delta v = 0$ seq.	3770
				$\Delta v = 1$ seq.	3830
	CaCl	Orange	B ² Σ -X ² Σ	$\Delta v = -1$ seq.	5809
				$\Delta v = 0$ seq.	5934
	CaCl	Red	A ² Π -X ² Σ	$\Delta v = -1$ seq.	6050
				$\Delta v = 0$ seq.	6190
				$\Delta v = 1$ seq.	6350
	CO? (weak)	Triplet	d ³ Δ -a ³ Π	(4, 0); ?	5053, 5071; 5430
	CuCl? (Weak)	B	B ¹ Π -X ¹ Σ	(0, 0)	4882
				(0, 1)	4982
<u>Mg/CCl₄/O₂:</u>	C ₂ ? (weak)	Deslandres- D'Azambuja	c ¹ Π -b ¹ Π_u	(0, 0)	3852
				(1, 1)	3826
	MgCl	_____	A ² Π -X ² Σ	$\Delta v = -1$ seq.	3700

Table XIII (continued)

<u>Flame</u>	<u>Emitter</u>	<u>Band System</u>	<u>Transition</u>	<u>(v', v'')</u>	<u>Approximate $\lambda, \text{\AA}$</u>
	MgCl (continued)				
				$\Delta v=0$ seq., $v=0-7$	3750-3780
				$\Delta v=1$ seq.	3845
	CH (some runs)	4300 \AA	$A^2\Delta-X^2\Pi$	(0,0)	4314
				(1,0)	3627
<u>Mg/CCl₄/N₂O:</u>	SAME AS Mg/CCl ₄ /O ₂ PLUS THE FOLLOWING:				
	CN	Violet	$B^2\Sigma-X^2\Sigma$	(0,1), (1,2)	4216, 4181
				(0,0), (1,1), (2,2) (3,3), (4,4)	3883, 3871, 3862, 3855, 3851
				(1,0), (2,1), (3,2)	3590, 3586, 3584

Mg/CCl₄/N₂O flame) the same emissions were seen as with O₂, with the addition of the (0,1), (1,2), (0,0)-(4,4), (1,0), (2,1) and (3,2) bands of the CN violet system (B²Σ-X²Σ).

In addition to the lines and bands mentioned above a photoelectric scan of the spectrum of the Mg/CCl₄/O₂ flame showed weak resonance lines of the Na and K impurities. The Na line, which was very weak seemed to weaken further with O₂ addition, while the potassium line increased by nearly 2 orders of magnitude.

Another difference from the M+O₂ and M+N₂O flames (M=Mg,Ca) is that in the flames with CCl₄, no metal oxide bands were seen, nor were any bands which might be attributed to metal dimer, M₂.

The energy required to excite the observed Ca and Mg atomic lines are easily read from Figs. (III-16) and (III-17). The excitation energies of the observed molecular bands were estimated using the approximation (neglecting anharmonicity):

$$E \approx T_e + (v'_{\max} + 1/2) \omega_e$$

where T_e and ω_e are the electronic term value and vibrational constant as defined by Herzberg (1967) and v'_{\max} is the highest observed vibrational level in the upper electronic state. The results of these calculations are shown in Table XIV. In the case of the CaCl bands, the tabulated

Minimum Excitation Energies of Highest Observed Molecular Energy Levels**

ORIGINAL PAGE IS
OF POOR QUALITY

Emitter	State	T_e, cm^{-1} *	ω_e, cm^{-1} *	Excitation Energy		
				cm^{-1}	eV.	kcal/mol.
C ₂	A ³ Π _g , v'=6	19916	1788	31538	3.91	90.2
	C ² Π _g , v=1	34262	1809	36976	4.58	105.7
CaCl	A ² Π, v'=1	16093**	365	16640	2.06	47.6
****	B ² Σ, v'=1	16851	359	17390	2.16	49.7
	C ² Σ, v'=1	26499**	336	27003	3.35	77.2
CuCl	B ¹ Π, v'=0	20488	401	20688	2.56	59.1
MgCl	A ² Π, v'=7	26465**	492	30155	3.74	86.2
CH	A ² Δ, v'=1	23150	2921	27532	3.41	78.7
CN	B ² Σ, v'=4	25752	2164	35490	4.40	101.5
CO	d ² Δ, v'=4	61999	1138	67120	8.32	191.9

Notes: *Electronic term value, T_e and vibrational constant, ω_e , from Herzberg [30A]. C₂(A³Π_g)

T_e value corrected for revised C₂ ground state as described by Gaydon [47].

**When Herzberg [30A] lists 2 doublet components, the lowest one is listed here.

***Excitation energy = $T_e + (v'_{\text{max}} + 1/2)\omega_e$

****These energies are lower limits. CaCl sequences too closely spaced to identify individual bands, but since $\Delta v = -1$ sequences were seen, v'_{max} is at least 1. Higher values are possible.

values represent a lower bound, since individual bands were not separated. For these bands, (since the $\Delta v = -1$ sequences are seen and v' cannot be negative) v' was taken as 1 in Table XIV. The excitation energy of the presumed CO triplet band observed is nearly double that of any of the other observed bands and higher than that of any of the observed atomic lines. Thus there is some doubt in the identification of this band.

The intensity of metal atom line emission and MCl band emission was found to increase with addition of O_2 , while C_2 emission appeared unchanged (Fig. III-14). The quantitative dependence of line and band intensity upon O_2 and CCl_4 concentration was measured photoelectrically, and will be discussed in detail below. Metal atom and MCl emission was seen weakly, even in the absence of O_2 addition, probably as a result of minor air leakage into the system. The appearance of strong CN bands when N_2O is substituted for O_2 is shown in Fig. (III-14). Some weak CN bands are seen in the spectra without N_2O addition, probably due to the leakage of traces of N_2O through a closed valve, as they were not observed in other experiments when no N_2O supply was connected to the system. Fig. (III-14) also shows an apparent weakening of atomic Mg line emission by the addition of CO, while band emissions appeared unchanged. To the eye, the flame with added O_2 seemed less green

when CO was added, and the violet (C_2 emission) flame in the absence of O_2 seemed much brighter than in previous experiments. This increase in violet emission, rather than any decrease in green ($Mg\ 5180\ \overset{\circ}{\text{\AA}}$) emission, may be the reason for the color change in the green flame. An increase in C_2 emission is consistent with the observations of Tewarson et al. (1969) who observed a similar effect in CO addition to alkali metal - CCl_4 flames. The lack of apparent change in C_2 band emission in the spectra shown in Fig. (III-14) may be due to other changes in the flame during the hours-long spectrographic exposures and the fact that these strong bands were overexposed to begin with, and the plate would therefore be very insensitive to further increases in brightness. The limited intensity range of photographic plates, their non-linear exposure-density relation, and the necessity for long exposures during which the flame intensity can change due to exhaustion of metal supply or nozzle clogging make photographic plates useful primarily as a survey tool for determining the identity of species present in the flames. Quantitative studies of intensities, excited state population densities and the dependence of intensity on experimental conditions (pressure, mole fractions, flows) were therefore conducted using photomultiplier detection. Many of the stronger lines and bands

in Fig. (III-14) are overexposed. Consequently it is difficult to see changes in their intensity. Yet, if shorter exposures were used, many of the weaker lines and bands would be lost. Variation in flame intensity between exposures obscures the effect of added O_2 in Fig. (III-15) and may have something to do with the apparent effect of CO in Fig. (III-14) mentioned above. Photoelectric detection avoids many such difficulties.

(2) Molecular Excitation

The predominant emissions from the Mg and $Ca/CCl_4/O_2$ flames are, as noted above (Tables XIII, XIV, Figures III-16, III-17), numerous atomic singlet and triplet lines, MCl bands ($M=Mg, Ca$) and the C_2 Swan and "High Pressure" band systems. The distribution of population among the vibrational levels of the upper electronic state of the $C_2 A^3\Pi_g - X^3\Pi_u$ transitions have been studied in detail by Naegeli (1967), Naegeli and Palmer (1968) and Tewarson, Naegeli and Palmer (1969). They found a strongly inverted vibrational population in the $C_2 A^3\Pi_g$ state excited in the dilute diffusion flames of Na and K with CCl_4 . Bugrim et al. (1966) found a less extreme vibrational inversion in the Li/CCl_4 flame. Bugrim et al. (1966) also studied the Mg/CCl_4 flame but did not report a vibrational distribution.

A vibrational inversion in C_2 is useless as far as a rotation-vibration laser is concerned, since the radiative vibrational transition probability in a homopolar molecule such as C_2 is very small (zero for dipole radiation). The metal monohalide molecules do not suffer from this disability, but no evidence of inverted population has been found in MCl . Moreover, the focus of the present investigation is on electronic transitions presenting potentialities for laser applications in the visible and ultraviolet regions and a study of vibrational population distribution was therefore not made. Bugrim et al. (1966) suggested the possibility of an electronic population inversion in C_2 , based on the presumed formation of C_2 initially in the $A^3\Pi_g$ excited state. The high Franck-Condon factors (0.15 and 0.48, respectively) for the (6,5) and (6,4) C_2 "High Pressure" bands (Spindler, 1965) might suggest the possibility of an electronic transition laser. These transitions terminate on the $v=5$ and $v=4$ levels of $C_2 X^3\Pi_u$, which would not be thermally populated, even if C_2 were formed in the ground electronic state. However, the short radiative lifetime of the $A^3\Pi_g$ upper state, 1.7×10^{-7} sec (Smith, 1969), coupled with the long vibrational quenching time for emptying the lower state (about 10^{-6} sec, even if quenching occurs on every collision) would prevent this, as the lower state would quickly fill up. Under conditions of stimulated emission, what makes the situation worse is that the

radiative lifetime would be even shorter than the spontaneous emission value given above. The possibility, however, of a pulsed C_2 electronic laser cannot be completely ruled out (Naegeli, 1974a). The radiative lifetimes of electronically excited metal monochloride molecules (about 2×10^{-8} sec. for BaCl and CaCl), (Obenauf, Hsu and Palmer, 1973a, Capelle, Bradford and Broida, 1973) are even shorter than that of C_2 . Dagdigian et al. (1974) have recently reported radiative lifetime measurements on the Ca, Sr and Ba monohalides ranging from $15-50 \times 10^{-9}$ sec. The same difficulties regarding filling up of the lower laser state described above for C_2 would occur here in even more severe form. In the case of the Ca + CCl_4/O_2 flame where several electronic states are excited, the A-X bands are more intense than the B-X bands, which in turn are stronger than the C-X bands, which would seem to preclude electronic inversion on (unobserved) C-A and B-A transitions. This cannot be certain, in the absence of electronic transition probability and Franck-Condon factor data to relate the relative intensities of the CaCl A-X, B-X and C-X bands to the populations of the A, B and C electronic states. Dagdigian et al. (1974) have recently reported radiative lifetimes of about 28, 38 and 25×10^{-9} sec, respectively, for these states. This near equality would make the relative populations about the same as the observed relative intensities noted above, and hence no inversions seem to exist.

For these reasons, as well as the inherent advantages for laser applications of an atomic transition over a molecular transition where energy is divided over many levels, the present investigation concentrated on quantitative measurement of the atomic line emissions. Only flames with CCl_4 were studied since Zhitkevich et al. (1963a) reported stronger chemiluminescence with CCl_4 than with any other organic compound.

(3) Atomic Line Emission and Excitation Temperatures

As has been shown earlier (Chapter I of this thesis), observed atomic line intensities, I , can be related to excited state populations, N_u and excitation rates, n' , by:

$$N_u/g_u \sim \frac{I\lambda}{g_u A_{ul}} \sim \frac{I\lambda^3}{g_f} \quad \dots \dots \text{Eq. (III-1a)}$$

$$I\lambda/g_u \sim R_u/g_u = n'/g_u \quad \dots \dots \text{Eq. (III-1b)}$$

The transition probabilities and oscillator strengths are related by (Mavrodineanu and Boiteaux, 1965):

$$A_{ul} = \frac{8\pi^2 e}{\lambda^2 m c} f_{ul}$$

where e , m and c respectively are the charge and mass of the electron and the speed of light. Emission and absorption oscillator strengths, f_{ul} and f_{lu} are related by

$$g_u f_{ul} = g_l f_{lu} = g_f$$

R_u is the rate of radiative decay of the upper level.

For excited states whose radiative lifetime is much shorter than their mean lifetime for collisional quenching, the steady state radiative decay rate, R_u , will equal

the excitation ("pumping") rate n' . This will be the case for all the lines studied except the metastable Mg^* and Ca^* (3P) states.

Actually, only the first of Equations (III-1) is exact. Equation (III-1b) is an approximation for the case of only one downward transition from each excited state. The radiative decay rate is actually given by (Brennen and Kistiakowsky, 1966):

$$R_u = N_u / \tau_u$$

where τ_u is the radiative lifetime of the upper state, which is given by (Aller, 1963):

$$1/\tau_u = \sum_l A_{ul}$$

Thus:

$$R_u/g_u \sim \frac{I\lambda}{g_u} \frac{\sum_l A_{ul}}{A_{ul}} \quad \dots \dots \dots \text{Eqn. (III-2)}$$

where I and λ refer to a single transition of probability A_{ul} , and the summation is taken over all downward transitions originating in the same upper state "u". If one transition from each excited state is predominant, so $\sum_l A_{ul}/A_{ul} \approx 1$, then Equation (III-2) becomes identical to Equation (III-1b) given earlier, and transition probability values are not required to calculate excitation rates, though they are needed to calculate excited state populations. Examining the transi-

tion probability tables of Wiese et al. (1969) and assuming that those transitions not listed are of low intensity (small A_{ul}), it is found that in nearly every case only one transition from each upper state is listed. The simplified relation

$$R_u/g_u = I\lambda/g_u \quad \text{Eqn. (III-1b)}$$

has thus been used in correlating the data of the present study. As shown below, the excellent correlation obtained in this manner seems to justify this procedure.

An alternate approach would be to rearrange Equation (III-2) and sum over l to obtain the result:

$$R_u/g_u \sim \sum_l (I\lambda/g_u)$$

However, in this case the assumption must be made that all lines of significant intensity have been observed. This is harder to justify in view of the limited wavelength range of the spectrometer.

As shown earlier (Chapter I), for electronic populations following a Boltzmann distribution, a plot of $\log (I\lambda/g_u A_{ul})$ vs. upper state excitation energy, E_u , should give a straight line of slope $-1/kT_{\text{ex}}$, where T_{ex} is the excitation temperature corresponding to the Boltzmann distribution and k is the Boltzmann constant. For a Boltzmann distribution of population a similar plot of $\log \frac{R_u}{g_u}$ ($= \log \frac{I\lambda}{g_u}$) (excitation rate) vs. E_u could not be expected to correlate well, as N_u and R_u are rigidly tied together by the relation $R_u = N_u/\tau_u$, and the radiative lifetime τ_u varies irregularly from state to state. Such a $\log I\lambda/g_u$ plot would thus be expected to

show considerable scatter of the data points in a case where the excited state populations follow a Boltzmann distribution. This is indeed the case in the work of Brennan and Kistiakowsky (1966) on excitation of Fe and Ni in active N_2 , where populations correlate fairly well on a Boltzmann plot, but excitation rates show considerable scatter. (It should be noted, however, that Brennan and Kistiakowsky (1966) plotted R_u rather than R_u/g_u , which might tend to increase the scatter of their results). Duthler and Broida (1973a, 1973b) show similar results for potassium excited state populations in active N_2 . Mavrodineanu and Boiteux (1965) have plotted results of Gaydon and Wolfhard (1951) in a similar manner and obtained a fair Boltzmann plot of populations. Calculation of R_u/g_u from the same data by the present author showed much greater scatter than the Boltzmann plot of Mavrodineanu and Boiteux (1965).

The results of the present investigation of low pressure metal vapor flames are exactly the reverse of those cited above. The $\log I\lambda/g_u$ (excitation rate) vs. E_u plots exhibit a very good straight line correlation (scatter less than a factor of 2 compared with a factor of 10 or more for the studies cited above), and the $\log I\lambda/g_u A_{ul}$ (population) vs. E_u plots show much greater

scatter. Figs. (III-18) and (III-20) show excitation rate plots for Mg and Ca, respectively, and Figs. (III-19) and (III-21) show the corresponding population plots. In retrospect, it is easy to see that there is no mechanism by which the excited states could equilibrate among themselves and reach a Boltzmann distribution, unless they had been formed initially in such a distribution. Their radiative lifetimes are of the order of 10^{-8} sec, the mean time between collisions (at 1 torr, 500°K) is about 10^{-6} sec, and the mean time between potentially relaxing collisions (in \approx 99% argon) is $\sim 10^{-4}$ sec. Thus, collisional equilibration is impossible before the atoms radiate, and they radiate from the state to which they are initially excited. The states cannot equilibrate radiatively either, since for most lines the flame is optically thin and many states are not connected by optically allowed transitions. In the case of the studies cited earlier, where a Boltzmann distribution of population was found, gas temperatures (and in some cases pressures) were much higher than in the present study. The consequent higher collisional frequency thus made it easier to produce a Boltzmann distribution of population.

The straight line obtained on the plot of log

$I\lambda/g_u$ (excitation rate) vs. E_u suggests that the excitation process is controlled by a kinetic rate constant obeying an Arrhenius-type expression, $k \propto \exp(-E_u/kT_{ex})$. Here E_u , the energy required to excite the upper state, plays the role of an activation energy. This concept and its implications are considered further below in the discussion of experimental results and excitation mechanisms.

Even a cursory glance at the plots of $\log I\lambda/g_u$ (and $I\lambda/g_u A_{ul}$) vs. E_u reveals a number of important features. On the $\log I\lambda/g_u$ plots, it is seen that the excitation temperatures calculated from the slopes, $-1/kT_{ex}$ of the lines are of the order of thousands of degrees, although the translational temperature of the gas is only about 500K. A significant difference in excitation is seen to depend on the total spin, S , of the excited state. The excitation temperature of triplets ($S=1$) is about twice that of singlets ($S=0$). The radiative decay rates of the metastable Mg^* and $Ca^*(^3P)$ states are 3-4 orders of magnitude smaller than would be expected by extrapolation of the triplet Arrhenius line. It should be noted, however, that in the case of these metastable states, the rate of excitation, n' , is considerably larger than the rate of radiative decay, R_u . The primary decay process for these states

is not radiative but collisional (either physical or chemical quenching), due to their long radiative lifetimes, $\sim 2 \times 10^{-3}$ sec for $\text{Mg}^*(^3\text{P}_1)$, and $\sim 4 \times 10^{-4}$ sec for $\text{Ca}^*(^3\text{P}_1)$, using the A_{u1} values of Wiese et al. (1969). Also, these metastable states have an additional mechanism of formation. They can be formed, not only by direct excitation, but by cascading from higher levels. They are the lowest triplet states of their respective atoms, and many triplet transitions terminate on them.

The excitation rate of the $^1\text{P}^\circ$ upper state of the resonance line (for both Ca and Mg) is found to fall 1 to 2 orders of magnitude below the extrapolation of the singlet Arrhenius line. A similar effect was noted by Duthler and Broida (1973a, 1973b) for potassium and by Milne (1970) for sodium on their Boltzmann (population) plots. (In the present work, the resonance lines also appear anomalously low on population ($I\lambda/g_u A_{u1}$) plots, but the absence of a sharp Boltzmann line on these plots makes direct comparison with the above cited results difficult). In a number of experiments (with both Ca and Mg) a moderate correction of the resonance line intensity for self-absorption (measurement of self-absorption of the resonance line has shown reduction of intensity by a factor of 2-3) would place the $^1\text{P}^\circ$ state on the triplet rather than the singlet Arrhenius line on the $\log I\lambda/g_u$ vs. E_u graph.

Since both upper and lower states of this line are singlets, this behavior is difficult to explain and the proximity to the triplet Arrhenius line may be a coincidence.

It is observed (Fig. III-22) that in the vicinity of the ionization potential, E_I , of Ca or Mg, a number of triplet states deviate from the Arrhenius line and seem to approach the vertical line $E_u = E_I$ as an asymptote. This effect is discussed further later.

In experiments on the $\text{Ca}/\text{CCl}_4/\text{O}_2$ flame, it has been observed that a number of Ca triplet states in which two electrons are simultaneously excited (so-called "displaced terms", $4p^2\ ^3P$; $3d4p\ ^3P$, 3D , 3F ; $3d^2\ ^3P$) depart from the Arrhenius line drawn through the other triplet states. Another Arrhenius line, corresponding to $T_{\text{ex}} \sim 12,000\text{K}$ can be drawn through these two-electron states alone, and in many cases comes close to passing through the metastable 3P state. The "two-electron" singlet states show no such anomalous behavior. (In the case of Mg, only one "displaced term" is observed, $3p^2\ ^3P$, and it deviates from the Arrhenius line of the other triplet states). This is of interest since Zhitkevich et al. (1963a) reported an excitation temperature of $\sim 12,000\text{K}$ in the $\text{Ca}/\text{CCl}_4/\text{O}_2$ flame at atmospheric

pressure but did not specify which lines were used in calculating it.

The reasons why (1) the $1p^{\circ}$ resonance state, (2) the triplet states near the ionization limit and (3) the two-excited-electron states depart from the singlet and triplet Arrhenius lines followed by the other excited states are discussed later in the section on excitation mechanisms.

An examination of Figs. (III-18) and (III-20) shows that the rate of excitation of excited atomic electronic states is much lower in the case of Ca than in the case of Mg. Part of this difference is due to the lower Ca metal atom input to the flame (Tables I and IV), but much of it seems due to a much higher quantum yield for the excitation of metal atoms in the $Mg/CCl_4/O_2$ flame than in the $Ca/CCl_4/O_2$ flame. The calculation and interpretation of quantum yields are discussed in detail below.

At first glance, Figures (III-18) and (III-20) seem to indicate that in the $Ca/CCl_4/O_2$ flame Ca triplet and singlet states are excited at approximately the same rate, while in the $Mg/CCl_4/O_2$ flame Mg triplets are excited at a much higher rate than singlets. This would suggest that different excitation mechanisms are

operative in the two flames. This first impression, however, is shown to be erroneous by a careful examination of the $\log I\lambda/g_u$ vs. Eu plots (Figs. III-18 and III-20). In both the Ca and Mg cases the singlet and triplet Arrhenius lines are seen to cross at Eu about $45,000 \text{ cm}^{-1}$ ($\pm 3000 \text{ cm}^{-1}$). In the case of Mg, all the singlets observed (except the resonance line) are considerably higher in Eu than the crossing point of the two lines, and hence are lower in intensity than the triplets. In the case of Ca, many singlets are lower in Eu than the crossing point (hence higher in intensity than the corresponding triplets) and most of the singlets are near the crossing point. Thus the apparent difference in singlet and triplet excitation between Ca and Mg is purely an artifact of the arrangement of singlet energy levels in Ca and Mg atoms. For example, the lowest Mg singlet state (other than the $1P^\circ$ resonance state) is the $4s^1S$ level at 43503 cm^{-1} , but its only allowed transition ($4s^1S \rightarrow 3P^1P^\circ$) is in the infrared at 1.18μ , and hence is not observed. The lowest singlet Mg level producing a visible transition is the upper state of the $5s^1S \rightarrow 3p^1P^\circ$ line (5711\AA) with $\text{Eu}=52556 \text{ cm}^{-1}$. Ca, on the other hand, has numerous singlet states below $45,000 \text{ cm}^{-1}$, and many of them radiate in the visible. This

interpretation is confirmed by Fig. (III-23) in which $I\lambda/g_u$ is plotted on one graph for both Ca and Mg flames. The difference in absolute intensity of the two flames is compensated for by shifting all the Ca values upward by a factor of 300 (a linear shift of $\log 300$ on the log scale), to make the crossing points of singlet and triplet Arrhenius lines approximately coincide. It is seen that a single triplet line and a single singlet line can be drawn through both sets of data. (The lines are least square fits. The uncertainties given are \pm one standard deviation. Adjusting the vertical shift to a value slightly different than 300 would probably improve the fit slightly). It thus appears that there is no fundamental difference in the process of metal atom excitation between the $\text{Mg}/\text{CCl}_4/\text{O}_2$ and $\text{Ca}/\text{CCl}_4/\text{O}_2$ flames. While separate mechanisms may be required to explain the excitation of triplets vs. singlets (as indicated by their differing excitation temperatures), these processes seem likely to be the same in the Ca and Mg flames.

Examination of the plots of $\log \frac{I\lambda}{g_u A_{ul}}$ (population) vs. E_u shows a number of interesting features. It is

evident immediately that the population does not follow a Boltzmann distribution. While one might go through a formal least-squares procedure and plot some sort of line through the points, the correlation coefficient would be low and the meaningfulness of the result dubious. The metastable 3P state is seen to have a population 3-4 orders of magnitude larger than that of any other excited state. This is not surprising, since only a sizeable upper state population would make the "forbidden" $^3P_1 - ^1S_0$ transitions strongly visible in these flames, as they are. As mentioned earlier, the long radiative lifetimes of these states make collisional quenching their primary decay route. At 500°K, 1 torr, the mean time between collisions is 10^{-6} sec. If ~ 99% of the gas molecules are argon, the mean time between potentially quenching collisions (for gas-kinetic cross-sections) is 10^{-4} sec. The ratio of this "collisional lifetime" to typical radiative lifetimes of allowed transitions (10^{-8} sec) is 10^4 , in accord with the observed ratio of populations. Other factors which might contribute to the production of a high concentration of these metastable 3P states are their relatively low excitation energies ($15,210 \text{ cm}^{-1}$ for $\text{Ca}^*(^3P_1)$; 21870 cm^{-1} for $\text{Mg}^*(^3P_1)$) and radiative cascading from higher

levels into the metastable state.

Because the electronic state populations do not follow a Boltzmann distribution, but instead are determined jointly by their excitation rates and radiative lifetimes (and there are many instances where states of higher energy have longer radiative lifetimes than less energetic states), one would not be surprised to find population inversions in these flames. Detailed calculations of predicted inversions and comparison with experimental results are given in a later section. Here it will suffice to note that numerous cases were observed, in both Ca and Mg flames, where N_u/g_u was higher for a more energetic than for a less energetic state. Many such combinations are eliminated for laser consideration by the optical selection rules on spin ($\Delta S=0$), angular momentum ($\Delta L=\pm 1$ for one excited electron; $\Delta L=0, \pm 1$ for two excited electrons) and parity (odd \leftrightarrow even; even \leftrightarrow even, odd \leftrightarrow odd). However a number of cases were found where there appear to be population inversions between states connected by optically allowed transitions, and these are discussed below.

(4) Effect of Experimental Parameters on Flame Size, Intensity and Excitation Temperature.

(a) Flame Diameter

The present investigation was concerned with the spectra, emitted intensities, excited state

populations and excitation temperatures of the flames studied. The only interest in the effects of pressure and reactant concentrations on flame size was to allow the manipulation of these variables to provide a flame of suitable size, location and stability for spectroscopic study. Thus, accurate measurements of flame size were not required as they are in determination of reaction rate constants from flame diameters (Heller and Polanyi, 1936). Therefore, only approximate measurements were made of flame dimensions and their variations with experimental conditions. The direction and approximate extent of changes in flame dimensions were noted, and flame diameter was estimated by eye, using as references known dimensions of the furnace (the 1 inch diameter furnace tube and 4 inch diameter furnace insulator). An optimistic estimate of the uncertainty in these estimates of flame diameter is $\pm 1/4$ inch. Nevertheless, these estimates were found to yield useful information about the flames and will be discussed below.

It should be noted that the diameter considered is that observed when the flame is viewed along the furnace axis. Because of streaming flow, the flame was often elongated along the flow direction. Although the nozzle is not axisymmetric, but is a slit, rapid diffusion at low pressures caused the flame to approach cylindrical symmetry within a short distance from the nozzle.

The semi-quantitative flame diameter data discussed below were gathered in experiments on the $\text{Mg}/\text{CCl}_4/\text{O}_2$ flame, because of the wider range of conditions studied in that system and because regions of Mg atom emission and C_2 molecular emission could be more easily distinguished by a sharp difference in color (brilliant green Mg 5180\AA vs. blue-violet C_2 4350\AA , 4680\AA). However, similar trends were observed qualitatively in the $\text{Ca}/\text{CCl}_4/\text{O}_2$ flame.

The diameter of the green (Mg emission) region of the $\text{Mg}/\text{CCl}_4/\text{O}_2$ flame was found to decrease with increasing pressure (Fig. III-24, upper graph), as would be expected theoretically. The outer violet (C_2 emission) region of the flame did not appear to change in diameter with pressure. However this violet outer zone was much dimmer than the bright green inner zone, and hence was difficult to observe. Pressure was raised by partially closing the vacuum line valve, leaving all gas flow rates unchanged.

The region of metal atom emission (green) decreased in diameter as O_2 concentration was raised, while the outer region of C_2 emission appeared unchanged in diameter (Fig. III-25). At low O_2 concentrations it was difficult to estimate the diameter of the violet zone because of the proximity of the much brighter green region.

As CCl_4 mole fraction was increased, the (green) region of metal atom emission decreased in diameter. However in this case the (violet) outer region of C_2 emission also decreased in diameter (Fig. III-26). At CCl_4 mole fractions below about 0.4%, the violet region was seen as a thin halo around a green flame, and no difference could be seen in the rates at which these two zones shrank with increasing CCl_4 concentration. However, as $[\text{CCl}_4]$ was increased further, the green region decreased in diameter much more rapidly than the violet region, and finally almost disappeared. This is related to the quenching of metal atom chemiluminescence by CCl_4 which is discussed in detail later. Rapp and Johnston (1960) have noted that the emitted intensity, I , along a line of sight passing a distance r from the center of a low pressure dilute diffusion flame is given by

$$I(r) \sim K_0(Cr)$$

where $C^2 = \frac{kP_A}{D}$, k is the rate constant of the reaction of metal vapor with atmosphere reactant A, D is the metal vapor diffusion coefficient and P_A is the partial pressure of A and K_0 is the zero order Bessel function of the second kind. If the edge of the flame is defined by a minimum detectible value of I , then

$$r \sim \frac{1}{C} \sim \frac{1}{\sqrt{P_A}} \sim \frac{1}{\sqrt{X_A}}$$

at constant pressure. A log-log plot of r vs. X_{CCl_4} should thus be a straight line of slope $-1/2$. Identifying the outer, violet flame with the dilute diffusion flame governed by metal vapor reaction with CCl_4 , the data presented in Fig. (III-26) are found to fit such a line very well. The observation that when CCl_4 flow is shut off the flame expands to fill the chamber before fading out also supports such an inverse variation of r with X_{CCl_4} . Here, as in the variation with O_2 , at low concentrations, the green and violet flames are nearly coincident and only the brighter green flame can be measured. Insufficient data exist to define the form of the variation of the green flame diameter with X_{CCl_4} as it shrinks at higher X_{CCl_4} . It is clear however that it does not follow a line of slope $-1/2$ on Fig. (III-26). This is not surprising, as it is governed, not by consumption of metal vapor (as it exists within the violet flame where metal vapor and CCl_4 are reacting) but apparently by quenching of an active species responsible for metal atom excitation.

No attempt is made here to theoretically explain the variation of flame diameter with pressure and O_2 concentration, as the sparseness and uncertainty of the

data do not justify such an effort. Noting that the diffusion coefficient varies inversely with pressure, one might argue that:

$$r \sim \frac{1}{C} \sim \sqrt{\frac{D}{kP_A}} \sim \sqrt{\frac{1/P}{kPX_A}} \sim \frac{1}{P}$$

However, the data do not fit such a relation. Also, consideration of the fact that changing the pressure while maintaining all gas flows the same also changes the oxygen concentration and the carrier gas velocity, shows that such a treatment is too simplistic. The diameter vs. X_{O_2} data of Fig. (III-25) seem to correlate well on a semilog plot, but here too there is no theoretical basis for an $r \sim e^{-AP}$ relationship. An important conclusion, however, can be reached from the data of Figs. (III-24) through (III-26). Within a range of the experimental parameters containing most of the experiments performed ($X_{O_2} < 4\%$, $X_{CCl_4} < 0.4\%$, $P < 3$ torr), the flame diameter was 3 inches or greater and variations in diameter were not extreme and thus did not interfere with spectroscopic measurements.

(b) Flame Intensity

(i) Variation with Pressure:

Atomic line emission from the flames was found to show a weak dependence on pressure. The lower

curve of Fig. (III-24) shows data for the $3838\overset{\circ}{\text{A}}$ Mg triplet. Data from different experiments is normalized by its maximum value, to eliminate the effects of variations in metal atom flux on the absolute intensity. Over the range of pressures from 1.3 to 8.0 torr, the variation in intensity is less than $\pm 20\%$ from its average value, and intensity is nearly constant from 2. to 4. torr. The pressure was varied by manipulating the vacuum line valve, with all gas flows unchanged. A possible explanation of this variation with pressure is that at lower pressures the increase in flame diameter causes part of the flame to lie outside the field of view of the optical system, causing a loss in observed intensity. At the high end of the pressure range the condensation of the flame causes part of it to lie near to or even within the metal vapor nozzle, again out of the field of view. The decrease in intensity at the low end of the pressure range is easily estimated. Consider the flame to be spherical, of radius r and the field of view to be a cylinder of radius R . The total volume of the flame varies as r^3 , while the volume contained within the field of view varies approximately as $R^2 r$. The fraction of the flame volume viewed by the optical system thus varies as $1/r^2$. Since flame diameter is observed

to increase from 3 to 4 inches as pressure falls from 2.0 to 1.3 torr, one might expect a fall in intensity to a value $(3/4)^2 = 0.56$ times the peak value. This is good agreement with the observed value 0.65. Further support for this explanation comes from observations late in an experiment, when the metal sample is nearly exhausted. The flame is then observed to be smaller than earlier, and the I vs. P curve is found to decrease monotonically with P, without the low pressure falloff seen in Fig. (III-24). In this case, the smaller flame can be squeezed out of the field of view at higher pressures, but does not expand enough at lower pressures to overfill the field of view.

Apparently the intensities of all spectral lines change in proportion as pressure varies, since as discussed below, excitation temperature (from slope of $\ln(I\lambda/g_u)$ vs. Eu plot) is not found to vary with pressure. In any case the sensitivity of excitation temperature to changes in line intensity can be shown to be low. Let $I\lambda/g_u \equiv Y$. Excitation temperature is determined from the slope of a log Y vs. Eu plot using the relation:

$$\frac{\Delta \ln Y}{\Delta E_u} = - 1/kT_{ex}$$

where k is the Boltzmann constant. Rearranging and taking differentials:

$$d\Delta \ln Y = \frac{\Delta E_u}{k T_{ex}^2} dT_{ex}$$

$$dT_{ex} = \frac{k T_{ex}^2}{\Delta E_u} d\Delta \ln Y$$

Consider the extreme case of an excitation temperature determined from the intensities of two lines, one of which changes in intensity with pressure variation while the other line remains unchanged. Taking $k=0.69495 \text{ cm}^{-1}$, $\Delta E_u \approx 20,000 \text{ cm}^{-1}$, $d\Delta \ln Y=0.2$ (a variation of $\approx \pm 20\%$) and $T_{ex} \approx 5000^\circ\text{K}$ (typical value for triplets), one finds $dT_{ex} = \pm 174^\circ\text{K}$, which is smaller than the experimental scatter in the determination of T_{ex} . For $T_{ex} \approx 2500^\circ\text{K}$ (singlets) the sensitivity of T_{ex} to pressure variations is even smaller, by a factor of 4. In addition, since T_{ex} is determined using a curve fit by a least squares technique to data from many spectral lines, any variation in one or a few lines would be even further diluted.

(ii) Variation with Oxidizer Concentration

In the $\text{Mg}/\text{CCl}_4/\text{O}_2$ flames, the intensity of the MgCl bands and all metal atom lines was found to vary linearly with O_2 input. This is shown in Fig. (III-27) for the $\text{Mg } 3838\text{\AA}$ line. The $\text{Mg } ^3\text{P}_1 \rightarrow ^1\text{S}_0$ "forbidden" line, originates in a metastable state with a radiative lifetime about 2 milliseconds (vs. $\sim 10^{-8}$ sec. for the other lines which are therefore unquenched, as the mean time between collisions is 10^{-6} sec). It was found to

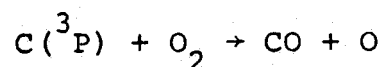
depart from this linear relation at about 0.3 mole % O_2 , probably due to reactive quenching of Mg^* (3P) by O_2 . The intensity of the C_2 "high pressure" band at 4860A was found to be essentially independent of O_2 except for a moderate falling off at very high O_2 inputs. This slight effect is probably due to lowering of the CCl_4 concentration by dilution with the 1.56% O_2 , 98.44% He mixture used to accurately meter low flows of O_2 . Helium was used in this mixture rather than argon to allow easier gas chromatographic analysis of the mixture. (O_2 in argon is very difficult to determine because the retention times of the two gases on most chromatographic column packing materials are nearly equal). Some reaction of O_2 with a precursor of C_2^* (e.g. C atoms) is also a possibility. Direct quenching of C_2^* is not a possibility because of its short radiative lifetime (Smith, 1969), 1.7×10^{-7} sec.

It should be noted that the absence of added O_2 does not imply zero intensity of the lines and bands showing linear dependence on O_2 . Even then, they are observed, but weakly. This is probably caused by O_2 impurities in the gases used and slight leakage of air into the system, and illustrates the sensitivity of these flames to small amounts of O_2 .

The slight departure of the 3838\AA curve of Fig. (III-27) from linearity at about 0.6% O_2 is due to dilution by the helium in the He/O_2 mixture, which causes a non-proportionality between O_2 input rate and mole % O_2 in the chamber. This is easily seen in Fig. (III-28) where the data of Fig. (III-27) plus data for two additional lines are plotted on a log-log plot vs. mole % O_2 . Here, there is no falloff in the intensity at the highest O_2 concentrations (except of course for the ^3P metastable). Departure from the plotted line is seen, at low O_2 concentrations, of the 4571\AA metastable line and (to a lesser degree) of the 2852\AA resonance line. This is probably due to their low excitation energies (21870 and 35051 cm^{-1} respectively), allowing some excitation by processes, not involving O_2 , which are not exothermic enough to excite states of higher energy. The slopes of the curves in Fig. (III-28) are not unity (which would indicate a first order dependence on O_2 concentration), but range from 1.12 to 1.19. This might be indicative of a complex reaction sequence resulting in a non-integral reaction order. Alternately, it might be due to rapid reaction of the O_2 so the actual O_2 mole fraction in the chamber is less than the molar ratio (O_2 input/total gas input), with more of the

input O_2 surviving at higher inputs.

Variation of intensity with O_2 input in $Ca/CCl_4/O_2$ flames was similar to that described above for $Mg/CCl_4/O_2$ flames. Here, however, departure from linearity and a definite maximum in intensity was observed at relatively low O_2 concentration (about 0.3% O_2 , Fig. III-29). This does not, however, represent any basic difference between Mg and Ca , as at high enough O_2 concentrations, the same behavior is shown in the Mg flames (Fig. III-30). An analysis of data from a number of experiments has revealed that the location of the peak in the intensity vs. O_2 curve is determined by the O_2/CCl_4 molar ratio. The maximum was reached at lower O_2 in the Ca data presented earlier because the CCl_4 mole fraction was lower than in the Mg experiment (0.042 vs. 0.27%). As shown in Table XV, over a wide range of CCl_4 and oxidizer concentrations, for Ca or Mg , and even for O_2 or N_2O oxidizer, the peak in the intensity vs. oxidizer curve always seems to occur for the $\frac{\text{oxidizer}}{CCl_4}$ molar ratio between 10 and 20. It would appear that an important intermediate species formed from CCl_4 is being destroyed by reaction with O_2 . Ground state carbon atoms are a likely responsible species, as the reaction



has a rate constant (at room temperature) of 1.1×10^{-10}

$\text{cm}^3 \text{ molecule}^{-1} \text{ sec}^{-1}$ (Braun et al., 1969) which is essentially gas kinetic (i.e. reaction on every collision). This hypothesis is discussed further below in the section on quenching experiments.

The O_2 quenching behavior of the metastable ($^3\text{P}_1 \rightarrow ^1\text{S}_0$) line is further contrasted with that of other atomic lines in Figs. (III-31) and (III-32), for Mg and Ca, respectively. A number of atomic lines, both singlets and triplets (plus one MgCl band in Fig. III-31) are plotted on each graph. The points are made to fall (approximately) on one curve by normalizing each data point by the peak value for that spectral line (or by the value at one specific O_2 concentration for Fig. III-38 where the peak is not reached). The divergence of the metastable from all the other lines is plainly seen. The falloff in metastable intensity with O_2 on Fig. (III-32) appears exponential, and a semilog plot (Fig. III-32) of the same data verifies this impression. It is shown below, how the slope of this plot can be used to estimate the rate constant for the quenching of $\text{Mg}^*(^3\text{P})$ by O_2 .

A single experiment on the $\text{Mg}/\text{CCl}_4/\text{N}_2\text{O}$ flame revealed behavior similar to that observed with O_2 , except that the intensity maximum vs. N_2O was flatter and broader.

In addition, CN violet system bands were seen. These bands increased in intensity with increasing $[N_2O]$, passed through a maximum, and then decayed at about the same rate as the atomic metal lines. The metastable Mg ($3P_1 \rightarrow 1S$) line ($4571\overset{\circ}{A}$) was very strongly quenched by N_2O , probably due to reactive quenching of the long-lived metastable 3P . It reached its intensity maximum at about 0.8 mole % N_2O as compared with about 6.% N_2O for the other metal atom lines and CN bands. In this experiment the CCl_4 mole fraction was about 0.32%.

As shown in Figs. (III-28, III-31 and III-32), all lines other than the metastable $^3P_1 \rightarrow 1S$ have the same variation in intensity with O_2 concentration, and one would therefore expect no dependence of T_{ex} on $[O_2]$. This is shown, below, to be the case. This identical variation in intensity of so many lines as O_2 flow is varied is further support for the hypothesis that a single intermediate species responsible for the excitation of all the lines is affected by O_2 (e.g. C atoms).

(iii) Variation with CCl_4 Concentration

All the emissions from the Mg/ CCl_4/O_2 flame, triplets and singlets, resonance and forbidden lines, C_2 and MgCl bands, were found to follow a similar variation

Table XV

(at peak of I vs. X_{oxidant} curve)

Run No.	Oxidant	Comments	Chamber Pressure, Torr	Mol.%Oxidant	Mol.%CCl ₄	Mol.ratio	Oxidant CCl ₄
Ca-4-2-74-1	O ₂	very flat peak: Lower limit peak Upper limit	1.4	0.566 1.066 1.485	0.0526 0.0525 0.0521	10.8 20.3 28.5	
Ca-3-26-74-1	O ₂	---	1.5	0.384	0.0369	10.4	
Mg-4-4-74-1	O ₂	---	1.4	4.67	0.390	12.0	
Mg-4-9-74-1	N ₂ O	very flat peak: Lower Limit Upper limit	1.5	3.40 9.42	0.328 0.307	10.4 30.7	
Mg-3-13-74-1	O ₂	No peak reached limits of broad peaks		0.594	0.210	2.83 (no peak)	
Range of $X_{\text{CCl}_4} \sim$		10.6:1		10.6:1			
Range of $X_{\text{oxidant}} \sim$		24.5:1		16.7:1			
Range of $\frac{X_{\text{CCl}_4}}{X_{\text{oxidant}}} \sim$		2.9:1		2.0:1			

in intensity with CCl_4 concentration. They increase from zero, go through a sharp maximum between 0.2 and 0.5 mole % CCl_4 and then continue to decrease more gradually with increasing CCl_4 . (Fig. III-34). (Each curve is normalized by its peak value). There seems to be a definite correlation between the CCl_4 concentration for peak intensity and the excitation energy of the emission, with no apparent relation to the multiplicity (singlet, doublet or triplet) or atomic or molecular species of the emitter (Fig. III-35). The concentration of CCl_4 at the maximum of each intensity vs. $[\text{CCl}_4]$ curve clearly varies inversely as the efficiency of CCl_4 as a quencher of that emission. Thus a decrease in this concentration with excitation energy of the emitter corresponds to an increase in quenching efficiency with excitation energy. This suggests the possibility that a vibrationally excited species may be involved in the excitation process. Such a species would have a radiative lifetime long enough to allow its collisional quenching. It could be readily quenched by CCl_4 with its multitude of internal modes, and might reasonably be expected to have a quenching cross-section which increases with vibrational level. This possibility is discussed further later in the section on mechanisms.

The curve of intensity vs. CCl_4 partial pressure (or concentration) for the Mg metastable 4571\AA line

does not differ significantly from that for other emissions (Fig. III-34), contrary to the O_2 case. However the maximum intensity occurs at a much lower CCl_4 concentration than would be expected from its excitation energy and the correlation of Fig. (III-35). This seems to indicate additional quenching of $Mg^*(^3P)$ itself by CCl_4 facilitated by its long radiative lifetime.

The early onset of quenching as CCl_4 concentration is increased makes it difficult to estimate a reaction order as was done above for O_2 . In addition, as $P_{CCl_4} \rightarrow 0$, changes in flame size and geometry, and a tendency for the flame to move toward the CCl_4 inlet make the data points nearest the origin of dubious value. The most that can be said is that for values of P_{CCl_4} below the maximum of the curve (Fig. III-34), the intensity seems to vary as a power of P_{CCl_4} less than 1. The portion of the curve past the maximum seems to decay exponentially, and a semilog plot of the same data points (Fig. III-36) is consistent with this description. A discussion is given later using the slope of this plot to estimate a rate constant for the quenching process by CCl_4 .

Quantitative measurements were not made of the variation of $Ca/CCl_4/O_2$ flame intensities with CCl_4 concentration. Qualitative observations were similar to

those in the $\text{Mg}/\text{CCl}_4/\text{O}_2$ flames, with flame intensity increasing at first with CCl_4 input, and then being quenched as CCl_4 input was increased further. As noted earlier, the quantitative variations of emissions with O_2 concentration were similar in the Ca and Mg flames, when the effect of O_2/CCl_4 ratio was taken into account.

(c) Excitation Temperatures

As discussed earlier, the observed excited state populations do not correlate well on a Boltzmann plot of log population ($I\lambda/g_u A_{ul}$) vs. E_u , and an excitation temperature based on such a plot therefore has little meaning. The rate of excitation of these states correlates very well on an Arrhenius plot of log production rate ($I\lambda/g_u$) vs. E_u , and such a plot can be used to define a chemical kinetic excitation temperature, T_{ex} related to the slope of the Arrhenius plot by: $\text{slope} = -\frac{1}{kT_{\text{ex}}}$. The present section discusses the differences in T_{ex} between singlets and triplets, Ca and Mg flames, and the variation of T_{ex} with experimental parameters such as pressure, oxygen concentration and CCl_4 concentration.

As described earlier, excitation temperatures were calculated from the slope of a least-squares line fit

to a $\log (I\lambda/g_u)$ vs. Eu plot, and are tabulated in Table XVI. There did not appear to be any appreciable dependence of excitation temperature on chamber pressure or oxidizer mole fraction, or on whether the oxidizer was O_2 or N_2O . When data were taken at more than one pressure or more than one O_2 concentration in the same experiment, lines with the same slope (i.e. same T_{ex}) could be faired through the data points on the Arrhenius plot, though the least-squares line-fit program sometimes gave T_{ex} values which differed somewhat.

Tables XVII and XVIII compare the average of all T_{ex} values for a number of categories of spectral lines. The average excitation temperature for triplets is seen to be about $2600^\circ K$ higher than that for singlets, for both Ca and Mg. Ca singlets and triplets, respectively, have average excitation temperatures about $800^\circ K$ higher than Mg singlets and triplets. The Ca states in which two electrons are excited show an excitation temperature of about $12,000^\circ K$. All of these excitation temperatures are far above the gas translational temperature of about $500^\circ K$. These averages should be taken with some degree of caution because of the relatively small number of data points in some cases (singlets and Ca lines). Also, data taken at different CCl_4 concentrations have been averaged together, and (as shown below) this variable

Excitation Temperatures, T_{ex} , and Experimental Conditions

Run Number	Chamber Pressure Torr	Mole Fraction O ₂ %	Mole Fraction CCl ₄ %	Mole Fraction Added Quencher %	T_{ex} , °K Singlets	T_{ex} °K Triplets	T_{ex} °K 2-Excited Electron Triplets	COMMENTS
MG-11-21-73	1.6	0.288-0.208	0.269-0.263	---	---	5552 [±] 276	---	
MG-12-21-73	1.9	0.893	0.341	---	---	5006 [±] 616	---	
MG-12-28-73	1.8-1.95	0.added	0.0506	---	---	4685 [±] 115	---	
" "	" "	0.added	0.300	---	---	5238 [±] 100	---	
" "	" "	0.1538	0.270	---	---	4223 [±] 129	---	possible error due to flame intensity change
MG-1-14-74	1.60	0.1536	0.283	---	---	6166 [±] 542	---	
MG-1-16-74	1.5-1.7	0.1537	0.315	---	---	*3171 [±] 330	---	possible systematic error due to inadequate correction for flame intensity changes with time might make these values all too low.
" "	1.5-1.7	0.306	0.281	---	---	*3490 [±] 532	---	
" "	4.9-5.5	0.1537	0.315	---	---	*3564 [±] 330	---	
" "	4.9-5.5	0.306	0.281	---	---	*3567 [±] 295	---	
MG-1-18-74	1.3	0.379	0.330	---	---	4715 [±] 93	---	
" "	4.1-4.5	0.379	0.330	---	---	5002 [±] 110	---	
MG-3-6-74	2.2	1.035	0.272	---	2391 [±] 110	6003 [±] 426	---	
MG-4-3-74	1.4	0.482	0.301	---	2709 [±] 229	5315 [±] 59	---	

Table XVI (continued)

Excitation Temperatures, T_{ex} , and Experimental Conditions								
Run Number	Chamber Pressure Torr	Mole Fraction O_2 %	Mole Fraction CCl_4 %	Mole Fraction Added Quencher %	$T_{ex}, ^\circ K$ Singlets	$T_{ex}, ^\circ K$ Triplets	$T_{ex}, ^\circ K$ 2-Excited Electron Triplets	COMMENTS
Mg-4-3-74	1.4	0.321	0.346	---	2699±266	5261±543	---	singlet temp. probably in error. Calc. from 4 points,* so one erroneous point has high weight. Note other temps. do not change
" "	"	0.1606	0.391	---	*3695±221	5215±74	---	
MG-4-5-74	1.4	1.075	0.405	---	2151±207	4514±417	---	
MG-4-9-74	1.49	0. added	0.339	---	---	5088±402	---	
" "	"	0.873 N_2O	0.336	---	2702±109	5373±110	---	flame dim. few singlets seen.
" "	"	1.84 N_2O	0.333	---	---	5411±208	---	
MG-6-14-74	0.90	0.340	0.1607	$N_2=78.0$	2359±296	4189±371	---	
MG-6-26-74	1.2	0.267	0.0849	NO-0.281	---	4771±391	---	
CA-2-13-74	1.5-1.6	0.319	0.0266	---	3452±317	4872±275	8909±1810	
CA-3-26-74	1.5	0. added	0.0502	---	---	6094±427	14,143±1720	2-electron triplet temp. from 2 points.
CA-3-28-74	3.0	0.237	0.0432	---	2948±345	5247±307	12,655	

-190-

Table XVI (continued)

Excitation Temperatures, T_{ex} , and Experimental Conditions

Run Number	Chamber Pressure Torr	Mole Fraction O_2 %	Mole Fraction CCl_4 %	Mole Fraction Added Quencher %	$T_{ex}, ^\circ K$ Singlets	$T_{ex}, ^\circ K$ Triplets	$T_{ex}, ^\circ K$ 2-Excited Electron Triplets	COMMENTS
CA-4-2-74	1.4	1.066	0.0524	---	3850 \pm 820	5844 \pm 296	12,217	2-electron triplet temp. from 2 points.
CA-6-19-74	0.95-1.15	0.221	0.0386	$N_2=45.1$	2341 \pm 316	4891 \pm 296	9194 \pm 121	
CA-7-2-74	0.75-0.9	0.215	0.0314	$NO=0.406$	3411 \pm 403	6793 \pm 510	12,373	2-electron triplet temp. from 2 points.

NOTE: The uncertainty appended to each T_{ex} value is \pm one standard deviation of the least squares line fit used to calculate T_{ex} .

TABLE XVII

Average Values of Excitation Temperature
and Effect of Nitrogen Addition

Category	N	\bar{T} , °K	σ , °K	T_{ex} with N ₂	$(T_{\text{ex}} - \bar{T})/\sigma$	P=Probability That N ₂ has no Real Effect (See Note Below)
Mg Triplets	18	5128	490	4182	-1.931	< .05
Mg Singlets	5	2530	252	2359	-0.679	< .25
Ca Triplets	6	5940	788	4891	-1.331	< .10
Ca Singlets	5	3414	320	2341	-3.353	< .0005
Ca 2-Excited Electron Triplets	6	12112	1720	9194	-1.696	< .05

NOTE: (1) In calculating this table, data points suspected of gross error (marked * in Table XVI) have been eliminated, and, of course, the data with N₂ added were not included in calculating \bar{T} .

(2) \bar{T} = Arithmetic Mean

σ = Standard Deviation of the T_{ex} values from \bar{T} .

P = Probability that the single T_{ex} value with N₂ addition was drawn from a population with the same mean, \bar{T} , as the runs without N₂.

N = Number of values

Table XVIII

A. Comparison of Average Excitation Temperatures, \bar{T} .

*95% Lower Confidence Limit

Triplets 2598°K Higher Than Singlets (Mg)	2332°K
2526°K " " " " " " (Ca) $\approx 2600^\circ\text{K}$	1947°K
Ca Triplets 812°K Higher Than Mg Triplets	250°K
Ca Singlets 884°K Higher Than Mg Singlets $\approx 800^\circ\text{K}$	584°K

B. Apparent Reduction By N_2 Addition ($\bar{T} - T(N_2)$):

Ca 2-Excited Electron Triplets:	2918°K
Ca Triplets	: 1049
Ca Singlets	: 1073
Mg Triplets	: 946
Mg Singlets	: 171

$\approx 1000^\circ\text{K}$

$$*95\% \text{ lower 1-sided confidence limit} = \bar{X}_1 - \bar{X}_2 + Z_{.05} \left(\frac{\sigma_1^2}{N_1} + \frac{\sigma_2^2}{N_2} \right)^{1/2}$$

where \bar{X}_1 and \bar{X}_2 are the two means being compared, σ_1 and σ_2 their standard deviations and N_1 and N_2 the number of values for each mean. $Z_{.05}$ is defined by:

$$\int_{Z_{.05}}^{\infty} \frac{1}{\sqrt{2\pi}} e^{-x^2/2} dx = .05 \quad (\text{Bowker and Lieberman, 1959}).$$

is found to have a strong effect on excitation temperature. However, as shown by the 95% confidence limits in Table XVIII-A, the differences in excitation temperature between triplets and singlets and between calcium and magnesium lines of the same multiplicity seem significant.

Attempts to correlate T_{ex} data for Mg triplets (for which the largest quantity of data exists) with X_{CCl_4} , X_{O_2} , or total molecular concentration by linear regression proved unsuccessful. The reason for this is seen in Fig. (III-37), which shows T_{ex} to be a strongly non-linear function of X_{CCl_4} , peaking at about 0.2 mole % CCl_4 . Since points from experiments with N_2O (instead of O_2) or with NO addition fell close to the other experimental points, they were included in the analysis which follows and in the averages shown in Tables XVII and XVIII. The remaining scatter in the points in Fig. (III-37) may be due partly to variations in metal vapor flux. This was not controlled closely enough to be used as an independent variable in the statistical analysis, and varied in the course of an experiment due to consumption of the metal sample and furnace temperature variations. Sufficient data points did not exist to perform similar regression analyses in the cases of Mg singlets and Ca singlets and triplets, but a similar variation seems plausible in these cases,

especially in view of the intensity variation with X_{CCl_4} shown in Figs. (III-34) and (III-35). If lines of higher excitation energy peak earlier and fall off sooner (with increase in X_{CCl_4}) than those of lower excitation energy, one might expect excitation temperature to rise and then fall with increasing X_{CCl_4} . This may represent the formation and subsequent quenching of an intermediate species in the excitation process. Possible excitation and quenching mechanisms are discussed in detail below.

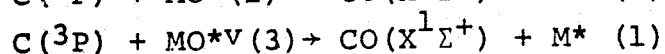
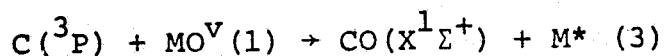
(5) Quenching Experiments

Chemical reaction mechanisms can often be elucidated through experiments in which a substance is added which can quench or otherwise remove a suspected reactive intermediate species. If the rate of the reaction is reduced (or the chemiluminescence quenched in the present case), the participation of the candidate intermediate species in the original reaction would be indicated. Although ideally a quencher affecting only one possible intermediate would be preferred, in practice such a selective quencher may not be available, and it may be necessary to deduce the identity of the unknown intermediate species from observations of the relative

effects of several less selective quenchers. In the present work, the effects of quenching by NO, O₂, CCl₄ and massive quantities of N₂ were studied.

The present section will discuss excitation mechanisms only to the extent required to explain why each type of quenching experiment was performed and what its results indicated. Detailed consideration of excitation mechanisms is deferred to a following section in which the results of all the quenching experiments, plus other experimental evidence, are drawn together to deduce the mechanisms by which the various excited species are produced. To clarify the following discussion of quenching experiments, the proposed primary mechanisms for M*, C₂* and MCl* excitation will be stated here. The detailed discussion of these processes and the evidence for choosing them over a host of alternative excitation mechanisms are reserved to the later section on mechanisms.

The proposed M* excitation mechanism is

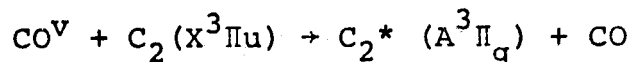
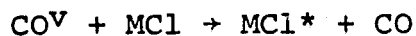


where "v" indicates vibrational and "*" electronic excitation, (1) and (3) denote singlets and triplets.

The excitation temperatures of triplet and singlet excited metal atoms are related to the respective vibrational tem-

peratures of singlet and triplet MO^V .

The proposed C_2^* and MCl^* excitation mechanisms are

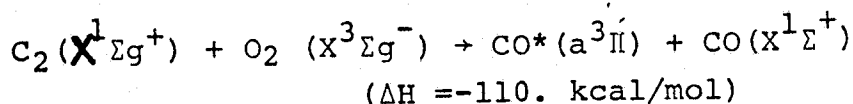
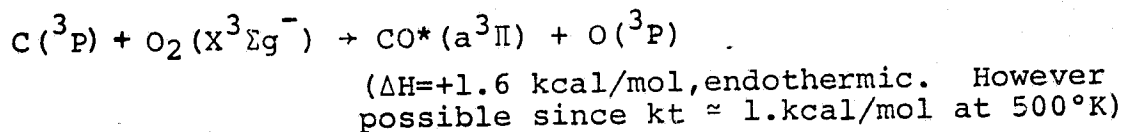
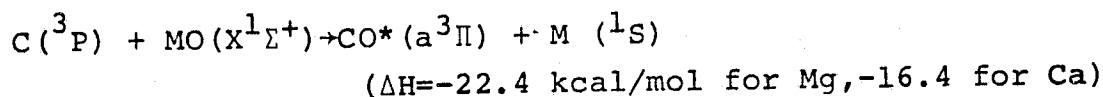
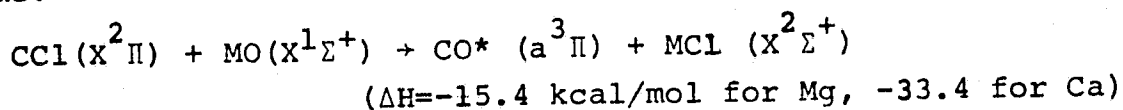


Spin conservation is definitely obeyed here since none of the species changes spin. (Spin conservation requires only constancy of the total spin). CO remains a singlet, MCl and MCl^* are both doublets and the initial state of C_2 is taken as the $\text{X}^3\Pi_u$ state which is 610 cm^{-1} ($\sim kT=350 \text{ cm}^{-1}$) above the true $\text{x}^1\Sigma_g^+$ ground state (Gaydon, 1968),

(a) Nitric Oxide Quenching

As has been discussed earlier, a likely source for the high electronic excitation energies observed (up to 7.6 eV.) is the formation of the C-O bond (11.1 eV.). Because of the dilute nature of the flame, the energetic species causing the metal atom excitation must be relatively long-lived, thus excluding all electronically excited states of CO except metastable states. The metastable $\text{a}^3\Pi$ state of CO, with electronic excitation energy of $\sim 6 \text{ eV}$ (and the possibility of additional vibrational excitation) and a radiative lifetime of 4.4 ± 1.1 milliseconds (Slanger and Black, 1971) is an excellent candidate for this role. $\text{CO}^*(\text{a}^3\Pi)$ can be

formed by a multitude of energetic, spin-allowed reactions between species likely to be present in the $M/CCl_4/O_2$ flame:

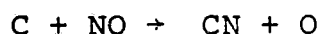


Note that the exothermicities quoted above have already had the ~ 6 eV excitation energy of $CO^*(a^3\Pi)$ subtracted from them.

Slanger and Black (1971) have demonstrated efficient electronic quenching of $CO^*(a^3\Pi)$ by ground state NO. They noted excitation of $NO^*(A^2\Sigma)$ and $NO^*(B^2\Pi)$ and emission of NO γ and β bands ($A \rightarrow X$ and $B \rightarrow X$ respectively), and showed that the NO γ bands are an effective tracer for small concentrations of $CO^*(a^3\Pi)$.

Experiments were therefore performed in which small amounts of NO (in the form of a 4.2-4.4% mixture in argon, to allow accurate control of small NO flows) were added to the $Mg/CCl_4/O_2$ and $Ca/CCl_4/O_2$ flames to detect any $CO^*(a^3\Pi)$ present. Overall NO concentration ranged up to 1.0% in the Mg flame and 1.7% in the Ca flame. All

optical emissions from the flames (M^* , both singlets and triplets; C_2^* , MCl^*) were strongly quenched by the addition of NO (with C_2^* much more strongly quenched than M^* or MCl^*). The NO β and γ bands were not seen at all indicating that $CO^*(a^3\Pi)$ is not present, since one would expect NO fluorescence of about the same strength as the M^* emission quenched. However, strong emission of the CN violet system was seen, which at first increased with increasing NO input, then peaked and decreased. The quenching of M^* emissions cannot be due to removal of metal atoms by reaction with NO, as the $M+NO \rightarrow MO + N$ reaction is about 50 kcal/mole endothermic. Its activation energy must thus be at least 50 kcal/mole, and at 500°K its rate would be negligible. The appearance of the CN violet band system suggests the reaction:



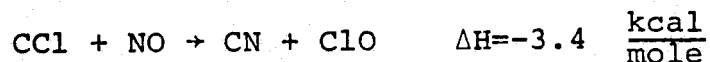
(with CN^* being excited by collision of CN with another energetic species, as this reaction lacks sufficient energy to excite the CN^* violet system). Braun et al. (1969) have reported near gas-kinetic rates for the reactions of 3P and 1D carbon atoms with NO. The quenching of the chemiluminescence by O_2 noted earlier suggests that the active species present in the flames is $C(^3P)$, as the rate constant for $C(^1D) + O_2 \rightarrow CO + O$ is smaller by at least a factor of 6 than that for $C(^3P) + O_2 \rightarrow CO + O$ and smaller by at least a factor of 20 than the $C + NO$

rate constant. Thus if $C(^1D)$ were the species involved, O_2 quenching should be almost unobservably small in comparison with NO quenching.

Another possible mechanism for quenching by NO would be the highly exothermic reaction:



Pearse and Gaydon (1963) and Herzberg (1950) list no spectral bands of NCl which might serve to indicate the occurrence of this reaction. The $b^1\Sigma^+ - X^3\Sigma^-$ band system of NCl (6200-7000Å) reported by Colin and Jones (1967) is extremely weak (being spin-forbidden) and might have gone undetected in the present study. However, the observed CN* emission would still require the occurrence of the $C+NO \rightarrow CN+O$ to produce CN. Excitation of CN* could then occur by collision of CN with an energetic species (probably CO^V). It does not appear likely that CN is formed by



as this reaction is far less exothermic than the reaction yielding $CO+NCl$. The extensive series of ClO bands in the 3500-4500Å region were not observed in the present work. However this is not conclusive proof that ClO is absent. This radical would be expected to be very

TABLE XIX

C Atom Reaction Rate Constants at Room Temperature
(Braun et al., 1969)

<u>Reaction</u>	<u>Rate Constant, cm³-sec⁻¹ molecule⁻¹</u>
$C(^1D) + N_2 \rightarrow C(^3P) + N_2$	$k \approx 2.5 \times 10^{-12}$
$C(^3P) + NO \rightarrow CN + O$	$k = 1.1 \times 10^{-10}$
$C(^1D) + NO \rightarrow CN + O$	$k = 9.2 \times 10^{-11}$
$C(^3P) + O_2 \rightarrow CO + O$	$k = 3.3 \times 10^{-11}$
$C(^1D) + O_2 \rightarrow CO + O$	$k < .5 \times 10^{-12}$

TABLE XX

Values Used in Estimating \bar{t} and \bar{X}

<u>Run</u>	<u>P, Torr</u>	<u>q_s std. cm³/min</u>	<u>$(X_{NO})_{1/2}$</u>	<u>$(X_{NO})_{1/2}^2 P^2 / q_s$</u>
MG-6-26-74	1.32	230.	0.205%	1.553×10^{-5}
CA-6-28-74	1.00	308	0.44%	1.428×10^{-5}

T=500°K (assumed)

$$\text{Shield slit area} = \frac{3}{16} \text{ inch} \times \frac{3}{4} \text{ inch} \times \left(\frac{2.54 \text{ cm}}{\text{inch}} \right)^2 = 0.9073 \text{ cm}^2$$

reactive with metal atoms and might be scavenged before excitation (e.g. by energy transfer from CO^V) could occur. However, as noted above, their relative exothermicities make the reaction of CCl with NO to form $\text{CO} + \text{NCl}$ much more likely than that to form $\text{CN} + \text{ClO}$. Thus, little CN is likely to be formed by the reaction of CCl with NO , yet strong CN^* emission is seen. Since the $\text{C} + \text{NO}$ reaction must occur to explain the appearance of CN , it is gratuitous to invoke the $\text{CCl} + \text{NO}$ reaction to explain the quenching of chemiluminescence, since the $\text{C} + \text{NO}$ reaction has a higher rate constant. Tyerman (1969) has reported a rate constant of $4.2 \times 10^{-12} \text{ cm}^3 \text{ molecule}^{-1} \text{ sec}^{-1}$ for the reaction of CCl with O_2 , which is a factor of 8 smaller than the value for $\text{C}(^3\text{P}) + \text{O}_2$ reported by Braun et al. (1969). It would seem reasonable that the relative rates of these two species with NO be in approximately the same ratio as those with O_2 .

The intensity of M^* emission was measured as a function of NO concentration and found to vary as $e^{-B[\text{NO}]}$ for both the Ca and Mg flames, where B is a constant and $[\text{NO}]$ is NO concentration, (Fig. III-38). Variation of O_2 concentration did not visibly affect the exponential decay of emitted intensity with $[\text{NO}]$. A Stern-Volmer plot of the same data

shows the experimental points rapidly diverging from the straight line given by the Stern-Volmer relation:

$$I_0/I = 1 + AP$$

where I_0/I is the ratio of the intensity with zero quencher (NO) concentration to the quenched intensity, P is the partial pressure of the quencher and A is proportional to the lifetime of the excited or active species in the absence of the quencher under consideration (NO).

The exponential decay of intensity with [NO] and the failure of the data to follow a Stern-Volmer line, both suggest that the process occurring is not a steady-state quenching process in which the concentration of the quenched species is determined by equating the rates of excitation and de-excitation (as is assumed in deriving the Stern-Volmer relation). It is instead a kinetic rate process in which the active species undergoes pseudo-first order decay in an excess of quencher (NO). A theory describing this process is derived below. It should be noted that except in the case of metastable $M^*(3P)$, direct quenching of M^* cannot occur, as the radiative lifetime ($\sim 10^{-8}$ sec) is much less than the time between collisions ($\sim 10^{-6}$ sec).

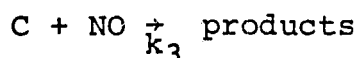
Consider a system where metal atoms are excited by a reaction represented schematically as



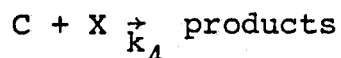
where C is an active species necessary for metal atom excitation to occur (which is probably carbon atoms, $C(^3P)$ as noted earlier).



Assume M^* has a short enough radiative lifetime $\tau_r = 1/k_2$ that M^* is not collisionally quenched. Since most M^* radiative lifetimes (other than metastable states) are $\sim 10^{-8}$ sec, this is reasonable. Represent the reaction of C and NO by



and all other reactions removing C (including that with Y) by:



The short radiative lifetime (large k_2) and absence of collisional quenching of M^* allows the equating of the excitation and radiative decay rates:

$$k_1 [C][Y] = k_2 [M^*] = I$$

Thus $I = k_1 [C][Y] \sim [C]$ if the concentration of Y does not vary with [NO]. Writing the rate equation for [C]:

$$\frac{d[C]}{dt} = -k_4 [X][C] - k_3 [NO][C]$$

Integrating this equation:

$$[C] = Ae^{-\{k_4[X] + k_3[NO]\}t}$$

$$\text{and } I = k_1 [C][Y] = k_1 [Y] Ae^{-\{k_4[X] + k_3[NO]\}t}$$

For [NO] = 0:

$$I_0 = k_1 [Y] Ae^{-k_4[X]t}$$

The constant A is the same in both cases as $A=[C]_{t=0}$ and at $t=0$ no reaction with NO has occurred yet. Dividing I by I_0 :

$$I/I_0 = e^{-k_3[NO]t}$$

where I_0 is the intensity value at zero [NO]. Defining \bar{t} as an average residence time in the flame, one may represent the effect of NO on the total emission from the flame by:

$$\bar{I}/\bar{I}_0 = e^{-k_3[NO]\bar{t}}$$

which is precisely the experimentally observed [NO] dependence, with $B=k_3\bar{t}$. Interpreting \bar{t} in this manner as a residence time in a fixed region, it is possible to estimate the effect upon \bar{t} of changes in carrier gas flow rate and chamber pressure. Let subscript "s" refer to a set of standard conditions for the carrier gas flowing through the nozzle (e.g. 1 atm at 70°F). Since nozzle area is fixed, the gas velocity is proportional to the volumetric flow rate at the nozzle exit. Since flow is subsonic (as shown above, Chapter II), the pressure at this point equals the chamber pressure. By continuity,

$$q_s \rho_s = q \rho = \text{constant}$$

where q is volumetric flow rate and ρ is gas density.

By the ideal gas law,

$$\rho = P/RT$$

whence:

$$q = q_s \rho_s / \rho = q_s \cdot \frac{P_s}{P} \cdot \frac{T}{T_s}$$

Comparing two different experimental conditons, 1 and 2, and noting that $\bar{t} \sim \frac{1}{V} \sim \frac{1}{q}$ (where V is gas velocity), it can be shown that

$$\frac{\bar{t}_1}{\bar{t}_2} = \frac{(q_s)_1}{(q_s)_2} \cdot \frac{P_2}{P_1} \cdot \frac{T_1}{T_2}$$

Heat losses occur during flow of the carrier gas through the nozzle (as evidenced by metal condensation) and mixing with the chamber gas occurs at the nozzle exit. Thus the isentropic relation cannot be used to relate T at the nozzle exit to the furnace temperature and pressure and the chamber pressure. Instead, since it has been observed that this exit temperature is relatively insensitive to furnace temperature (which itself varies only by about 200°C between Ca and Mg runs), it will be assumed that T at the nozzle exit is constant for all runs. Then the factor $T_1/T_2 \approx 1$ and

$$\frac{(\bar{t})_2}{(\bar{t})_1} \approx \frac{(q_s)_1}{(q_s)_2} \cdot \frac{P_2}{P_1}$$

Since $[NO] \equiv X_{NO}P$, where X_{NO} is the NO mole fraction, then

$$k[NO]\bar{t} \sim k X_{NO}^2 P^2 / q_s$$

Using the data presented in Table XX for NO quenching experiments in $Mg/CCl_4/O_2$ flames, the rate constants for the quenching reactions in the two flames can be compared.

Since both quenching curves (Fig. III-38) are exponential in form, the rate constants can be compared by comparing the value of $[\text{NO}]$ at which \bar{I}/\bar{I}_0 has some fixed value, e.g. $1/2$.

$$k_{\text{Ca}} [\text{NO}]_{1/2, \text{Ca}} \bar{t}_{\text{Ca}} = k_{\text{Mg}} [\text{NO}]_{1/2, \text{Mg}} \bar{t}_{\text{Mg}} = \ln 2$$

Using the relation for $k[\text{NO}]\bar{t}$ derived above:

$$(kX_{\text{NO}1/2} P^2 / q_s)_{\text{Ca}} = (kX_{\text{NO}1/2} P^2 / q_s)_{\text{Mg}}$$

$$\frac{k_{\text{Mg}}}{k_{\text{Ca}}} = \frac{1.428 \times 10^{-5}}{1.553 \times 10^{-5}} = 0.920 \approx 1.$$

The two rate constants are thus the same within the accuracy of the experimental data and the assumptions made. This equality of the rate constants for NO quenching in the Ca and Mg flames suggests that neither Ca nor Mg is involved, but that the same active species is being quenched in both cases. The observation of CN* emission in both flames shows that the reaction $\text{C} + \text{NO} \rightarrow \text{CN} + \text{O}$ is occurring in both flames, and as noted earlier, the rate constant of this reaction is nearly gas-kinetic. It thus appears that NO quenching of the chemiluminescent emission from Ca and Mg/ CCl_4/O_2 flames occurs by destruction of C atoms which are necessary to the excitation of the

chemiluminescence.

Assuming that this is the case, the known rate constant for the $C(^3P) + NO \rightarrow CN + O$ reaction, $1.1 \times 10^{-10} \text{ cm}^3 \text{ molecule}^{-1} \text{ sec}^{-1}$ (Braun et al., 1969) can be used to estimate \bar{t} from the NO quenching results. A corresponding distance \bar{X} may be defined, $\bar{X} = U\bar{t}$, where U is the carrier gas flow velocity. In the calculation which follows, Ca flame data are used, as the Ca and Mg results were shown above to be equivalent.

$$[NO]_{1/2} = 0.44 \times 10^{-2} \times \frac{1.00 \text{ torr}}{760 \text{ torr}} \times \frac{273^\circ K}{500^\circ K} \times \frac{6.025 \times 10^{23} \text{ molecules}}{2.24 \times 10^4 \text{ cm}^3} =$$

$$= 0.849 \times 10^{14} \text{ molecules/cm}^3$$

$$\therefore \bar{t} = \frac{\ln 2}{k_3 [NO]_{1/2}} = \frac{0.693}{1.1 \times 10^{-10} \text{ cm}^3 \text{ molecule}^{-1} \text{ sec}^{-1} \times 0.849 \times 10^{14} \text{ molecules/cm}^3} =$$

$$= \bar{t} = 0.742 \times 10^{-4} \text{ sec}$$

$$U = \frac{308 \text{ Std. cm}^3/\text{min} \times \frac{760 \text{ torr}}{1.00 \text{ torr}} \times \frac{500^\circ K}{273^\circ K}}{0.9073 \text{ cm}^2 \times 60. \text{ sec/min}} = 7.88 \times 10^3 \text{ cm/sec}$$

$$\therefore \bar{X} = U\bar{t} = 7.88 \times 10^3 \times 0.742 \times 10^{-4} = 0.584 \text{ cm} = 5.84 \text{ mm.}$$

It is at once evident that the value of \bar{X} calculated above is far smaller than the observed dimensions of the flame (5-10 cm.), and a simple calculation serves to show that the value of \bar{t} calculated above is far smaller than the residence time in the observed flame volume. The mean

residence time in a volume V , through which a volumetric flow q is passing may be expressed as

$$\bar{\tau} = V/q$$

(This quantity is more precisely denoted as the space-time in chemical reactor theory. However for constant density and number of moles it is identical to the mean residence time). (Cooper and Jeffreys, 1971, Denbigh and Turner, 1971; Boudart, 1968).

Consider a typical flame about 5cm diameter x 10cm long, with a volume of $\sim 200 \text{ cm}^3$, and the same flow conditions used earlier

$$\therefore q = 308 \text{ std cm}^3/\text{min} \times \frac{760 \text{ torr}}{1.00 \text{ torr}} \times \frac{500}{273} = 6.50 \times 10^3 \text{ cm}^3/\text{sec}$$

$$V_{\text{obs}} = 200 \text{ cm}^3$$

$$\therefore \tau_{\text{obs}} = V_{\text{obs}}/q = \frac{2 \times 10^2}{6.50 \times 10^3} = 30.8 \text{ milliseconds}$$

(where the subscript "obs" indicates a value based on the observed flame volume, 200 cm^3).

$$\therefore \frac{\bar{\tau}}{\tau_{\text{obs}}} = \frac{0.742 \times 10^{-4} \text{ sec}}{3.08 \times 10^{-2} \text{ sec}} = \frac{1}{415} = 2.41 \times 10^{-3}$$

The value of $\bar{\tau}$ calculated from NO quenching is thus a factor of more than 400 smaller than the mean residence time calculated from carrier gas flow rate and flame volume.

This difficulty is easily resolved, however by noting

that in a low pressure flame where the rates of chemical reaction and light emission vary as $I(t)/I(t=0)=e^{-Bt}$, the volume corresponding to the observed flame boundary is not the appropriate volume to use in calculating the mean residence time. Since the location of the flame boundary is defined by the emitted intensity, I , falling to the limit of detectability, (Reed and Rabinovitch, 1957; Heller and Polanyi, 1936) it is clear that most of the observed emission comes from far inside this boundary, and the effective volume (and hence mean residence time) relevant to light emission is much smaller. In effect each volume element is weighted by the factor e^{-Bt} .

A quantitative estimate of this effect may be obtained by considering the simplified case of constant flow velocity, $U=U_0=\text{const.}$ and spherical flame shape centered on the nozzle as $r=0$.

Then $dr/dt = U_0$ and $r=U_0t$.

The effective volume, V_{eff} is then given by multiplying each volume element by the weighting factor e^{-Bt} and integrating:

$$V_{\text{eff}} = \int_0^{t_{\text{max}}} e^{-Bt} dV$$

where t_{max} is the value of t at the edge of the flame and

$$dV = 4\pi r^2 dr = 4\pi r^2 dr = 4\pi U_0^3 t^2 dt.$$

$$\therefore V = \int_0^{t_{\text{max}}} 4\pi U_0^3 t^2 e^{-Bt} dt$$

V_{eff} has the physical meaning of the volume with constant

$I=I(t=0)$ which would produce the same total emission as the actual flame.

$$\therefore \frac{\bar{\tau}_{\text{eff}}}{\bar{\tau}_{\text{obs}}} = \frac{V_{\text{eff}}}{V_{\text{obs}}}$$

and the effective residence time might be expected to be in the range $\approx 10^{-3}$ - 10^{-2} times $\bar{\tau}_{\text{obs}} = V_{\text{obs}}/q$. It is now clear that the quantity \bar{t} calculated from NO quenching is identical to $\bar{\tau}_{\text{eff}}$ and the observed ratio

$$\frac{\bar{t}}{\bar{\tau}_{\text{obs}}} = 2.41 \times 10^{-3} = \frac{\bar{\tau}_{\text{eff}}}{\bar{\tau}_{\text{obs}}}$$

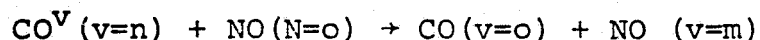
is explained, as it falls within the range just calculated.

RATIO is the intensity at the visible flame boundary (i.e. the least detectible brightness) divided by that at the center of the flame (i.e. $t=0$). Using the value of Hardy and Perrin (1932) for the "least perceptible brightness" detectible by the dark-adapted human eye and measured total photon emission rates (discussed later in the section on quantum yields), a value of 1.6×10^{-8} is found for RATIO (Zwillenberg, 1975). This corresponds to $V_{\text{eff}}/V_{\text{obs}} = 1.04 \times 10^{-3} = 1/965$.

In view of the many approximations made, this is excellent agreement with the value of $2.4 \times 10^{-3} = 1/415$ obtained from NO quenching. Thus, the apparent discrepancy between \bar{t} (from NO quenching) and $\bar{\tau}_{\text{obs}}$ (from flame size and

flow rate) is explained by the similar difference between V_{eff} and V_{obs} .

Several tenths of a percent of added NO (Table XVI, Fig. III-37) did not appear to appreciably affect the metal atom excitation temperature. This was not surprising, since (as discussed later) this temperature is believed to correspond to a vibrational temperature of vibrationally excited metal oxide, MO^V . As described below, hundred-fold larger additions of N_2 produced only moderate reductions in T_{ex} . Examining the vibrational frequencies of the species involved, NO (1904 cm^{-1}) would not be expected to be more efficient in vibrational relaxation of MO^V (700-800 cm^{-1}) than N_2 (2345 cm^{-1}), but might possibly more effectively relax certain vibrational levels of CO^V due to the near resonance at $v=10$ of CO^V (1898 cm^{-1}). Such vibrational relaxation of CO^V by NO cannot, however, account for the overall quenching of emitted intensity (the I vs. [NO] curves). The most likely v-v exchange process is the transfer of a single vibrational quantum, with the transition probability falling off rapidly with increasing number of quanta. Complete quenching of CO^V :

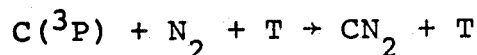


would have a negligible probability. However, since the removal of C atoms by reaction with NO would also

reduce the rate of formation of CO^{V} (by the $\text{C} + \text{O}_2$ reaction), the quenching of M^* emission by NO proves only that C atoms are necessary to the excitation process. It does not differentiate between the direct $\text{C} + \text{MO} \rightarrow \text{CO} + \text{M}^*$ excitation process and the alternative, vibrational-electronic energy transfer between CO^{V} and metal atoms.

(b) N₂ Quenching

Addition of massive quantities of N₂ (by substitution for argon) to Ca/CCl₄/O₂ and Mg/CCl₄/O₂ flames (45% and 78% N₂ respectively) produced no visible decrease in overall emitted intensity, in contrast to the strong effect of much smaller amounts of NO described above. However, N₂ was observed to reduce the excitation temperatures (from Iλ/gu vs. Eu plot) of both singlet and triplet metal atoms by about 1000°K (Tables XVII and XVIII). These observations are consistent with the mechanism $C + MO^V \rightarrow CO + M^*$ mentioned earlier. C atoms are not removed by reaction with N₂ as they are with NO. The reaction $C + N_2 \rightarrow CN + N$ is 47 kcal/mole endothermic and hence of negligible importance at 500°K. Braun et al. (1969) have noted that C(³P) atoms react with N₂ primarily by the pressure-dependent reaction



where T is a third body. Husain and Kirsch (1971) give a rate constant of $(3.1 \pm 1.5) \times 10^{-33} \text{ cm}^6 \text{ molecule}^{-2} \text{ sec}^{-1}$ for this reaction. At a total gas density of $\sim 10^{16} \text{ cm}^{-3}$, this is equivalent to a bimolecular rate constant of $3 \times 10^{-17} \text{ cm}^3 \text{ molecule}^{-1} \text{ sec}^{-1}$, which is extremely small. N₂ would be expected to reduce the MO^V vibrational temperature by vibrational relaxation, as indicated by the observed re-

duction in M^* excitation temperature. However, as noted earlier, removal of more than one vibrational quantum from MO^V in each collision with N_2 has a low probability, and hence complete removal of all vibrational energy from MO^V is unlikely. Moreover, even if this occurred, M^* could still be produced by the quite exothermic reaction $MO(v=0) + C \rightarrow CO + M^*$. One would therefore not expect quenching of overall emitted intensity by N_2 addition.

Referring to Tables XVII and XVIII, it is seen that N_2 addition reduces the excitation temperatures of Ca triplets and singlets and Mg triplets by about $1000^\circ K$ and of the Ca triplet states with two excited electrons by about $2900^\circ K$. These reductions are statistically significant at the $P=0.10$ level or better. (Tables XVII and XVIII). An apparent reduction of Mg singlet excitation temperature by about $170^\circ K$ is not statistically significant at this level. These reductions are with respect to \bar{T} , the average of all runs for a given metal and multiplicity except those with N_2 . However, as shown in Fig. (III-37) excitation temperature is a function of $[CCl_4]$, and when this variation is considered, the reduction of T_{ex} by N_2 is seen to be greater, about $1600^\circ K$ for Mg triplets, vs. the $1000^\circ K$ reduction relative

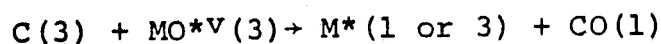
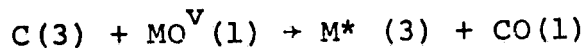
to T noted above.

It thus appears that Mg(3), Ca(3) and Ca(1) excitation temperatures are significantly reduced by N₂ addition, while Mg(1) is affected little if at all. ((1) and (3) denote singlets and triplets). Because these conclusions are based on only one N₂ quenching experiment for each flame, the possibility that the anomalously low quenching of Mg(1) is erroneous cannot be excluded, except by further experiments. However, the effect may be real and could be explained as follows.

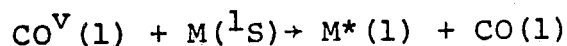
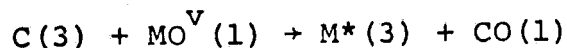
Although it appears likely that the effect of N₂ addition is produced by vibrational relaxation of a vibrationally excited species, the first question to be answered is whether this is CO^V or MO^V. There is not good resonance between the vibrational frequencies of MO, N₂ (v=0) and CO(v=n). The situation becomes worse as n increases. The existence of resonances at high vibrational levels of N₂ is irrelevant, as all N₂ present will be in v=0. Callear and Lambert (1969) have noted that vibrational relaxation occurs more rapidly for species with a higher dipole moment (MO vs. CO), which might produce more efficient quenching of MO^V. Resonance might occur by transfer of several vibrational quanta of MO^V into one vibrational quantum of N₂.

Consider the two alternative sets of reactions :

I:



II.



together with the following data rearranged from Table XVII:

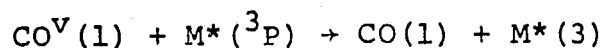
Table XXI

	<u>T, °K</u>	<u>T(N₂), °K</u>
Mg(3)	5128	4182
Ca(3)	5940	4891
Mg(1)	2530	2359
Ca(1)	3414	2341

It is seen that $T(\text{N}_2)$ is nearly equal for Mg(1) and Ca(1), and only slightly lower than the unquenched value, \bar{T} , for Mg(1). Thus, there may be a limit to how far T_{ex} can be quenched. The C+MO reaction may produce M^* with $T_{\text{ex}} \approx 2300^\circ\text{K}$ for MO in $v=0$, and any vibrational energy in MO^{V} would serve to raise T_{ex} . Thus in the case of Mg, $\text{MO}^*\text{V}(3)$ may be formed with very little vibrational energy and therefore cannot lose very much to N_2 . In the case of Ca the rate of reaction with O_2 is faster than that of Mg (as observed in Ca/ O_2 and Mg/ O_2 flames). Hence a higher

steady state vibrationally excited population of MO^V can be maintained against quenching processes and there can be significant vibrational energy in $CaO^*(3)$ which can be lost to N_2 . The excitation of high vibrational levels of singlet excited states of CaO (observed in the Ca/O₂ flame and discussed earlier) makes similar vibrational excitation of unobserved metastable triplet states of CaO seem plausible.

Note that in both Reactions I and II above, all triplets are formed from the $C(^3P) + MO^V$ reaction, and none from CO^V . Since triplets are quenched by NO addition, it must be MO^V rather than CO^V which is being vibrationally quenched by N_2 . The only way triplets could be formed from CO^V would be



However as shown below, the metastable $M^*(^3P)$ level is quenched much more strongly by O₂ than any other triplet (or singlet) excited state. This could not be the case if the other triplets were being formed from metastable $M^*(^3P)$. The formation of $M^*(1)$ from CO^V as shown in Reaction II does not seem plausible. It would be fortuitous if quenching of CO^V by N_2 should produce precisely the same degree of reduction of \bar{T} of Ca singlets as quenching of MO^V by N_2 does for triplets. The large difference

in vibrational frequency between CO and MO should cause their rates of vibrational relaxation by N₂ to differ considerably. Also, it does not seem plausible that CO_v would be quenched less by N₂ in Mg than in Ca flames, as evidenced by the greater quenching of Ca(1) than Mg(1). It thus appears that MO^V rather than CO_v is the species whose relaxation by N₂ addition effects Tex. Even more conclusively, measurements of M(¹S) concentration (by self-absorption), discussed later, show that [M(¹S)] is too low for collisional excitation by CO^V to account for measured rates of photon emission.

(c) Quenching by O₂ and CCl₄

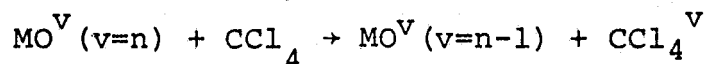
Quenching of chemiluminescence by O₂ and CCl₄ differs from the quenching processes discussed earlier in that the same reactant is responsible both for excitation and quenching. One would therefore expect a curve of emitted intensity vs. reactant concentration which rises, reaches a maximum and then decays, and this is what is observed (Figs. III-29 through III-32, III-34. It has been found that if the experimental data are normalized by plotting $Y = I/I_{\max}$ (where I_{\max} is the peak value of each curve) vs. $u = [X]/[X]_{\max}$ (where $[X]_{\max}$ is the reactant concentration at the maximum) then data from many experiments, including singlets, triplets and metastable lines, and both I vs. [O₂] and I vs. [CCl₄] data fit very well the equation

$$Y = eue^{-u}$$

This is shown in Fig. (III-39) in which data from Figs. (III-29, III-31, III-36 and III-33) are fit to a single normalized curve. The data of Fig. (III-30) also are fit well by this curve, but were omitted from Fig. III-39 because the large degree of scatter in Fig. (III-30) would obscure the good fit of the other data plotted in Fig. (III-39). Simplified kinetic schemes have been proposed (Zwillenberg, 1975) which can reproduce the behavior of these normalized I vs. [X] curves. Estimates for the rate constants of the quenching reactions can then be obtained, and are discussed in detail below.

A necessary prerequisite to a quantitative treatment of chemiluminescence quenching is the identification of the species affected by the additive. In the case of quenching by O_2 , the nearly gas kinetic rate constant of $C(^3P) + O_2 \rightarrow CO + O$ makes this reaction a more likely candidate than either of the slower reactions $C(^1D) + O_2$ and $CCl + O_2$, as has been discussed earlier. In addition, the participation of $C(^1D)$ in the excitation of chemiluminescence would lead one to predict a large difference in O_2 quenching of M^* singlet and triplet emission, which is not observed. In the case of quenching by CCl_4 , two possibilities are suggested by the proposed $C + MO^V \rightarrow CO + M^*$ excitation mechanism. These are the removal of C atoms by reaction with CCl_4 or one of its degradation products (e.g. CCl),

or the vibrational quenching of MO^{V} by CCl_4 which has close vibrational frequency resonances with MgO and CaO . However, MO^{V} quenching by CCl_4 could remove only 1 or 2 vibrational quanta per collision. Thus, even if this process occurred on every collision, about 40 collisions would be needed to remove all vibrational energy from MO^{V} (assuming vibrational frequency $\sim 700 \text{ cm}^{-1}$ and about $28,000 \text{ cm}^{-1}$ of vibrational energy in MO^{V}). Also, the process $\text{C} + \text{MO}(\text{v}=0) \rightarrow \text{CO} + \text{M}^*$ is quite exothermic and could produce M^* with energies up to about 7 eV., and this would not be quenched by CCl_4 . Thus it appears that quenching of chemiluminescence by CCl_4 is a result of the removal of C atoms. However, some vibrational relaxation of MO^{V} by CCl_4 :



may occur, having the effect of lowering the vibrational temperature of MO^{V} (and hence the excitation temperatures of M^*) as has been observed (Fig. III-37). The close resonance in vibrational frequency between CCl_4 and MO makes CCl_4 at $\sim 0.4\%$ as efficient in this respect as a mixture containing 40-80% N_2 (no resonance). Such vibrational relaxation might also account for the displacement of the peak of the I vs. $[\text{CCl}_4]$ curve to lower

$[\text{CCl}_4]$ for higher Eu (Fig. III-35). The similar I vs. $[\text{CCl}_4]$ behavior of M^* , MCl^* and C_2^* emission may be explained by a reduction in the rate of production of CO^V (which excites C_2^* and MCl^*) by consumption of C atoms. Since this is the same reaction quenching the M^* emission, the similar I vs. $[\text{CCl}_4]$ curves are thus explained.

The proposed M^* excitation mechanism, $\text{C}(^3\text{P}) + \text{MO} \rightarrow \text{CO} + \text{M}^*$, plus the conclusions reached above that quenching by both O_2 and CCl_4 is due to destruction of C atoms, form the basis upon which a quantitative model of the variation of I with $[\text{O}_2]$ and $[\text{CCl}_4]$ can be constructed. A simple approach is to assume (as was done earlier in the case of NO quenching) that carbon atoms are formed initially by reaction of metal vapor and CCl_4 at a rate much faster than any processes removing C atoms, so an initial carbon atom concentration is produced which then decays by reaction with O_2 and CCl_n ($n=1, \dots, 4$). This does not require that the rate constant for C atom production be larger than those for C atom decay. As the C atom concentration builds up from zero, there must be a region near the nozzle (where metal atom concentration is a maximum and both $[\text{O}_2]$ and $[\text{CCl}_4]$ a minimum) where the rate of production of C atoms $\sim [\text{CCl}_4] [\text{M}]$ is much larger than

the rate of decay $\sim [C] [X]$. Of course, the larger the rate constant for C atom production, the larger this region can be. Rate constant values for the reactions of CCl_4 with Ca and Mg are not available. Nearly gas-kinetic values for the analogous $Na + CCl_4$ reaction have been published, but some disagreement exists in the literature. Polanyi and Heller (1936) reported a rate of $1.6 \times 10^{-10} \text{ cm}^3 \text{ molecule}^{-1} \text{ sec}^{-1}$ at $543^\circ K$. Kaufman and Reed (1963), using a correction of Reed and Rabinovitch (1955) for convective flow and considering reaction of Na with CCl_n ($n=1, \dots, 3$), reported rates of 2.5×10^{-12} and $0.99 \times 10^{-11} \text{ cm}^3 \text{ molecule}^{-1} \text{ sec}^{-1}$ for the initial Cl abstraction and for the overall reaction respectively. Steinfeld and Kinsey (1970) report molecular beam data (for which the corrections of Kaufman and Reed are not relevant as only single collisions are involved) showing a total reactive cross section of $25. \text{ \AA}^2$ which is equivalent to a rate constant of $2.2 \times 10^{-10} \text{ cm}^3 \text{ molecule}^{-1} \text{ sec}^{-1}$ at $500^\circ K$, nearly the same as the original result of Heller and Polanyi (1936).

Assuming "instantaneous" C atom formation (fast enough so all CCl_4 is converted quantitatively to C atoms before any C atoms are consumed) yields the following expression for emitted intensity, I as a function of $[O_2]=a$ and

$$[\text{CCl}_4] = b:$$

$$I \sim a b e^{-(k_2 b + k_3 a) \bar{t}}$$

Here \bar{t} is the effective mean residence time in the flame determined from NO quenching, and k_2 and k_3 respectively are the rate constants for removal of C atoms by O_2 and CCl_4 . The derivation of this expression, which reproduces the experimental $I \sim u e^{-u}$ relation, is detailed elsewhere (Zwillenberg, 1975). Differentiating with respect to $[\text{O}_2]$ and $[\text{CCl}_4]$ respectively yields the following expressions for the rate constants in terms of the maxima of the experimental I vs. $[\text{O}_2]$ and $[\text{CCl}_4]$ curves:

$$k_3^{(2)} = \frac{1}{[\text{O}_2]_{\text{max}} \bar{t}} = \frac{1}{b_{\text{max}} \bar{t}}$$

$$k_3^{(2)} = \frac{1}{[\text{CCl}_4]_{\text{max}} \bar{t}} = \frac{1}{a_{\text{max}} \bar{t}}$$

where the superscript (2) denotes this particular method of calculation, to distinguish it from others presented below.

The above analysis does not, however, account for the experimental observation that $[\text{O}_2]_{\text{max}}$ seems to increase with increasing $[\text{CCl}_4]$, and $[\text{CCl}_4]_{\text{max}}$ with increasing $[\text{O}_2]$. This can be corrected by considering that the rate of C atom formation, though rapid, is not instantaneous. If the initial C atom concentration

is assumed to be a steady state value obtained by equating production and decay rates (Zwillenberg, 1975) the emitted intensity is found to be

$$I \sim \frac{ab}{k_2b + k_3a} e^{-(k_2b + k_3a)\bar{t}}$$

which no longer exactly fits the relation $I \sim ue^{-u}$, but which approximates it at low b or low a . Finding the maximum and making several approximations based on an order-of-magnitude analysis (Zwillenberg, 1975), yields the following expressions for the rate constants:

$$k_2^{(3)} = \frac{1}{b_{\max}} \sqrt{\frac{k_2a}{\bar{t}}}$$

$$k_3^{(3)} = \frac{1}{a_{\max}} \sqrt{\frac{k_2b}{\bar{t}}}$$

These are seen to include variation in the proper sense with the concentration of the reactant not varied.

Another approximate method of deriving rate constant values from the experimental I vs. $[O_2]$ and $[CCl_4]$ curves is to consider the decay portion of the curve as a pure exponential taking the slope as a measure of the rate constant (see Figs. III-33, 34, and 35), and neglecting additional excitation by the added reactant. Then, since $I \sim e^{-k[X]\bar{t}}$ in this portion of the curves, the rate constants are given by:

$$k_2^{(1)} = - \frac{1}{\bar{t}} \frac{d \ln I}{d[O_2]}$$

$$k_3^{(1)} = - \frac{1}{\bar{t}} \frac{d \ln I}{d[CCl_4]}$$

for atomic lines radiated by non-metastable excited states. For metastable states, this would give the sum of the rate constants for quenching of C atoms and the metastable. In that case:

$$k_2^{(1)} + k_4^{(1)} = - \frac{1}{\bar{t}} \frac{d \ln I}{d[O_2]}$$

$$k_3^{(1)} + k_5^{(1)} = - \frac{1}{\bar{t}} \frac{d \ln I}{d[CCl_4]}$$

where k_4 and k_5 are the rate constants, respectively, for quenching of metastable M^* by O_2 and CCl_4 respectively. Since $k_2^{(1)}$ and $k_3^{(1)}$ can be found from the slopes for non-metastable lines, $k_4^{(1)}$ and $k_5^{(1)}$ can be estimated. However, it is clear that since this method of calculation neglects added excitation in the exponential portion of the I vs. $[O_2]$ and $[CCl_4]$ curves, the decay rate constants calculated will probably be too small.

The use of the effective mean residence time \bar{t} in the calculations above is actually equivalent to determining the various rate constants $k^{(1)}$ in terms of the rate constant, k_{C-NO} , for the $C + NO$ reaction, since this value was used in determining \bar{t} . Thus, letting \bar{t}' refer to the NO quenching experiment:

$$\frac{k_2^{(1)}}{k_{e-NO}} = \frac{\bar{t}'}{\bar{t}} \frac{d \ln I / d [O_2]}{d \ln I / d [NO]}$$

$$\frac{k_3^{(1)}}{k_{C-NO}} = \frac{\bar{t}'}{\bar{t}} \frac{d \ln I / d [CCl_4]}{d \ln I / d [NO]}$$

and we are actually comparing the slopes of the exponential tails of the $[O_2]$ and $[CCl_4]$ quenching curves with that of the $[NO]$ quenching curve. The ratio \bar{t}'/\bar{t} can be calculated from the relation derived earlier between residence time, carrier gas flow and chamber pressure:

$$\frac{\bar{t}'}{\bar{t}} = \frac{q_s}{q'_s} \cdot \frac{p}{p'}$$

where the primed quantities refer to the NO quenching case and subscript "s" refers to standard conditions.

A better method for calculating the rate constant for quenching of metastable M^* by O_2 is the following: The rate equations are set up for all excitation and quenching processes. The approximations $k_2b \gg k_3a$ and $k_4b \gg k_6$ (where k_6 is the radiative transition probability of the metastable) are made. dI/db is set equal to zero to find the maximum, yielding the equation

$$(k_4^{(4)}/k_2) = 1 + \frac{\ln(k_4^{(4)}/k_2)}{b_{\max} k_2 \bar{t}}$$

which can be solved iteratively for $(k_4^{(4)}/k_2)$ being careful to avoid the trivial solution, $(k_4^{(4)}/k_2)=1$. This solution is rejected since for $k_4=k_2$, the I vs. O_2 curve would have no maximum (Zwillenberg, 1975).

Rate constant values calculated by each of these methods, where applicable and where experimental data are available, are shown in Table XXII. Values shown for the rates of quenching of C atoms and $Mg^*(^3P)$ metastable by N_2O were calculated from one experiment on the $Mg/CCl_4/N_2O$ flame. As was expected, the $k^{(1)}$ values for each rate constant are the lowest, since the effect of excitation in partially offsetting decay was neglected in this method. $k^{(3)}$ values were, in general, smaller than $k^{(2)}$ values. There was fair agreement between $k^{(2)}$ and $k^{(3)}$ values and literature values (where available). Near gas kinetic values of 1.9, 2.1 and $6.5 \times 10^{-11} \text{ cm}^3 \text{ molecule}^{-1} \text{ sec}^{-1}$ were obtained for $Mg^*(^3P)+N_2O$, $Mg^*(^3P)+O_2$ and $Ca^*(^3P)+O_2$, respectively. No literature values of these rates could be found for comparison, but the exothermicity of these reactions (due to the energy carried by the excited metastable atom) and the possibility of an electron-jump mechanism make such high rates quite plausible. The O_2 quenching rate for $Ca^*(^3P)$ is approximately three times that of $Mg^*(^3P)$, which is consistent with the observation that O_2 quenching

Table XXII

Rate Constants Calculated From I vs. [O₂] and [CCl₄]

Curves by Different Methods. (All values in cm³molecule⁻¹sec⁻¹.)

<u>Reaction</u>	<u>k (1)</u>	<u>k (2)</u>	<u>k (3)</u>	<u>k (4)</u>	<u>Literature Values</u>
Quenching by CCl ₄ , probably C(3P)+CCl	**2.0x10 ⁻¹¹	(4.4±0.2)x10 ⁻¹¹	3.6x10 ⁻¹¹	NA	see discussion
C(3P)+O ₂	---	(3.4±2.0)x10 ⁻¹¹	(8.3 ⁺ 3.4x10 ⁻¹²	NA	3.3x10 ⁻¹¹ (Braun et al., 1969) (3.3±1.5)x10 ⁻¹¹ (Husain & Kirsch, 1971)
C(3P)+N ₂ O	---	0.94x10 ⁻¹¹	0.58x10 ⁻¹¹	NA	(2.5±1.6)x10 ⁻¹¹ (Husain & Kirsch, 1971)
Ca*(3P)+O ₂	**1.2x10 ⁻¹¹	NA	NA	6.5x10 ⁻¹¹	---
Mg*(3P)+O ₂	---	NA	NA	2.1x10 ⁻¹¹	---
Mg*(3P)+N ₂ O	---	NA	NA	1.9x10 ⁻¹¹	---

--- = insufficient data

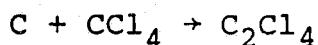
NA = method not applicable

** = probably low as neglects additional excitation by quencher

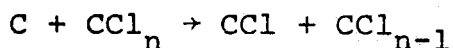
Uncertainties listed in experimental values are mean deviation of several values.

of the two species is of about the same magnitude, despite the ~ 5 times longer radiative lifetime of $\text{Mg}^*(^3\text{P})$ vs. $\text{Ca}^*(^3\text{P})$.

It should be noted that the purpose of the present investigation is not the precise determination of rate constants, nor was the experimental technique chosen with that goal in mind. For this reason, in only a few of the many experiments performed was the complete I vs. $[\text{O}_2]$ or $[\text{CCl}_4]$ curve measured, which explains the blank spaces in Table XXII. However approximate values of rate constants can be extracted from data of experiments not originally designed for their determination. These values can help identify the excitation and quenching processes governing the excited state populations which were the primary subject of the present investigation. A case in point is the quenching of $\text{C}(^3\text{P})$ atoms by a species derived from CCl_4 , for which a near gas kinetic rate constant of $\sim 4 \times 10^{-11} \text{ cm}^3 \text{ molecule}^{-1} \text{ sec}^{-1}$ was obtained. Possible reactions of C atoms include insertion (addition)



abstraction,



and



Rate constant values for some related reactions are shown in Table XXIII.

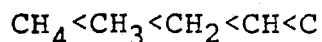
Table XXIII

Literature Rate Constant Values for Reactions of C, CCl₄ and Related Molecules

<u>Reaction</u>	<u>cm³ molecule⁻¹ sec⁻¹</u>	<u>Reference</u>	<u>Comments</u>
H+CCl ₄ →HCl+CCl ₃	~10 ⁻¹³	Seidel, Martin & Mietzner (1965)	Calculated for 500°K from steric factor =0.13, Ea=5kcal/mol.
C(³ P)+CH ₄ →C ₂ H ₄	<2x10 ⁻¹⁵	Husain & Kirsch (1971)	300°K
" " " "	<5x10 ⁻¹⁵	Braun et al. (1969)	300°K
C(¹ D)+CH ₄ →C ₂ H ₂ +H ₂	3.2x10 ⁻¹¹	" "	"
D+CH ₃ Br→CH ₃ +DBr	1.2x10 ⁻¹²	Davies, Thrush and Tuck (1970)	Calculated for 500°K from published Arrhenius constants
CH ₃ [•] +CCl ₄ →CH ₃ Cl+CCl ₃	1.0x10 ⁻¹⁶	Danen (1974)	" "
CCl+O ₂ →?	4.2x10 ⁻¹²	Tyerman (1969)	298°K
C(¹ D or ¹ S)+CCl ₄ →C ₂ Cl ₄	---	Skell & Harris (1965)	on solid substrate at 77°K
C(³ P)+CCl ₄ →no reaction	---	" "	" "

In the case of CH_4 , addition of $\text{C}(^3\text{P})$ is seen to be 4 orders of magnitude slower than addition of $\text{C}^*(^1\text{D})$, and addition to CCl_4 would be sterically more difficult because of the larger size of Cl vs. H atoms. As discussed earlier, $\text{C}^*(^1\text{D})$ atoms do not seem to play a role in the excitation of the observed chemiluminescence. Skell and Harris (1965) found that $\text{C}^*(^1\text{D}$ or $^1\text{S})$ would add to CCl_4 , but $\text{C}(^3\text{P})$ would not. However, their experiments were at liquid N_2 temperature (77°K) on a solid substrate, and the situation might be quite different in the gas phase at 500°K .

Little data are available on abstraction reactions by C atoms. Abstraction of Cl from CCl_4 by H atoms has a rate constant $\sim 10^{-13} \text{ cm}^3 \text{ molecule}^{-1} \text{ sec}^{-1}$ (Table XX III), and there is no reason to expect abstraction by C to be 400 times faster ($4 \times 10^{-11} \text{ cm}^3 \text{ molecule}^{-1} \text{ sec}^{-1}$). The abstraction of Cl from CCl_4 by methyl radicals is quite slow, $k \sim 10^{-16} \text{ cm}^3 \text{ molecule}^{-1} \text{ sec}^{-1}$. However MacKay and Wolfgang (1965) note that reactivity increases in the series:

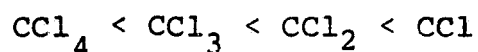


and since C is the most electron-deficient in this series it should have the highest reactivity. The rate of

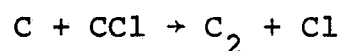
$C(^3P) + CCl_4 \rightarrow CCl + CCl_3$ could thus be much greater than $10^{-16} \text{ cm}^3 \text{ molecule}^{-1} \text{ sec}^{-1}$, but probably not 5 or 6 orders of magnitude larger.

To summarize, abstraction of Cl from CCl_4 by $C(^3P)$, a reaction only mildly exothermic, seems too slow to account for the observed C atom quenching rate constant $\sim 4 \times 10^{-11} \text{ cm}^3 \text{ molecule}^{-1} \text{ sec}^{-1}$. Insertion of C into CCl_4 would be sterically very difficult. A more probable mechanism for C atom decay would be the highly exothermic reaction $C(^3P) + CCl \rightarrow C_2 + Cl$ between two highly reactive free radicals. The rate constant k_3 determined experimentally would thus refer to this reaction. Gaydon (1968) has invoked this mechanism to explain the production of C_2^* in flames containing chlorine. Naegeli (1967) has expressed doubts that sufficient energy is available in this reaction to excite C_2^* , but there is no reason to doubt that the reaction forming ground state C_2 should be extremely rapid, in agreement with the observed near gas kinetic rate constant values. The preceding discussion has not considered possible reactions of C atoms with CCl_3 or CCl_2 , but these appear only slightly more favorable than the reactions with CCl_4 . The energy release is about the same and the steric problems slightly less severe. However, the formation of C_2 by the reaction of C atoms with CCl_3 or CCl_2 would require the breaking of 3 or

2 C-Cl bonds. These reactions are thus thermoneutral or endothermic, as opposed to the very exothermic $C + CCl \rightarrow C_2 + Cl$. Also, commensurate with the reactivity series for CH_n discussed by MacKay and Wolfgang (1965) it is reasonable to assume similar reactivity series of



for CCl_n . Thereby, the only fast reaction appears to be



(6) Excitation Mechanisms

At this point, it is appropriate to discuss briefly criteria for choosing between alternative excitation mechanisms. Because of the low temperatures ($\sim 500^\circ\text{K}$) of the chemiluminescent flames studied, the overall sequence of excitation reactions must be exothermic (though individual reactions may be endothermic if the required energy is supplied by an exothermic reaction occurring in a preceding step). The exothermicity must be large enough to account for the excitation of the most energetic excited species observed. The rate of the candidate reaction must be high enough to account for the observed rate of photon emission (from absolute intensity measurements). Thus, reactions with very small rate constants or involving more than one reactant present in very low concentration are not favored. Although, as has been shown earlier, spin conservation is not an infallible guide for systems containing heavier atoms, spin and energy conservation are sometimes the only guides available in a thicket of possible mechanisms. Thus, when a choice must be made between equally plausible mechanisms, only one of which obeys spin conservation, the spin-conserving mechanism will be chosen.

Reactions involving oxygen atoms were not considered as possible excitation mechanisms, since evidence from a number of sources suggests that O atom concentrations are very low. Processes such as $M + O_2 \rightarrow MO + O$ are endothermic and the flame temperature is low. The flames studied contain many species capable of scavenging O atoms including metal atoms, CCl_4 , CCl_3 , CCl_2 , CCl , C and C_2 . Ung and Schiff (1962) report reaction of O atoms with CCl_4 to form Cl_2 , CO, CO_2 and $COCl_2$, with even more rapid disappearance of O atoms when O_2 is present (as in the present system). They postulate that the primary reaction is addition of O to CCl_4 and this might occur even more readily with the radicals produced by stripping Cl atoms from CCl_4 . Cl_2 , one of the products of the $O + CCl_4$ reaction reported by Ung and Schiff (1962) has been found by Kaufman (1958) to catalyze the recombination of O atoms. In the present system however any Cl_2 produced would probably be scavenged by reaction with metal vapor. In addition, the green band system of MgO ($B^1\Sigma^+ - X^1\Sigma^+$) reported by Johnson (1971) in the reaction of Mg vapor with O atoms (but not with O_2) was not observed in the Mg/ CCl_4/O_2 flame. In experiments with added NO, the yellow-green NO-O continuum described by Gaydon (1957) as a test

for the presence of atomic O was not observed in either the Mg or Ca/CCl₄ O₂ flames. It thus appears that little O could be present.

As mentioned earlier, the observed M* excitation energies of up to 7.5 eV. suggest that the C-O bond formation energy (~11.eV.) must be involved in the M* excitation process. The M-O bond energies are only about 4 eV. and the M-Cl bond energies even lower, and thus cannot account for the observed excitation. The question to be answered, however, is the manner in which the C-O bond energy is transferred into M* excitation so as to yield the observed intensity distributions. In the discussion which follows, a number of candidate mechanisms are examined critically in the search for a mechanism which can explain the experimental observations.

The observed excitation of atomic states up to the ionization limit, plus the observed asymptotic approach of the $I\lambda/gu$ vs. Eu plots near the ionization limit (described earlier) suggests that processes involving ionization, recombination or free elections may play a part in M* excitation. One possible mechanism could be the formation of excited states of neutral metal atoms by ion-electron recombination occurring preferentially into lower excited states (thus giving the observed ex-

citation rate vs. Eu distribution). However a simplified theoretical calculation of the variation of recombination rate vs. bound state energy (Zwillenberg, 1975) shows that although the asymptotic behavior near the ionization limit is predicted qualitatively, the overall form of the excited state formation rate ($I\lambda/gu$) vs. Eu variation is not in agreement with experimental results. In addition, this mechanism would predict $I\lambda[M^+][e^-]$, and since both species are likely to be present in low concentration, this process would seem unlikely.

Another possibility would be the formation of M^* by excitation of ground state metal atoms by "hot" free electrons. A simplified theoretical treatment (Zwillenberg, 1975) shows that the mechanism gives approximately the correct $I\lambda/gu$ vs. Eu dependence (including a straight line region on a log $I\lambda/gu$ vs. Eu plot and asymptotic behavior at the ionization limit). The question remains, however, where electrons could get 6.-7.5 eV. in addition to the 6.-7.6 eV. ionization energy required to free each electron. This would require 12.-15. eV., which is more than available, even from formation of the C-O bond (≈ 11 .eV.).

However, von Engel and Cozens (1964) and von Engel (1967) have described a mechanism whereby free electrons

(formed initially in small concentration, thermally or otherwise), can be "overheated" to electron temperatures as high as $30,000^{\circ}$ K by superelestatic collisions.

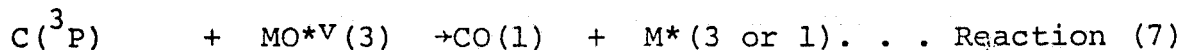
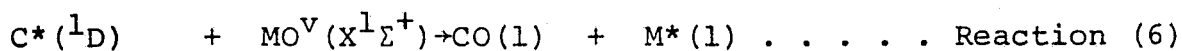
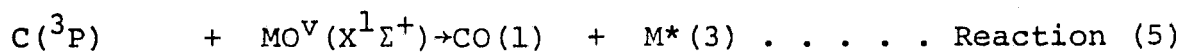
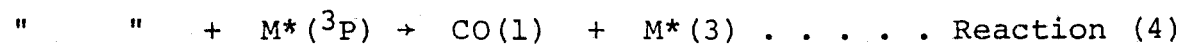
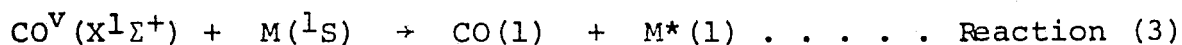
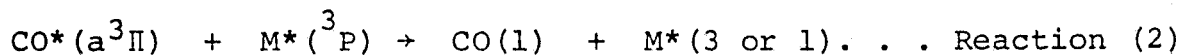
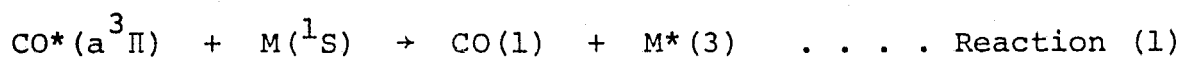
Bradley and Matthews (1967) have measured such electron temperatures in CO flames and explained it in terms of electron heating by collision with excited CO.

However, despite the attractiveness of this "hot electron" mechanism, there seem to be overwhelming objections to it. Since the positive ion concentration would be expected to approximately equal the electron concentration (assuming no negative ions), the direct excitation of a metal ion by collision with the excited species should be about as likely as the heating of a free electron, and ionic lines should be visible in the spectrum. However, as noted earlier, the ionic resonance lines were not observed, even though their excitation energy (above the ion ground state) is less than that of neutral lines which were observed ($\sim 25,000 \text{ cm}^{-1}$ for Ca^{+} ; $36,000 \text{ cm}^{-1}$ for Mg^{+}). Hinnov and Hirschberg (1962) have noted that excited states within about kT_e of the ionization limit should be in Saha equilibrium with free electrons and should follow a Boltzmann population

distribution corresponding to the electron temperature, T_e . For $T_e \sim 5000^\circ\text{K}$ (corresponding to observed excitation temperatures), $kT_e \approx 10 \text{ kcal/mole} \approx 3500 \text{ cm}^{-1}$. Yet, as is shown in Figs. (III-19 and III-21), excited states within this range of the ionization limit show no signs of following a Boltzmann distribution. In fact, they show population inversions (described further below), the very opposite of a Boltzmann distribution. Saha equation calculations (Zwillenberg, 1975) of the free electron concentration which would be expected in equilibrium with observed excited state population densities near the ionization limit, predicted almost complete ionization of the metal. Yet as noted earlier, no ionic lines were observed, indicating that there is no significant concentration of ions (or free electrons). In fact in some cases the Saha equation calculations predicted electron densities higher than the input concentration of metal atoms, a sure sign that the observed excited state populations are not in Saha equilibrium with free electrons, and the metal atom excitation is thus not due to "hot" free electrons. The asymptotic behavior on the $\log(I\lambda/g_u)$ vs. E_u plot of some transitions near the ionization limit (described earlier) can be explained in terms of depletion of long-lived highly excited states by thermal collisions with argon molecules (500K) involving anomalously high ionization cross sections of the type described for alkali metals by Kelly and Padley (1972) and Ashton and Hayhurst (1973). This is treated in detail elsewhere (Zwillenberg, 1975).

Since electron excitation mechanisms have been eliminated, the only remaining possibilities to explain the observed

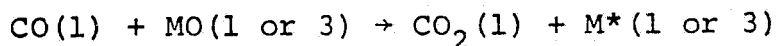
chemiluminescent emissions are collisional processes between atomic or molecular species, in which excitation occurs either directly by chemical reaction, or indirectly by energy transfer from a previously excited species. Considering the chemical species likely to present in the $M/CCl_4/O_2$ flames, the most plausible excitation mechanisms seemed to be:



The mechanisms listed above all obey spin conservation, and the excited reactant species indicated are all long-lived (i.e. vibrationally excited or metastable electronically excited species). In the detailed discussion which follows, the results of various quenching experiments will be used to eliminate most of the possible mechanisms listed above, and it will be shown that only one mechanism is consistent with all the experimental data. The line of reasoning used is summarized here for clarity. The results of NO

quenching experiments showed the absence of $\text{CO}^*(a^3\Pi)$ and thus eliminate Reactions (1) and (2). Since $\text{M}^*(^3\text{P})$ metastable is much more strongly quenched by O_2 than any other excited state, it cannot be their precursor, thus eliminating Reactions (2) and (4). The results of the O_2 quenching experiments in conjunction with the much lower rate constant for $\text{C}^*(^1\text{D}) + \text{O}_2$ than for $\text{C}(^3\text{P}) + \text{O}_2$ argue against Reactions (6) and (8). Calculated maximum possible rates of collision of CO^V with metal atoms (based on measured metal atom concentrations) show that Reactions (3) and (4) cannot account for the measured rates of photon emission, thus ruling out these mechanisms. Reactions (3) and (4) are also inconsistent with the results of N_2 quenching experiments. These arguments are all treated in more detail later. Thus the combination of Reactions (5) and (7) is the only possibility remaining, and is discussed in detail below. Mechanisms for the production of both singlet and triplet MO^V were presented earlier in the section on the M/O_2 and $\text{M}/\text{N}_2\text{O}$ flames.

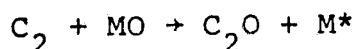
A number of other mechanisms were considered briefly, but found less plausible than reactions (5) and (7) above. The reaction



is only about 30 kcal/mole exothermic, and this falls far short of the required energy to excite the observed M^* . Trying to make up a deficit of ~ 6 eV by invoking vibrational excitation of both CO and MO seems implausible.

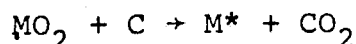
Moreover, this reaction would lead one to expect emitted intensity to vary as $[O_2]^2$ instead of the observed first power dependence, since both $[CO]$ and $[MO]$ should vary as $[O_2]$.

The reaction

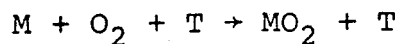


was considered, since C_2^* (and hence presumably C_2) is known spectroscopically to be present in the flame, but the available energy release is insufficient (Naegeli, 1974b).

The reaction



is a possibility, as the formation of MO_2 was postulated earlier in explaining the M/O_2 flames. However, since MO_2 would be formed by the three body reaction



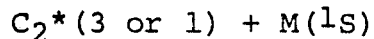
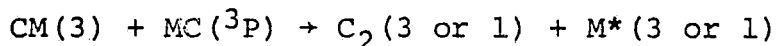
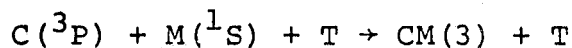
its production rate would be low at low pressures. (This is not a problem in the M/O_2 flames where the emitted intensities, and hence reaction rates, are low). Moreover, one might expect some formation of CO_2^* which would be indicated by emission of the so-called "carbon monoxide flame spectrum" described by Pearse and Gaydon (1963). A further objection is that this reaction would be difficult sterically since the carbon atom must insert

itself between the two O atoms to form CO₂. If one wishes to invoke the reaction of MO₂ with carbon atoms, the reaction



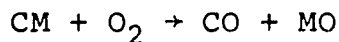
appears more likely. It is not subject to steric difficulties and has nearly the same exothermicity as $\text{MO}_2 + \text{C} \rightarrow \text{M}^* + \text{CO}_2$. However, one would then expect at least some production of MO* with emission of MO bands, and this is not observed. It thus appears that reaction of MO₂ with C is not occurring to any significant extent.

The sequence of reactions



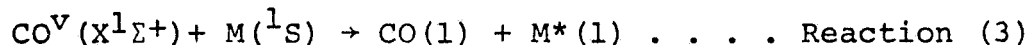
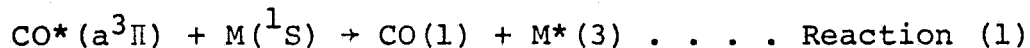
has an overall energy release equal to the bond energy of C₂, 144 kcal/mole (6.2 eV.). This falls somewhat short of the ~7.5 eV. maximum excitation observed in the Mg/CCl₄/O₂ flame. It would appear difficult for this mechanism, not involving O₂, to explain the observed first order dependence of the M* emitted intensity on [O₂]. Neither does it explain why C₂* emission is independent of [O₂], as [C] should decrease as [O₂] rises. Moreover, as noted by Naegeli (1967), no evidence for the existence of the MC molecule has been reported, and there is hence no spectroscopic,

thermochemical or kinetic data regarding it. Any mechanism involving MC must thus remain purely speculation. For this same reason, the reaction



is not considered a plausible source of either MO^V or CO^V , and moreover, as a four-center reaction it might be expected to be slow.

Returning now to the set of Reactions (1) through (8), the arguments for and against each one will be discussed in detail. The most obvious choice to explain the observed difference in excitation temperature between M^* singlets and triplets would be the combination of reactions (1) and (3):



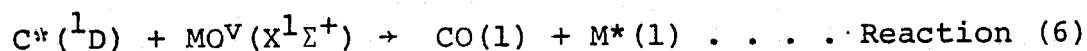
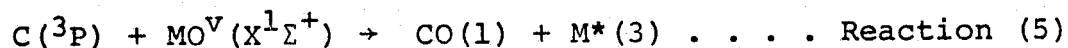
Since singlets and triplets are formed by two different exciting species, it is simple to explain their different excitation temperatures by differing internal (i.e. vibrational) excitation of $\text{CO}^*(a^3\Pi)$ and ground state CO, or by differences between the processes of electronic-electronic and vibrational-electronic energy transfer. Both should be efficient since resonance to within one vibrational quantum of CO is automatically attained.

However, the appearance of the NO β and γ bands upon NO addition was found by Slinger and Black (1971) to be a sensitive test for the presence of $\text{CO}^*(a^3\Pi)$, and these bands were not observed when NO was added to the $\text{M}/\text{CCl}_4/\text{O}_2$ flames. Thus, $\text{CO}^*(a^3\Pi)$ is not present, the mechanism proposed above is incorrect, and Reactions (1) and (2) are eliminated from further consideration.

The excitation of M^* singlets and triplets by vibrational-electronic energy transfer from $\text{CO}^V(X^1\Sigma^+)$ to $\text{M}(^1\text{S})$ and $\text{M}^*(^3\text{P})$ metastable (Reactions (3) and (4)) might offer a possible explanation of the higher excitation temperature observed for triplets than for singlets, due to the additional energy supplied by the excited $\text{M}^*(^3\text{P})$ vs. ground state $\text{M}(^1\text{S})$. However, $\text{M}^*(^3\text{P})$ is quenched much more strongly by O_2 than other triplets, and triplets and singlets are quenched equally by O_2 (Fig. III-31, 32). This indicates that $\text{M}^*(^3\text{P})$ cannot play a part in the M^* excitation process, thus eliminating Reaction (4) from consideration. (It would also eliminate Reaction (2), which has previously been eliminated). Since O_2 quenching measurements were not made on any of the two-excited electron $\text{M}^*(3)$ states (Fig. III-16, 17), Reaction (4) is not yet eliminated as far as they are

concerned. Indeed, the fact that these states show an anomalously high excitation temperature ($\sim 12,000^\circ\text{K}$) and fall on a line on the $\log(I\lambda/gu)$ vs. E_u plot which often passes through the metastable $M^*(^3P)$ state, would tend to suggest production of these states from $M^*(^3P)$ by Reaction (4). However, serious objections raised later to any excitation of M^* by collision of metal atoms with CO^V apply also to this case and would appear to eliminate this mechanism. The measured metal atom concentration is simply too low for collisional excitation by CO^V to account for observed rates of photon emission.

Reaction (5) is an attractive one, since NO and O_2 quenching experiments described earlier indicated the presence of C atoms and the study of the M/O_2 and $\text{M}/\text{N}_2\text{O}$ flames indicated the presence of highly vibrationally excited metal oxide. The only drawback for Reaction (5) is that it can (by spin conservation) produce only triplet M^* . This can be corrected by combining Reactions (5) and (6):



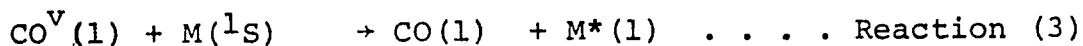
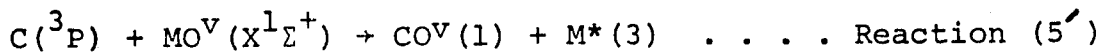
The relatively low excitation energy of $\text{C}^*(^1\text{D})$, 10,194 $\text{cm}^{-1} \approx 29$ kcal/mole makes its excitation by energy transfer

from a vibrationally excited species (CO^V , MCl^V) quite possible. The reaction $\text{CCl}(2) + \text{M}(^1\text{S}) \rightarrow \text{MCl}(2) + \text{C}^*(^1\text{D})$ is endothermic, and hence could only occur if CCl had high vibrational excitation.

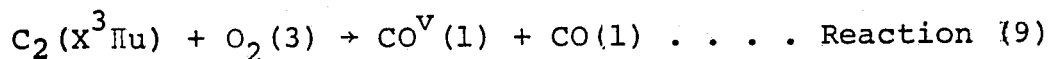
This mechanism is eliminated, however, by the observation that the quenching of M^* emission by NO and O_2 was of about the same magnitude, and that both singlets and triplets were equally quenched by O_2 . Examining the rate constants for the reactions of $\text{C}^*(^1\text{D})$ and $\text{C}(^3\text{P})$ with NO and O_2 , (Table XIX) it is seen that both rate constants with NO are $\sim 10^{-10} \text{ cm}^3 \text{ molecule}^{-1} \text{ sec}^{-1}$, while the $\text{C}(^3\text{P}) + \text{O}_2$ and $\text{C}^*(^1\text{D}) + \text{O}_2$ rate constants are 3.3×10^{-11} and $< 5 \times 10^{-12} \text{ cm}^3 \text{ molecule}^{-1} \text{ sec}^{-1}$ respectively. Thus, if singlet M^* were formed by Reaction (6), one would expect singlet quenching by O_2 to be less than triplet quenching, and much less than NO quenching, contrary to observation. Thus, Reaction (6) is eliminated, and since this probably indicates the absence of $\text{C}^*(^1\text{D})$, so is Reaction (8). In any event, if $\text{C}^*(^1\text{D})$ were formed by collisional excitation of $\text{C}(^3\text{P})$ its concentration would be much less than that of $\text{C}(^3\text{P})$, and production of $\text{M}^*(3)$ by Reaction (8) would be negligible relative to that by Reaction (5).

If one modifies Reaction (5) to allow vibrational

excitation of the product CO, and combines this with Reaction (3), the following interesting mechanism results:



Note that since the lowest triplet state is the $\text{M}^*(^3\text{P})$ metastable, the energy available for excitation of singlets is automatically smaller than that available for triplets by the energy of $\text{M}^*(^3\text{P})$, 15,000-20,000 cm^{-1} , which might explain the lower excitation temperature for singlets than for triplets. There are other reactions conceivable which might produce CO^{V} but they do not seem likely to affect Reaction (3). The four-center reaction



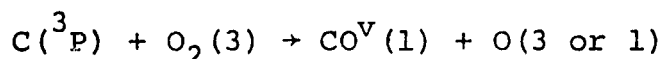
would have a much lower rate than the simple abstraction reaction



Hirschfelder's (1941) semiempirical rules would predict an activation energy of 28% of the sum of the energies of the bonds being broken for the first type of reaction and only 5% of the energy of the one bond being broken in the second type of reaction. In addition, Reaction (9) is sterically less favorable than Reaction (10).

C_2O produced in Reaction (10) might react

with carbon atoms, regenerating C_2 and partially explaining why C_2 emission is independent of $[O_2]$ over a wide range. The reaction



$$\Delta H = -137.6 \text{ kcal/mole for } O(^3P)$$

seems certain to occur. C atoms and O_2 are present, the rate constant is large (Braun, 1969) and all the energy released is unlikely to go into translational energy. However Ogryzlo, Reilly and Thrush (1973) have shown that CO^V is excited only up to $v=17$ ($93 \text{ kcal/mole} \approx 32,500 \text{ cm}^{-1}$), with the remainder of the energy taken up by $O(^1D)$. Thus CO^V produced by this reaction would not have sufficient energy to excite any M^* excited states other than the lowest-lying ones, the (3P) metastable and perhaps the resonance line. The reaction



is very exothermic, 7.5 eV. for Ca and 6.7 eV. for Mg. However if this reaction occurred, at least part of the energy would excite MCl^* . However, neither MO nor CCl are likely to react rapidly with NO, and the rate of the $CCl+O_2$ reaction is much lower than that of the $C(^3P) + O_2$ reaction (Tyerman, 1969). Thus if the $MO+CCl$ reaction occurred to any significant extent, one would expect quenching of MCl^* emission by NO and O_2 to be much less than that of M^* emission, contrary to observation that they are about the same. Thus, Reaction (5') appears

to be the only remaining source of CO^V for Reaction (3).

A strong argument against the combination of Reactions (5') and (3) is found, however, in the results of the N_2 quenching experiments described earlier, (Table XXI). In the case of Ca, the reduction in both triplet and singlet excitation temperatures is about the same. This indicates that the same vibrationally excited species is being relaxed vibrationally by N_2 . The combination of Reactions (5') and (3) has triplets produced from MO^V and singlets from CO^V . It does not seem likely that both these species would be vibrationally relaxed at the same rate by N_2 , since they have greatly differing dipole moments and vibrational frequencies. Thus, the vibrational frequency of N_2 ($v=0$) is 2345 cm^{-1} . The vibrational frequency of CO^V ranges from 2157 cm^{-1} ($v=0$) to 1231 cm^{-1} ($v=40$). The vibrational frequencies of MO^V are in the range $400\text{--}700 \text{ cm}^{-1}$ for low-lying electronic states of CaO and MgO.

Another difficulty is presented by the observed difference in the degree of relaxation of excitation temperature of Mg and Ca singlets by N_2 , (Table XXI). If one assumed that CO^V is exciting both Ca(1) and Mg(1) as in Reaction (3), it is difficult to explain why vibrational relaxation of CO^V by N_2 has such different

efficiencies in the two cases (Table XXI). This is not a problem in mechanisms in which MO^V is the species vibrationally relaxed by N_2 . In such mechanisms, two different species, CaO^V and MgO^V are involved in the Ca and Mg flames respectively. Differences in degree of relaxation by N_2 can thus be explained in terms of differing degrees of initial vibrational excitation of CaO^V and MgO^V .

A more serious objection to Reaction (3), however, is that measured metal atom concentrations are too low to allow a high enough rate of collision between CO^V and metal atoms to account for observed photon emission rates. Self absorption (for $M(^1S)$ and $M^*(^3P)$) and absolute emitted intensity (for $M^*(^3P)$) measurements described below indicated $Mg(^1S)$ and $Mg^*(^3P)$ concentrations of the order of 10^{14} cm^{-3} , based on the effective radiating volume $V_{eff} = 1/2 \text{ cm}^3$. This concentration is much lower than the ~ 1 mole % input metal atom concentration $\sim 10^{-2} \times 3 \times 10^{16} = 3 \times 10^{14} \text{ cm}^{-3}$, and probably indicates that most metal reacts rapidly with CCl_4 or O_2 , leaving few free metal atoms. The observed M^* is then formed by a secondary process such $C + MO \rightarrow CO + M^*$ rather than by collisional excitation of free metal atoms. In the discussion earlier of NO quenching, it was shown that most reaction and light emission occurs in an effective

volume, V_{eff} , which is much smaller than the observed volume V_{obs} which merely indicates a surface at which emission has fallen below the eye's detection limit. For $V_{eff}/V_{obs} \approx 1/400$, $V_{obs} \approx 200 \text{ cm}^3$, then $V_{eff} \approx 1/2 \text{ cm}^3$.

The mole fraction of metal atoms is then $10^{11}/3 \times 10^{16} \approx 3 \times 10^{-6}$. Assuming that $[CO^V]$ or $[C]$ are $\approx [CCl_4]$ input, then $X_{CO^V} \sim X_C \sim 10^{-3}$. (They can be no higher as CCl_4 is the only source of carbon in the system). The total number of collisions per unit volume under the experimental conditions is:

$$Z = v_C n = 10^6 \text{ sec}^{-1} \times 3 \times 10^{16} \text{ cm}^{-3} = 3 \times 10^{22} \text{ cm}^{-3} \text{ sec}^{-1}.$$

The rate of collision between CO^V and M (which is the maximum rate of excitation of M^* by this mechanism) is thus:

$$ZX_{CO^V}X_M V_{eff} = 3 \times 10^{22} \times 10^{-3} \times 3 \times 10^{-6} \times 1/2 = 5 \times 10^{13} \text{ quanta/sec.}$$

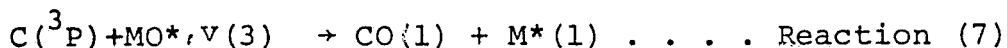
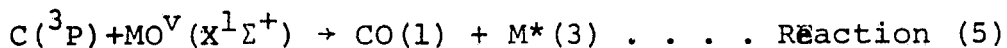
However the observed maximum rates of M^* photon emission in the $Mg/CCl_4/O_2$ flame was $\sim 10^{16}$ quanta/sec and in the $Ca/CCl_4/O_2$ flame $\sim 10^{15}$ quanta/sec. Thus, the CO^V+M mechanism cannot account for the observed rate of photon emission in these flames. (In the $Ca/CCl_4/O_2$ flame, $[M(^1S)]$ was not measured. However estimates of $[M(^3P)]$ from absolute emitted intensities were about

equal to those for Mg. Estimates of metal atom input flux were lower for Ca, suggesting that the ground state Ca atom concentration is no higher and might be smaller than that for Mg. Thus the $\text{CO}^V + \text{M}$ mechanism falls short of explaining the Ca^* photon emission rate).

It is interesting to apply this same analysis to the $\text{C} + \text{MO} \rightarrow \text{CO} + \text{M}^*$ mechanism. Assuming as before, $[\text{C}] \approx [\text{CCl}_4]_{\text{input}}$ so $X_{\text{C}} \approx X_{\text{CCl}_4} \approx 10^{-3}$, and taking $[\text{MO}] \approx \frac{1}{10} [\text{M}]_{\text{input}}$, so $X_{\text{MO}} \approx \frac{1}{10} \times 10^{-2} = 10^{-3}$ (i.e. assuming most M forms MCl), the collision rate between C and MO is thus $3 \times 10^{22} X_{\text{C}} X_{\text{MO}} = 3 \times 10^{22} \times 10^{-3} \times 10^{-3} = 3 \times 10^{16} \text{ cm}^{-3} \text{ sec}^{-1}$. Since $V_{\text{eff}}/V_{\text{obs}} \approx 1/400$, $V_{\text{obs}} \approx 200 \text{ cm}^3$, then $V_{\text{eff}} \approx 1/2 \text{ cm}^3$. The total rate of C-MO collisions is thus $1.5 \times 10^{16} \text{ sec}^{-1}$, in agreement with the observed photon emission rate of 10^{16} sec^{-1} . Thus, the excitation of M^* by the C+MO mechanism is possible, but the $\text{CO}^V + \text{M}$ mechanism is not a possibility. It should be noted that if the difference between V_{obs} and V_{eff} had not been considered in this calculation the above conclusions would not be changed. The calculated number of $\text{CO}^V - \text{M}$ collisions would be unchanged while that of C-MO collisions would have been larger by a factor of $V_{\text{obs}}/V_{\text{eff}} \approx 400$, making the latter mechanism even more attractive.

Since Reaction (5) can produce only triplet M^* ,

Reaction (7) is needed to explain the observed excitation of singlets. The proposed M^* excitation process is thus:



This mechanism explains the equal quenching of triplets and singlets by O_2 , CCl_4 and NO , since the same species, $C(^3P)$ is removed in both cases. The effect of N_2 addition is explained by vibrational relaxation of MO^V . The results of the Ca/O_2 and Ca/N_2O flame experiments, described earlier, proved that the $CaO(A^1\Sigma^+)$ state is formed with high vibrational excitation, and similar excitation in the ground electronic state would be plausible in view of the polarity of the bond formed. The increased effectiveness of CCl_4 as a quencher at high Eu (Fig. III-35) is explained by the increase in probability of vibrational relaxation of high vibrational levels (e.g. of MO^V) noted by Callear and Lambert (1969). They gave the vibrational transition probability of the relaxation process

$$A(v=n) + A(v=m) \rightarrow A(v=n-1) + A(v=m+1)$$

as

$$P_{m,m+1}^{n,n-1} = n(m+1)P_{0,1}^{1,0}$$

for the harmonic oscillator case, where $P_{m,m+1}^{n,n-1}$ is the transition probability for the process shown and $P_{0,1}^{1,0}$ is that for $n=1, m=0$. If m is zero (a vibrationally cold quencher), the transition probability is seen to be proportional to the vibrational level (n) of the excited species. The equation above was derived for two identical molecules, but it is a good approximation for unlike partners (i.e. MO^V and CCl_4). Jones and Broida (1974) have reported vibrational excitation in BaO formed in the $Ba+N_2O$ flame. Field (1974) has published potential curves for low-lying triplet and singlet states of CaO, SrO and BaO, and Schamps and Lefebvre-Brion (1972) have done the same, (Fig. III-5) in much greater detail for MgO. Thus accessible triplet states appropriate to Reaction (7) exist. It is proposed that the observed excitation temperatures of $M^*(3)$ and $M^*(1)$ correspond to the vibrational temperatures of $MO^V(X^1\Sigma^+)$ and $MO^*,V(3)$ respectively. It is of interest that vibrational population data reported for $BaO(A^1\Sigma^+)$ by Jones and Broida (1974b) can be fit very closely on a Boltzmann plot by a line with slope corresponding to 5000K (Fig. III-40), which is approximately the excitation temperature observed

for triplet M^* in the present work. (By Reaction (5), triplet M^* is formed from singlet MO). (Jones and Broida (1974b) emphasized the deviations of Fig. (III-40) from a Boltzmann distribution. However these deviations are actually quite small and a small amount of experimental scatter would make the differences indetectable.)

The "best value" dissociation energy for CaO selected from a variety of experimental data by Gaydon (1968), ~ 100 kcal/mole, corresponds to the dissociation of Field's (1974) $a^3\Pi$ state into ground state atoms. The dissociation of $CaO(X^1\Sigma^+)$ into $O(^3P) + Ca^*(^3P)$ would require $49,400\text{ cm}^{-1} \approx 141$ kcal/mole. It thus appears that $CaO(X^1\Sigma^+)$ dissociates by a curve crossing into the $a^3\Pi$ state. The maximum excitation energy (electronic plus vibrational) of either $CaO(X^1\Sigma^+)$ or $CaO^*(a^3\Pi)$ would thus be the same, ~ 100 kcal/mole. Assuming CaO is formed with this maximum internal energy, the vibrational energy in $CaO^*(a^3\Pi)$ would be less than that in $CaO(X^1\Sigma^+)$ by an amount equal to the electronic energy of $CaO^*(a^3\Pi)$. This lower vibrational energy in $CaO^*(a^3\Pi)$ compared with $CaO(X^1\Sigma^+)$ might correspond to a lower vibrational temperature for the triplet CaO , and thus a lower excitation temperature for M^* singlets produced by Reaction (7). The same arguments apply to

Mg. Alternatively, one might simply hypothesize a higher vibrational temperature produced in the formation of $MO^V(1)$ than of $MO^*,V(3)$, but the first argument based on constant excitation energy which is divided between vibrational and electronic excitation seems more plausible.

In the earlier discussion of the plots of $\log(I\lambda/gu)$ vs. Eu (Arrhenius plots), the excited state energy (Eu) was considered to play the role of an activation energy for the excitation process. In effect it was assumed that $\Delta(\text{activation energy}) = \Delta Eu$. It is clear that this would be justified if the excitation were produced by collisional energy transfer from an active species to a metal atom (e.g. $A^* + M \rightarrow A + M^*$ or $A^V + M \rightarrow A + M^*$). The excitation of M^* by these processes is clearly endothermic by an amount Eu , and the activation energy must equal at least this endothermicity.

However, it has been shown earlier that the excitation mechanism is not of this type at all. Instead, the reaction $C + MO \rightarrow CO + M^*$ was proposed. This reaction is highly exothermic for all but the very highest excited states of M^* , even in the absence of internal excitation of MO .

The Polanyi-Semenov (Semenov, 1958; Johnston, 1966; Laidler, 1965) correlation between activation energy (E_a) and heat of reaction is a strictly empirical relation for certain restricted sets of reactions occurring on one potential surface and not involving excited products (Kaufman, 1966). It thus may not apply to the present systems where excited products are formed and numerous intersecting potential surfaces are involved. The same might be said of other published correlations between activation energies and bond energies (Laidler, 1965). The difficulty of estimating activation energies for reactions involving excited products or reactants has been commented upon by Laidler (1955). Some idea of the difficulty of this problem may be gained by imagining a set of potential surfaces for the $C(^3P)-O-M^*$ system constructed using CO and MO potential curves in the manner described by Laidler (1955) and including MO potential curves correlating with higher excited states of M^* (as in Fig. III-5). The resulting multitude of intersecting potential surfaces is too complex to be helpful in drawing quantitative conclusions about the variation of activation energy with E_u . What can be said is that the products, $CO+M^*(n,L,J,S)$ (where n,L,J and S are quantum numbers specifying M^*) must be reached via a

potential surface which correlates both the products and the reactants, $C(^3P)+MO^V$, with the separated atoms, $C(^3P)+O+M^*(n,L,J,S)$ (Laidler, 1955). Thus, as Eu increases, higher excited states of MO must be reached for reaction to occur and a qualitative increase of activation energy with Eu is indicated.

Somewhat more quantitative conclusions may be reached by making several reasonable assumptions regarding the C-O-M activated complex in the $C+MO \rightarrow CO+M^*$ reaction. The problem will be simplified by assuming a linear complex. Since one bond is in the process of forming while the other bond is being broken, the C-O and M-O bonds will be weaker in the activated complex than they are in CO and MO respectively. It will be assumed that each bond has the same fraction, K, of its full strength. The total atomization energy of the C-O-M complex will then be:

$$D(C-O-M) = K[D(CO) + D(MO)]$$

$D(CO)$ and $D(MO)$ are the dissociation energies of CO and MO respectively. Bonding between the non-adjacent C and M atoms is implicitly neglected in the above equation. Some upper bounds may be placed on K by the consideration that the activation energy must be non-negative. For the case of three identical atoms (e.g.

$H_2 + H \rightarrow H + H_2$) it is clear that K must be less than $1/2$, since otherwise a negative activation energy would result. The energy of a system consisting of ground state C , O and M atoms at infinite separation is the same whether this system was produced from $(C+MO)$ by dissociating MO or by atomizing the complex $C-O-M$. Thus, the activation energy, E_a for the $C+MO \rightarrow CO + M(\text{ground state})$ reaction is:

$$E_a(M) = D(MO) - D(C-O-M) = (1-K)D(MO) - KD(CO)$$

(Only the ground electronic state of CO will be considered since the $a^3\Pi$ state was shown to be absent by NO addition and the singlet states of CO are at energies above $60,000 \text{ cm}^{-1}$. The lowest of these, the $A^1\Pi$ state is not present as the fourth positive bands of CO were not observed). The condition that $E_a \geq 0$ inserted in the above equation, together with $D(CO) = 256 \text{ kcal/mole}$, $D(MO) \approx 100 \text{ kcal/mole}$, yields $K \leq 0.281$.

For the reaction $C+MO \rightarrow CO+M^*$ yielding excited metal atoms, the activated complex will be denoted $C-O-M^*$, since it must correlate with separated C , O and M^* atoms. The energy required to transform a ground state C atom and a ground state MO molecule into separated C, O and M^* atoms is clearly $D(MO) + E_u$. The activation energy for $C+MO \rightarrow CO+M^*$ is thus:

$$E_a(M^*) = D(MO) + E_u - D(C-O-M^*)$$

Denote the (excited) MO state which correlates with C-O-M* as M*O. Then, using the same approximation as before,

$$D(C-O-M^*) = K[D(CO) + D(M^*O)]$$

and

$$E_a(M^*) = D(MO) + E_u - K[D(CO) + D(M^*O)]$$

Note that $D(MO)$ and $D(CO)$ are constants. Assume the same value of K (≤ 0.28) found earlier for the ground state M case. Then:

$$E_a(M^*) - E_a(M) = E_u + K [D(MO) - D(M^*O)]$$

Except for extremely unusually shaped potential curves, an excited molecular electronic state which crosses the ground state potential curve (at $r > r_{\text{equilibrium}}$) must have a lower dissociation limit than the latter. Thus $D(MO) > D(M^*O)$ and $E_a(M^*) - E_a(M) > E_u(M^*)$. Examining the potential curves for CaO (Field, 1974) and MgO (Schamps and Lefebvre-Brion, 1972), the difference in dissociation energies between the ground state and nearly all excited states it crosses is seen to be less than $20,000 \text{ cm}^{-1}$ (Fig. III-5). Thus $D(MO) - D(M^*O) \leq 20,000 \text{ cm}^{-1}$ and $K[D(MO) - D(M^*O)] \leq 0.28(20,000) = 5600 \text{ cm}^{-1}$.

This is much smaller than the excitation energies under consideration ($\approx 30,000$ – $60,000 \text{ cm}^{-1}$) and may thus be neglected. Thus, $E_a(M^*) - E_a(M) \approx E_u$ and $\Delta E_a(M^*) \approx \Delta E_u$ as originally assumed in the analysis of the Arrhenius plots.

It was noted earlier that on the plots of excitation rate ($I\lambda/gu$) vs. E_u (Arrhenius plots), the $M^*(^1P^o)$ resonance state fell far below the straight line drawn through the other singlet excited states. This may result from the relative probabilities of different distributions of energy between the products CO^V and M^* . It is clearly unlikely that all the exothermicity would appear in vibration of CO^V and none in M^* or vice-versa. Some intermediate distribution of energy between M^* and CO^V is much more likely than either extreme. As a partition of energy departs from this most probable partition, its likelihood of occurrence decreases. If this most probable partition of energies occurs for $E_u(M^*)$ somewhat higher than that of the $^1P^o$ resonance state, the observed behavior of the latter is explained. Ogryzlo, Reilly and Thrush (1973) have presented data showing that in the reaction $C+O_2 \rightarrow CO^V + O$, the most probable vibrational excitation of the product CO is $v=8-10$ although excitation up to $v=17$ is observed.

The partition of energy between CO^V and M^* mentioned above is statistical in nature. Statistical energy distributions often contain a factor $e^{-\text{const.} \times E}$. One might therefore be tempted to explain the observed log excitation rate vs. E_u straight line plots entirely in terms of such a statistical distribution rather than

an Arrhenius rate law whose activation energy varies with E_u , as done earlier. Indeed since it was not feasible to perform experiments in which temperature was an independent variable, the experimental data show only that excitation rate $\propto e^{-BE_u}$. The assignment $B = 1/kT_{ex}$ was done by analogy with other chemical kinetic processes and is somewhat arbitrary. However, the observation that the values of T_{ex} so obtained agree with the MO vibrational temperatures obtained from the data of Jones and Broida (1974) lends support to the identification of B with $1/kT_{ex}$.

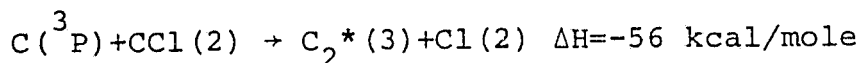
A few words are in order about the mechanism of excitation of the C_2^* , MCl^* and CN^* (when NO or N_2O were added) bands observed. As noted earlier, the MCl bands were quenched about equally with M^* by CCl_4 , O_2 and NO. The C_2 band intensity was independent of $[O_2]$ up to fairly high values ($\sim 0.6\%$) when some falloff occurred, and were quenched much more by NO than M^* or MCl^* . The CN bands reached a peak as NO was added and then rapidly fell off.

$C(^3P)$ atoms and O_2 are both present and the $C(^3P) + O_2 \rightarrow CO + O$ reaction is known to be fast (Braun, 1969). Ogryzlo et al. (1973) have demonstrated the production of CO^V with vibrational energy up to 93 kcal/mole ($v=17$) by this reaction, which is more than enough energy to excite all the emissions observed. The excitation of the ground state molecule by collision with $CO^V(1)$ is spin-allowed in all cases. Thus the excitation of all three molecular species is easily explained by collisional excitation of the ground state molecule by CO^V :

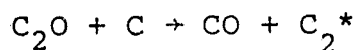


The energy produced by the $C + O_2$ reaction is sufficient to excite these molecular species, but not sufficient to excite any of the M^* metal atom excited states, except

the metastable $M^*(^3P)$ (whose formation by $CO^V + M(^1S)$ is spin-forbidden), and the $M^*(^1P)$ resonance state whose excitation was noted earlier to be unusual. This separation in energy justifies the use of two different mechanisms to explain M^* and molecular band emission. C_2^* cannot be excited by



since 86 kcal/mole are needed to excite the observed (6,5) "high pressure" bands, although this reaction probably does produce ground state C_2 . The reaction



is probably also insufficiently energetic, if one takes $\Delta H_f(C_2O) = 2.47 \text{ eV}$. (Naegeli, 1974b).

The quenching of MCl^* by O_2 , CCl_4 and NO is due to the reduction in CO^V caused by the consumption of C atoms by these quenchers, as is the falloff in C^*_2 emission at high $[O_2]$ and in CN^* emission at high $[NO]$. The greater quenching of C^*_2 by NO is due to the twofold effect produced by the reduction in $[C_2]$ due to C atom destruction as well as the reduction in $[CO^V]$. The independence of $[O_2]$ shown by C_2^* may be due to the counteracting effects of the formation of additional CO^V and the destruction of C atoms by the reaction of C with O_2 .

(7) Ground and Excited State Population Densities and Quantum Yields.

Population densities of the metal atom ground (1S) and metastable (3P) states can be calculated from measurements of self-absorption of transitions with high Aul terminating in these states (since the absorption coefficient $K^{\nu}Aul$), as described earlier in Chapter I. The population densities of excited states can be estimated from the relation $(I\lambda/gu) \sim N_u V_{eff} Aul$, where N_u is population density of the upper state and V_{eff} is the effective emitting volume defined earlier by NO quenching data. For the metastable $M^*(^3P)$ these two methods overlap and their results can be compared. Because it is the orders of magnitude rather than the precise values of populations and quantum yields which are important, calculations will be simplified by considering the increase in signal due to the White cell (\sim a factor of 8) to cancel the effect of statistical weight g_u (1-21, average value 11) so that the total population and photon emission rate of each excited state may be obtained from the $I\lambda/gu$ and $N_u/g_u = I\lambda/gu$ vs. E_u plots, by use of the appropriate conversion factors $\frac{4 \times 10^{10}}{V_{eff}} \frac{cm^{-3}}{mV-A-sec.}$ and $4 \times 10^{10} \frac{photons/sec}{mV-A}$, respectively).

Self-absorption measurements were made using the first of the two methods described in Chapter I, in which the ratio of single-pass to multiple-pass intensity measurements is used (i.e. the effect of varying the path length). The other method described in Chapter I, using the ratio of triplet component intensities, is not valid in the present case since the assumption made in its derivation, $n_1/g_1 = n'_1/g'_1$ (equal population of the lower state sublevels) is not likely to be satisfied by the $^3P_{0,1,2}$ sublevels. The radiative decay rates of the 3P_0 and 3P_2 sublevels are much lower than that of the 3P_1 level, since they are strictly forbidden by the strong $\Delta J=0, \pm 1$, $J=0 \rightarrow J=0$ selection rule as well as the weaker $\Delta S=0$. (This is why the $^3P_1 \rightarrow ^1S_0$ line is seen, while the other two components of this "triplet" are not). In addition, the collisional quenching rates of the 3P sublevels are likely to be quite different. In the case of mercury, Massey (1971) lists quenching cross sections for $Hg(6^3P_1)$ which are 1-3 orders of magnitude larger than those for $Hg(6^3P_0)$ with the same quenching species.

Measurements of the multipass/single-pass intensity ratio were made for a number of spectral lines, including some known to be optically thin (either because of low transition probability A_{ul} or because of a sparsely populated lower state). These measurements also allowed detection of any change in the multipass/single-pass intensity due to change in mirror reflectance with wave-

length. It was found (Fig. III-41) that such variation exists. This variation plus other experimental scatter in the data made it impossible to detect self-absorption in any of the transitions terminating in the metastable $M^*(^3P)$ state. An upper bound could however be placed on the $Mg^*(^3P)$ population by estimating how low the multi-pass/single-pass intensity ratio could fall before self-absorption would be detected (a value of 3. for the 3838\AA triplet was assumed). The value of $[M^*(^3P)]$ corresponding to $m=5.50$, $\phi=3.0$ was then calculated (where m is the effective number of passes through the cell as measured by the intensity ratio for an optically thin line and ϕ is the ratio for the self-absorbed line). Since the resonance line (2852\AA , $^1P^o \rightarrow ^1S$) was closely bracketed by two lines within 100\AA on either side, variation of mirror reflectance with wavelength was no problem and $[M(^1S)]$ could be calculated, using $m=6.48$, $\phi=2.20$ (Fig. III-41).

Population density values for $Mg(^1S)$ and $Mg^*(^3P)$ calculated from self-absorption and of $Mg^*(^3P)$ and $Ca^*(^3P)$ metastables calculated from absolute emitted intensities are shown in Table XXIV. The higher value for $[Mg^*(^3P)]$ than for $[Mg(^1S)]$ in the first column of

TABLE XXIV

Ground and Metastable State Population Densities Calculated
From Absorption and Emission Data.

<u>State</u>	<u>Population Density, cm⁻³</u>	
	<u>From Self-Absorption</u>	<u>From Emitted Intensity</u>
Mg(¹ S)	2.8×10^{10} **	Not applicable (ground state)
Mg*(³ P)	$< 4.4 \times 10^{10}$ **	3.6×10^{11}
Ca*(³ P)	---	2.4×10^{11}

**See discussion

NOTE: In self-absorption calculation the Doppler linewidth at 500°K was used. $\Delta\nu_D = 1.26 \times 10^9 \text{ sec}^{-1}$ for Mg 3838Å triplet and $1.70 \times 10^9 \text{ sec}^{-1}$ for Mg 2852Å resonance line.

TABLE XXV

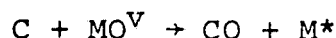
Maximum Observed Excited State Population Densities From
Absolute Emitted Intensities.

	<u>Population Density, cm⁻³</u>		
	<u>Highest Population Non-Metastable State</u>	<u>Highest Population States within kTex of Ionization Limit</u>	<u>Highest Inversion Density</u>
<u>Mg</u>	7×10^7	1×10^5	2×10^6
<u>Ca</u>	3×10^6	9×10^5	5×10^5

of the table does not indicate a possible inversion between the $\text{Mg}^*(^3\text{P})$ state and the ground state. Even if $[\text{Mg}^*(^3\text{P})]$ equalled the upper bound value given, because of the higher statistical weight of the ^3P vs. the ^1S state, n/g would not be inverted. Moreover, an extremely high inversion density ($\sim 10^{14} \text{ cm}^{-3}$) would be necessary to lase on this "forbidden" transition whose transition probability is $\sim 10^{-6}$ that of allowed transitions.

The $\text{Mg}^*(^3\text{P})$ population density calculated from emitted intensity is larger by a factor of 8 than the upper bound estimated from self-absorption. A possible explanation would be for the highly excited atoms which emit radiation (while falling to the ^3P state) to be translationally "hotter" than the $\text{M}^*(^3\text{P})$ atoms absorbing the radiation, and thus to have a broader spectral linewidth than the absorbers. This difference in linewidth would reduce the self-absorption produced by a given $\text{M}^*(^3\text{P})$ concentration, and cause the self-absorption measurement to yield population density values which are too low. Such a difference in translational energy between $\text{M}^*(^3\text{P})$ metastable and other excited states is quite plausible. Because the lifetime of the metastable is long enough to equilibrate with the argon molecules which make up the bulk of the gas, the $\text{M}^*(^3\text{P})$ trans-

lational temperature is $\sim 500^\circ\text{K}$. The allowed ($A \sim 10^8 \text{ sec}^{-1}$) atomic transitions cannot relax ($\nu_c \sim 10^6 \text{ sec}^{-1}$) and thus could exhibit broadening. As a result of the highly exothermic reaction

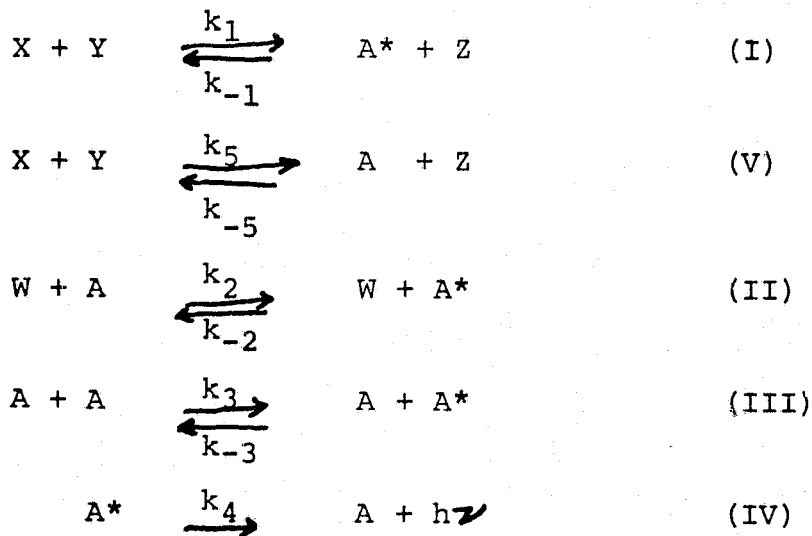


some share of the energy could possibly appear as translationally hot M^* . Translational energy corresponding to 5000°K would be only 15 kcal/mole ($3/2 kT$) which is a small fraction of the total energy release. Duthler and Broida (1973) reported increased emission vs. absorption linewidth in Li excited by active N_2 , which they attributed to Doppler broadening caused by translational energy ~ 25 kcal/mole. When comparing the two methods of measuring $\text{M}^*(^3\text{P})$ population density, the emission result ($\sim 10^{11} \text{ cm}^{-3}$) appears more reliable than the self-absorption result. Similar linewidth arguments apply to the self-absorption measurement of the ground state population which is also probably too low, and the correct (^1S) ground state population would also appear to be $\sim 10^{11} \text{ cm}^{-3}$. Both the (^1S) and (^3P) population densities are much smaller than the $\sim 10^{14} \text{ cm}^{-3}$ metal atom input, which would appear to indicate that nearly all the metal reacts initially to form MO or MCl and lends

support to the hypothesis that the observed M^* (and perhaps $M(^1S)$) is formed by a secondary reaction, such as $C+MO$.

Maximum observed non-metastable excited state populations (calculated from emitted intensities) are shown in the first column of Table XXV. The second column shows similarly calculated populations of states near the ionization limit. These were used in the Saha equation estimates of equilibrium electron densities described earlier.

The ratios of metastable and non-metastable populations to the ground state population are thus about 10^{-4} and 1 respectively. It is of interest to compare these ratios with the theoretical predictions of Shuler (1953) who considered the system of reactions:



Here Reactions I and V are the chemical formation of electronically excited A^* and ground state A (and their reverse reactions). Reaction IV is radiative decay and II and III are thermal excitation processes where $[W]=[X]+[Y]+[Z]$. Since thermal excitation is negligible in low temperature chemiluminescent flames, set $k_2=k_3=0$. Shuler's result then simplifies to:

$$\frac{[A^*]}{[A]} = \frac{1/t}{k_{-2}[W] + 1/t + 1/\tau}$$

where τ , the radiative lifetime is $1/k_4$ and t is the residence time in the volume of observation, V/q . Identify t with \bar{t} measured in the NO quenching experiments $\sim 10^{-4}$ sec, and take $\tau \sim 10^{-8}$ sec for non-metastable excited states and $\tau \sim 10^{-3}$ sec for metastable states. $[W] \sim 10^{14} \text{ cm}^{-3}$ and assume gas kinetic $k_{-2} \sim 10^{-10} \text{ cm}^3 \text{ molecule}^{-1} \text{ sec}^{-1}$. Then $k_{-2}[W] \sim 10^4 \text{ sec}^{-1}$. Then for non-metastable states:

$$\frac{[A^*]}{[A]} = \frac{10^4}{10^4 + 10^4 + 10^8} \approx 10^{-4}$$

and for metastable states:

$$\frac{[A^*]}{[A]} \approx \frac{10^4}{10^4 + 10^4 + 10^3} \approx 1/2 \sim 1$$

Thus, the experimental ratios presented earlier agree with Shuler's (1953) theory which assumed a mechanism of

excitation similar to the $C+MO \rightarrow M^*+CO$ mechanism.

Quantum yields (photons per reactant molecule) were calculated by taking the ratio of photon emission rate to reactant input rate. In the $M/CCl_4/O_2$ flames, quantum yields were generally calculated on a "per CCl_4 molecule" basis, to put different flames on a common basis for comparison. Since the CCl_4 input rate was less than those of O_2 or metal vapor, CCl_4 was the limiting reactant. It is not meant to imply that all CCl_4 is consumed in the flame, as due to the CCl_4 and metal vapor input geometry this is unlikely. Only part of the CCl_4 is consumed, while the remainder leaves via the vacuum port. (It could, in principle, be measured by trapping a sample, but this was not done). Thus, the calculated quantum yields are lower bounds. The true values are probably somewhat higher, and might tend to increase with increasing metal vapor input, due to more efficient collecting of the CCl_4 . For molecular bands, the total photon emission was estimated by integrating the chart of a wavelength scan of the band by planimeter and using an average photomultiplier sensitivity over the band. For atomic lines, in principle the total photon emission could be obtained by summing

the intensities of all the lines emitted. In practice this is not feasible since not all lines were observed, but only a sufficient number to define the singlet and triplet Arrhenius plots ($\log I\lambda/g_u$ vs. E_u). The fact that most observed transitions fell on a straight line on a $\log (I\lambda/g_u)$ vs. E_u plot was therefore used to relate the total emitted intensity of all transitions to that of the strongest observed spectral line. By using the equation of the Arrhenius line, making the approximation of equally spaced lines and summing the resulting geometric progression it may be shown (Zwillenberg, 1975) that

$$\bar{N} = \frac{F}{(I\lambda/g_u)_{\max}} = \frac{NkT_{\text{ex}}}{E_H - E_L}$$

Here, F is the total rate of photon emission, $(I\lambda/g_u)_{\max}$ is that for the strongest (lowest) energy line, T_{ex} is the excitation temperature and $(N+1)$ is the number of spectral lines with upper states in the energy range from E_L to E_H over which the Arrhenius plot is linear.

Let:

$E_H - E_L \approx (\text{lowest energy triplet}) - E \text{ (ionization)}$
 since the linear portion of the $\log (I\lambda/g_u)$ vs. E_u plot

extends between approximately these limits. N is estimated by taking the total number of neutral Ca and Mg lines respectively listed in the Handbook of Chemistry and Physics spectral tables (Hodgman, 1957), dividing by 2 (average between 3 for triplets and 1 for singlets) since the tables list each triplet component as a separate line, and subtracting 2 (the metastable and resonance lines which fall below E_L). This yields N equal to 62 for Ca and 24 for Mg. Taking $T_{ex} \approx 4000^\circ K$ (an average between triplet and singlet values), $kT_{ex} \approx 2800 \text{ cm}^{-1}$.

Thus

$$\bar{N} = \frac{NkT_{ex}}{E_H - E_L} = \frac{62(2800)}{49306 - 31539} = 9.8 \text{ for Ca}$$

$$= \frac{24(2800)}{61669 - 41197} = 3.3 \text{ for Mg}$$

Overall line quantum yields can now be calculated by multiplying the quantum yield for the strongest triplet observed by this factor. Since the resonance and metastable lines are below E_1 and do not fall on the linear portion of the $\log(I\lambda_{gu})$ vs. E_u plot, the quantum yields calculated may be low by as much as a factor of 2. Maximum observed photon emission rates in the strongest triplet were 3.6×10^{15} photons/sec for Mg and 9×10^{13} photons/sec for Ca, while typical CCl_4 input rates were $\sim 2 \text{ std. cm}^3/\text{min} \sim 10^{18}$ molecules/sec. Thus, the quantum yields

for the strongest triplet of Mg and Ca respectively (in photons/molecule CCl_4) were 3.6×10^{-3} and 9×10^{-5} respectively. Estimated overall line emission quantum yields are thus $3.6 \times 10^{-3} \times 3.3 \approx 1.2 \times 10^{-2}$ for Mg and $9 \times 10^{-5} \times 9.8 \approx 9 \times 10^{-4}$ for Ca. Corresponding maximum photon emission rates are 1.2×10^{16} photons/sec for Mg and 9×10^{14} photons/sec. for Ca. Estimated maximum quantum yields for line and band emission in the various flames studies are shown in Table XXVI. Note that despite the large difference in quantum yield for Ca vs. Mg line emission and CaCl vs. MgCl band emission, the total quantum yield (including both atomic and molecular emissions) for both flames is about the same. This is consistent with the observation that visually, the brightnesses of the two flames are about the same. The much higher CaCl vs. MgCl emission is probably due to the lower energy of the CaCl electronically excited states.

From Figs. (III-34 and III-39) it is plain that as $[\text{CCl}_4]$ is increased from low values, the quantum yield of M^* emission (per CCl_4 molecule) remains approximately constant in the region where emission is roughly proportional to $[\text{CCl}_4]$, and then decreases rapidly as quenching by CCl_4 becomes important and the I vs. $[\text{CCl}_4]$

TABLE XXVI

Quantum Yields

<u>Flame</u>	<u>Emitter</u>	<u>Quantum Yield, Photons/Molecule</u>	
Ca/CCl ₄ /O ₂	Ca	9x10 ⁻⁴	per CCl ₄
	CaCl	1x10 ⁻²	" "
	C ₂	1x10 ⁻⁴	" "
Mg/CCl ₄ /O ₂	Mg	1.2x10 ⁻²	" "
	MgCl	1x10 ⁻⁵	" "
	C ₂	1x10 ⁻⁵	" "
Mg/CCl ₄ /N ₂ O	CN	1x10 ⁻⁶	" "
		2x10 ⁻⁶	" N ₂ O
Ca/O ₂	CaO	2x10 ⁻⁴ -2x10 ⁻³	" O ₂
Ca/N ₂ O	CaO	2x10 ⁻³	" N ₂ O
Mg/O ₂	MgO?	6x10 ⁻⁷	" O ₂
Mg/N ₂ O	MgO?	1x10 ⁻⁵	" N ₂ O

curve departs from linearity. Figs. (III-29 through III-32 and III-39) show that M^* emission quantum yield (photons/ CCl_4 molecule) increases with $[\text{O}_2]$ until the peak in the I vs. $[\text{O}_2]$ curve is reached, and then declines. (If quantum yield were calculated per O_2 molecule, the roles of O_2 and CCl_4 in the previous two sentences would be interchanged).

(8) Population Inversions, Predicted and Observed

It has been shown experimentally that the production rate (R_u) of excited metal atoms in the Mg and $\text{Ca}/\text{CCl}_4/\text{O}_2$ flames follows an Arrhenius-type expression:

$$R_u/g_u \sim \frac{I\lambda}{g_u} \frac{1}{\sum A_{ul}} \approx \frac{I\lambda}{g_u} \sim e^{-E_u/kT_{\text{ex}}}$$

while excited state populations (for negligible collisional quenching) are related to production rates by

$$n_u/g_u = \frac{1}{\sum A_{ul}} \quad R_u/g_u = \frac{I\lambda}{g_u A_{ul}}$$

These relationships can now be used to predict, for a given value of T_{ex} , just what relative populations and inversions should be expected and where one should look for them. This calculation can conveniently be performed graphically on a semi-log graph with a linear

Eu abscissa. A line is drawn with slope $-1/kT_{\text{ex}}$, corresponding to the relative production rates at the assumed T_{ex} , and relative populations are obtained by graphically subtracting $\log (\sum_1 A_{ul})$ from each point on the line corresponding to a transition. Transition probabilities, A_{ul} are available in the excellent tables of Wiese et al. (1966, 1969). Such calculations for Ca and Mg respectively are shown in Figures III-42 and III-43. A single T_{ex} of 6000°K has been used for both singlets and triplets, but the effect of varying T_{ex} can be readily seen by imagining the excitation rate line to pivot about one end (changing its slope $\sim 1/kT_{\text{ex}}$) while each excited state point stays the same vertical distance (equal to $\log \sum_1 A_{ul}$) from the line. It is readily seen that higher T_{ex} favors the production of population inversions. Figs. III-42 and III-43 predict a number of sizeable inversions in Ca and Mg at values of T_{ex} comparable with those experimentally observed. This does not automatically occur for all metals. Similar calculations show T_{ex} of 12,000°K necessary to produce much smaller inversions in beryllium, while $T_{\text{ex}}=6000^\circ\text{K}$ would produce none at all.

Some of these predicted inversions have been observed experimentally by monitoring upper and lower state populations by means of visible and ultraviolet transitions originating in these states. The actual transitions on which inversions

are believed to exist are in the infrared, beyond the range of sensitivity of the detectors used in this investigation. For this reason, no measurements of gain could be made. A number of the predicted inversions could not be verified because of difficulties in measuring the populations of their upper and lower states. Either there were no allowed visible or ultraviolet transitions originating in these states, or else such transitions were too weak to detect (low A_{ul} or λ near the sensitivity limits of the detector). However, direct detection of the inverted transitions using an infrared detector and detecting gain (negative absorption) by the variation of signal with optical path length may be possible. In the infrared the multiple reflection mirrors would have higher reflectance than in the visible increasing the effective number of optical passes through the flame.

Fig. III-44 shows typical excited state populations and population inversions in calcium, observed in a $\text{Ca/CCl}_4/\text{O}_2$ flame at 3. torr pressure. The resemblance to the distribution predicted in Fig. III-42 is clear. Similar inversions were observed at different pressures and with NO addition, which is consistent with the observation earlier that excitation temperature does not

vary with pressure or NO addition over the range studied. When ~45% N_2 was added, the populations of the highest $^3F^o$ and 3D excited states were reduced to the point where inversion no longer occurred, but some inversions, originating in lower-lying states, remained. This is consistent with the observed reduction of T_{ex} by N_2 addition discussed earlier and with the interpretation that the effect of N_2 is due to the relaxation of highly vibrationally excited metal oxide molecules.

Observed population inversions and upper state population densities are summarized in Table XXVII. Inversion ratios (the ratio of n/g in the upper state to that in the lower state) ranged from 1 to about 6, with most in the vicinity of 2. Upper state densities ranged from $2 \times 10^4 \text{ cm}^{-3}$ to $3 \times 10^6 \text{ cm}^{-3}$. This considers only states which were inverted. As noted in Table XXV, somewhat higher populations were observed in states not inverted. All the transitions on which inversions existed correspond to wavelengths in the infrared, in the range from 1.02 to 19.68 microns.

However, as noted earlier in Chapter I, a population inversion is a necessary but not sufficient

Table XXVII

Observed Population Inversion Ratios and Upper State Population Densities

Upper State	Lower State	E_u, CM^{-1}	E_l, CM^{-1}	λ_{ul} Microns	Observed inversion ratios and upper state population densities (10^5 CM^{-3})						
					Run No: CA2-13	CA7-2	CA6-19	CA4-2	CA3-28	CA3-26	MG3-6
Calcium:											
8f ³ F°		47550			(1.04)	(2.00)	---	---	(2.53)	(0.449)	---
	8d ³ D		47042	19.68	2.29	1.74	---	---	1.26	2.22	---
	7d ³ D		46305	8.03	1.80	---	---	---	---	2.93	---
	6d ³ D		45051	4.00	2.56	2.65	---	---	2.00	---	---
	5d ³ D		42746	2.08	2.25	2.32	---	---	2.73	1.86	---
	4d ³ D		37754	1.02	---	2.74	---	---	1.78	1.80	---
7f ³ F°		47006			(0.856)	(1.70)	---	---	(2.11)	(0.875)	---
	7d ³ D		46305	14.26	1.48	---	---	---	---	5.72	---
	6d ³ D		45051	5.12	2.11	2.25	---	---	1.67	---	---
	5d ³ D		42746	2.35	1.85	1.97	---	---	2.28	3.63	---
	4d ³ D		37754	1.08	---	2.32	---	---	1.49	3.52	---
6f ³ F°		46165			(1.18)	(1.41)	(1.76)	(8.54)	(2.08)	(0.432)	---
	6d ³ D		45051	8.98	2.91	1.87	---	2.87	1.65	---	---
	5d ³ D		42746	2.92	2.55	1.64	1.29	2.80	2.25	---	---
	4d ³ D		37754	1.19	1.22	1.93	---	2.00	1.46	1.74	---

Table XXVII (continued)

Observed Population Inversion Ratios and Upper State Population Densities

Upper State	Lower State	E_u, CM^{-1}	E_l, CM^{-1}	λ_{ul} Microns	Observed inversion ratios and upper state population densities (10^5 CM^{-3})						
					Run No: CA2-13	CA7-2	CA6-19	CA4-2	CA3-28	CA3-26	MG3-6
5f ³ F°		44763			(0.960)	(1.32)	(2.06)	(6.50)	(1.38)	---	---
	5d ³ D		42746	4.96	2.08	1.53	1.51	2.13	1.49	---	---
	4d ³ D		37754	1.43	---	1.80	---	1.52	---	---	---
4f ³ F°		42171			---	(1.45)	(3.86)	---	---	(0.417)	---
	4d ³ D		37754	2.26	---	1.99	1.91	---	---	1.68	---
8d ³ D		47042			---	---	---	---	(2.00)	---	---
	5f ³ F°		44763	4.39	---	---	---	---	1.45	---	---
5p ³ P		36565			---	---	---	---	(9.36)	---	---
	5s ³ S		31539	1.99	---	---	---	---	1.07	---	---
4p ³ P°		39338			(1.65)	(1.18)	(6.08)	---	(2.14)	---	---
	4d ³ D		37754	6.31	1.71	1.62	3.01	---	1.50	---	---
	4p ² ³ P		38508	12.05	4.81	3.70	---	---	---	---	---
4f ¹ F°		42344			(1.51)	---	---	---	---	---	---
	4p ² ¹ D		40720	6.16	1.36	---	---	---	---	---	---
5d ¹ D		42919			---	---	---	(4.93)	(2.03)	---	---

Table XXVII (continued)

Observed Population Inversion Ratios and Upper State Population Densities

Observed inversion ratios and upper state population densities (10^5 CM^{-3})

<u>Upper State</u>	<u>Lower State</u>	<u>E_u, CM^{-1}</u>	<u>E_l, CM^{-1}</u>	<u>λ_{ul} Microns</u>	<u>Run No:</u> <u>CA2-13</u>	<u>CA7-2</u>	<u>CA6-19</u>	<u>CA4-2</u>	<u>CA3-28</u>	<u>CA3-26</u>	<u>MG3-6</u>
	$4p^{-1}F^\circ$		40538	4.20	---	---	---	1.10	1.22	---	---
$6p^1P^\circ$		41679			---	---	---	---	---	(0.208)	---
	$4p^2 \ ^1D$		40720	10.42	---	---	---	---	---	1.35	---
<u>Magnesium:</u>											
$4d^1D$		53135									(33.1)
	$4p^1P^\circ$		49346	2.64	---	---	---	---	---	---	2.22
					1.5	0.80	1.0	1.4	3.0	1.5	2.2
Chamber Pressure, Torr:					0.319	0.215	0.221	1.066	0.237	zero	1.035
Mole % O_2 :										added	
Mole % CCl_4 :					0.0266	0.0314	0.0386	0.0524	0.0432	0.050	0.272
Mole % NO (If any):					---	0.406	---	---	---	---	---
Mole % N_2 (If any):					---	---	45.1	---	---	---	---

Note: Numbers in () are upper state densities in 10^5 CM^{-3}

$$\lambda_{ul} \text{ (Microns)} = \frac{10^4}{E_u - E_l}$$

$$\text{Inversion Ratio} = (N/g)_u \div (N/g)_l$$

condition for laser action. There must also be a high enough density of the inverted state for the gain produced to overcome the losses in the system. Bennett (1965) gives the following formula for the gain per unit path length at the center of a spectral line:

$$G_0 = \sqrt{\frac{\log_e 2}{16\pi^3}} \left[N_2 - \frac{g_2}{g_1} N_1 \right] \lambda^2 A_{21} / \Delta \nu_D$$

where:

G_0 = gain per unit length (cm^{-1}).

N_2, N_1 = upper and lower state population densities (cm^{-3}).

g_2, g_1 = upper and lower state statistical weights.

λ = wavelength of line (cm).

A_{21} = Einstein coefficient (transition probability) for spontaneous emission (sec^{-1}).

$\Delta \nu_D$ = Doppler linewidth (frequency), (sec^{-1}).

Taking as the most favorable case, $N_2 \gg \frac{g_2}{g_1} N_1$,
or $[N_2 - \frac{g_2}{g_1} N_1] \approx N_2$, and the following typical values:

$$A_{21} \approx 10^8 \text{ sec}^{-1}$$

$$\Delta \nu_D \approx 10^9 \text{ sec}^{-1}$$

$$\lambda \approx 0.5 \mu = 0.5 \times 10^{-4} \text{ cm.}$$

one obtains the result, $G_0 \approx 10^{-11} N_2$. For $N_2 \approx 10^6 \text{ cm}^{-3}$,
 $G_0 \approx 10^{-5} \text{ cm}^{-1}$, a very low gain. Assuming that mirror losses

are the only losses, the condition for oscillation is $G_0 L = (1-r)$, or $G_0 = (1-r)/L$, where r is the mirror reflectance and L the single pass length. Table XXVIII shows the minimum inversion density (or N_2 in the best case, $N_2 > \frac{g_2}{g_1} N_1$) necessary for oscillation, for several assumed path lengths and values of mirror reflectance. A mirror with 99.9% reflectance stretches the current state of the art (about 99.7%) and a single pass length of 100 cm is rather long to be practical with a metal vapor flame or an array of such flames. It is thus clear that the observed inversion densities of 10^4 - 10^6 cm^{-3} are at least two orders of magnitude too small to lase under even these most favorable conditions. Of course, in a practical laser system one of the mirrors must have net reflectance considerably less than 99.9% to allow output power to be extracted. Thus, unless the inversion densities can be increased by 2 or 3 orders of magnitude over the values observed, lasing on these transitions is impossible, no matter how high the inversion ratio (N_2/g_2)/(N_1/g_1). Factors limiting such increases to relatively small values are considered later. The more attractive possibility of utilizing the much higher ($\sim 10^{11} \text{ cm}^{-3}$) metastable $M^*(^3P)$ densities observed (which exceed the threshold values shown in Table XXVIII) is discussed below.

Table XXVIII

Minimum Inversion Density Necessary for Oscillation

	<u>Inversion Density, cm⁻³</u>		
<u>L, cm:</u>	<u>1</u>	<u>10</u>	<u>100</u>
r : 0.99	10 ⁹	10 ⁸	10 ⁷
0.999	10 ⁸	10 ⁷	10 ⁶

Table XXIX

Calculated Inversion Ratios for Potassium

<u>λ_{ul}, Å</u>	<u>Transition, u → l</u>	<u>A_{ul}, sec⁻¹</u>	<u>g_u</u>	<u>Inversion Ratio</u>
12,522	5s ² S _{1/2} 4p ² P _{3/2}	0.156x10 ⁸	2	2.48
12,432	5s ² S _{1/2} 4p ² P _{1/2}	0.079x10 ⁸	2	4.84
11,773	3d ² D _{5/2} 4p ² P _{3/2}	0.259x10 ⁸	6	0.896*
11,690	3d ² D _{3/2} 4p ² P _{1/2}	0.220x10 ⁸	4	0.868
11,770	3d ² D _{3/2} 4p ² P _{3/2}	0.0434x10 ⁸	4	0.896*
7,665	4p ² P _{3/2} 4s ² S _{1/2}	0.387x10 ⁸	4	— (resonance lines)
7,699	4p ² P _{1/2} 4s ² S _{1/2}	0.382x10 ⁸	2	—

*states with common lower level

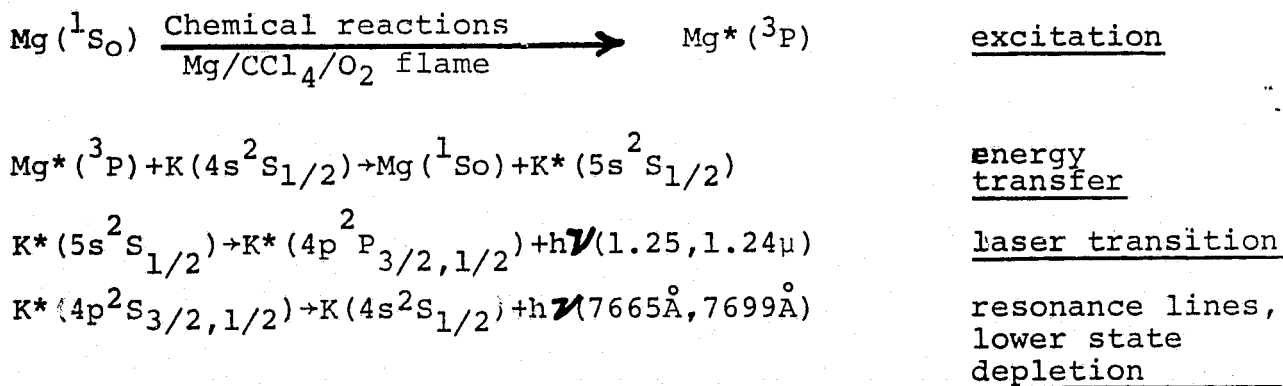
A_{ul} values from Wiese et al. (1969).

(9) Mg*(³P) - K Collisional Transfer Laser

The most highly populated electronically excited state produced in the M/CCl₄/O₂ low pressure flame is the metastable M*(³P). This occurs because M*(³P) has a long radiative lifetime and a relatively low excitation energy. In addition, transitions from many more highly excited states terminate in the ³P metastable state. Of course, the ³P metastable cannot serve as the upper level of a laser since the only state below it is the ground state. The low transition probability of the "forbidden" ³P → ¹S transition would require extremely high inversion density, since the laser gain equation presented earlier shows the gain to be proportional to A_{ul}. However, the possibility suggests itself of using this high population density of chemically produced metastable M*(³P) to pump (by resonant collisional energy transfer) a laser transition in another species. This excitation mechanism is illustrated schematically in Fig. (III-45). The energy gap between the ³P metastable state of M and state B of lasing species Z should be as small as possible to enhance collisional energy transfer, certainly no more than ≈ several kT. The rate of the B → A transition should be sufficiently slower than that

of the A→X transition to allow a population inversion to be produced. One possibility would be for A→X to be the resonance line of species Z. Thus, the criteria for the selection of species Z are that it (1) have a state in near resonance with the M*(³P) metastable which (2) has a relatively slow allowed transition to a short-lived intermediate state.

A less than exhaustive examination of the literature has revealed that these conditions can be satisfied by Mg*(³P) metastable and the 4s²S_{1/2} state of potassium. In the Mg*-K case, the steps would be:



This is illustrated in Fig. (III-46). Indeed, laser action on these very transitions has been reported in pulsed electrical discharges (Willett, 1971; Mishakov et al., 1971; Tibilov and Shukhtin, 1968). The present scheme represents the possibility of achieving the same result continuously and via chemical excitation.

An even closer resonance exists between the M^* ($3p$) levels and the K^* ($3d^2D_{5/2,3/2}$) levels at 21534 and 21537 cm^{-1} ($\Delta E = 313 \text{ cm}^{-1} \approx kT$ at 500°K). This could then radiate on the $3d^2D_{5/2,3/2} \rightarrow 4p^2P_{3/2,1/2}$ transitions (1.1773, 1.1770 and 1.1690 μ). However, no laser action has ever been reported on these transitions (Willett, 1971). A brief calculation however, considering the values of A_{ul} for the various transitions, shows clearly why this is so.

The intensity of a transition is given by

$$I = N_u A_{ul} \cdot h\nu_{ul}$$

and the decay rate in quanta per second is thus $I/h\nu_{ul} = N_u A_{ul}$. In the steady state, with no collisional quenching, the excitation equals the decay rate $= N_u A_{ul}$. Let the upper and lower laser states and the ground state be designated as states 3, 2 and 1 respectively. The decay rate of the upper laser state equals the excitation rate of the lower laser state (assuming no direct excitation of the lower state, and that the direct decay of the upper state to the ground state is forbidden, as it is in the example discussed).

$$\therefore N_3 A_{32} = N_2 A_{21}$$

and

$$N_3/N_2 = A_{21}/A_{32}$$

The inversion ratio is $(N_3/g_3) \div (N_2/g_2)$, where g_3 and g_2 are statistical weights of states 3 and 2 respectively. Then:

$$\text{inversion ratio} = \frac{(N_3/g_3)}{(N_2/g_2)} = \frac{A_{21}}{A_{32}} \cdot \frac{g_2}{g_3}$$

In a case where two sublevels of the same upper state decay to a single sublevel of the lower state (as in the $K^*(3d^2D_{5/2,3/2} \rightarrow 4p^2P_{3/2})$ transitions), an analogous result may be obtained, as follows: If the two sublevels of the upper state are denoted by states 3 and 3', then

$$N_3 A_{32} + N_{3'} A'_{32} = N_2 A_{21}$$

Assuming the sublevels populated in proportion to their statistical weights, i.e. $N_3/g_3 = N_{3'}/g_{3'}$, then

$$\text{inversion ratio} = \frac{(N_3/g_3)}{(N_2/g_2)} = \frac{(N_{3'}/g_{3'})}{(N_2/g_2)} = \frac{A_{21}}{(g_{3'}/g_2)A'_{32} + (g_3/g_2)A_{32}}$$

Calculations of inversion ratios to be expected in the transitions discussed earlier are presented in Table (XXIX). The predicted inversion ratios for the 1.25 and 1.24 μ ($5s^2S_{1/2} \rightarrow 4p^2P_{3/2,1/2}$) transitions are 2.48 and 4.84 respectively, explaining why lasing has been reported on these transitions in pulsed electric discharges (Willett, 1971; Mishakov et al., 1971; Tibilov

and Shukhtin, 1968). The inversion ratios predicted for the transitions originating in $3d^2D_{5/2,3/2}$ are all less than unity, explaining why no lasing has been reported there.

In summary, the high inversion ratios calculated above for the $K(5s^2S_{1/2} + 4p^2P_{3/2,1/2})$ transitions plus the relatively high $Mg^*(^3P)$ populations observed in the $Mg/CCl_4/O_2$ low pressure flame make the $Mg^*(^3P)$ -K transfer laser described above an attractive possibility worthy of investigation. Because of the long radiative lifetime (~ 2 milliseconds for 3P_1 , much longer for $^3P_{0,2}$) of the metastable, this species can be separated spatially from the flame reaction zone by readily attainable flow velocities. Potassium could be added downstream of the reaction zone so it would not react with reactive and energetic species in the flame and so that the $(4p^2P_{3/2,1/2})$ lower laser states should not be directly excited. The proportions of Mg vapor, CCl_4 and O_2 could be adjusted so the O_2 and CCl_4 were exhausted by reaction with Mg before injection of potassium.

CHAPTER IV - CONCLUSIONS

Two types of low pressure metal vapor flames were studied in the present investigation: (1) Flames of Ca and Mg with O_2 and N_2O , and (2) Flames of Ca and Mg with CCl_4/O_2 . Excitation in both types of flames was shown to be chemiluminescent in origin rather than thermal.

The Ca/O_2 and Ca/N_2O flames showed band emission which was assigned to high vibrational states ($v=20-30$) of the CaO ($A^1\Sigma^+$) state (and in the Ca/N_2O flame the $A^1\Pi$ state as well) whose only known transitions are to the ground electronic state. These bands were completely different from those observed by Sullivan (1969) because of the differing conditions of excitation. His flames were at considerably higher temperature and pressure, with consequent thermal excitation and collisional relaxation of the higher vibrational levels.

Relatively low quantum yields ($\sim 0.01-0.1\%$) observed in the present work suggest that most CaO is formed in the ground electronic state, which makes the excited states observed unpromising for lasers. The $A(v=n) \rightarrow X(v=m)$ transition (where n and m are both high vibrational levels) might be useful in pulsed laser applications if $X(v=m)$ is only thermally populated. However, continuous operation would not be possible as $X(v=m)$ would be filled quickly and due to the large difference

between electronic radiative lifetimes and collisional vibrational relaxation times, could not be emptied fast enough collisionally to maintain an inversion. Any additive which would increase vibrational relaxation of the ground electronic state would probably do so for the excited state as well. However, vibrational excitation in the product CaO molecule might be useful in a vibrational transition (IR) laser, making possible on a continuous basis results similar to those achieved by Rice and Jensen (1973) and Rice and Beattie (1973) using exploding wires of various metals. The results of Jones and Broida (1974) indicate the presence of small inversions of vibrational sublevels of the $A(^1\Sigma^+)$ state of BaO produced in the $Ba+N_2O$ reaction. Zare (1974), in a recent review, describes vibrationally inverted populations observed in the ground electronic state by BaX produced in the $Ba+HX$ reaction ($X=Cl, Br, I$).

The Mg/O_2 and Mg/N_2O flames showed only a broad continuum which has been attributed to the formation of a weakly bound $^3\Sigma^-$ state of MgO which then falls to a lower bound triplet state. Because of the weakly bound upper state, production of high enough excited state densities for lasing seems unlikely. The MgO green system ($B^1\Sigma^+-X^1\Sigma^+$) does not appear, supporting

Sullivan's (1969) conclusion that the excitation in his flames at higher temperature and pressure is thermal in origin.

The Mg and Ca/CCl₄/O₂ flames showed extensive metal atom line emission up to the ionization limit of each metal, but no ionic lines. Metal monochloride and C₂ band emission were also observed. Because of the advantages for laser application of energy concentrated in atomic states (rather than spread over the vibrational and rotational sublevels of molecular states), attention was concentrated on the atomic transitions, many of which had a lower state other than the ground state. (All the molecular transitions observed terminated in the ground state and had short radiative lifetimes, thus sharing the disadvantages for laser use described above for CaO.)

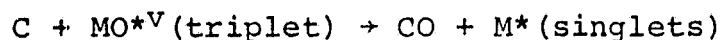
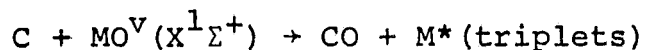
A log (population) vs. upper state energy plot (Boltzmann plot) of the observed atomic excited states revealed extreme non-equilibrium excitation, showing wide scattering of the points with no Boltzmann distribution. However, a log (excitation rate) vs. energy plot (Arrhenius-type plot) showed a straight line with slope corresponding to a temperature ~5000°K for triplets and ~2500°K for singlets when the gas temperature was 500°K. What appears

to be happening is excitation by chemical reaction with the upper state energy playing the role of an activation energy. The populations are governed purely by the rate of excitation and the radiative transition probabilities of the excited states. There is no chance for establishment of a Boltzmann distribution of population because the radiative lifetime, $\sim 10^{-8}$ sec, is much shorter than the mean time between collisions, $\sim 10^{-6}$ sec at ~ 1 torr, 500°K .

Extensive studies were made of the effects of CCl_4 and O_2 concentration, various quenchers (N_2 , NO , etc.) and pressure on the observed emissions, in an effort to elucidate the excitation mechanism. The emitted intensity was found to vary linearly with O_2 concentration and to increase with CCl_4 concentration, but to reach a maximum and then decay as these reactant concentrations were increased further. In Chapter III a wide range of possible excitation mechanisms was examined critically in the light of the results of these experiments, with the conclusion that the source of the up to 7.5 eV. excited state energy observed must be the ~ 11 eV. bond energy of CO , since the MO bond energies are ~ 4 eV. and the MCl bond energies are lower, and thus could not supply all the energy required. C_2 and MCl are believed to be excited by energy transfer from vibrationally excited CO ,

but it has been shown that this type of mechanism cannot account for the observed metal atom excitation.

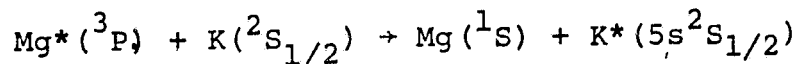
That is explained by the mechanism:



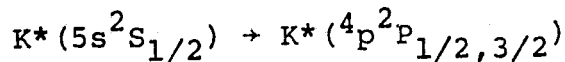
where "*" and "v" are electronic and vibrational excitation respectively. The different excitation temperatures observed for triplet and singlet metal atoms are explained in terms of different vibrational temperatures of singlet and triplet metal oxide molecules, respectively. Low-lying triplet states of MgO have been described by Schamps and Lefebvre-Brion (1972) and similar states of CaO, SrO and BaO by Field (1974). Jones and Broida (1974) have published vibrational population distributions for singlet BaO produced in low pressure flames which can be described well by a vibrational temperature $\sim 5000^\circ K$. NO quenching experiments have shown that electronically excited $CO(a^3\Pi)$ is not involved in the metal atom excitation process, nor in the excitation of C_2 or MCl.

Monitoring of relative populations of upper and lower electronically excited states showed that population inversions appear to have been established on a number of electronic transitions, on a continuous (rather than pulsed) basis, by means of purely chemical excitation. However,

absolute population estimates (based on self-absorption and absolute emitted intensity measurements) showed that the inversion densities were $\sim 10^5 \text{ cm}^{-3}$ while reasonable estimates of path length and mirror reflectance would require $\sim 10^8 \text{ cm}^{-3}$ for lasing. Another possibility for laser action has been found, based on estimated populations of $\sim 10^{11} \text{ cm}^{-3}$ in the $\text{Mg}^*(^3\text{P})$ metastable state. A close resonance has been noted between this state and the $5s^2\text{S}_{1/2}$ state of potassium. If the collisional energy transfer



could be efficiently achieved, then lasing might be possible at 1.25μ via the



transitions. The lower state is connected to the ground state by the K resonance lines and would be rapidly depleted. The relative transition probabilities are such as to favor inversion, and lasing has been reported on these transitions in pulsed electric discharges (Willett, 1971; Tibilov and Shukhtin, 1968; Mishakov et al., 1971).

The $\sim 10^5 \text{ cm}^{-3}$ inversion densities in Ca^* and Mg^* mentioned earlier might be increased by raising O_2 , CCl_4 and metal atom concentrations and pressure. However,

this would be limited by quenching of the chemiluminescence observed as $[O_2]$ and $[CCl_4]$ are raised, and raising pressure would eventually reduce the time between collisions to the point where thermalization of the excited states occurred. Certainly, the increase by a factor of 10^3 required to lase does not appear feasible. However the changes mentioned above might increase the metastable $M^*(^3P)$ concentration and make the $M^* - K$ transfer laser suggested above seem even more feasible. Here too however, there is a limit to improvement set by the quenching of the long-lived (~ 2 milliseconds) $Mg^*(^3P)$ state.

A few words are in order here regarding several possibilities suggested by the present work which are not connected with lasers. The low pressure $M/CCl_4/O_2$ flame may prove a useful technique for studying carbon atom reactions via the quenching effect on chemiluminescent emission of different additives by consuming C atoms. C atom reactions have hitherto been studied using arc or hot wire sources (where the species produced is not definite), flash photolysis of carbon suboxides and isotope decay ("hot-atom") techniques. The $Mg/CCl_4/O_2$ flame may be useful as a chemical source of discrete ultraviolet and visible wavelengths, as most of the emission is in a few strong lines. It may also prove the basis

of a linear detector of low concentrations of oxygen in inert gases.

A number of possibilities for future research are suggested by the results of the present study. The $\text{Mg}^*(^3\text{P}) - \text{K}$ transfer system described above could be investigated to determine if a laser along these lines is practical. Other possible $\text{M}^*(^3\text{P}) - \text{Z}$ resonances (where Z is some atom other than K) could be sought. The flames of Sr and Ba with CCl_4/O_2 would be of interest (particularly Ba because of its many low-lying states). Examination of the spatial distribution of emitters in the flames already studied (by photographs taken through interference filters centered on specific atomic and molecular transitions) might reveal that actual point inversion ratios are even higher than the overall average values measured in the present work. Studies of the $\text{M}/\text{CCl}_4/\text{O}_2$ system at higher pressures might be of some interest. Zhitkevich et al. (1963a) reported chemiluminescence with Boltzmann (population) temperatures $\sim 12,000^\circ\text{K}$ at atmospheric pressure in these metal/ CCl_4/O_2 systems, but gave few details of the temperature measurement. If a "two-line" method (Gaydon and Wolfhard, 1960) was used, non-equilibrium excitation of a single line could produce serious errors. However, the occurrence of even the weakest chemiluminescence at such high pressure is of interest, and may involve

different mechanisms than those operative at lower pressures. Although thermalization of excited state populations is likely at atmospheric pressure, a significantly higher $M^*(^3P)$ population for use in a collisional transfer laser might be present.

Another possibility is presented by the Ba/N_2O system. Based on an assumed kinetic scheme which matches experimental quantum yield vs. pressure data, Hsu, Krugh and Palmer (1974) concluded that 99.6% of the BaO produced in the Ba/N_2O reaction is produced originally in the $(a^3\Pi)$ state and the observed emission is due to collisionally induced curve-crossing into singlet states. Many workers (Hsu et al., 1974; Field, Jones and Broida, 1974) have concentrated on using higher pressures (~ 10 torr) to facilitate this process and increase quantum yield. However, since the observed singlet emission is from transitions terminating in the ground state, they may be proceeding in the wrong direction. It might be better to keep pressure low and minimize pressure-induced crossing, to keep the BaO in the triplet state in which it is formed and build up a large population of $BaO(a^3\Pi)$, while minimizing the production of ground state BaO . Although the triplet state is nominally metastable, it should be remembered that the high atomic weight of

barium makes the spin selection rule much less rigorous. Kuhn (1962) notes that the "forbidden" 3P_1 -1s line of Ba is weaker than the resonance line by a factor of only 146. If the analogous transition in BaO is no more "forbidden" than this, then a laser operating upon the BaO $a^3\Pi-X^1\Sigma^+$ transition might be feasible. Using Johnson's (1971) value of 3.5×10^{-7} sec for the radiative lifetime of BaO($A^1\Sigma^+$) and assuming the same ratio between transition probabilities of allowed and "forbidden" transitions in BaO and Ba gives a radiative lifetime of about 5×10^{-5} sec for BaO($a^3\Pi$). Using an assumed mirror reflectance of 99% and a path length of 10. cm, the laser gain equation predicts a threshold inversion density of $\sim 10^{17}$ cm $^{-3}$. (admittedly optimistic since the energy is spread over a band rather than concentrated in a line). Such a density appears quite attainable in view of total density of $\sim 10^{16}$ cm $^{-3}$ at 1. torr and the hypothesized formation of 99.6% of the BaO in the excited state. Using Field's (1974) value for the energy of the BaO($a^3\Pi$) state would predict emission on this transition at about 5756Å. The corresponding transition in CaO is at 1.216 microns.

In conclusion, the present work has indicated the production by chemical means of continuous population

inversions in Mg and Ca/CCl₄/O₂ flames at inversion densities below threshold, and has suggested possible systems which might produce high enough inversion densities to lase. In many respects the present situation with respect to electronic transition chemical lasers is similar to that of vibration-rotation chemical lasers in 1965. Then, many approaches were being pursued in the effort to produce a chemical laser, a few weak inversions had been observed, but no successful chemical laser had been produced. Several years later, however, chemical lasers were an actuality. It is to be hoped that similar success will crown the efforts in electronic transition lasers, and that perhaps the present work will have made a small contribution to that achievement.

References

- Aller, L. H. (1963). Astrophysics: The Atmospheres of the Sun and Stars. N.Y. Ronald Press.
- Applied Optics, Suppl. 2: Chemical Lasers, New York, Optical Society of America (1965).
- Arnold, S.J. and Rojeska, H. (1973). Chemical lasers: A comprehensive literature survey. Applied Optics, 12, 169.
- Askar'ian, G. A., Gol'ts. E. Ia. and Rabinovich, M.S. (1966). Use of artificial meteors for laser pumping. JETP Letters 4, 305.
- Balfour, W. J. and Douglas, A. E. (1970). Absorption spectrum of the Mg_2 molecule, Can. J. Phys. 53, 901.
- Balfour, W. J. and Whitlock, R. F. (1971). Ca_2 : a van der Waals molecule. J. Chem. Soc. (Lond.), 13D, 1231.
- Batalli-Cosmovici, C. and Michel, K.-W. (1971). "Reactive scattering of a supersonic O_2 beam on Ba atoms," Chem. Phys. Lett., 11, 245.
- Bauman, R. P. (1962). Absorption Spectroscopy, N.Y., Wiley.
- Bennett, W. R., Jr. (1965). Inversion mechanisms in gas lasers. Applied Optics, Suppl. 2: Chemical Lasers, 3.
- Beutler, H. and Polanyi, M. (1928). Uber hochverdunnte Flammen. I. Flammen in einfachen Rohr, vor lavfige Analyse des Reactionmechanismus. Reaction-geschwindigkeit Leuchtvorgang. Z. Physik.Chem., 1B, 3.
- Birely, J. H. et al. (1969). Molecular beam kinetics: reactions of Na with CH_3I , Br_2 and ICl . J. Chem. Phys. 51, 5461.
- Black, G., Luria, M., Eckstrom, D. J., Edelstein, S. A. and Benson, S. W. (1974). Chemiluminescence photon yields for some encapsulated metal system flames". J. Chem. Phys., 60, 3709.

- Boudart, M. (1968). Kinetics of Chemical Processes. Englewood Cliffs, Prentice-Hall.
- Bowen, J. R. and Overholser, K. A. (1969). An appraisal of the continuous explosion laser. Astronautica Acta, 14, 475.
- Bowker, A. H. and Lieberman, G. J. (1959). Engineering Statistics. Englewood Cliffs, Prentice-Hall.
- Bradley, D. and Matthews, K. J. (1967). Ionization and electron temperatures in carbon monoxide and hydrogen flames with added methane. in Eleventh Symposium (International) on Combustion, Pittsburgh, The Combustion Institute, p. 359.
- Braun, W. et al. (1969). Flash photolysis of carbon suboxide: Absolute rate constants for the reaction of C(3P) and C(1D) with H₂, N₂, CO, NO, O₂ and CH₄. Proc. Roy. Soc. (Lond.) A312, 417.
- Brennen, W. R. and Kistiakowsky, G. B. (1966). Reactions of metal carbonyls with active nitrogen. J. Chem. Phys., 44, 2695.
- Brewer, L. and Hauge, R. (1968). Near infrared bands of diatomic CaO and SrO. J. Mol. Spectrosc., 25, 330.
- Bugrim, D. E. et al. (1966). Excitation Characteristics of the Swan bands of C₂ in streams of metals and organic compounds. Optics and Spectroscopy, 20, 360.
- Bundy, F. P. and Strong, H. M. (1954). Measurement of flame temperature, pressure and velocity. In: Physical Measurements in Gas Dynamics and Combustion. B. Lewis, R. N. Pease and H. S. Taylor, eds. Princeton, Princeton University Press.
- Callear, A. B. and Lambert, J. C. (1969). The transfer of energy between chemical species. Comprehensive Chemical Kinetics, Vol. 3: The Formation and Decay of Excited Species, Bamford, C. H. and Tipper, C. F. H. eds. Elsevier, New York, Chapter 4, pp. 182-273.
- Capelle, G. A., Bradford, R. S. and Broida, H. P. (1973). Chemiluminescence and laser photoluminescence of some diatomic metal halides. Chem. Phys. Lett., 21, 418.

- Carabetta, R. and Kaskan, W. E., "The oxidation of sodium, potassium and cesium in flames," J. Phys.Chem., 72, 2482 (1968).
- Carrington, T. and Garvin, D. (1969). The chemical production of excited states. Comprehensive Chemical Kinetics, Vol. 3: The Formation and Decay of Excited Species, Bamford, C. H. and Tipper, D. F. H. eds., Elsevier, New York, Chapter 3, pp. 107-181.
- Chandrasekhar, S. (1960a) Radiative Transfer, N.Y., Dover.
- Chapman, A. J. (1967). Heat Transfer, 2nd ed. London, Macmillan.
- Charters, P. E. and Polanyi, J. C. (1960). An improved technique for the observation of infrared chemiluminescence. Can. J. Chem., 38, 1742.
- Chester, A. N. (1971). Chemical lasers: a status report. Laser.Focus, 25, Nov.
- Clough, P. N. and Thrush, B. A. (1967). Mechanism of chemiluminescent reaction between nitric oxide and ozone. Trans. Faraday Soc., 63, 915.
- Cohen, Wilkins, R. and Jacobs, T. A. (1970). Theoretical calculations of detonation initiated chemical lasers. IEEE J. Quantum Electronics, QE-6, 168.
- Colin, R. and Jones, W. E. (1967). The $b^1\Sigma^+ - x^3\Sigma^-$ band system of NCl. Can. J. Phys., 45, 301.
- Conger, R. L., Johnson, J. H. et al. (1966). Argon bomb pumping of ruby laser. Applied Optics 5, 1240.
- Cool, T. A. (1971a). CW chemical lasers, IEEE International Convention Digest 348.
- Cool, T. A. (1971b). A summary of recent research on continuous-wave chemical lasers. Modern Optical Methods in Gas Dynamic Research, Dosanjh, D.S., ed., New York. Plenum Press.
- Cool, T. A. et al. (1969). A continuous-wave chemically excited CO₂ laser. Int. J. Chem. Kinetics. 1, 495.

- Cooper, A. R. and Jeffreys, G. V. (1971). Chemical Kinetics and Reactor Design. Edinburgh, Oliver and Boyd.
- Corliss, C. H. and Bozman, W. R. (1962). Experimental Transition Probabilities for Spectral Lines of Seventy Elements. NBS Monograph 53. Washington, National Bureau of Standards.
- Corneil, P. H. and Kasper, J. V. V. (1970). Computer simulation of the HCl explosion laser. IEEE J. Quantum Electronics, QE-6, 170.
- Corneil, P. H. and Pimentel G. C. (1968). Hydrogen-chlorine explosion laser. J. Chem. Phys. 49, 1379.
- Dagdigian, P. J., Cruse, H. W. and Zare, R. N. (1974), Radiative lifetimes of the alkaline earth monohalides. J. Chem. Phys., 60, 2330 (1974).
- Danen, W. C. (1974). Abstraction of halogen atoms by free radicals. Ch. 1 in Methods in Free Radical Chemistry, Vol. 5, E. S. Huyser, ed. N. Y., Marcel Dekker.
- Davies, P. B., Thrush, B. A. and Tuck, A. F. (1970). Reaction of deuterium atoms with methyl bromide studied by gas phase ESR spectroscopy. Trans. Faraday Soc., 66, 886.
- Denbigh, K. G. and Turner, J. C. R. (1971). Chemical Reactor Theory, 2nd ed. Cambridge, Cambridge University Press.
- Duthler, C. J. and Broida, H. P. (1973b). Excitation of Group Ia and IIb metal atoms by a Lewis-Rayleigh nitrogen afterglow. J. Chem. Phys., 59, 167.
- Duthler, C. J. and Broida, H. P. (1973a). Chemiluminescence reactions involving metal vapors. in Chemiluminescence and Bioluminescence, M. J. Cormier, D. J. Hercules and J. Lee, eds. N.Y., Plenum.
- Eckstrom, D. J., Edelstein, S. A. and Benson, S. W. (1974). "Chemiluminescence photon yields for several alkaline earth metal-halogen/oxygen reactions". J. Chem. Phys., 60, 2930.

- von Engel, A. (1967). Collisions in gases and flames involving excited particles. Brit. J. Appl. Phys. 18, 1661.
- von Engel, A. and Cozens, J. R. (1964). Origin of excessive ionization in flames. Nature, 202, 480.
- Evans, M. G. and Polanyi, M. (1939). Notes on the luminescence of sodium vapor in highly dilute flames. Trans. Faraday Soc., 35, 178.
- Ewing, J. Milstein, R. and Berry, R. S. (1970). Population inversions in shock-induced dissociation of alkali halides. Shock Tubes, Proc. of the 7th Int. Symposium, University of Toronto, June 23-25, 1969, I. I. Glass, ed., University of Toronto Press.
- Field, R. W. (1974). "Assignment of the lowest 3Π and 1Π states of CaO, SrO and BaO". J. Chem. Phys., 60, 2400.
- Field, R. W., Capelle, G. A. and Jones, C. R. (1974). "The $A^1\Pi-X^1\Sigma$ system of CaO". submitted to J. Mol. Spectroscopy.
- Field, R. W., Jones, C. R. and Broida, H. P. (1974). Gas-phase reaction of Ba with N_2O . II. Mechanism of reaction". J. Chem. Phys., 60, 4377.
- Fristrom, R. M. and Westenberg, A. A. (1965). Flame Structure, McGraw-Hill, N.Y., pp. 11-13.
- Garvin, D. and Kistiakowsky, G. B. (1952). The kinetics of coordinate bond formation. J. Chem. Phys., 20, 105.
- Gaydon, A. G. (1957). The Spectroscopy of Flames. London, Chapman and Hall.
- Gaydon, A. G. (1968). Dissociation Energies and Spectra of Diatomic Molecules, 3rd ed., London, Chapman and Hall.
- Gaydon, A. G. and Wolfhard, H. H. (1950). "Spectroscopic studies of low pressure flames: IV. Measurement of light yield for C_2 bands". Proc. Roy. Soc. (Lond.), 201A, 570.

- Gaydon, A. G. and Wolfhard, H.G. (1951). Spectroscopic studies of low pressure flames. V. Evidence for abnormally high electronic excitation. Proc.Roy.Soc.(Lond.), A205, 118.
- Gaydon, A. G. and Wolfhard, H. G. (1960). Flames, Their Structure, Radiation and Temperature, 2nd ed., rev. N.Y., Macmillan.
- Gebbie, H.A. and Bohlander, R. A. (1972). Non resonant cavity as a long path absorption cell. Applied Optics, 11, 723.
- Gerry, E. T. (1971). Gas dynamic lasers. IEEE International Convention Digest, 352.
- Glasstone, S., Laidler, K. J. and Eyring, H. (1941). The Theory of Rate Processes, First Ed. N.Y., McGraw-Hill.
- Glasstone, S. and Lewis, D. (1960). Elements of Physical Chemistry. Princeton, Van Nostrand.
- Gole, J. L. (1973). Private communication. Solid State Materials Physics Seminar, Princeton University, March 26, 1973.
- Gole, J. L. and Zare, R. N. (1972). Determination of D_0° (AlO) from crossed beam chemiluminescence of $Al+O_3$. J.Chem.Phys., 57, 5331.
- Gorog, I. (1961). Coherent optical emission from molecular beams. Cal.U.Berkeley, Electronics Research Laboratory. Inst.Eng.Res., Ser.60/I-418.
- Graham, B. J. (1971). Combustion laser. U.S. Patent 3,573, 655, April 6. [This describes a hydrogen-oxygen explosion laser, in a rather vague manner, with very fragmentary information. No working laser of this design has been reported.]
- Green, D. W. (1968). Arc spectrum of magnesium oxide. Ph.D. Thesis. Univ. of California, Berkeley. UCRL-17878-Rev.
- von Haber, F. and Zisch, W. (1922). Anregung von Gasspectern durch chemische Reaktionen, Zeit.Physik, 9, 302.
- Hajdu, L. (1963). Diatomic gas optical maser with exploding wire pumping source. Cal. U. Berkeley, Electronics Research Laboratory, Report 63-12, (AROD-33233).

- Hansel, J. G., Mellor, A. M. and Sullivan, H.F. (1967). The combustion of metals, final report, 1 July 1964 to 30 June 1966, to Sandia laboratories. Report SC-CR-67-2611, Princeton University, May.
- Hardy, A. C. and Perrin, F. H. (1932). The Principles of Optics. N.Y., McGraw-Hill.
- von Hartel, H. and Polanyi, M. (1930). Z.physikal.Chem., 11B, 97. Quoted in Heller and Polanyi (1936).
- Hauge, R. H. (1966). Spectra of CaO. Ph.D. Thesis, Dept. of Chemistry, University of California, Berkeley.
- Heller, W. (1937). A critical investigation and development of the diffusion method for determining speeds of atomic reactions, Trans.Faraday Soc., 33, 1556.
- Heller, W. and Polanyi, M. (1936). Reactions between sodium vapour and volatile polyhalides. Velocities and luminescences. Trans.Faraday Soc. 32, 633.
- Herzberg, G. (1944). Atomic Spectra and Atomic Structure. N.Y., Dover.
- Herzberg, G. (1950). Molecular Structure and Molecular Spectra, I. Spectra of Diatomic Molecules, Second ed., Princeton, Van Nostrand.
- Herzberg, G. (1967). Molecular Spectra and Molecular Structure. III. Electronic Spectra and Electronic of Polyatomic Molecules. N.Y., Van Nostrand.
- Hill, R. A. and Hartley, D. L. (1974). Focused, multiple-pass cell for Raman scattering. Applied Optics, 13, 186.
- Hinnov, E. and Hirschberg, J. G. (1962). Electron-ion recombination in dense plasmas. Phys.Rev., 125, 795.
- Hirschfelder, J. (1941). Semi-empirical calculations of activation energies. J.Chem.Phys., 9, 645.
- Hodgman, C. D., Weast, R.C. and Selby, S. M., eds. (1958). Handbook of Chemistry and Physics, 39th ed. Cleveland, Chemical Rubber Publishing Co.
- Hurle, I. R. and Hertzberg, A. (1965). Electronic population inversions by fluid mechanical techniques. Physics of Fluids 8, 1601.

- Husain, D. and Kirsch, L. J. (1971). Reactions of atomic carbon $C(2^3P_J)$ by Kinetic absorption spectroscopy in the vacuum ultraviolet. Trans. Faraday Soc. 67, 2025.
- Hsu, C. J., Krugh, W. D. and Palmer, H. B. (1974). Pressure dependence of the $A(1\Sigma) \rightarrow X(1\Sigma)$ photon yield in the reactions of $Ba(g)$ with N_2O and NO_2 . J. Chem. Phys., 60, 5118.
- IEEE (1970). IEEE J. Quantum Electronics, QE-6, 168-186.
- JANAF Thermochemical Data, Interim Tables, Dow Chemical Co., Midland, Michigan, 1960-64.
- Jesson, P. F. and Gaydon, A. J. (1967). Study of the absorption spectra of free radicals in flames. Combustion and Flame, 11, 11.
- Johnson, S. E. (1971). Spectroscopy of selected diatomic metal and metal-oxide molecules using laser excited fluorescence. Ph.D. Thesis, University of California, Santa Barbara, Physics Department.
- Johnston, H. J. (1966). Gas Phase Reaction Rate Theory, N.Y., Ronald Press.
- Jonah, C. D. and Zare, R. N. (1971). Formation of group II dihalides by two-body radiative association. Chem. Phys. Lett., 9, 65.
- Jonah, C. D., Zare, R. N. and Ottinger, Ch. (1972). Crossed-beam chemiluminescence studies of some group IIa metal oxides. J. Chem. Phys. 56, 263.
- Jones, C. R. and Broida, H. P. (1973). An efficient chemiluminescent reaction. J. Chem. Phys., 59, 6677.
- Jones, C. R. and Broida, H. P., (1974a). "Chemical lasers in the visible." Laser Focus, 10, 37 (1974a).
- Jones, C. R. and Broida, H. P., (1974b). Gas-phase reaction of Ba with N_2O . I. Measurement of production efficiency of excited states. J. Chem. Phys., 60, 4369.

- Kaufman, E. D. and Reed, J. F. (1963). The vapor phase diffusion flame reaction of sodium with fluorinated chloromethanes. J.Phys.Chem., 67, 896.
- Kaufman, F. (1958). The air afterglow and its use in the study of some reactions of atomic oxygen. Proc.Roy.Soc.(Lond.), A247, 123.
- Kikuchi, T. T. and Broida, H. P. (1965). Laser possibilities of chemically excited molecules formed with atomic species. Applied Optics, Suppl. 2: Chemical Lasers, New York, Optical Society of America.
- Klemsdal, H. (1973). The variation of the electronic transition moment, M_e , in the intensity theory of diatomic molecules. J. Quant. Spectrosc. Radiat. Transfer, 13, 517.
- Kuhn, H.G. (1962). Atomic Spectra. N.Y., Academic Press.
- Kwei, G. H. and Herschbach, D. R. (1969). Molecular beam kinetics: reactions of K, Rb, and Cs with ICl and IBr. J.Chem.Phys. 51, 1742.
- Ladenburg, R. W. et al., eds. (1954). Physical Measurements in Gas Dynamics and Combustion. Princeton, Princeton University Press. p.300.
- Lagerqvist, A. and Huldt, L. (1954). The height of the excited electron states of calcium, strontium and barium oxides. Ark.Fys., 8, 427.
- Laidler, K. J. (1955). The Chemical Kinetics of Excited States. Oxford, Clarendon Press.
- Laidler, K.J. (1965). Chemical Kinetics, 2nd ed. N.Y., McGraw-Hill.
- Lin, S. M., Mims, C.A. and Herm., R.R. (1973). Crossed beams chemistry: Reactions of Ba, Sr, Ca and Mg with Cl₂ and Br₂. J.Chem.Phys., 58, 327.
- Mackay, C. and Wolfgang, R. (1965). Free carbon atom chemistry. Science, 148, 899.

- Marchenko, V. M. and Prokhorov, A. M. (1971). Possibility of producing an inverted medium for lasers by means of an explosion. JETP Lett., 14, 76.
- Markstein, G. H. (1963). Magnesium-oxygen dilute diffusion flame. 9th Symposium (International) on Combustion. N.Y., Academic Press.
- Markstein, G. H. (1967). Heterogeneous reaction processes in metal combustion. 11th Symposium (International) on Combustion. Pittsburgh, The Combustion Institute.
- Marr, G. V. (1968). Plasma Spectroscopy. N.Y., Elsevier.
- Massey, H. S. W., Burhop, E. H. S. and Gilbody, H. B. (1971). Electronic and Ionic Impact Phenomena, 2nd ed. Vol. III. Collisions of Heavy Particles. Oxford, Clarendon Press.
- Mavrodineau, R. and Boiteux, H. (1965). Flame Spectroscopy. N. Y., Wiley.
- McCubbin, T. K., Jr. and Grosso, R. P. (1963). A White-type multiple pass absorption cell of simple construction. Applied Optics, 2, 764.
- Mellor, A. M. (1967). Heterogeneous ignition of metals: Model and experiment. Ph. D. Thesis. Princeton Univ., Dept. of Aerospace and Mech. Sci.
- Menzinger, M. and Wren, D. J. (1973). Hermaphroditism in chemical dynamics: The reaction $\text{Ba} + \text{Cl}_2 \rightarrow \text{BaCl} + \text{Cl}$. Chem. Phys. Lett., 18, 431.
- Miller, W. J. and Palmer, H. B. (1963). Spectra of alkali metal-organic halide flames. 9th Symposium (International) on Combustion. N.Y., Academic Press. p. 137.
- Milne, E. L. (1970). Sodium-atom excitation in nitrogen afterglows. J. Chem. Phys., 52, 5360.
- Mims, C. A., Lin, S. M. and Herm, R. R. (1972). Crossed beam collision mechanics: Reactions of Ca, Sr and Ba with HI and limits on D₀ for CaI, SrI and BaI. J. Chem. Phys., 57, 3099.
- Mims, C. A., Lin, S. M. and Herm, R. R. (1973). Crossed beams product angular distributions: MCl and MI from Ba, Sr, Ca and Mg + ICl and BaCN and BaBr from Ba + BrCN. J. Chem. Phys., 58, 1983.

- Mishakov, V. G. Tibilov, A. S. and Shukhtin, A. M. (1971).
Laser action in Na-H₂ and K-H₂ mixtures with pulsed
injection of metal vapor into a gas discharge plasma.
Opt. Spectry., 31, 176.
- Naegeli, D. W. (1967). Chemiluminescence in diffusion
flames of halides burning in vapors of alkali metals.
Ph.D. Thesis. Pennsylvania State University. Depart-
ment of Fuel Science.
- Naegeli, D. W. (1974a). Private communication.
- Naegeli, D. W. (1974b). Unpublished manuscript.
- Naegeli, D. W. and Palmer, H. B. (1968). Creation of
Population inversion in the A³Πg state of C₂ by
chemical reaction. J. Chem. Phys., 48, 2372.
- Nieuwpoort, W. C. and Bleekrode, R. (1965). Chemical
lasers, I. Z. Angew. Math. Phys., 16, 101.
- Obenauf, R.H., Hsu, C. J. and Palmer, H. B. (1972a).
Mechanism of production of electronically excited
BaO in the reaction of Ba vapor with O₂. Chem. Phys.
Lett., 17, 455.
- Obenauf, R. H., Hsu, C. J. and Palmer, H. B. (1972b).
Distribution of electronic states in products of
elementary reactions. Ba + N₂O → BaO(A¹Σ or X¹Σ) + N₂
or NO. J. Chem. Phys., 57, 5607.
- Obenauf, R. H., Hsu, C. J. and Palmer, H. B. (1973a).
Distribution of electronic states in products of
elementary reactions. II. Ba(g) or Ca(g) + ONCl → NO
BaCl(C²Σ, A²Σ or X²Σ) or CaCl(B²Σ, (g) A²Σ or X²Σ).
J. Chem. Phys., 58, 4693.
- Obenauf, R. H., Hsu, C. J. and Palmer, H. B. (1973b).
Production of electronically excited species in some
exothermic elementary reactions. Combustion Institute
European Symposium 1973, Proceedings. Weinberg, F. J.,
ed. London, Academic Press.
- Ogryzlo, E. A., Reilly, J. P. and Thrush, B. A. (1973).
Vibrational excitation of CO from the Reaction C + O₂.
Chem. Phys. Lett., 23, 37.

- Ortenberg F. S. and Antropov, E. T. (1967). Probability of electron-vibrational transitions in diatomic molecules. Soviet Physics Uspekhi, 9, 717.
- Ottinger, C. and Zare, R. N. (1970). Crossed beam chemiluminescence. Chem. Phys. Lett., 5, 243.
- Padley, P. J. and Sugden, T. M. (1960). Chemiluminescence and radical recombination in hydrogen flames. 7th Symposium (International) on Combustion. London, Butterworths. p. 235.
- Parrish, D. D. and Herm, R. R. (1969). Molecular beam kinetics. I. Magnetic deflection analysis of reactions of Li with Cl_2 , ICl , Br_2 , SnCl_4 and PCl_3 . J. Chem. Phys. 51, 5467.
- Pearse, R. W. B. and Gaydon, A. G. (1963). The Identification of Molecular Spectra, 3rd ed., N.Y., Wiley.
- Perry, J. H., ed. (1950). Chemical Engineers' Handbook, 3rd ed. N.Y., McGraw-Hill.
- Peyron, M. (1971). Le Laser Chimique, J. Chim. Phys. 68, 1391.
- Pimentel, G. C. (1966). Chemical lasers, Scientific American 214, 32.
- Polanyi, J. C. (1959). Energy distribution among reagents and products of atomic reactions. J. Chem. Phys. 31, 1338.
- Polanyi, J. C. (1961). Proposal for an infrared maser dependent on vibrational excitation. J. Chem. Phys., 34, 347.
- Polanyi, J. C. (1965). Vibrational-rotational population inversion. Applied Optics, Suppl. 2: Chemical Lasers, 109.
- Polanyi, J. C. (1971). Nonequilibrium processes. Applied Optics 10, 1717.
- Polanyi, J. C. and Cashion, J. K. (1960). Infrared chemiluminescence, I. Infra-red emission from hydrogen chloride formed in the hydrogen plus hydrogen chloride, atomic hydrogen plus deuterium chloride and atomic deuterium plus hydrogen chloride. Proc. Roy. Soc., (London) A258, 529.
- Polanyi, M. (1932). Atomic Reactions, London, Williams and Norgate.

- Polanyi, M. and Schay, G. (1928). Eine Chemilumineszenz Zwischen Alkalimetалldampfen und Zinnhalogeniden. Z. Physik 47, 814.
- Pressman, J., Wentink, T. and Schuler, C. (1967). Study on theory and applicability of laser techniques for measuring atmospheric parameters. Appendix I.: Compilation of known Franck-Condon factors and r-centroids. Second Quarterly Report, Contract NAS 12-540 NASA-CR-94513.
- Rapp, D. and Johnston, H. S. (1960). Nitric Oxide Dilute Diffusion Flame. J. Chem. Phys., 33, 695.
- Reed, J. F. and Rabinovitch, B. S. (1955). The sodium diffusion flame method for fast reactions. I. Theory of the experimental method. J. Phys. Chem., 59, 261.
- Reed, J. F. and Rabinovitch, B. S. (1957). The sodium diffusion flame method for fast reactions. II. Reactions of fluorinated methyl chlorides. J. Phys. Chem. 61, 598.
- Rice, W. W. and Beattie, W. H. (1973). Metal atom oxidation lasers. Chem. Phys. Lett., 19, 82.
- Rice, W. W. and Jensen, R. J. (1973). Aluminum fluoride exploding wire laser. Applied Phys. Lett., 22, 67.
- Sakurai, K., Johnson, S. E. and Broida, H. P. (1970). Laser-induced fluorescence of BaO. J. Chem. Phys., 52, 1625.
- Schamps, J. and Lefebvre-Brion, H. (1972). SCF calculations of the electronic states of magnesium monoxide. J. Chem. Phys., 56, 573.
- Schultz, A. and Zare, R. N. (1974). Comparison of Ba + O₃ and Ba + N₂O chemiluminescence, J. Chem. Phys., 60, 5120.
- Seidel, W., Martin H. and Mietzner, F. G. (1965). Reaction between hydrogen atoms and carbon tetrachloride by a molecular beam method. Z. Physik, Chem., 47, 348. Quoted in Chemical Abstracts, 65, 82d (1966).

- Semenov, N. N. (1958). Some Problems of Chemical Kinetics and Reactivity, rev.ed., Vol.I. N.Y., Pergamon Press.
- Shuler, K.E. (1953). On the kinetics of elementary reactions in flames and its relation to the energy distribution of active species. J. Phys. Chem., 57, 396.
- Shuler, K. E., Carrington, T. and Light, J. C. (1965). Nonequilibrium chemical excitation and chemical pumping of lasers. Applied Optics, Suppl. 2: Chemical Lasers, 81.
- Skell, P. S. and Harris, R. F. (1965). The reaction of carbon atoms with chlorinated hydrocarbons. J. Amer. Chem. Soc., 87, 5807.
- Slanger, T. G. and Black, G. (1971). $\text{CO}(a^3\Pi)$, its production, detection, deactivation and radiative lifetime. J. Chem. Phys., 55, 2164.
- Smith, F. T. (1954). Theory of the spherical diffusion flame: The effect of atmosphere depletion. J. Chem. Phys., 22, 1605.
- Smith, W. H. (1969). Transition probabilities for the Swan and Mulliken C_2 bands. Astrophys. J., 156, 791.
- Sorokin, P. P. and Lankard, J. R. (1971). Infrared lasers resulting from giant pulse laser excitation of alkali metal molecules. J. Chem. Phys. 54, 2184.
- Spindler, R. J. (1965). Franck-Condon factors based on RKR potentials with applications to radiative absorption coefficients. J. Quantative Spectrosc. Rad. Transfer, 5, 165.
- Spinnler, J. F. and Kittle, P. A. (1970). Hydrogen fluoride chemical laser-a demonstration of pure chemical pumping. IEEE J. Quantum Electronics QE-6, 169.
- Steinfeld, J. I. and Kinsey, J. L. (1970). The determination of chemical reaction cross sections.

Ch.1 in Progress in Chemical Kinetics, Vol.5., G. Porter, ed. N.Y., Pergamon.

Stokes, C. S. (1970). The investigation of the use of high brightness flames of a possible source for pumping solid laser rods. Report GL-1970-8 (AD-709698), Philadelphia, Temple University.

Sullivan, H. F. (1969). The structure of the alkaline-Earth metal diffusion flame. Ph.D. Thesis, Princeton University. Department of Aerospace and Mechanical Sciences.

Tewarson, A., Naegeli, D. W. and Palmer, H. B. (1969). Further observations of chemiluminescence in diffusion flames of alkali metals and halogenated methanes. Twelfth Symposium (International) on Combustion, Pittsburgh, Combustion Institute.

Tibilov, A. S. and Shukhtin, A. M. (1968). Investigation of generation of radiation in the Na-H₂ mixture. Opt. Spectry., 25, 221.

Tully, J. C. (1974). Collision complex model for spin forbidden reactions: Quenching of O(¹D) by N₂. J.Chem.Phys., 61, 61

Turner, E. B. (1965). Optical and Ultraviolet techniques. Plasma Diagnostic Techniques. Huddleston, R. H. and Leonard, S. L. Eds. N.Y., Academic Press. Ch.7.

Tyerman, W. J. R. (1969). Rate constants for reaction of the chloromethylidyne radical with olefins, alkynes, chloroalkanes, hydrogen and oxygen. J.Chem.Soc. (Lond.), 16A, 2483.

Ung, A. Y.-M. and Schiff, H. I. (1962). The reaction of oxygen atoms with carbon tetrachloride. Can. J. Chem., 40, 486.

Walker, S. and Straw, H. (1962). Spectroscopy. N.Y., Macmillan. Vol. 2.

Weast, R. C. ed. (1967). Handbook of Chemistry and Physics, 48th ed., Cleveland, Chemical Rubber Publishing Co. p. E-154.

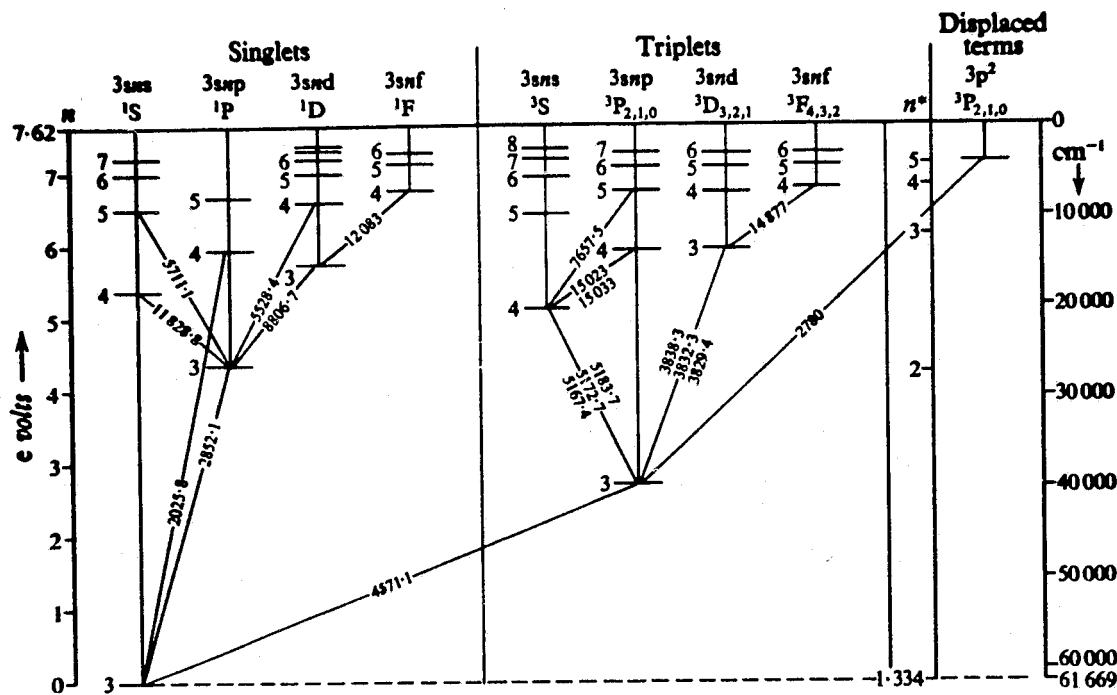
- Welsh, H. W., Cumming, C. and Stansbury, E. J. (1951). Multiple reflection Raman tubes for gases. J. Opt. Soc. Amer., 41, 712.
- Welsh, H. W. Stansbury, E. J., Romanko, J. and Feldman, T. (1955). Raman spectroscopy of gases. J. Opt. Soc. Amer., 45, 338.
- White, J. V. (1942). Long optical paths of large aperture. J. Opt. Soc. Amer., 32, 285.
- Wieder, I. (1970). Flame pumped lasers. IEEE J. Quantum Electronics, QE-6, 182.
- Wieder, I., Neiman, R. R. and Rodgers, A. P. (1965). Exploratory research on population inversions in gaseous explosions. Applied Optics, Supp. 2: Chemical Lasers. 187.
- Wiese, W. L., Smith, M. W. and Glennon, B. M. (1966). Atomic Transition Probabilities. Vol. I. Hydrogen through Neon. NSRDS-NBS 4-. Washington. U.S. Bureau of Standards.
- Wiese, W. L., Smith, M. W. and Miles, B. M. (1969). Atomic Transition Probabilities. Vol. II. Sodium Through Calcium. NSRDS-NBS 22. Washington. U.S. National Bureau of Standards.
- Willet, C. S. (1971). Laser lines in atomic species, in Progress in Quantum Electronics, J. H. Sanders and K. W. H. Stevens, eds. Vol. I, part 5. N.Y., Pergamon.
- Wilson, L. E. et al. (1973). New gas lasers committee report on electronic transition chemically and electrically excited lasers: Meeting of 20-22 September 1972. Technical Report No. AFWL-TR-73-60. Air Force Weapons Laboratory, Kirtland Air Force Base, May.
- Wren, D. J. and Menzinger, M. (1973). Quenching of the Ba + Cl₂ chemiluminescence: Estimate of BaCl₂* radiative lifetime. Chem. Phys. Lett., 20, 471.
- Zhitkevich, V. F., Lyutyi, A. I., Nesterko, N. A., Rossikhin, V. S. and Tsikora, I. L. (1963b). Excitation of atomic spectra in the reaction zone of the acetylene-air flame. Optics and Spectroscopy, 14, 180.
- Zhitkevich, V. F., Lyutyi, A. I., Rossikhin, V. S. and Tsikora, I. L. (1963a). Anomalous excitation of metals in flames and in the vapors of certain organic compounds. Optics and Spectroscopy, 15, 217.

Zwillenberg, M. L. (1975). Chemical laser action in low pressure metal vapor flames. Aero. and Mech. Sci. Tech. Rept. No. 1219. Dept. of Aerospace and Mech. Sci., Princeton University.

Zwillenberg, M. L., Naegeli, D. W. and Glassman, I. (1973). Additional work on chemical laser action in low pressure metal vapor flames. Aero. and Mech. Sci. Tech. Rept. No. 1143, Guggenheim Laboratories, Dept. of Aerospace and Mech. Sci., Princeton University.

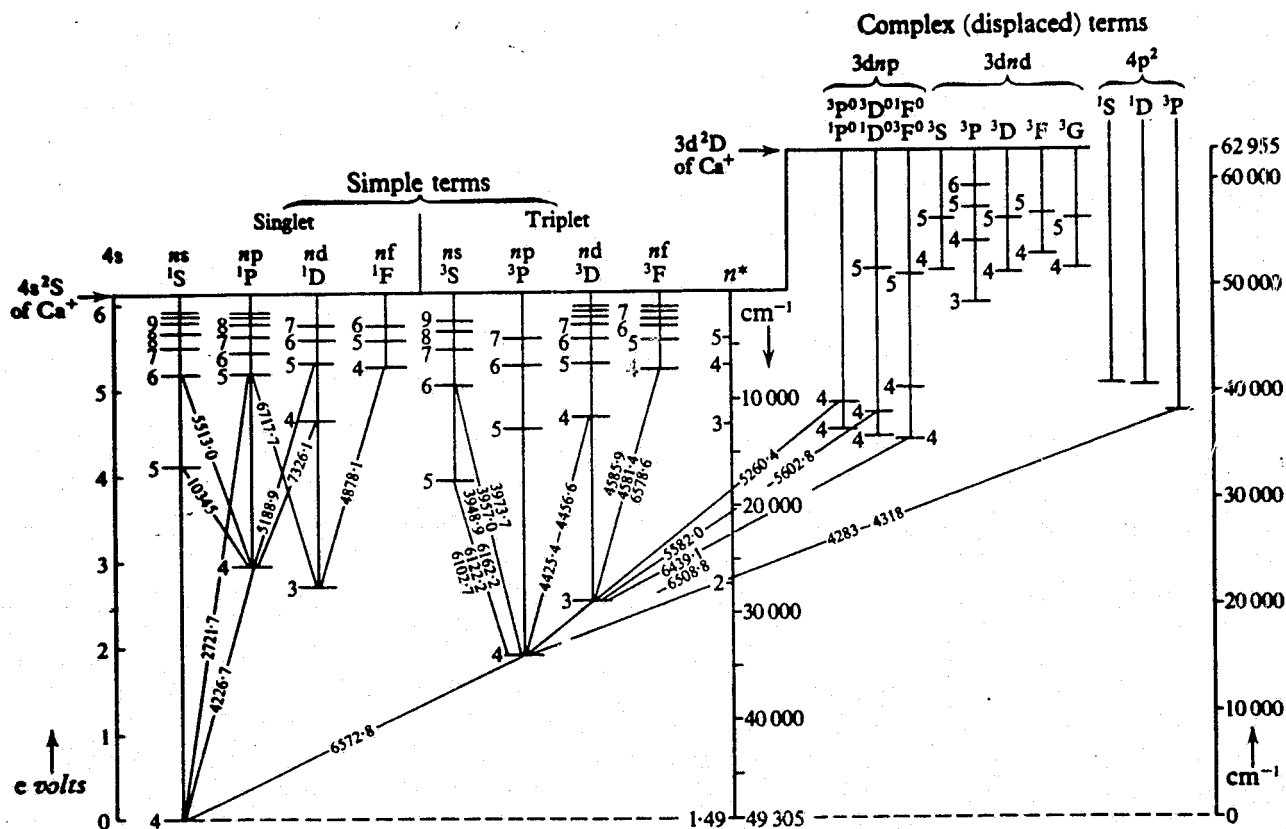
Zwillenberg, M. L., Naegeli, D. W. and Glassman, I. (1974). Chemical laser action in low pressure metal vapor flames. Combustion Science and Technology, 8, 237.

FIGURES



Energy Level Diagram of Mg (After Kuhn, 1962)

FIGURE I-1



Energy Level Diagram of Ca (After Kuhn, 1962)

Note: $\frac{\phi}{m} = \frac{1}{m} \cdot \frac{1-e^{-mx}}{1-e^{-x}}$

$\frac{\phi}{m} = \frac{1}{m} \cdot \frac{\text{multiple pass signal}}{\text{single pass signal}}$

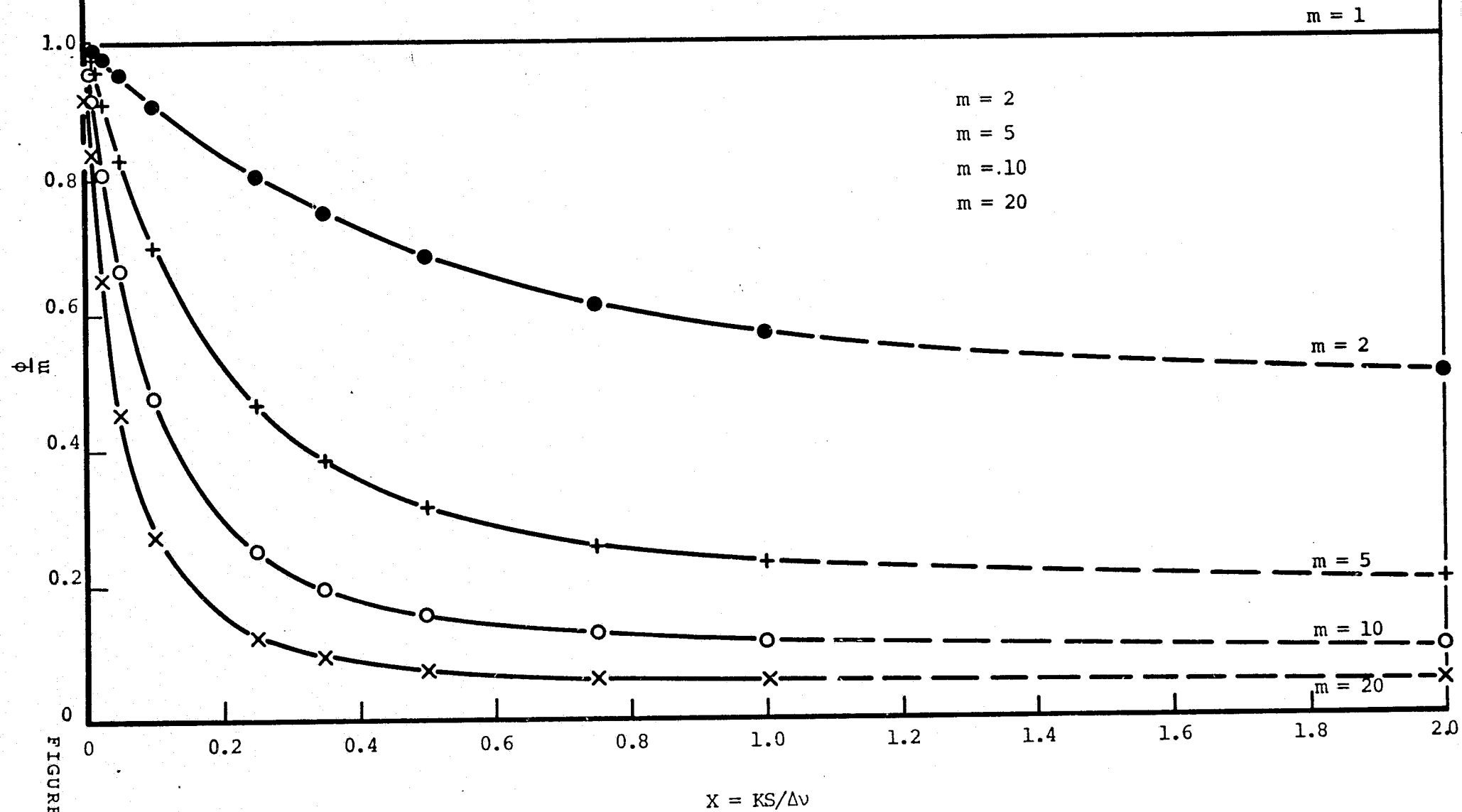


FIGURE I-3

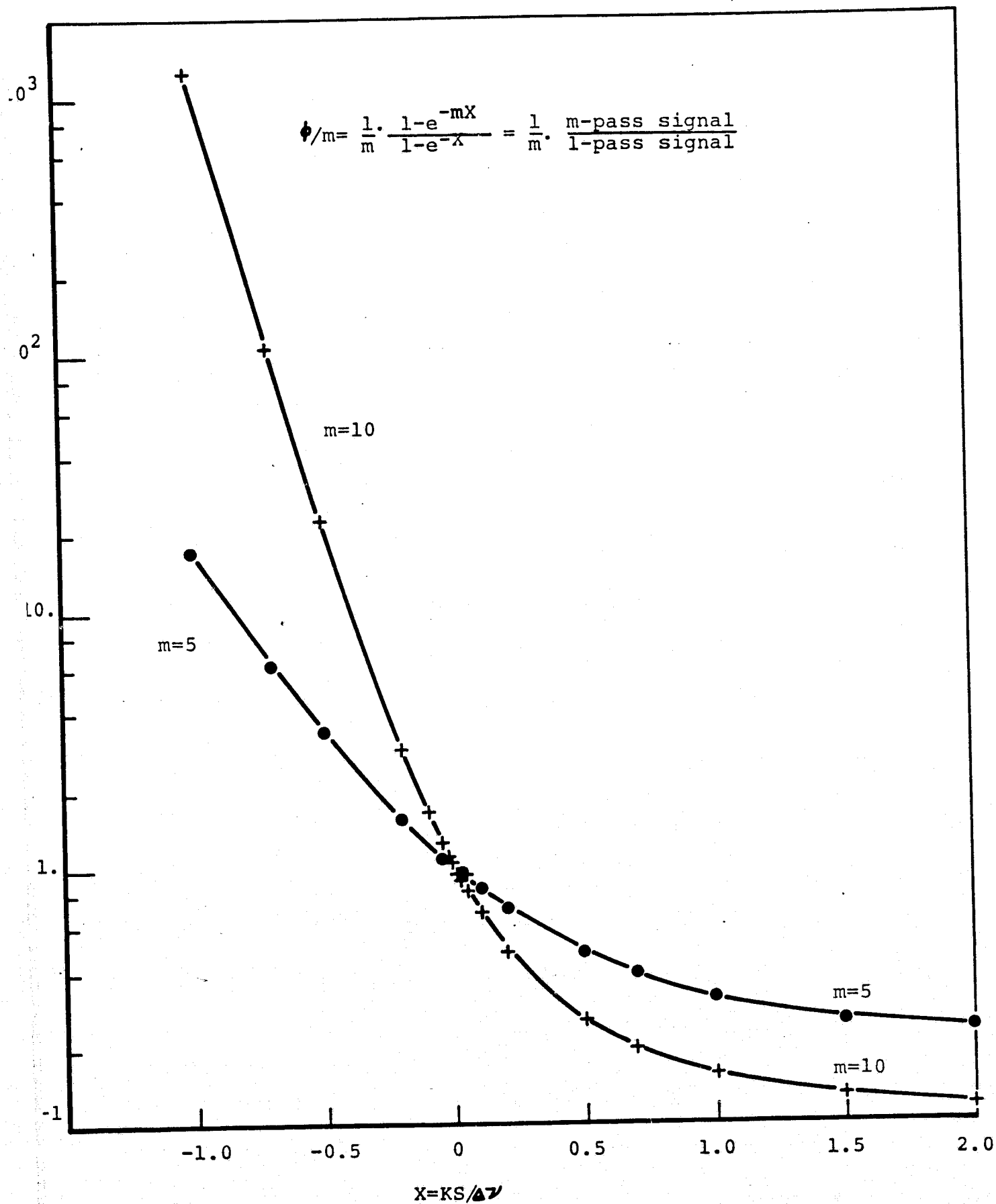
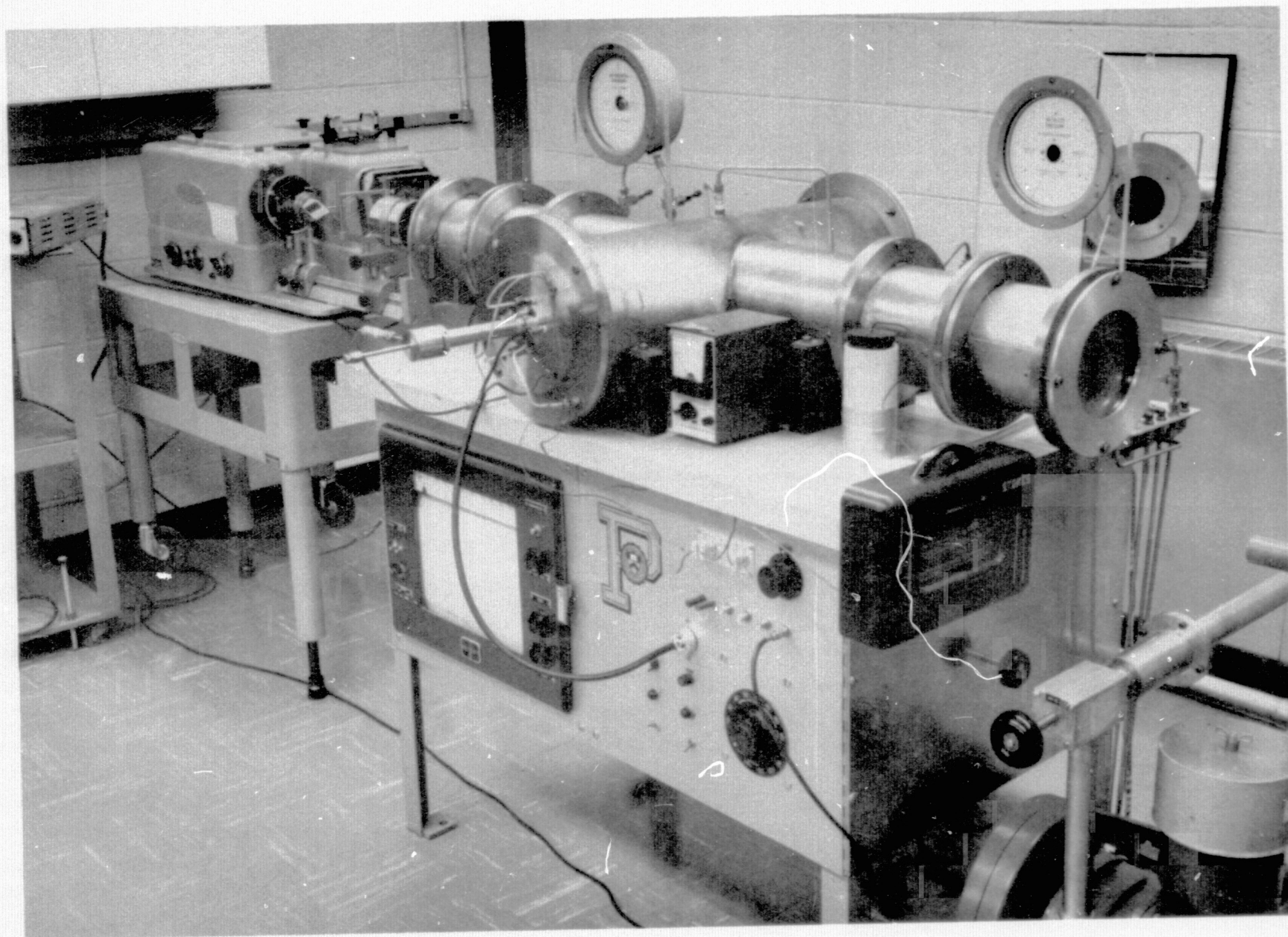


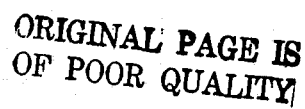
FIGURE I-4

ORIGINAL PAGE IS
OF POOR QUALITY

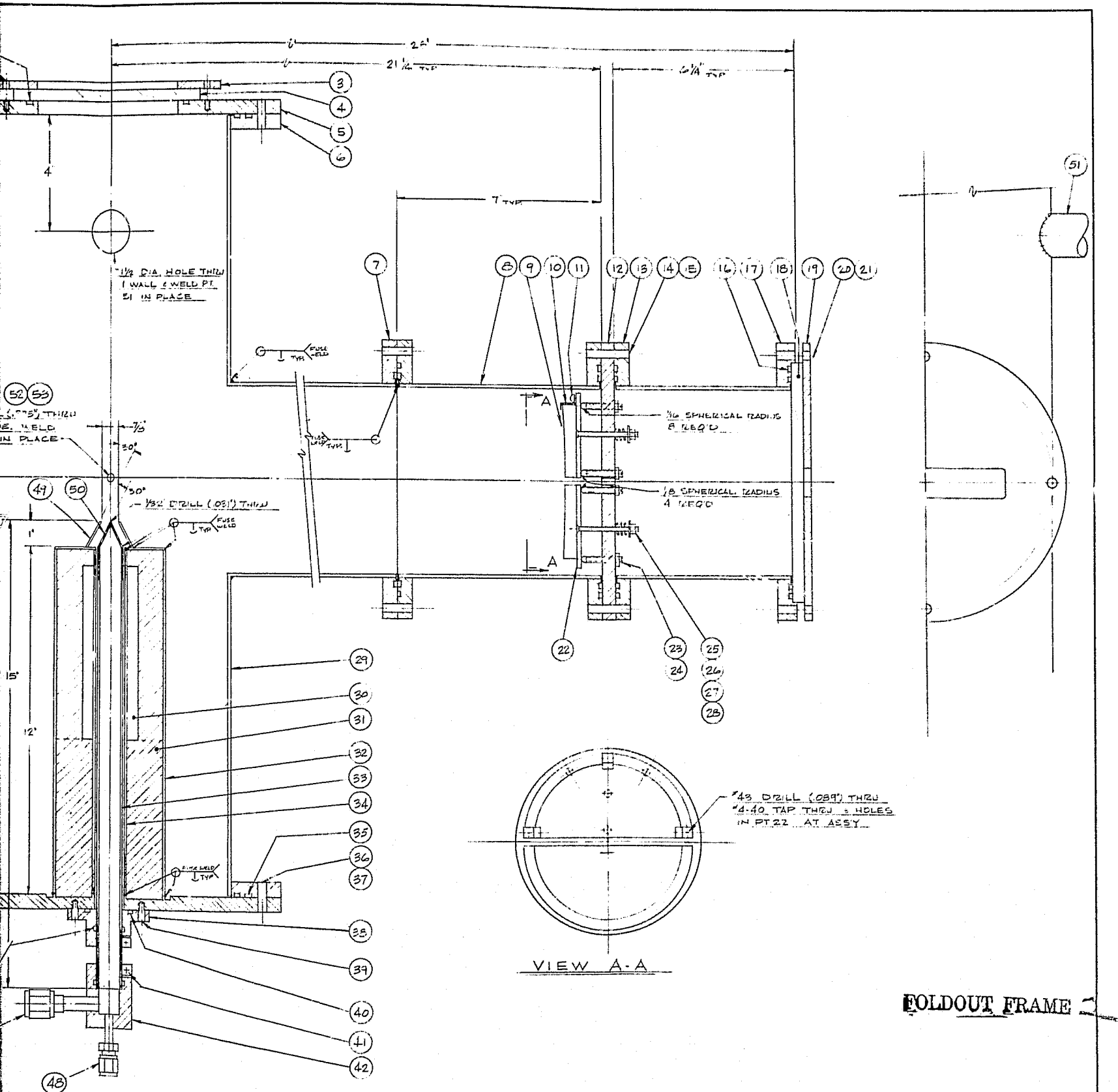


Low Pressure Metal Vapor Flame Apparatus

FIGURE II-1



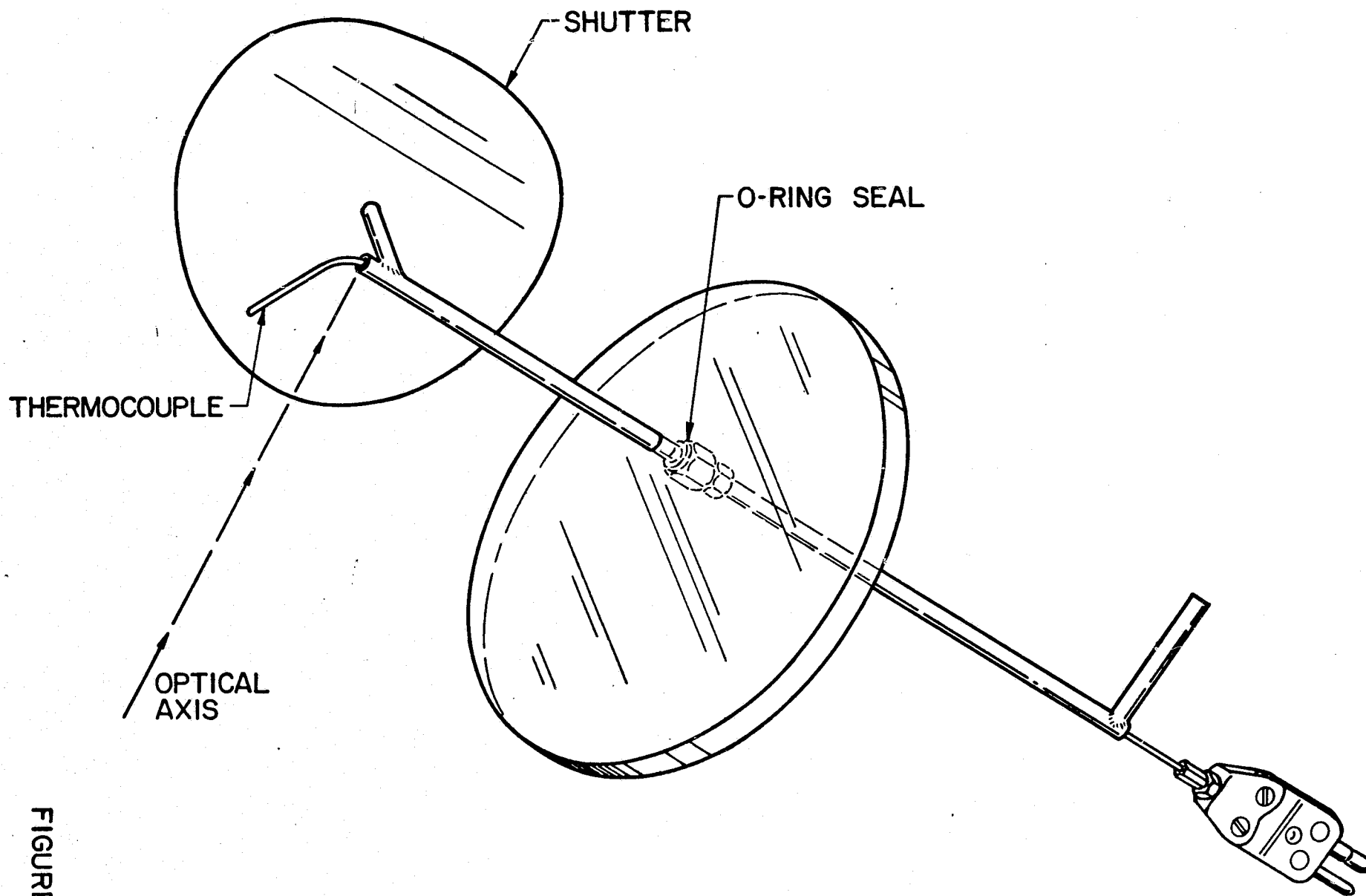
FOLDOUT FRAME



FOLDOUT FRAME

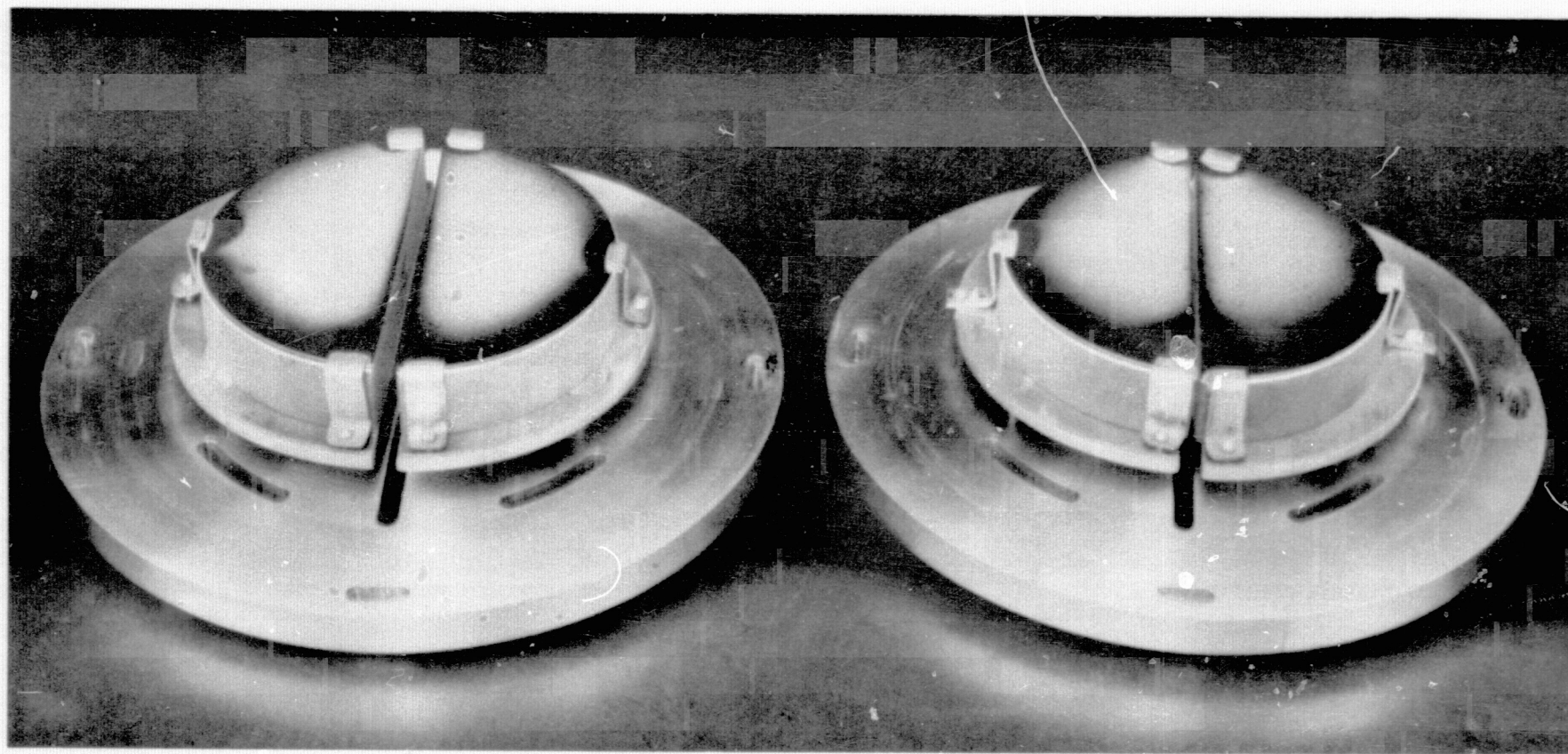
FIGURE II-2

SCALE: 1" = 1"	TOLERANCES UNLESS NOTED (NON-ACCUMULATIVE)	NO. CHANGE	BY	APP.
DATE: 6-11-76	XXX = ± .002"	NO. REQ'D		
DESIGNED: W. Z. TF	XX = ± .005"	MAT'L		
DRAWN: E	FRACTIONS = 1/32"	FINISH UNLESS NOTED		
CHECKED:	ANGLES = 1°	TITLE		
APP'D:		LOW PRESSURE BURNER ASSEMBLY		
GUGGENHEIM LABORATORIES DEPARTMENT OF AERONAUTICAL ENGINEERING PRINCETON UNIVERSITY		DWG NO. 6105 L 01 A		



THERMOCOUPLE / SHUTTER ASSEMBLY

ORIGINAL PAGE IS
OF POOR QUALITY



WHITE CELL MIRROR MOUNTING
(Mirrors removed from chamber
for removal of oxide deposits)

FIGURE II-4

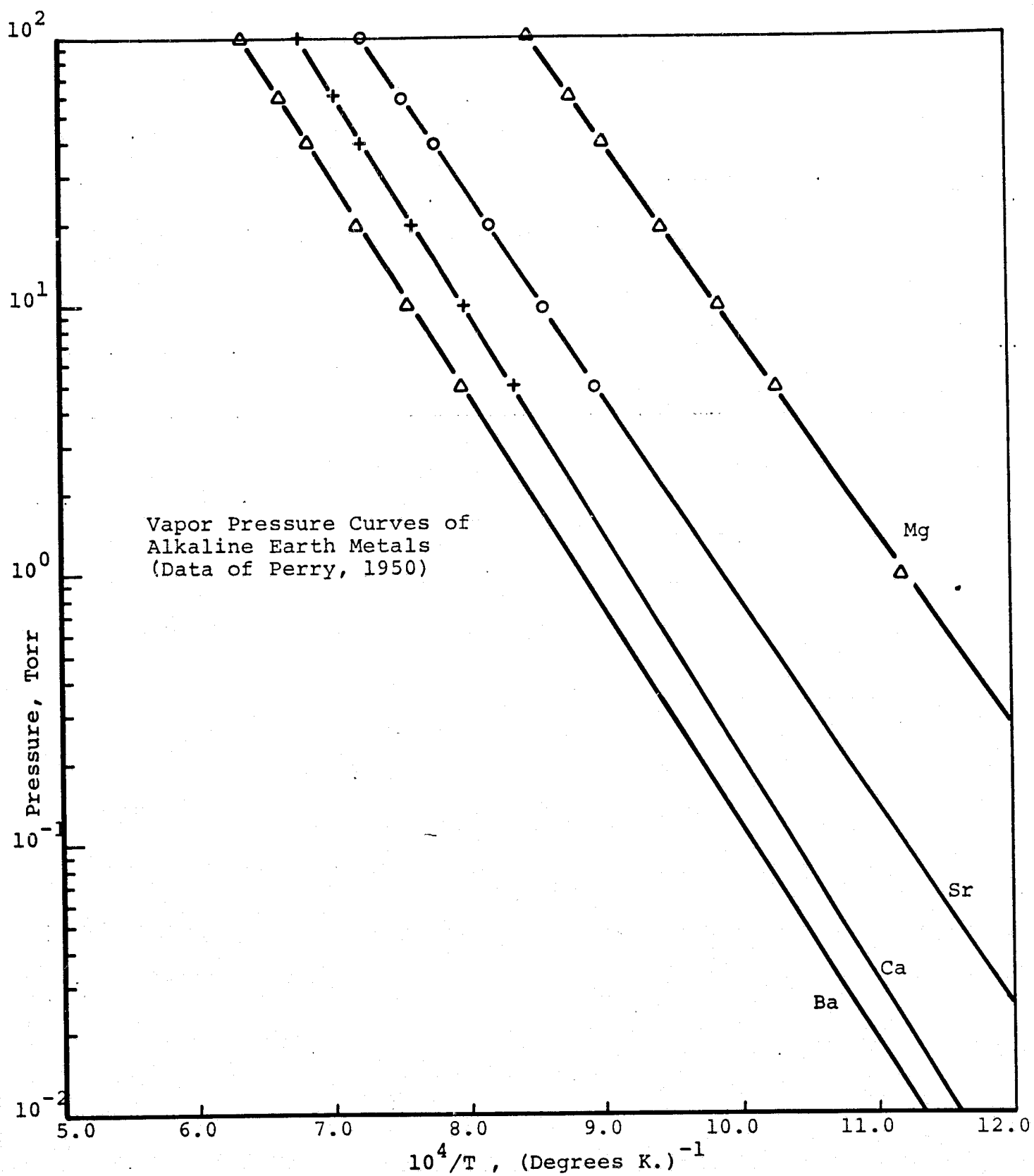
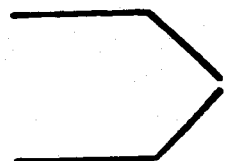
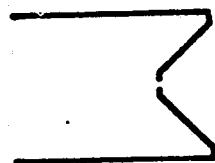


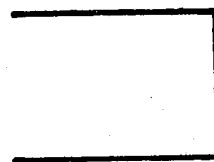
FIGURE II-5



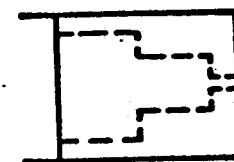
a) 0.032" dia.
0.042" dia.



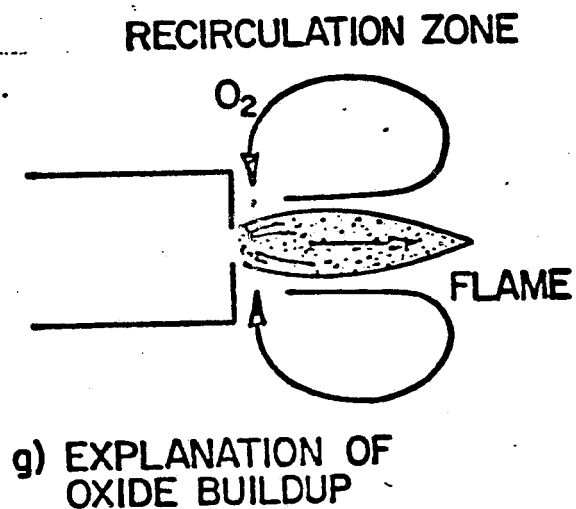
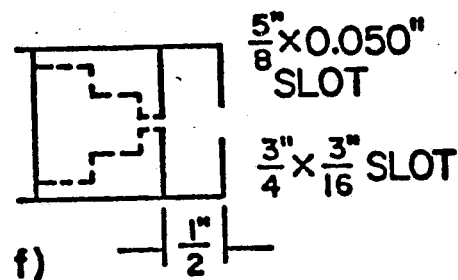
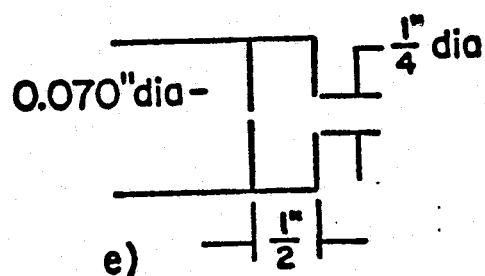
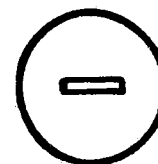
b) 0.042 dia.



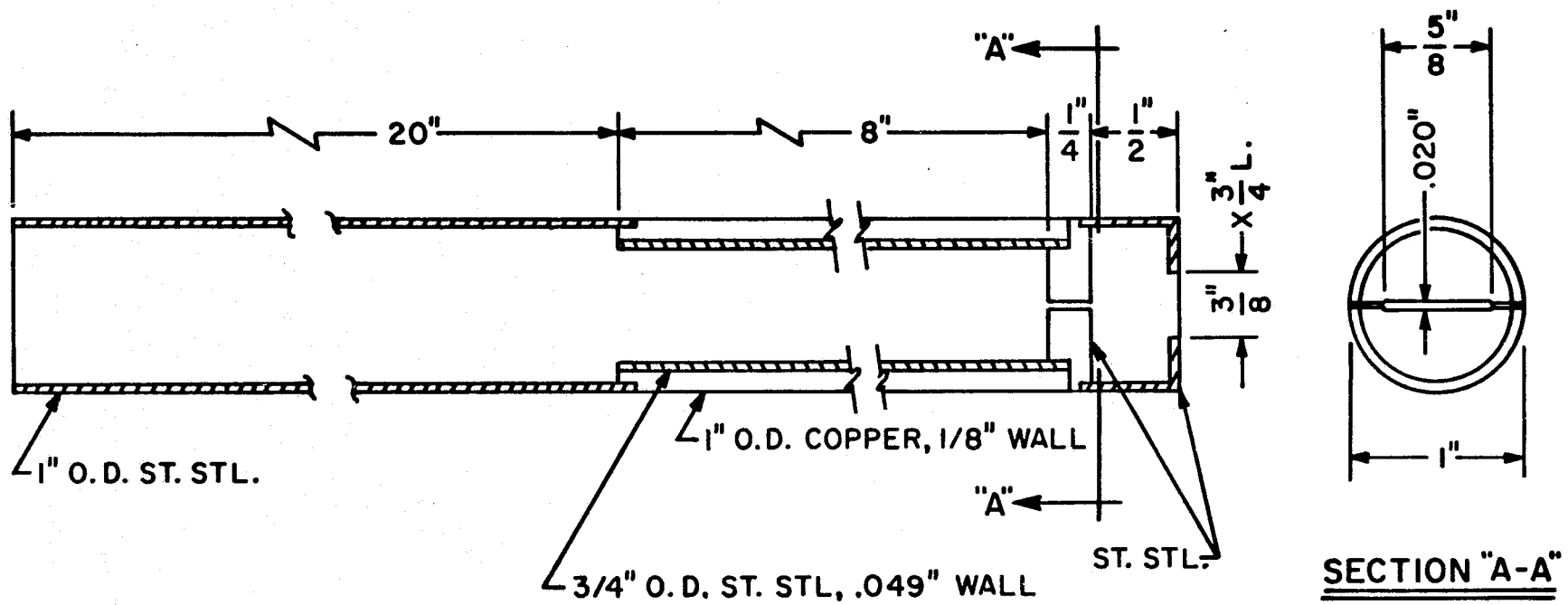
c) 0.042" dia.
0.070" dia.



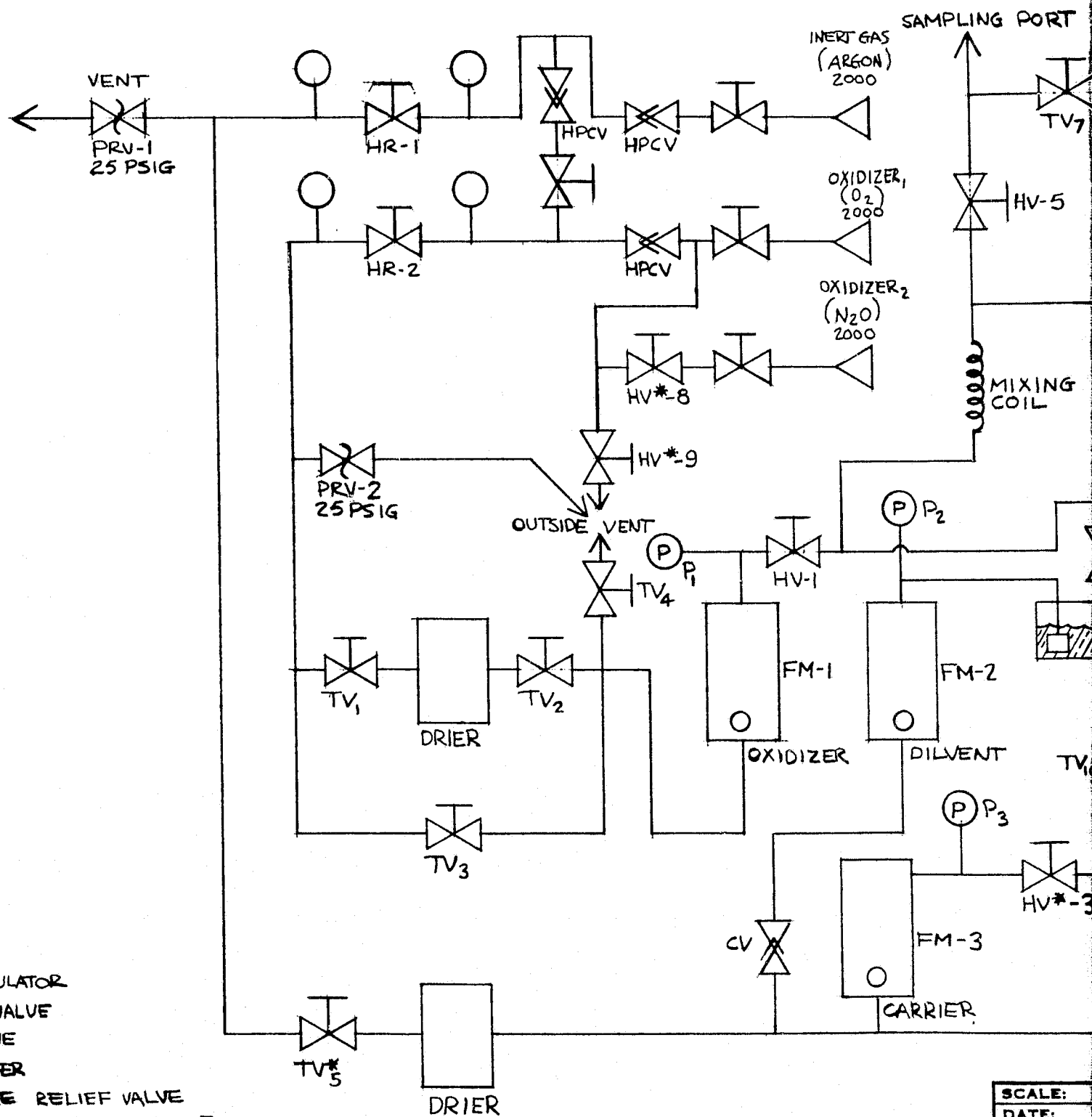
d) $\frac{5}{8} \times \frac{1}{32}$



TYPES OF METAL VAPOR NOZZLES USED
(ORIFICE DIMENSIONS GIVEN UNDER EACH SCETCH)
ALL TUBES 1" dia



FURNACE TUBE, SLIT NOZZLE AND SHIELD ASSEMBLY



HR = HAND REGULATOR
 TV = TOGGLE VALVE
 HV = HAND VALVE
 FM = FLOWMETER
 PRV = PRESSURE RELIEF VALVE
 PTC = THERMISTOR VACUUM GAUGE
 P = PRESSURE GAUGE (BOURDON OR BELLOWS TYPE)
 ΔP = DIFFERENTIAL PRESSURE GAUGE
 CV = CHECK VALVE
 HPCV = HIGH PRESSURE CHECK VALVE

FOLDOUT FRAME

SCALE:
DATE:
DESIGNED:
DRAWN:
CHECKED:
APP'D:
G DEPA

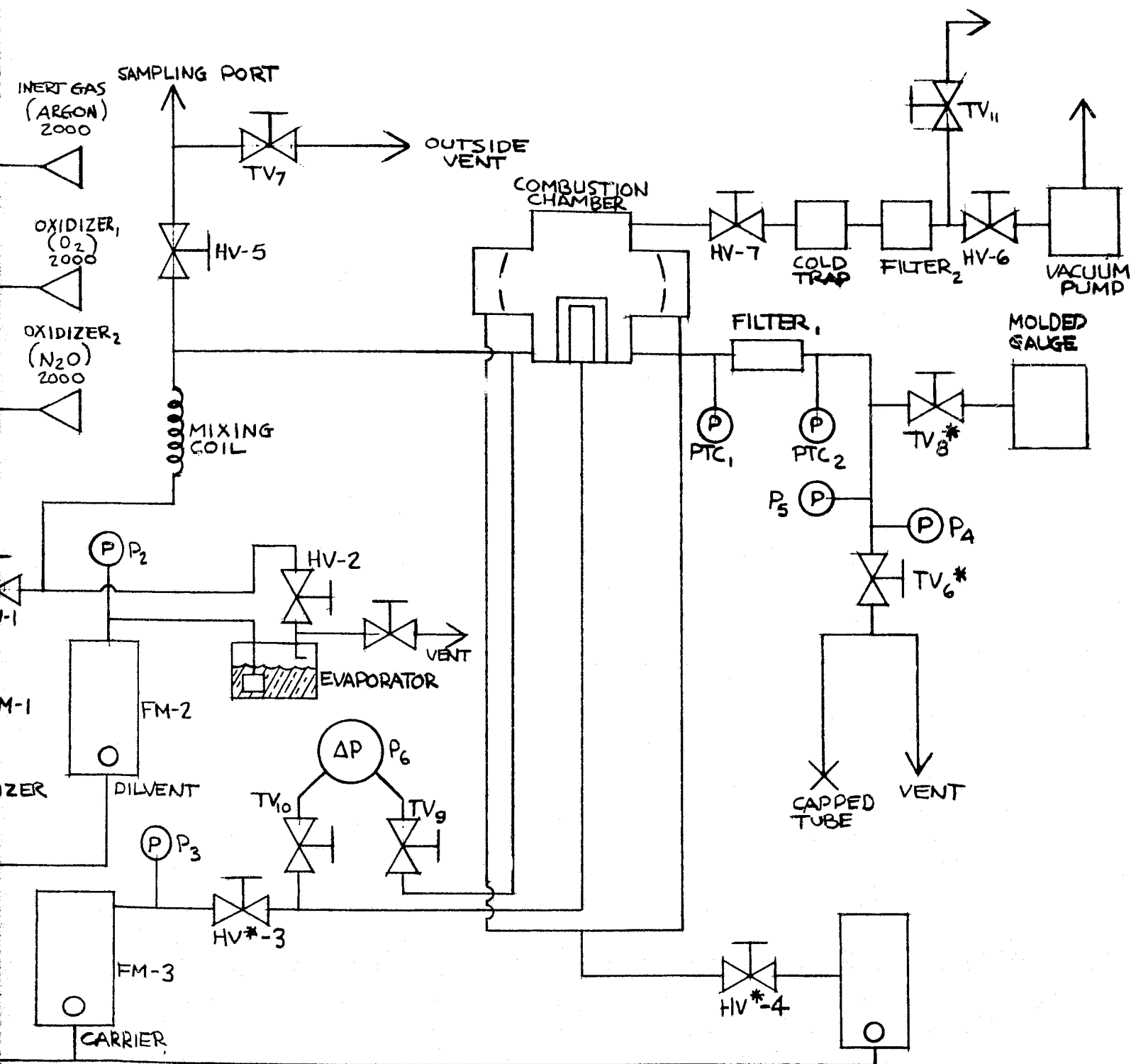
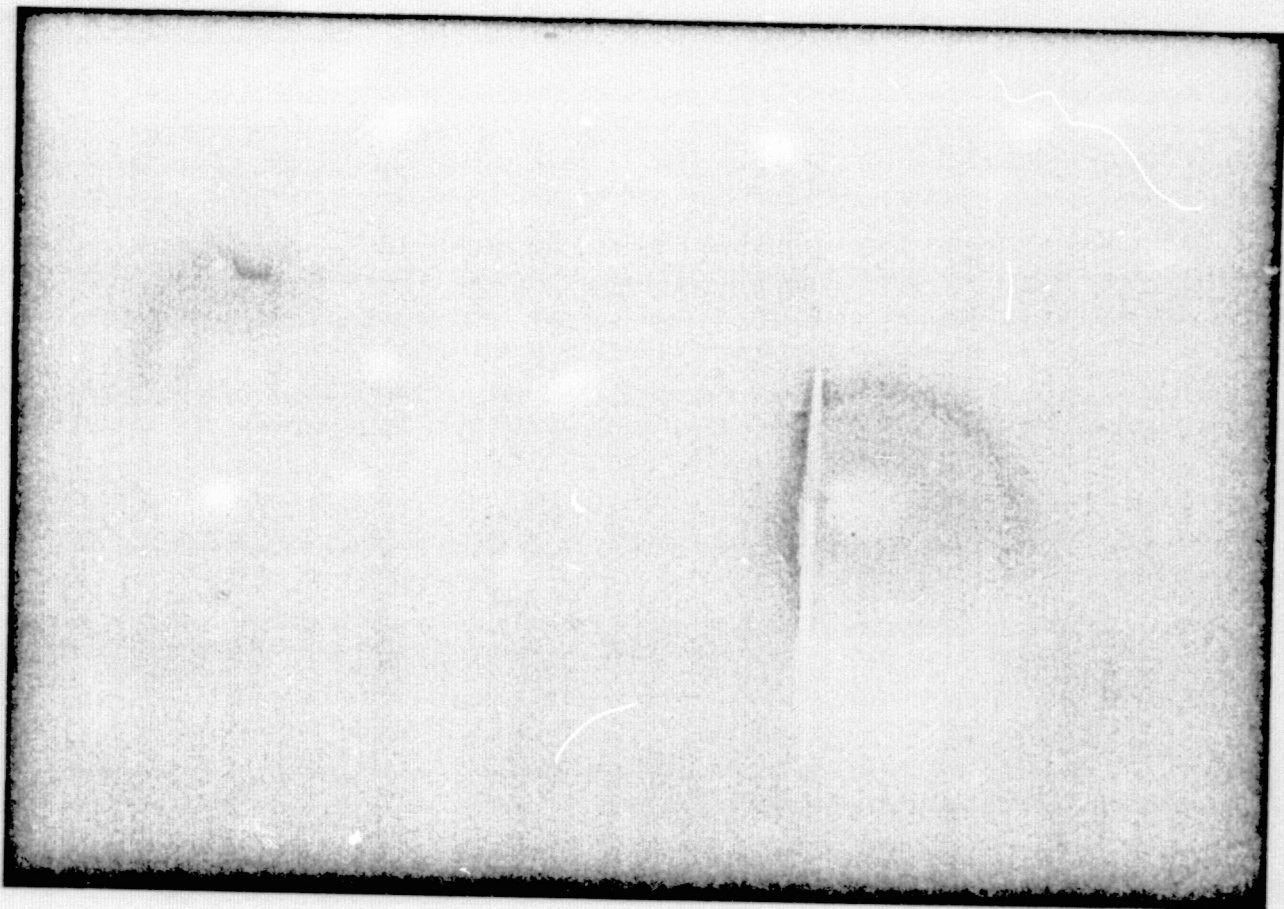


FIGURE II - 8

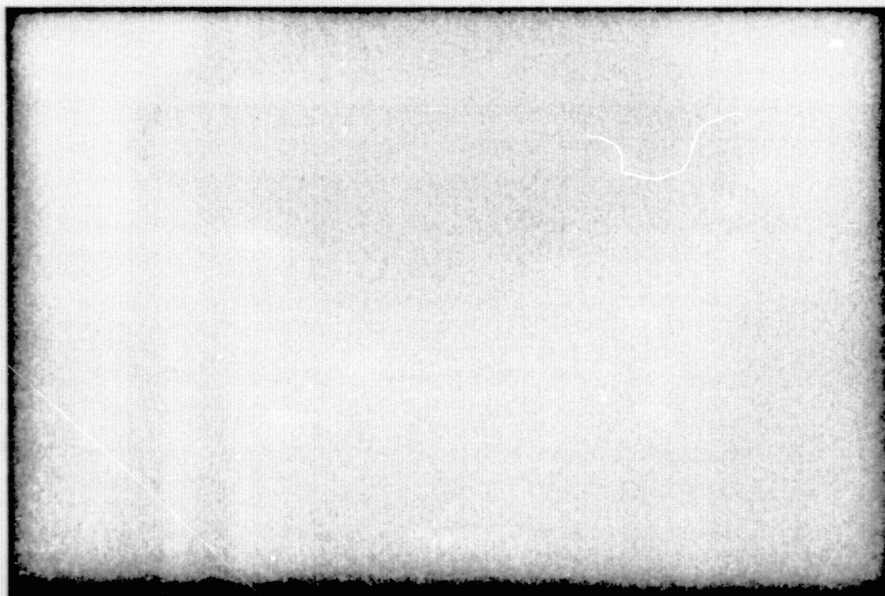
SCALE:	TOLERANCES UNLESS NOTED (NON-ACCUMULATIVE)	NO.	CHANGE	BY	APP.
DATE:		NO. REQ'D:			
DESIGNED:	.XXX = ± .002"	MAT'L:			
DRAWN:	.XX = ± .005"	FINISH UNLESS NOTED:V			
CHECKED:	FRACTIONS = ± 1/32"	TITLE:			
APP'D:	ANGLES = ± 1°	LOW PRESSURE METAL VAPOR FLAME FLOW SYSTEM			
GUGGENHEIM LABORATORIES DEPARTMENT OF AERONAUTICAL ENGINEERING PRINCETON UNIVERSITY		DWG. NO.			

FOLDOUT FRAME

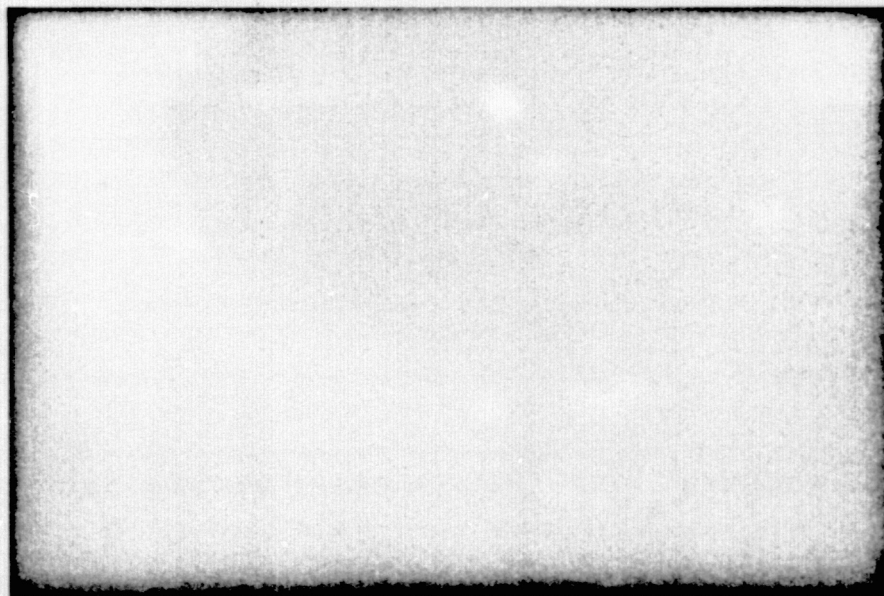


Dilute calcium vapor flame at 1.8 torr pressure
in 5.3% O₂/Argon

ORIGINAL PAGE IS
OF POOR QUALITY



a.
(Violet Flame)



b.
(Green Flame)

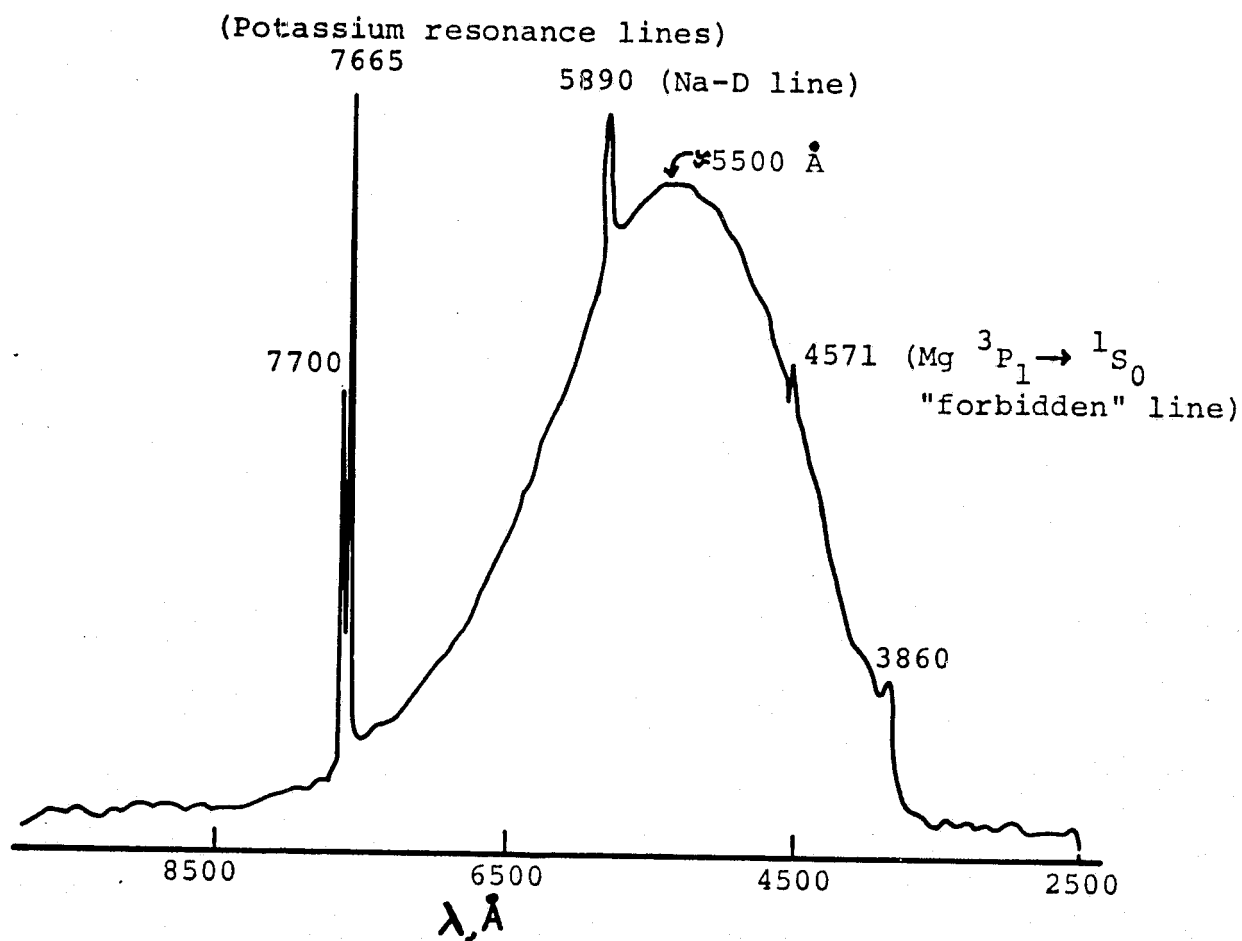
Dilute $\text{Mg}/\text{CCl}_4/\text{O}_2$ Flame, showing effect of O_2

Pressure = 1.3 torr. Object in flame is thermocouple probe.

a. zero added O_2 , 0.46% CCl_4 , balance Ar and He.

b. 0.38% O_2 , 0.34% CCl_4 (CCl_4 flow unchanged), balance Ar and He.

ORIGINAL PAGE IS
OF POOR QUALITY



Mg-N₂O Flame Spectrum. 400 micron slits (6. Å nominal resolution. RCA 7326 photomultiplier.
P= 3.59 torr

FIGURE III-3

7700 (Potassium resonance line)

Mg-O₂ Flame Spectrum

2. mm. slits (30 Å nominal resolution)

RCA 7326 photomultiplier

P= 0.4-1.4 torr

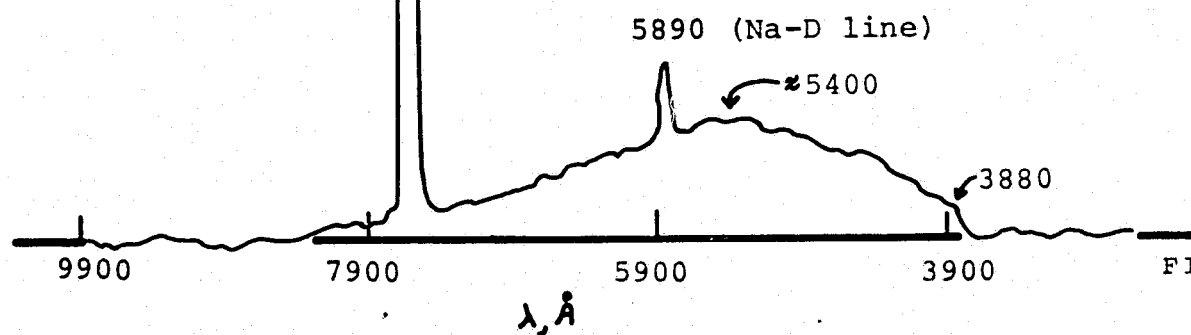
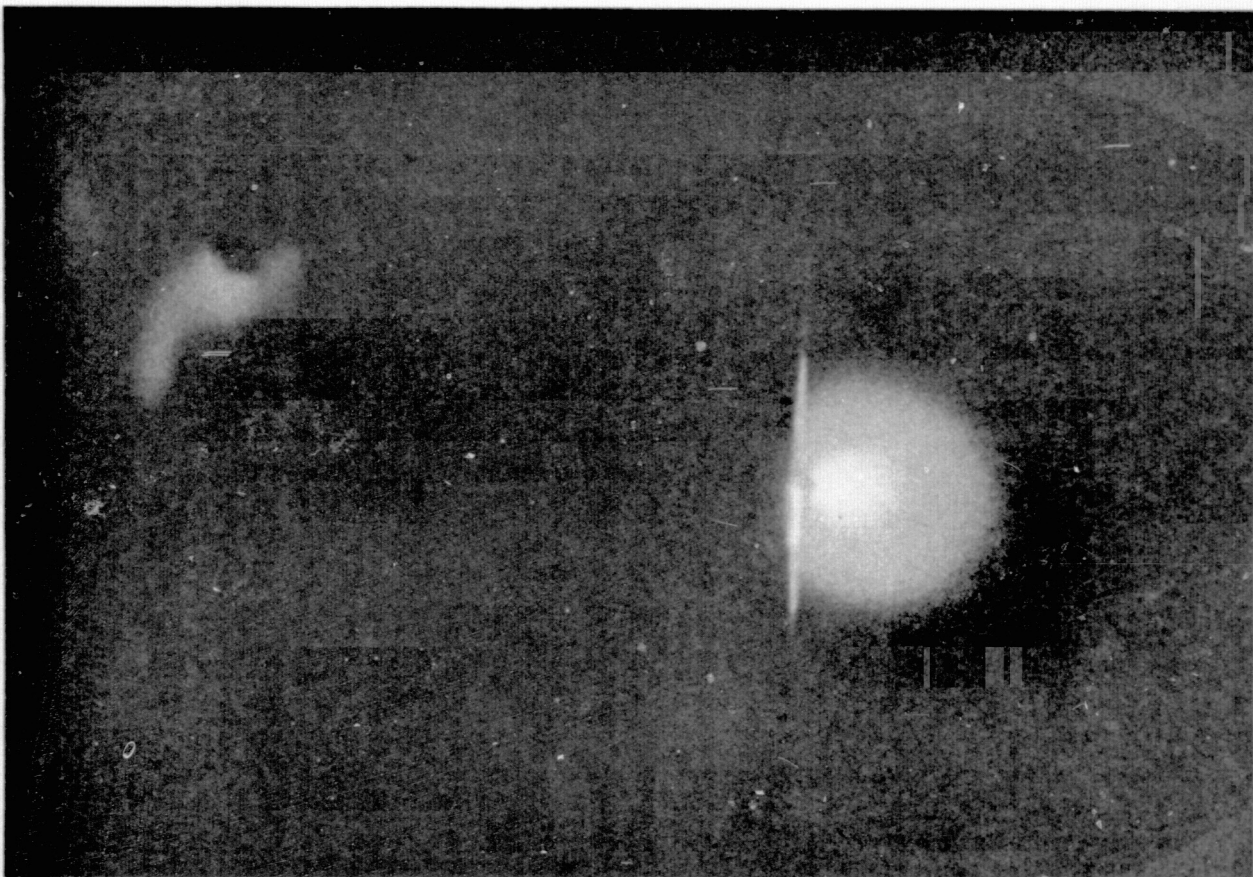
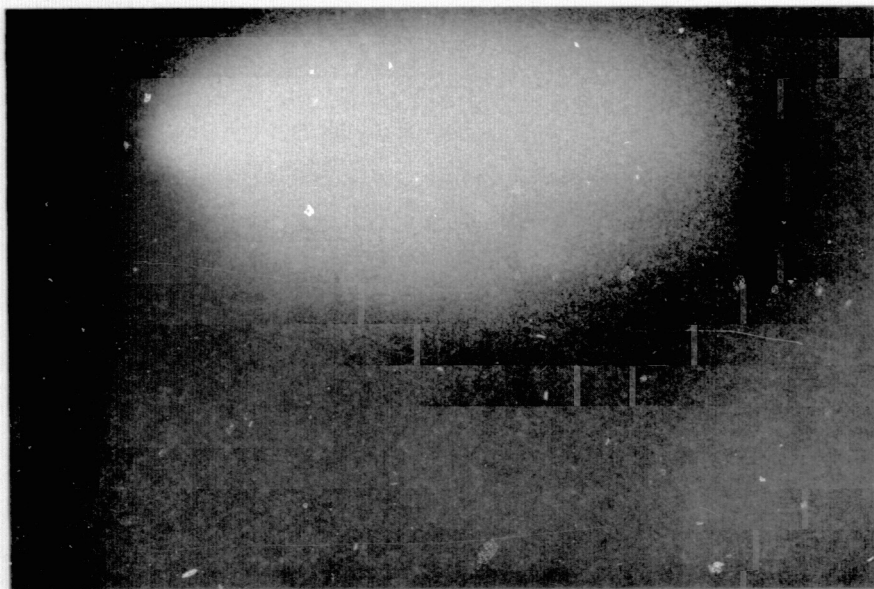


FIGURE III

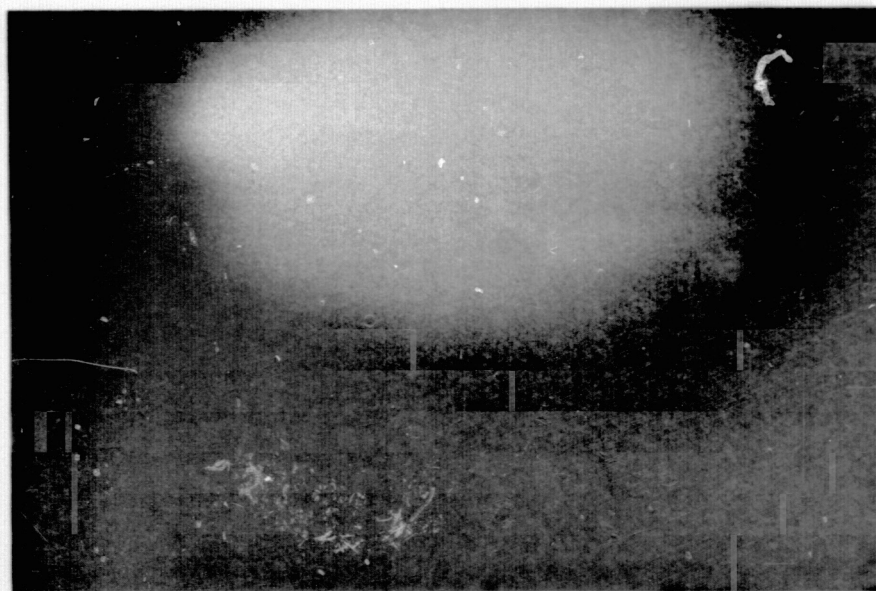
ORIGINAL PAGE IS
OF POOR QUALITY



Dilute calcium vapor flame at 1.8 torr pressure
in 5.3% O₂/Argon



a.
(Violet Flame)



b.
(Green Flame)

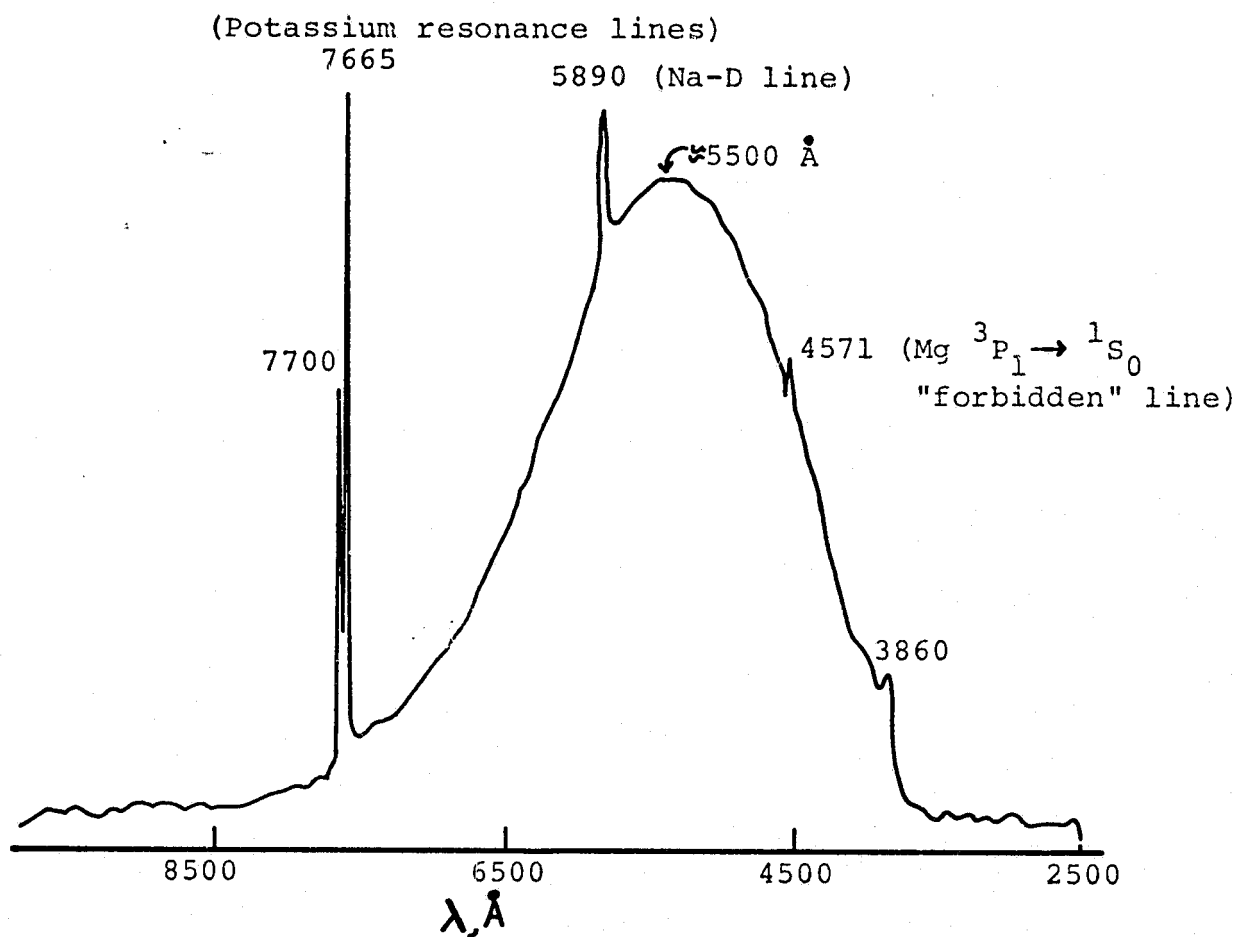
Dilute $\text{Mg}/\text{CCl}_4/\text{O}_2$ Flame, showing effect of O_2

Pressure = 1.3 torr. Object in flame is thermocouple probe.

a. zero added O_2 , 0.46% CCl_4 , balance Ar and He.

b. 0.38% O_2 , 0.34% CCl_4 (CCl_4 flow unchanged), balance Ar and He.

ORIGINAL PAGE IS
OF POOR QUALITY



Mg-N₂O Flame Spectrum. 400 micron slits (6. Å nominal resolution. RCA 7326 photomultiplier.
P= 3.59 torr

FIGURE III-3

7700 (Potassium resonance line)

Mg-O₂ Flame Spectrum

2. mm. slits (30 Å nominal resolution)

RCA 7326 photomultiplier

P= 0.4-1.4 torr

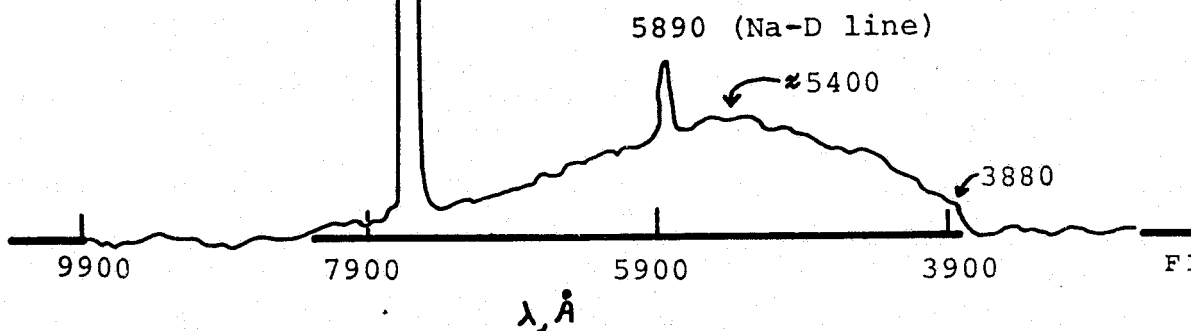
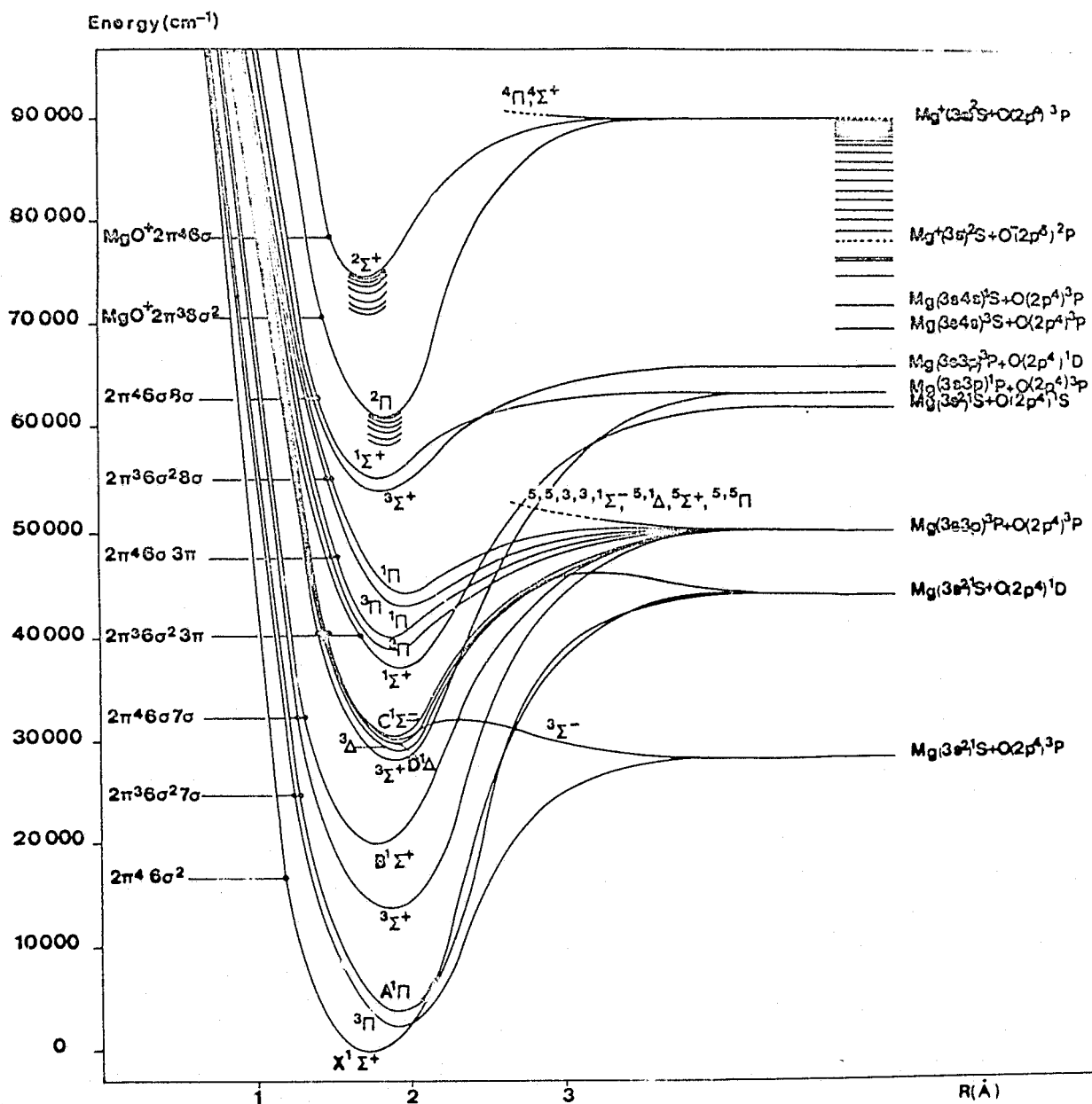


FIGURE III-



Potential Energy of MgO
(After Schamps and Lefebvre-Brion(1972))

FIGURE III-5

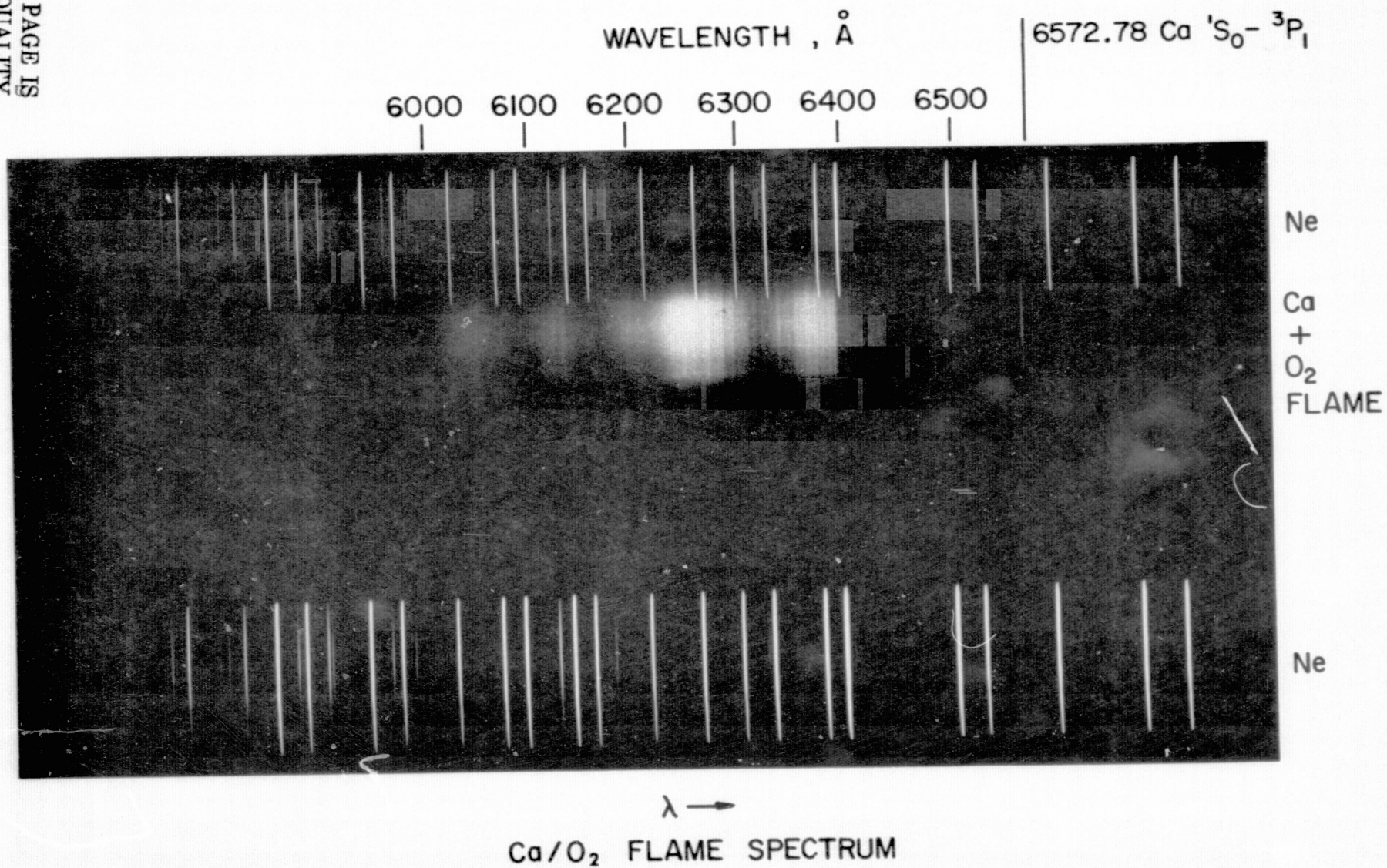


FIGURE 111-6

ORIGINAL PAGE IS
OF POOR QUALITY

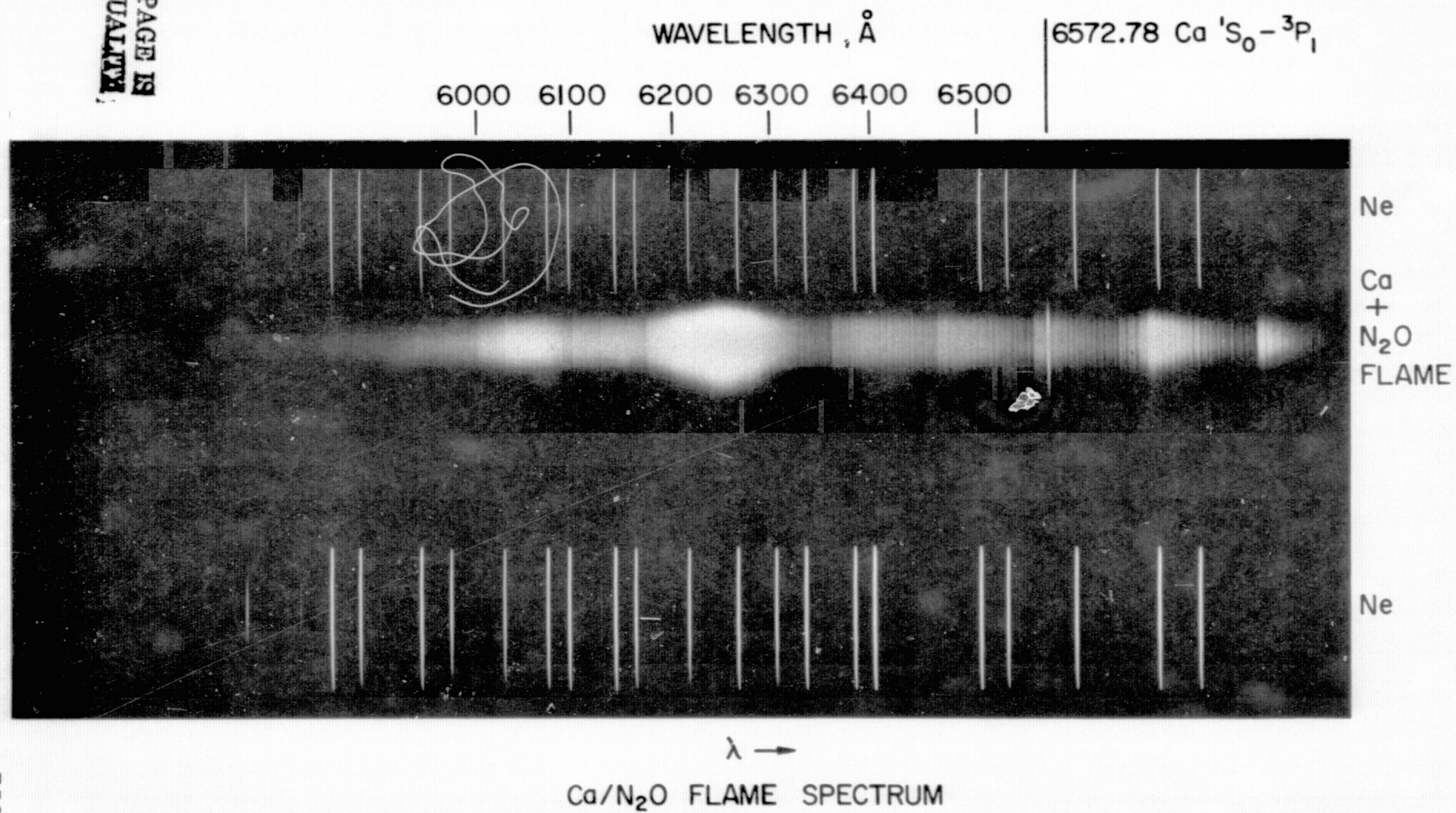
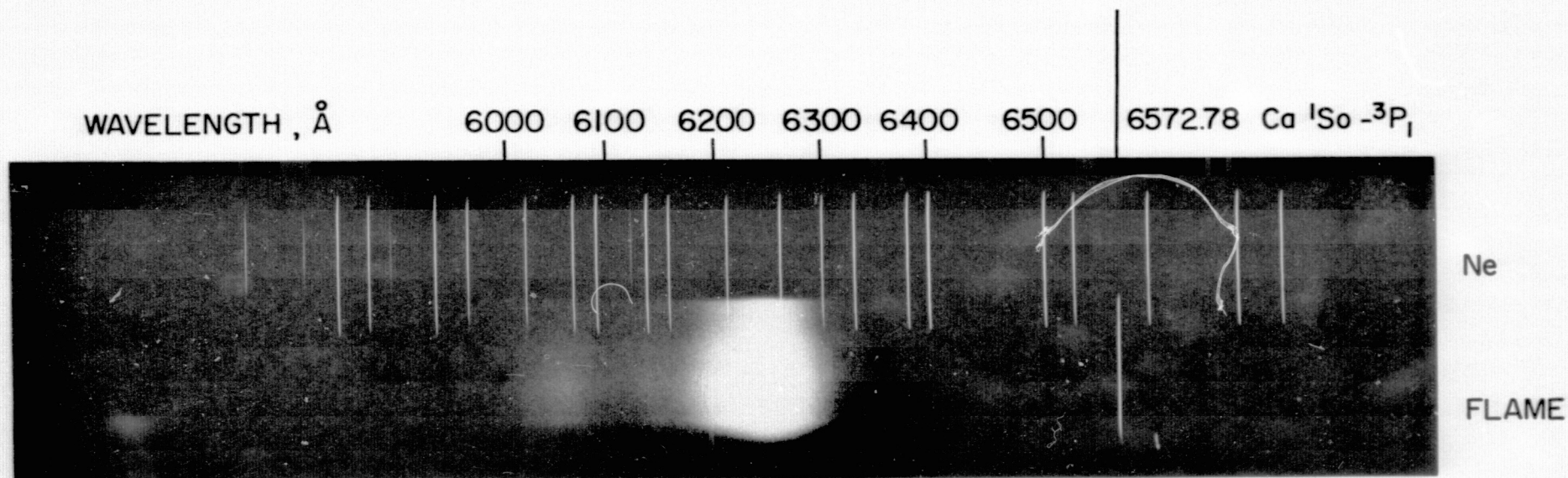
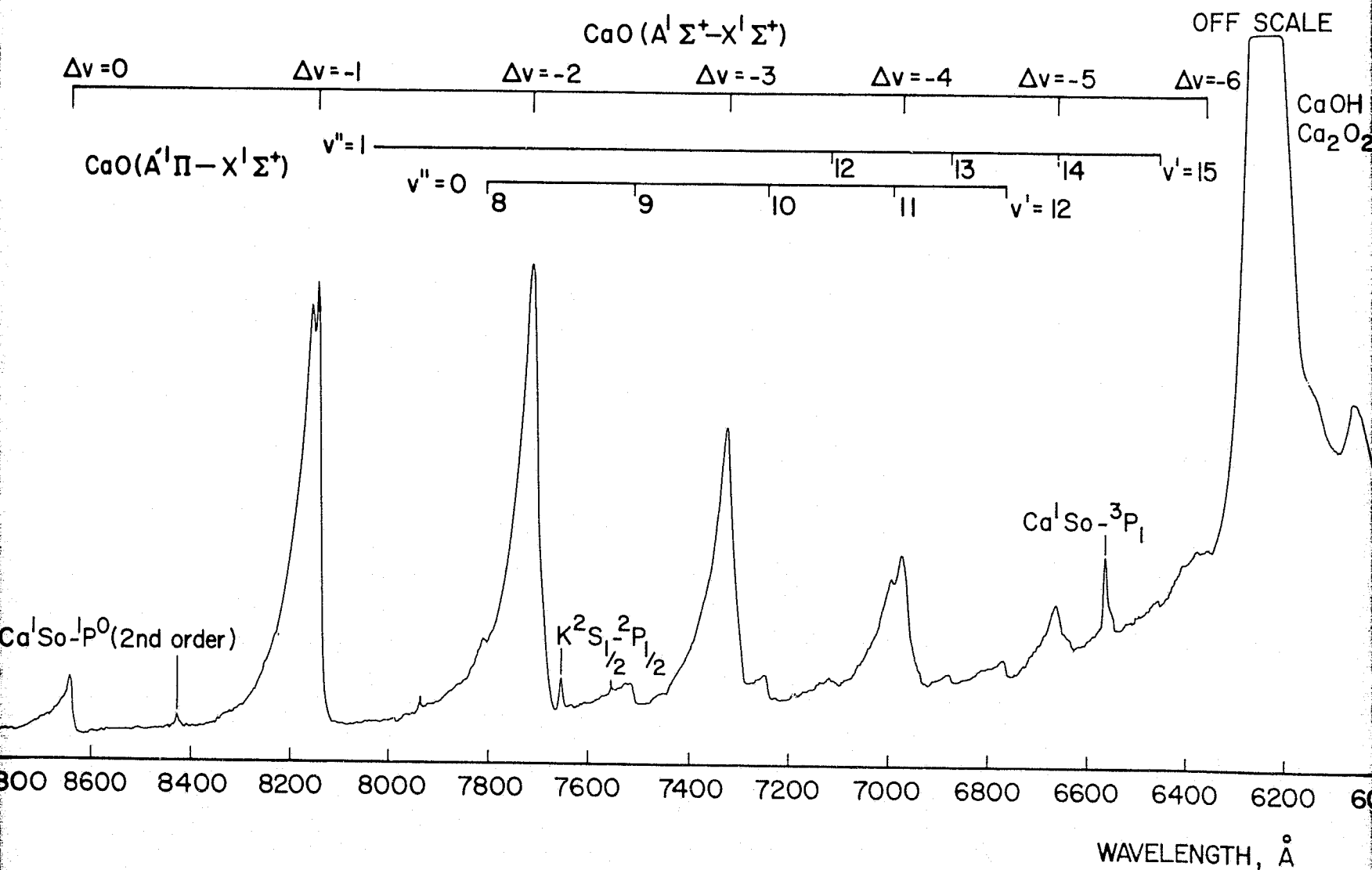


FIGURE III-7



SPECTROGRAM OF FLAME OF Ca VAPOR IN 214 ppm. O₂, 6.87% N₂ (BALANCE ARGON) AT 1.5 TORR PRESSURE

JP13 4329 75



FOLDOUT FRAME

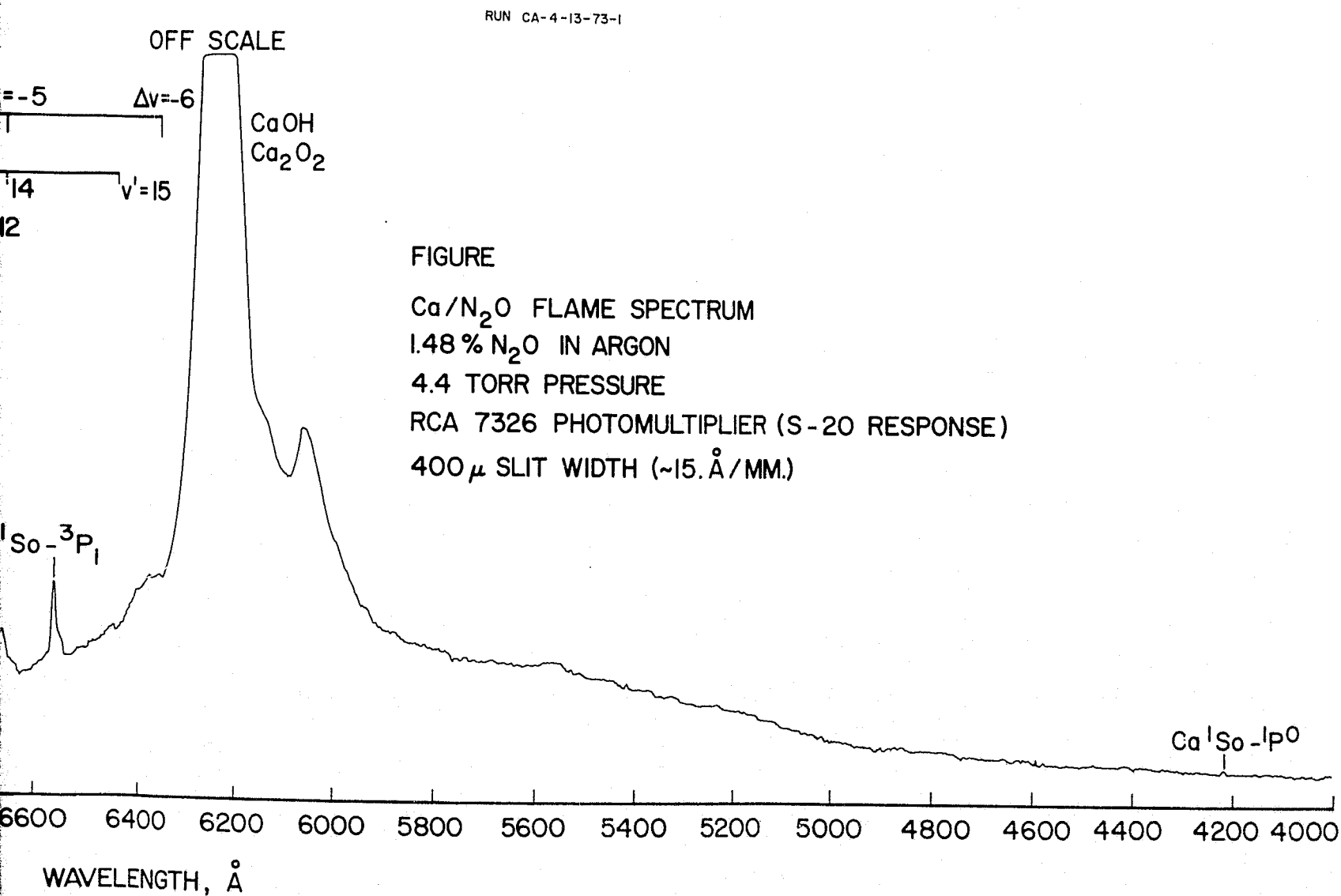
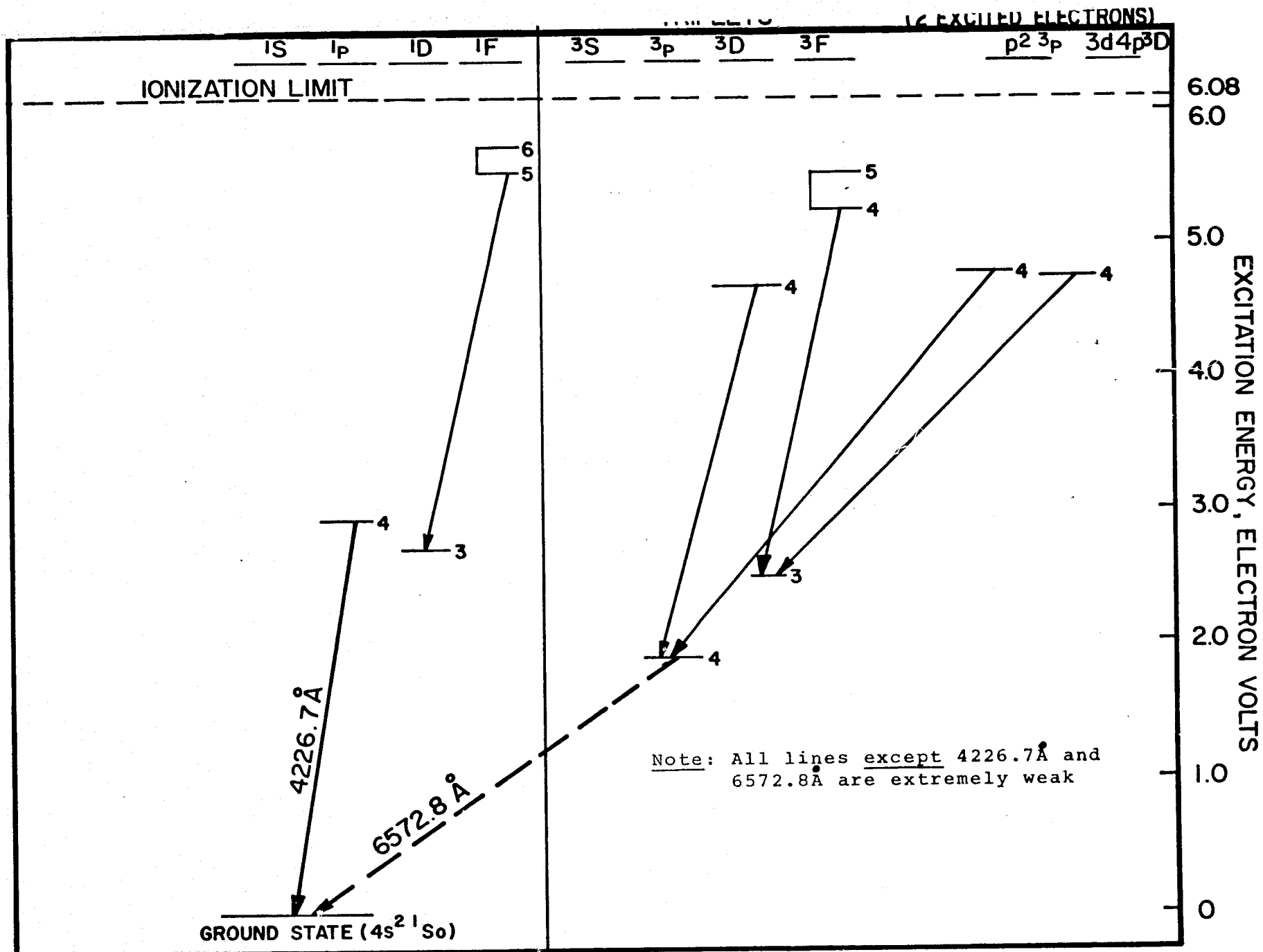


FIGURE III - 9

FOLDOUT FRAME 2

Cd ATOMIC TRANSITIONS OBSERVED IN
Cd + N₂O FLAMES

FIGURE III-10



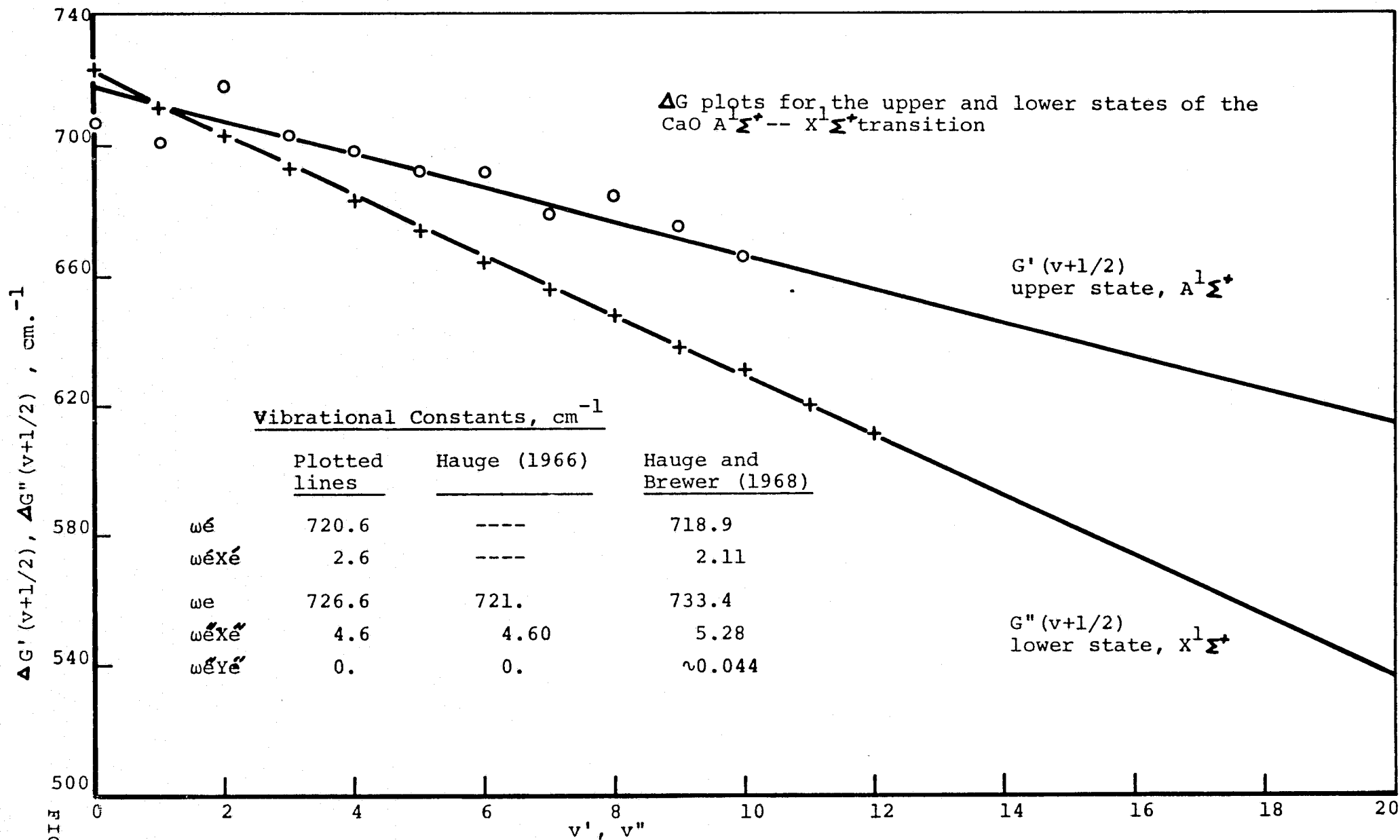


FIGURE III-1

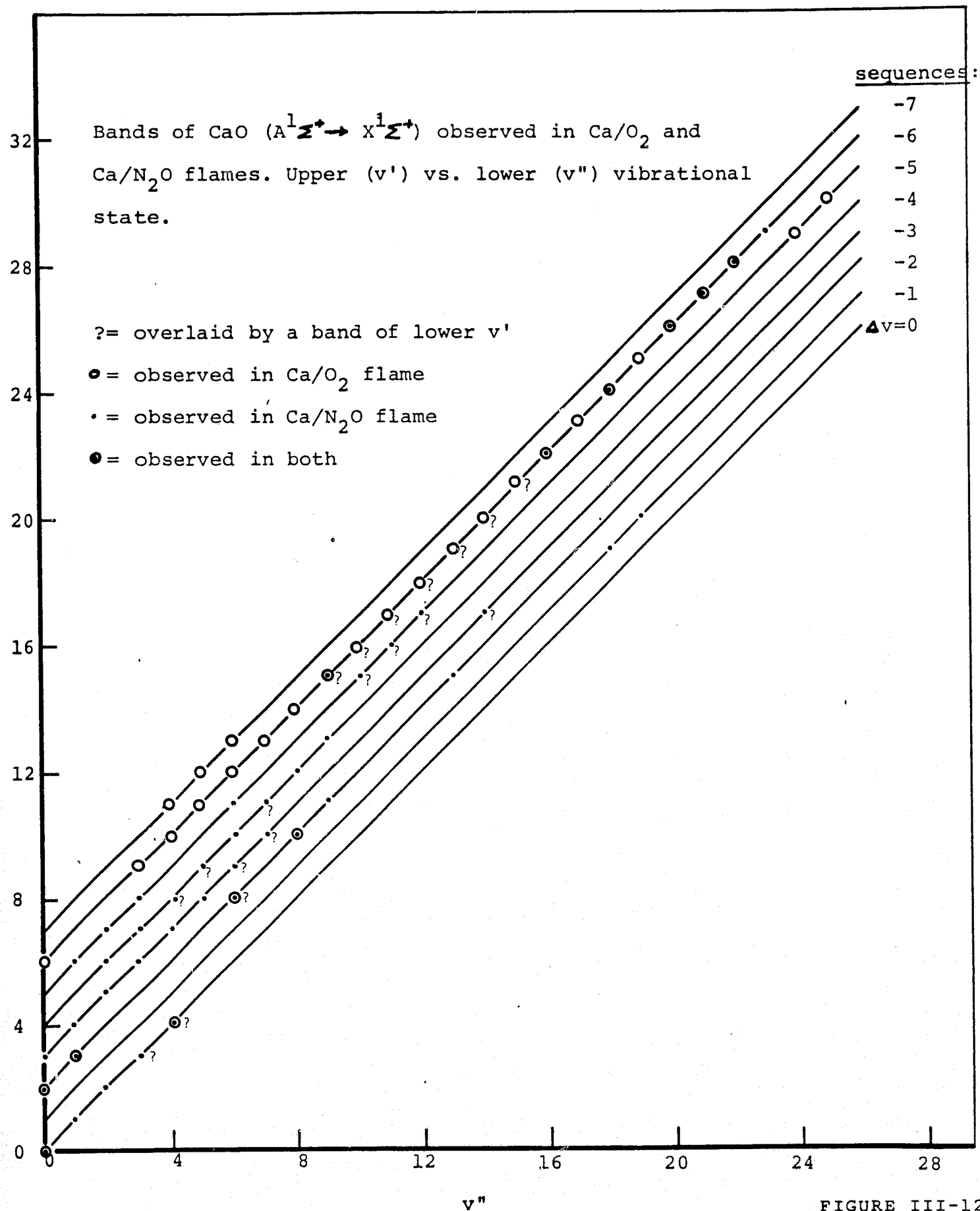


FIGURE III-12

($\Delta v = -5$)

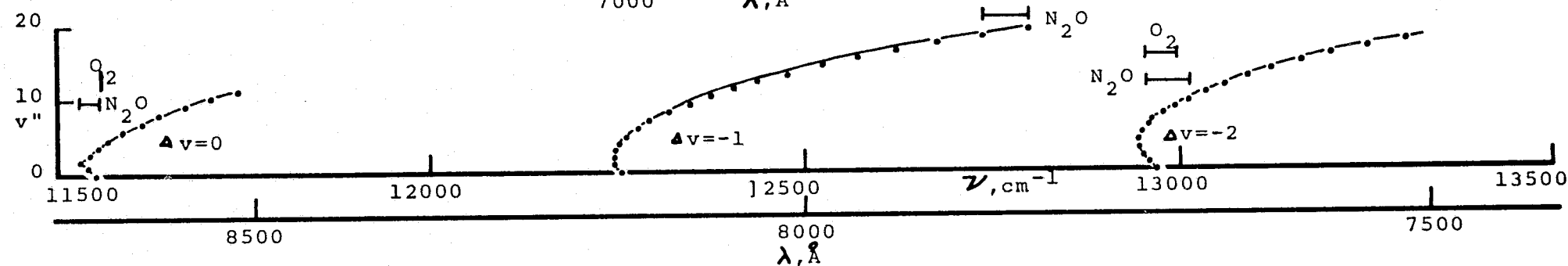
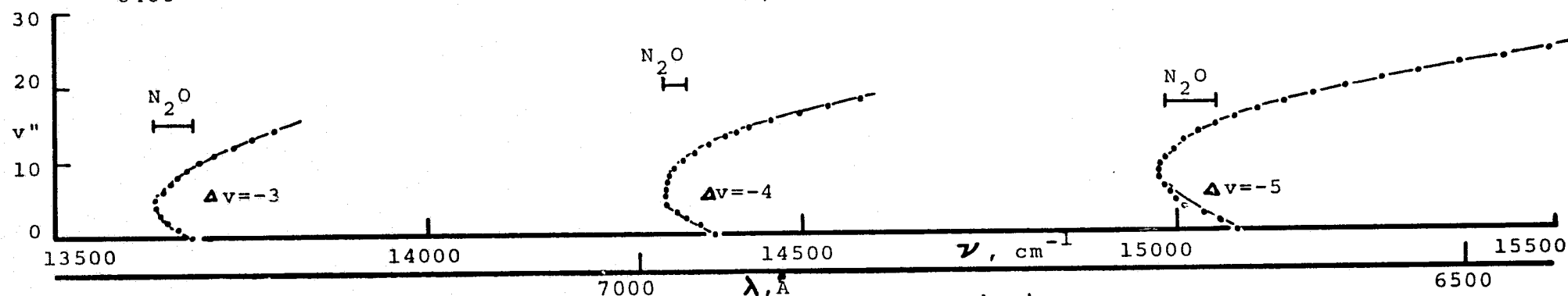
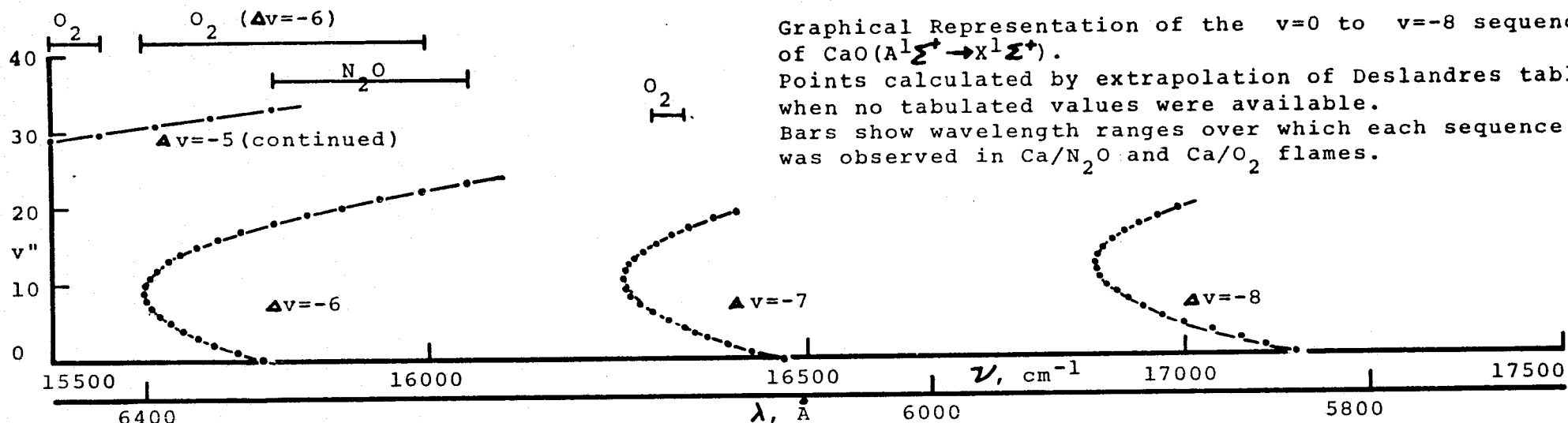
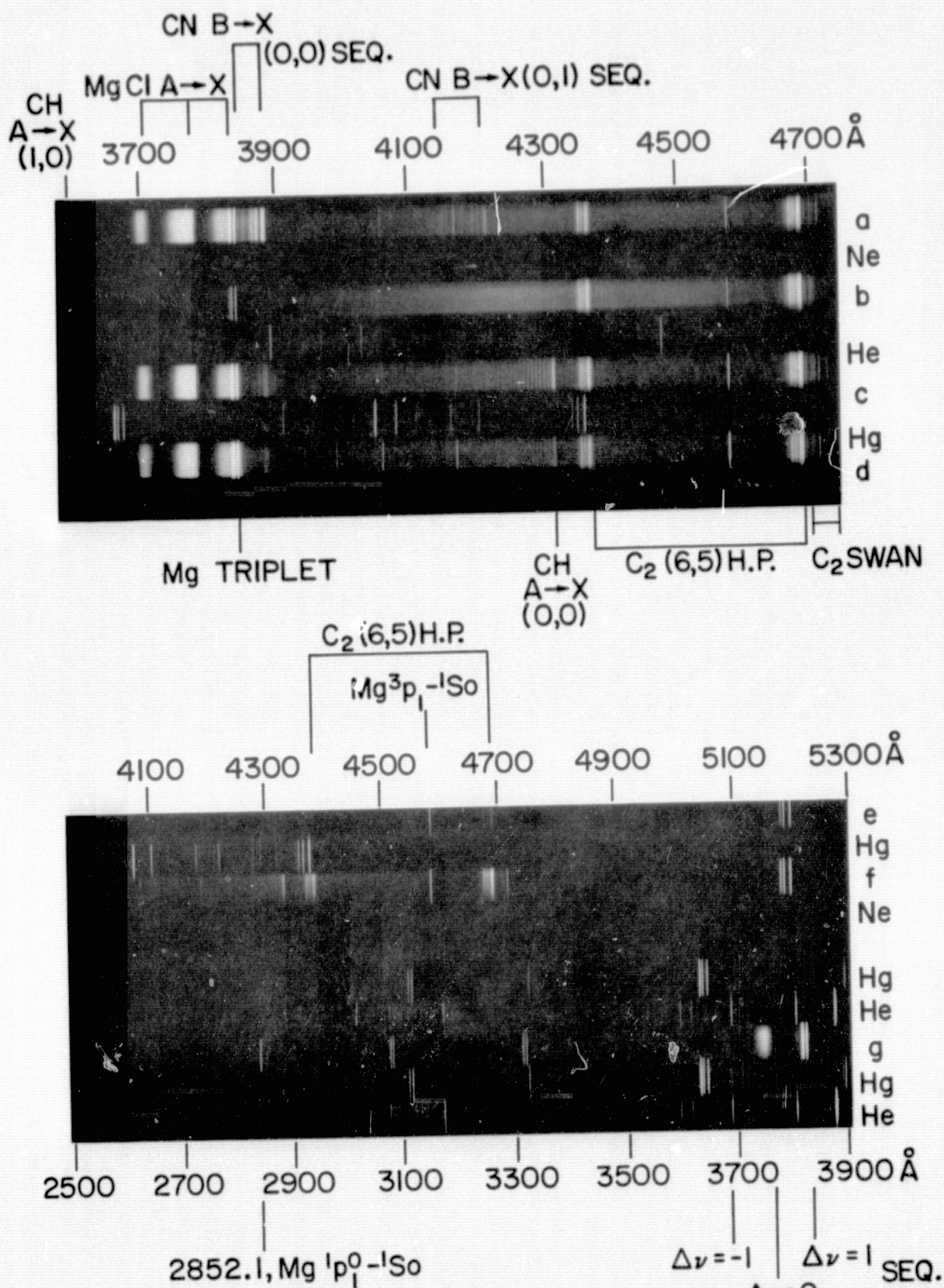
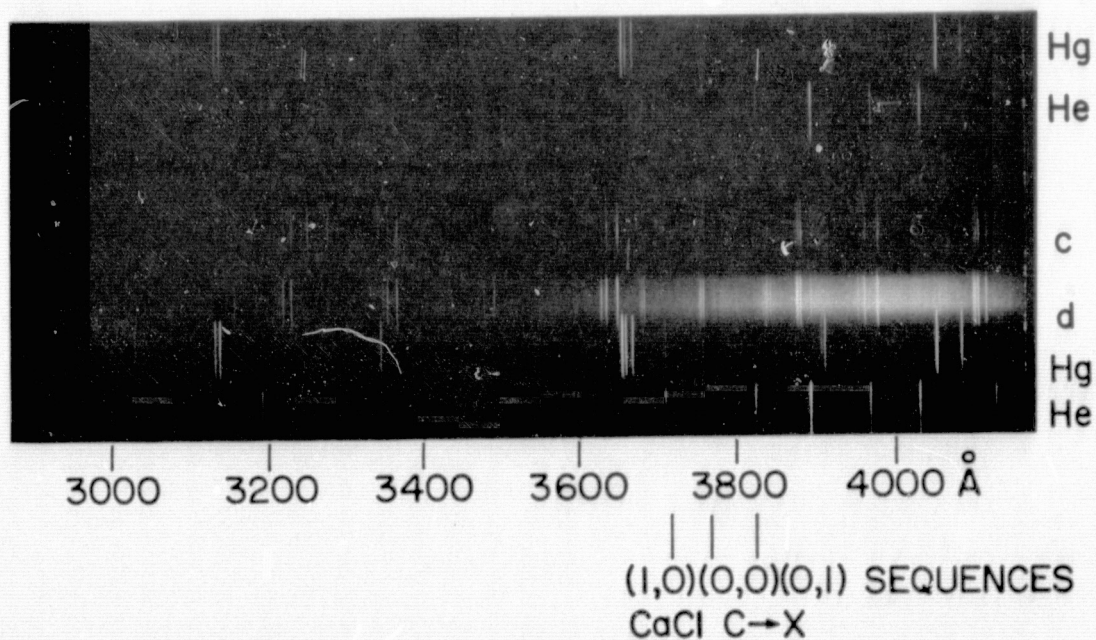
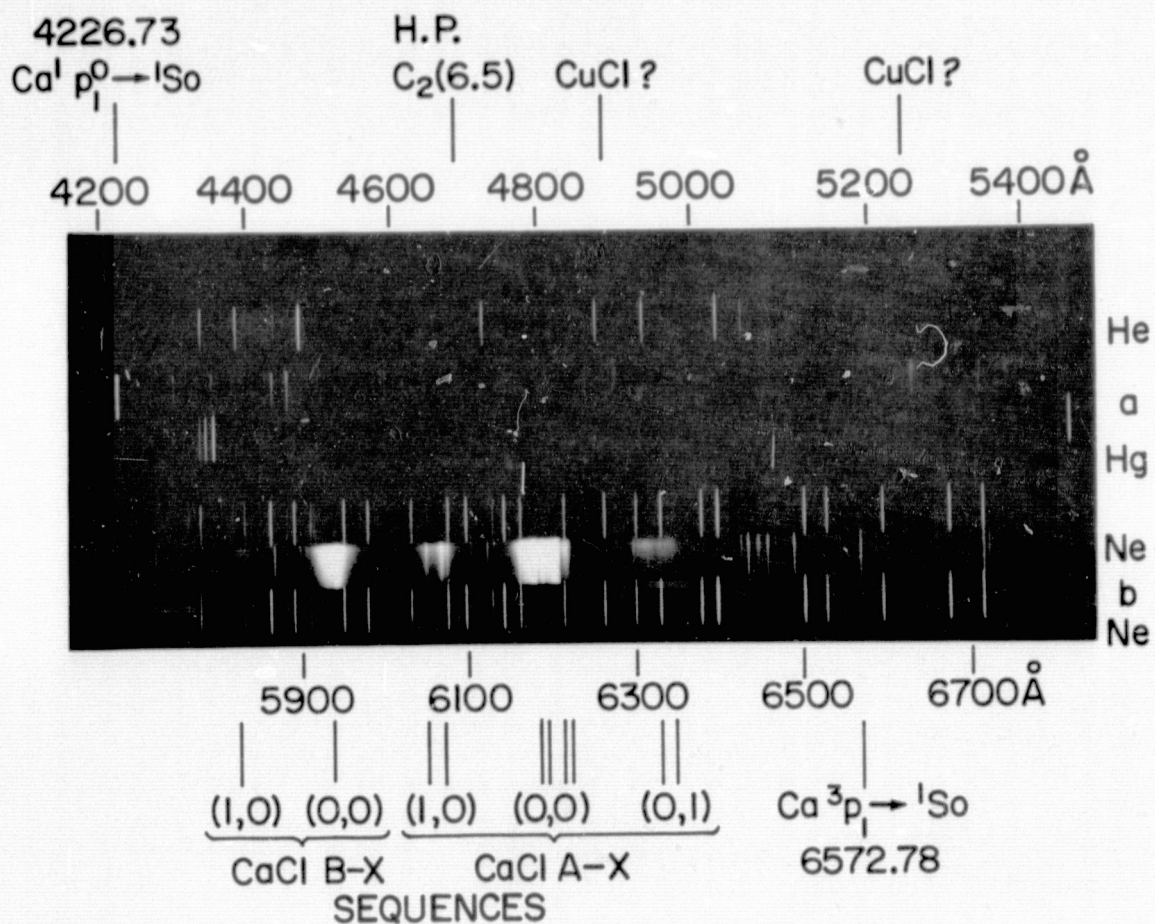


FIGURE
III-13



Mg/CCl₄/O₂ FLAME SPECTRA
a, b, c, d: Run MG-10-30-73-1, 50 Micron slit
P=1.6 torr, 0.23% CCl₄
a: 0.55% N₂O; b: no oxidizer added
c: CO+0.65% O₂; d: 0.65% O₂
e, f, g: Run MG-9-25-73-1, 50 Micron slit
P=0.9 torr, 0.60% CCl₄, 1.65% O₂
Exposure: e-11 min, f-71 min, g-66 min

FIGURE III-14



Ca/CCl₄/O₂ FLAME SPECTRA

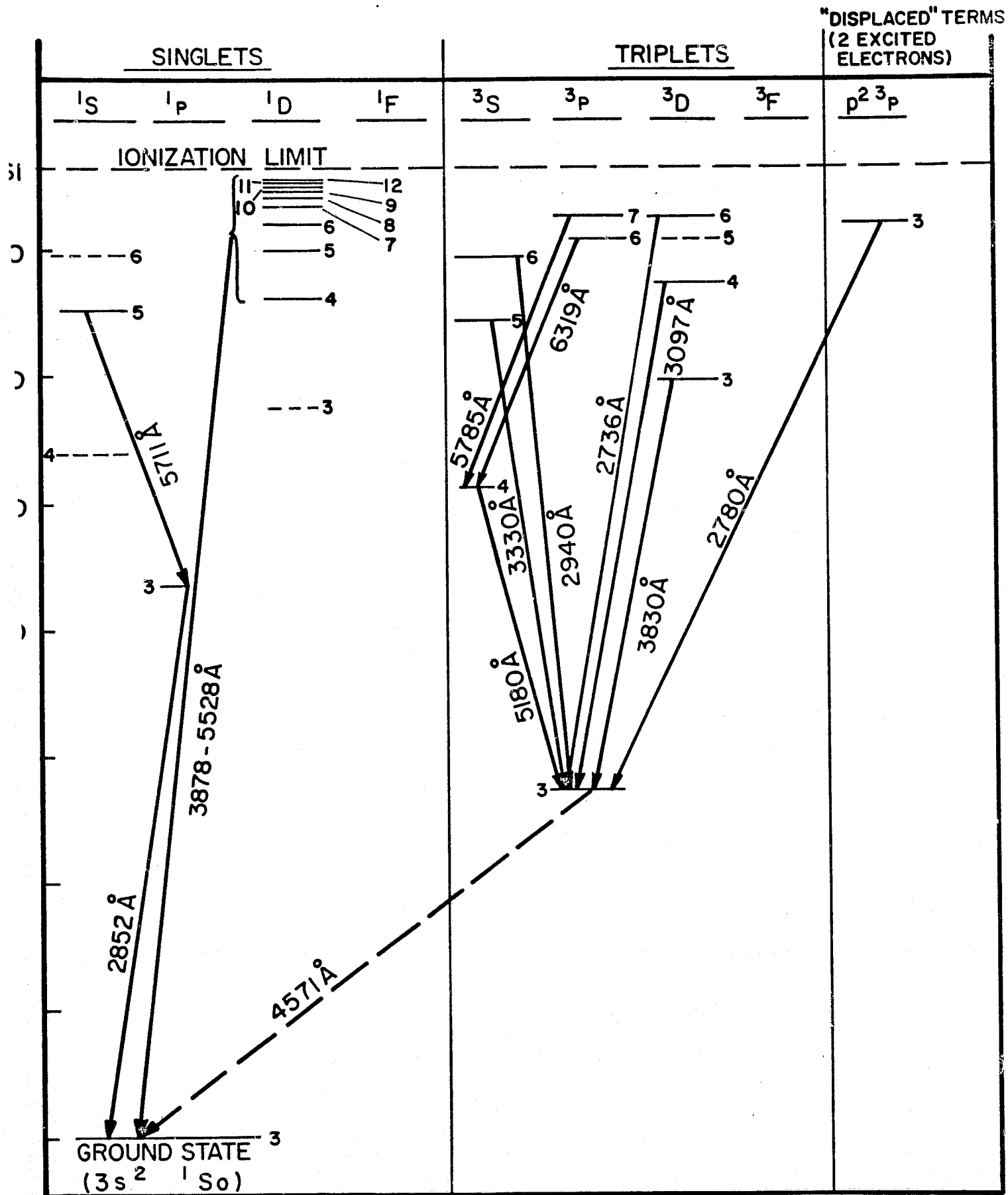
a. & b. : Run CA-9-26-73-1, P=0.9 torr, 0.47% CCl₄, 1.28% O₂

c. & d. : Run Ca-7-18-73-1, P=0.9 torr, 0.54% CCl₄

c. : 1.53% O₂ (near end of run, Ca nearly exhausted)

d. : zero O₂ (beginning of run)

Slit widths: 50 microns.



Mg ATOMIC TRANSITIONS OBSERVED IN $Mg+Ar/CCl_4/O_2$
FLAME

Cd ATOMIC TRANSITIONS OBSERVED IN Cd + Ar/CCl₄/O₂ FLAMES

SINGLETs

TRIPLETs

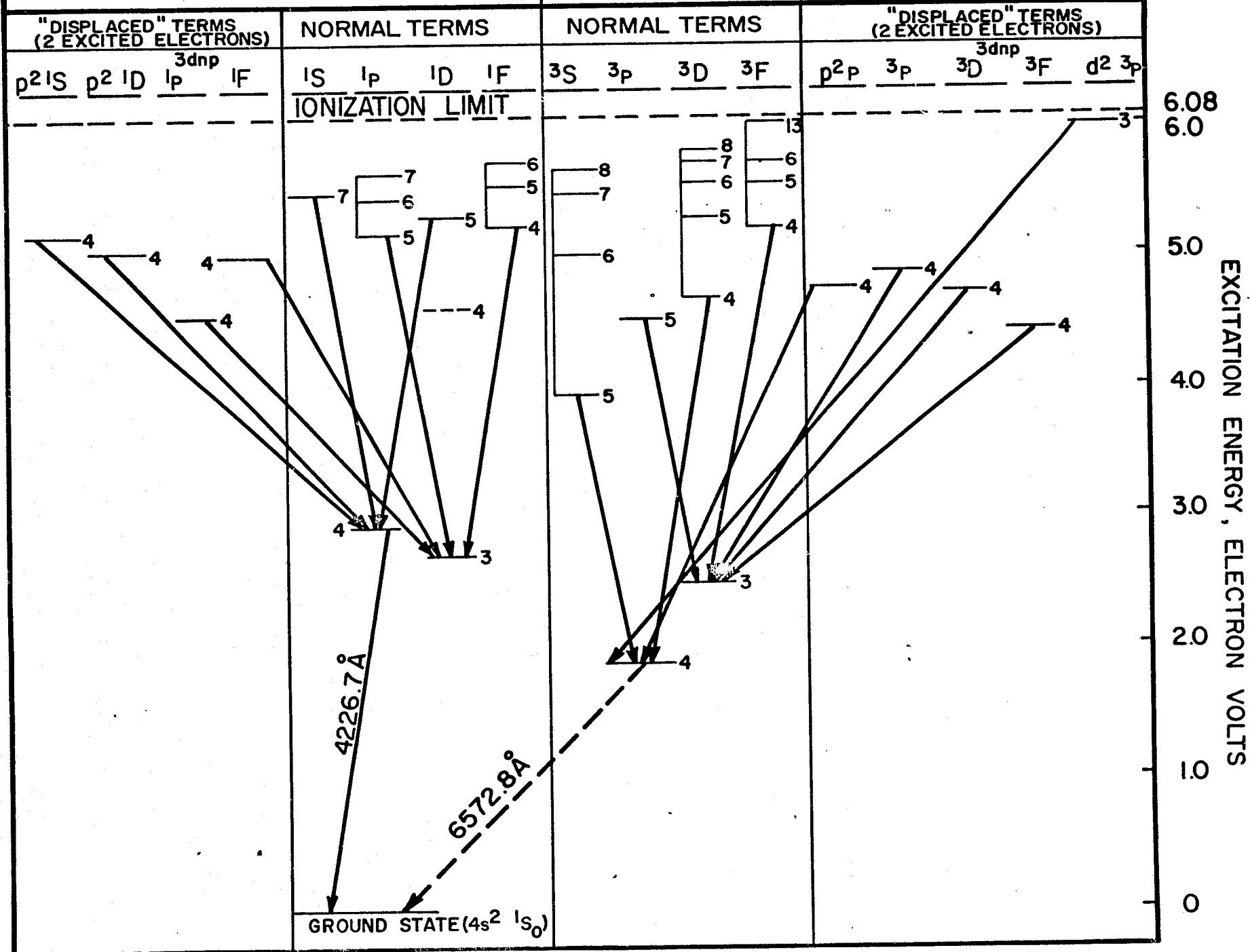


FIGURE
III-17

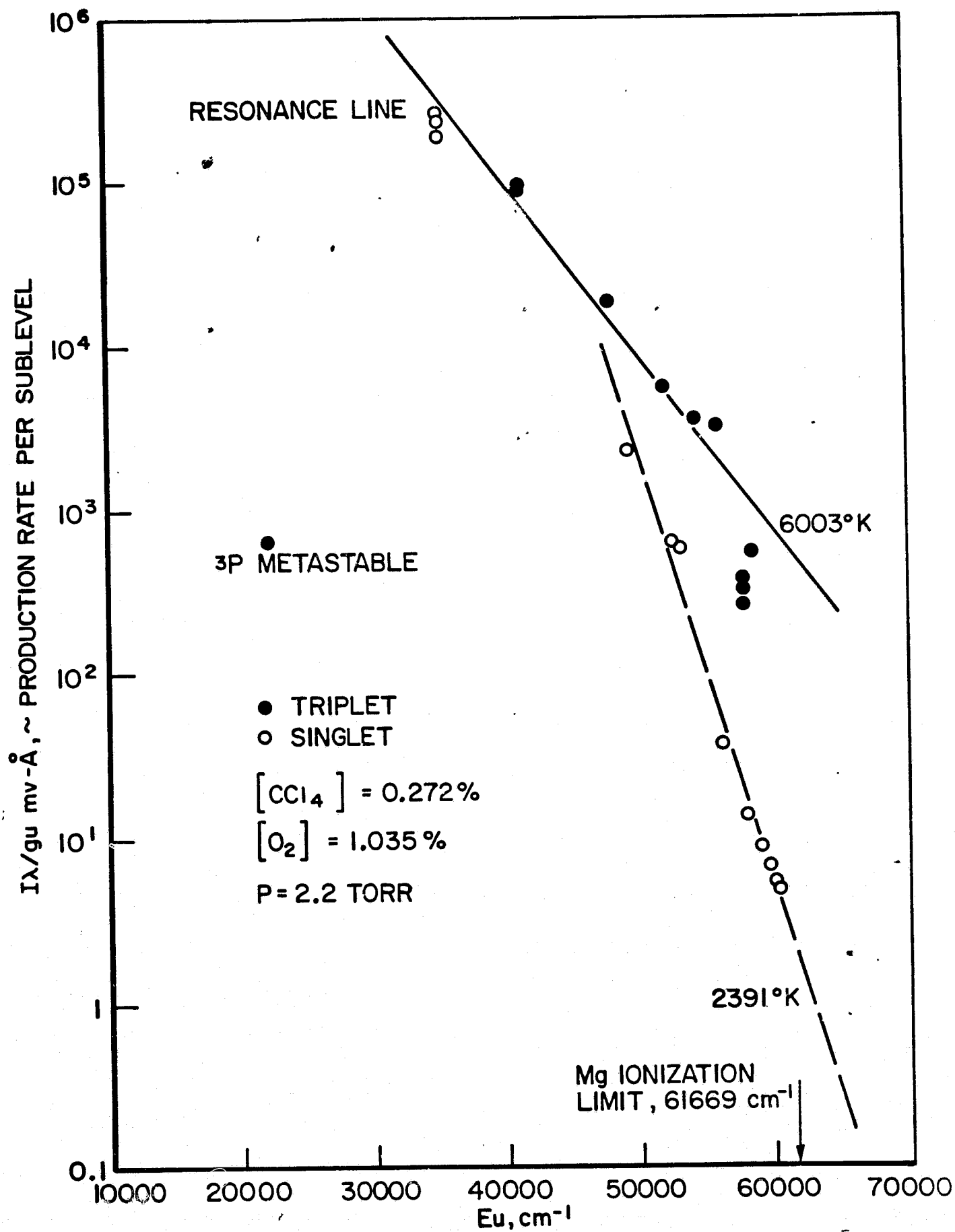


FIGURE III-18

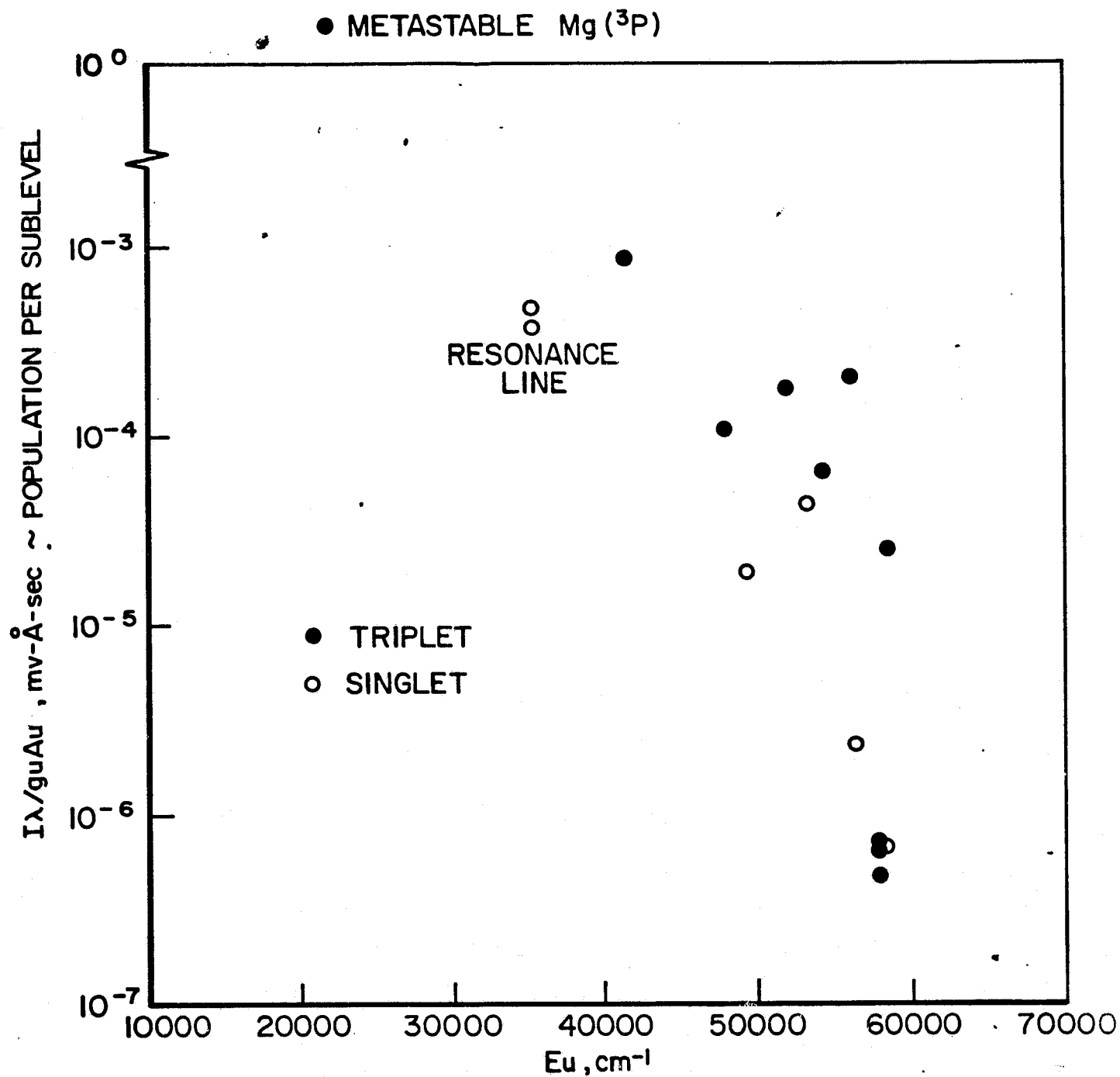


FIGURE III-19

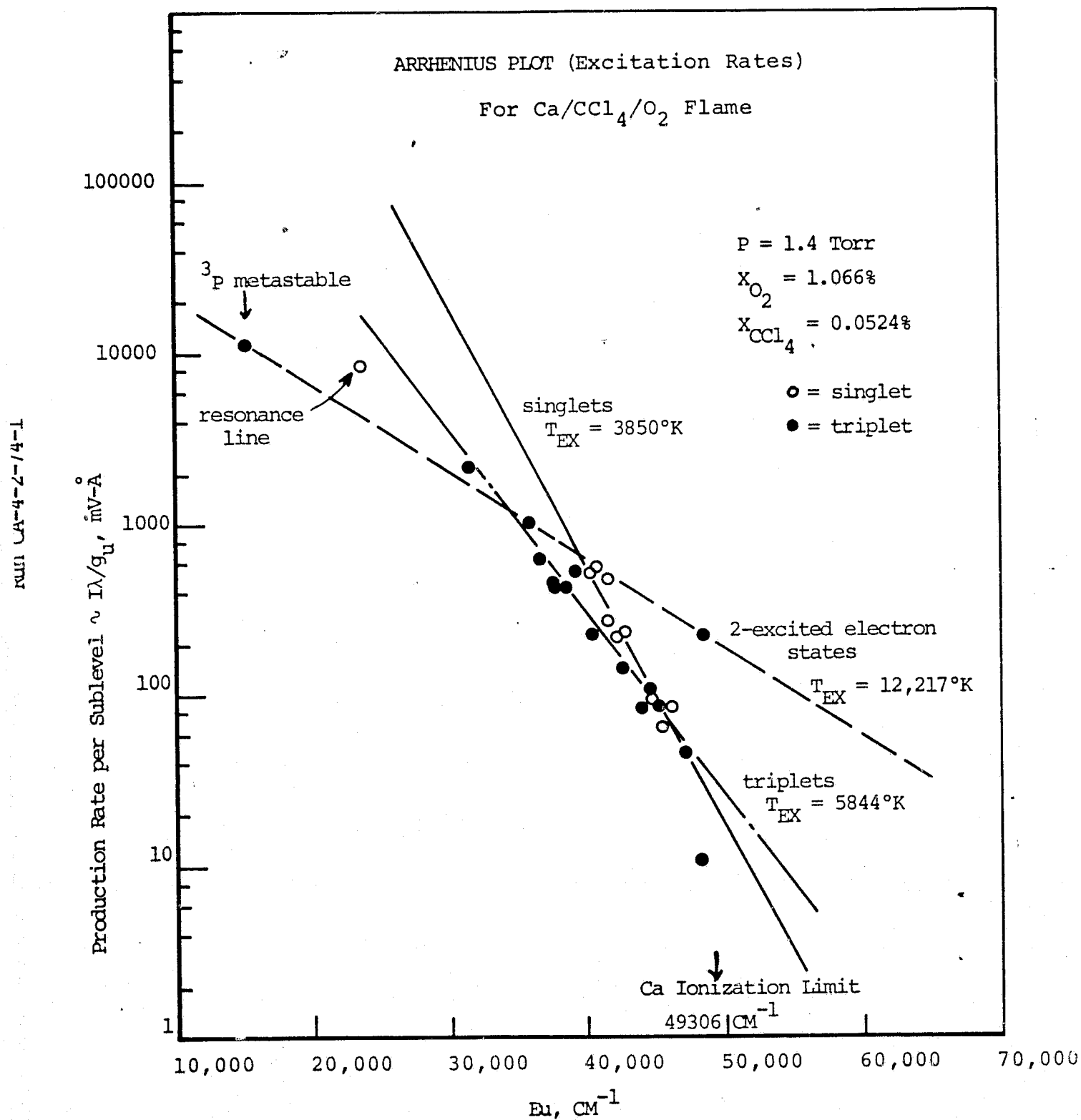


FIGURE III-20

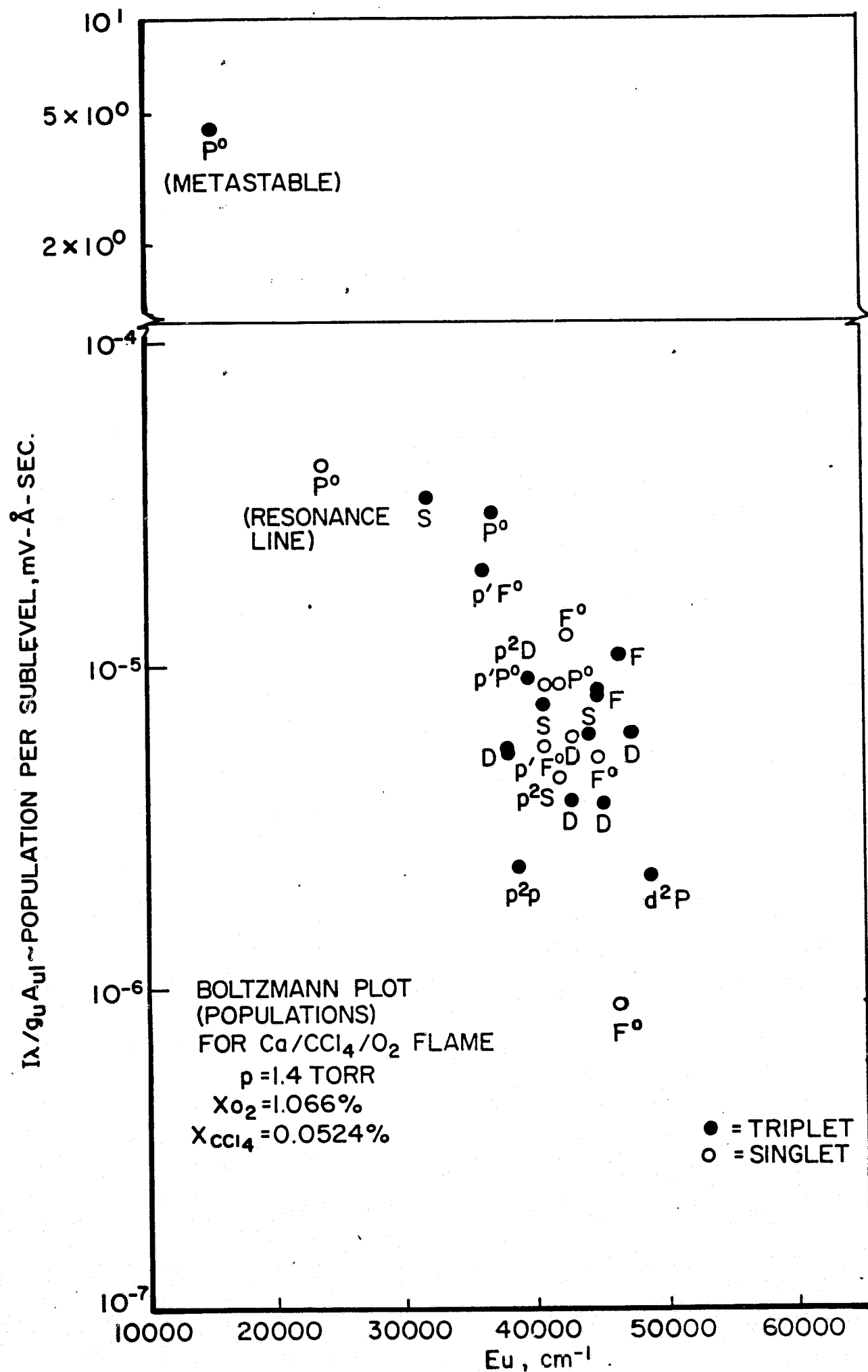


FIGURE
III-21

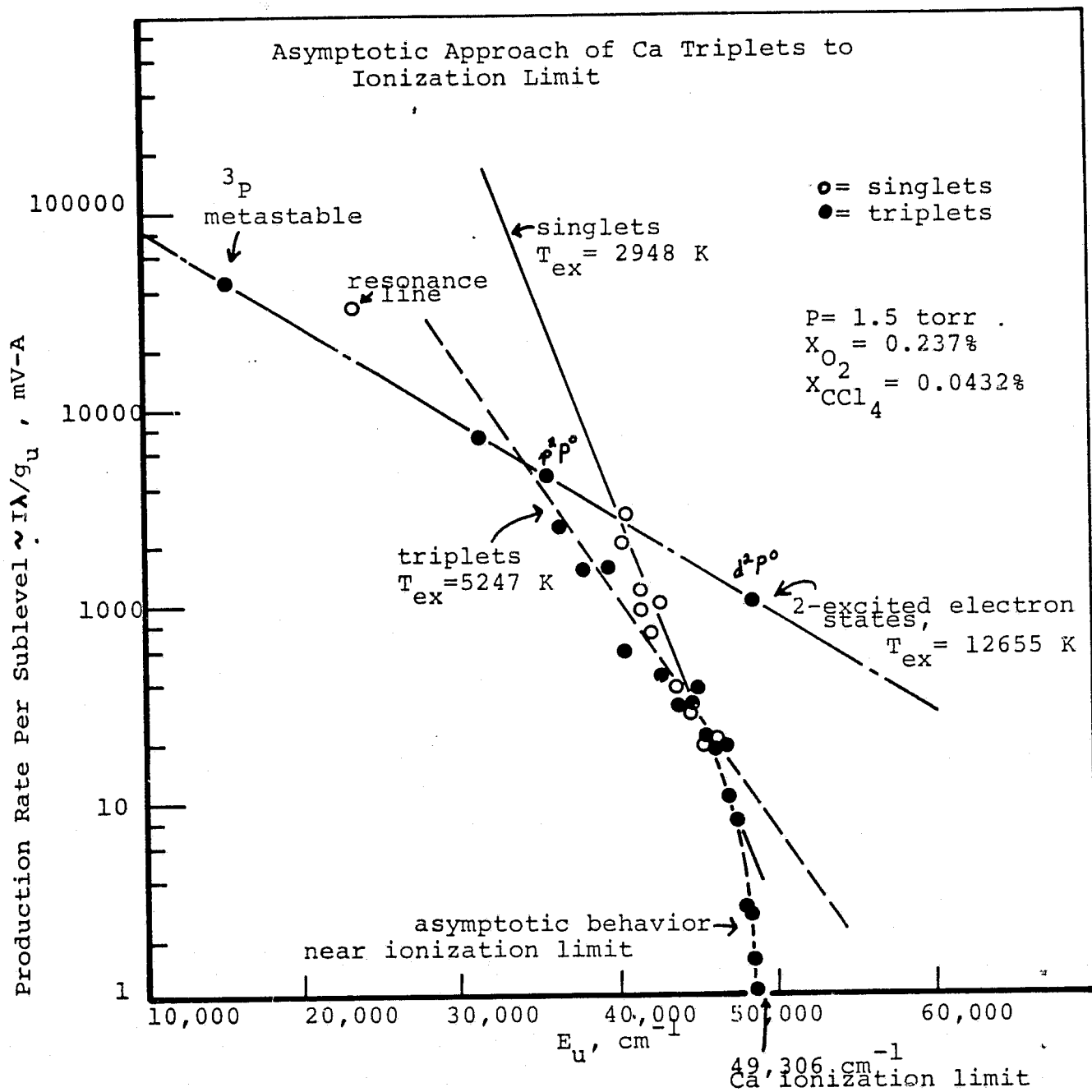


FIGURE III-22

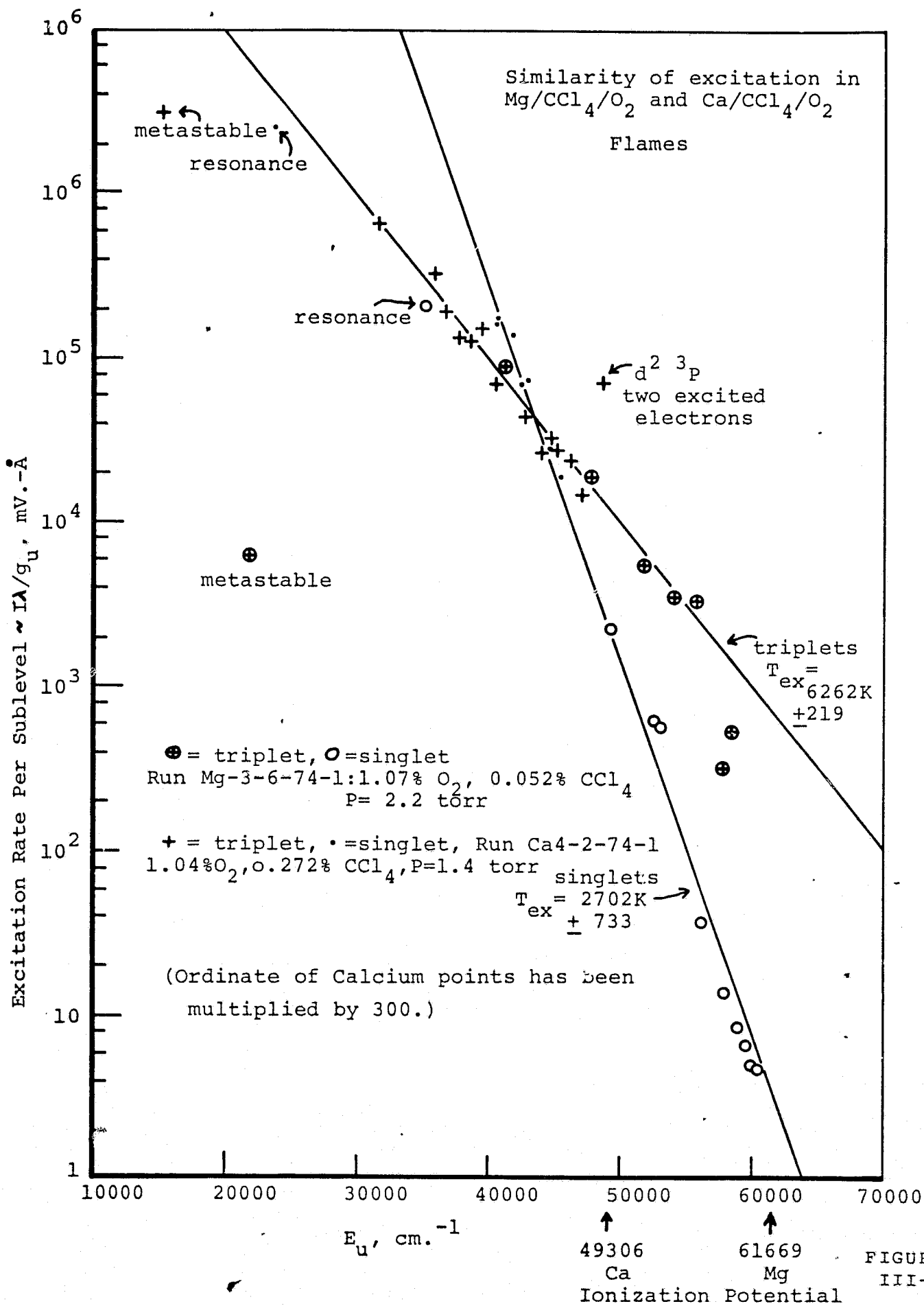
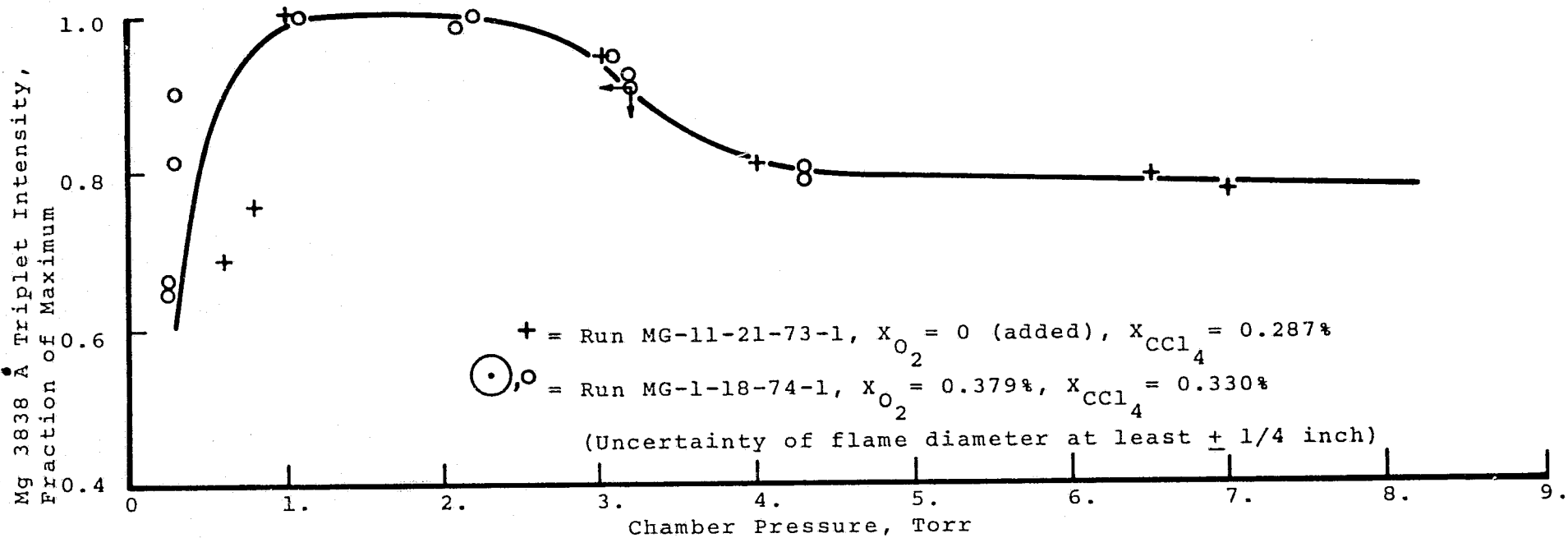
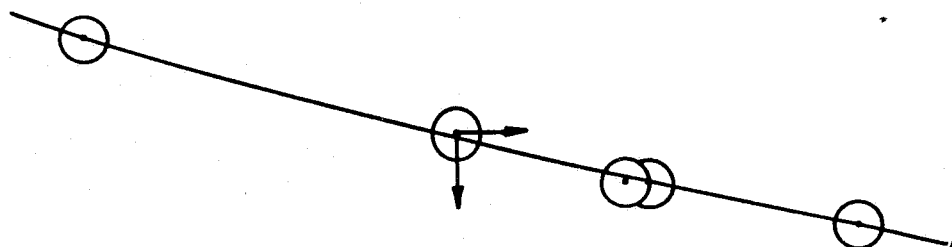


FIGURE
III-23



Mg/ CCl_4/O_2 Flame:
Flame Diameter and Emission Intensity
vs. Chamber Pressure

Approximate Flame Diameter,
inches



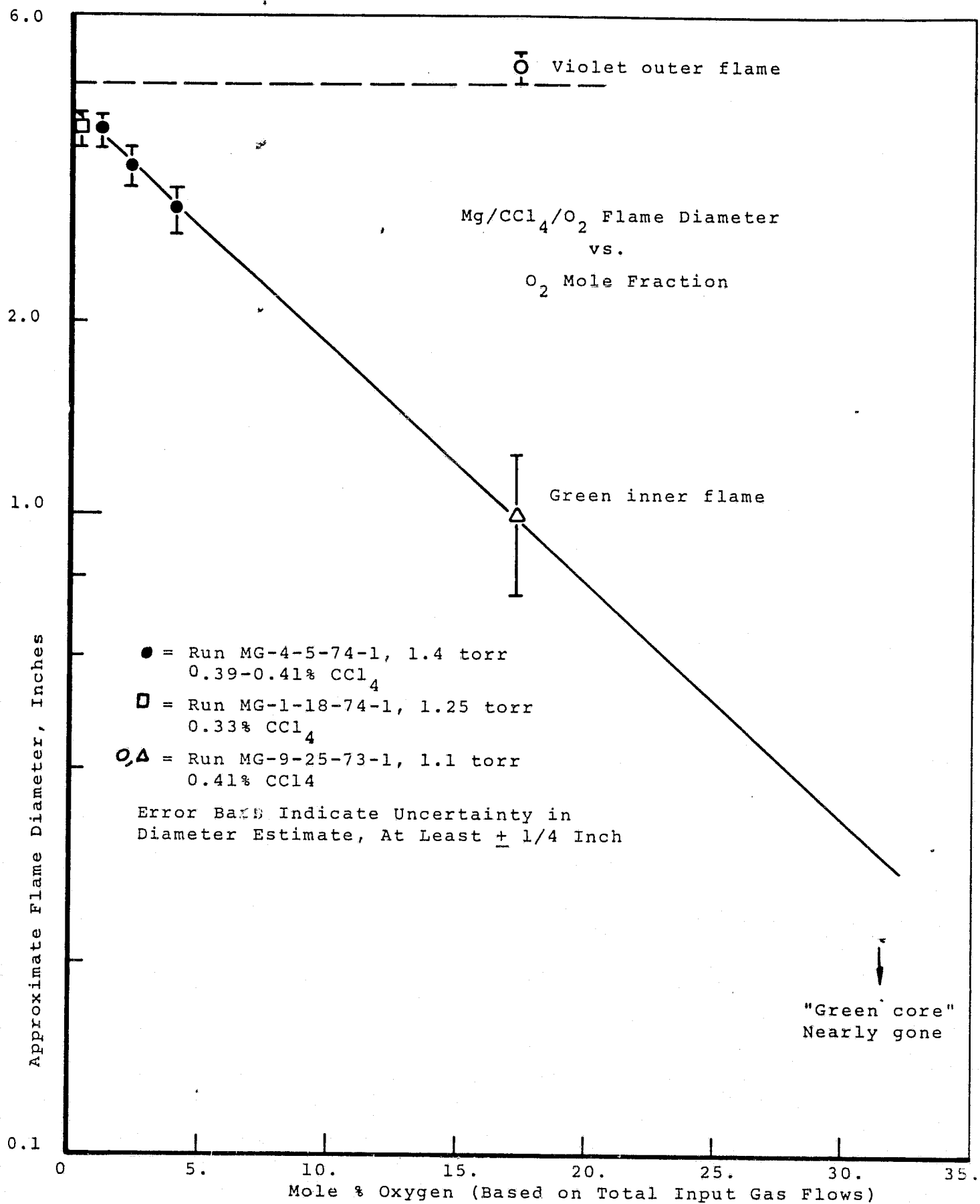


FIGURE III-25

Estimated Flame Diameter, Inches

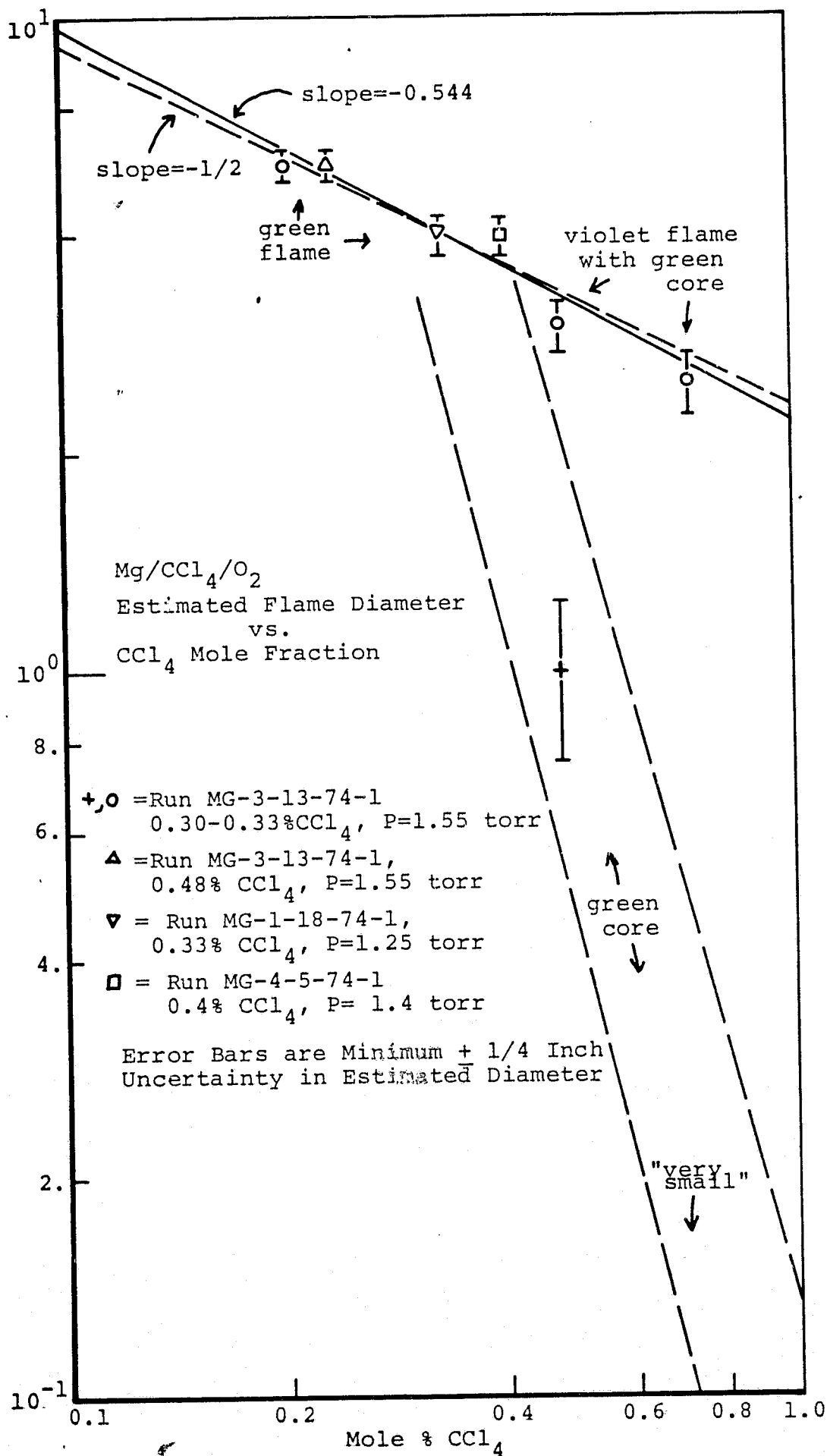


FIGURE III-26

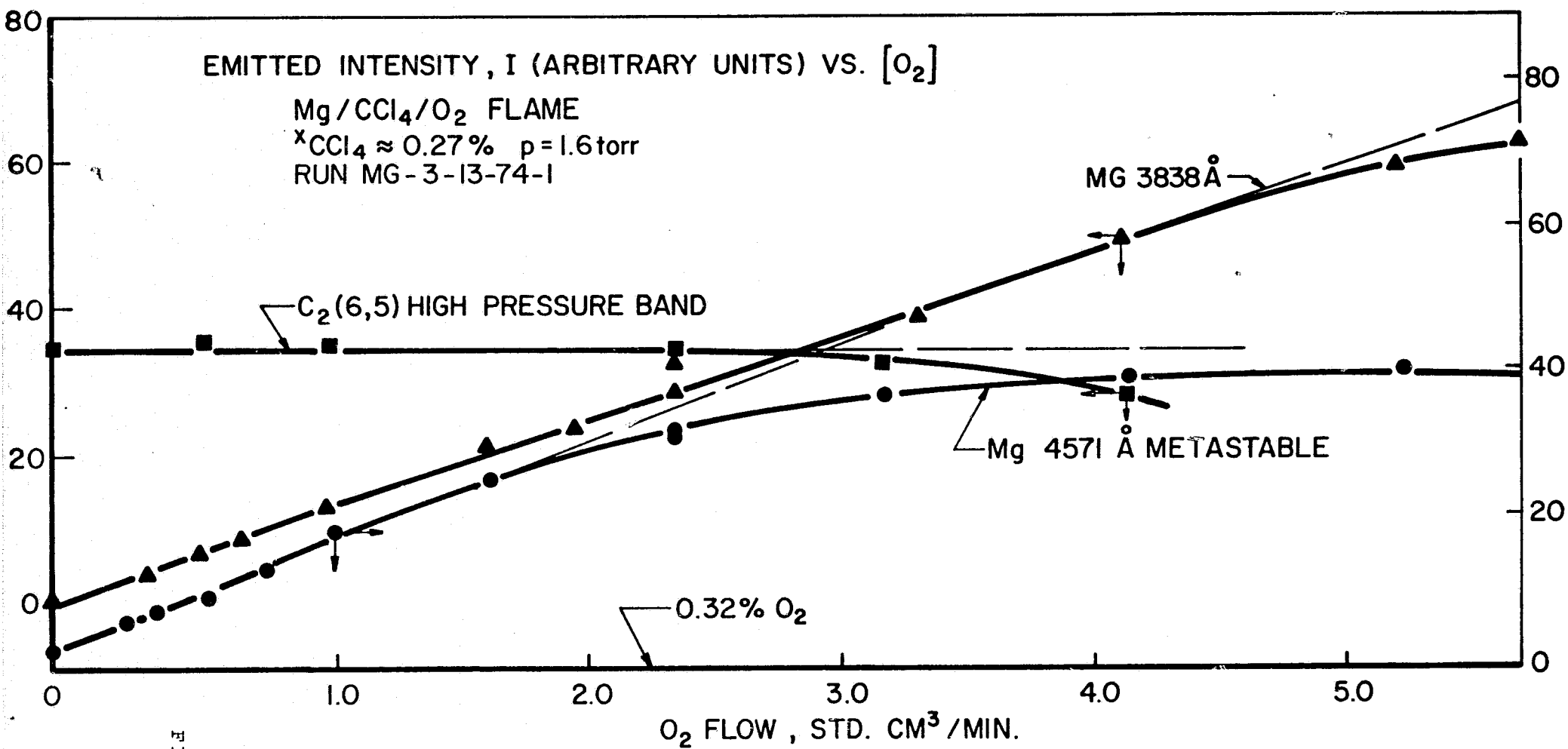


FIGURE III-27

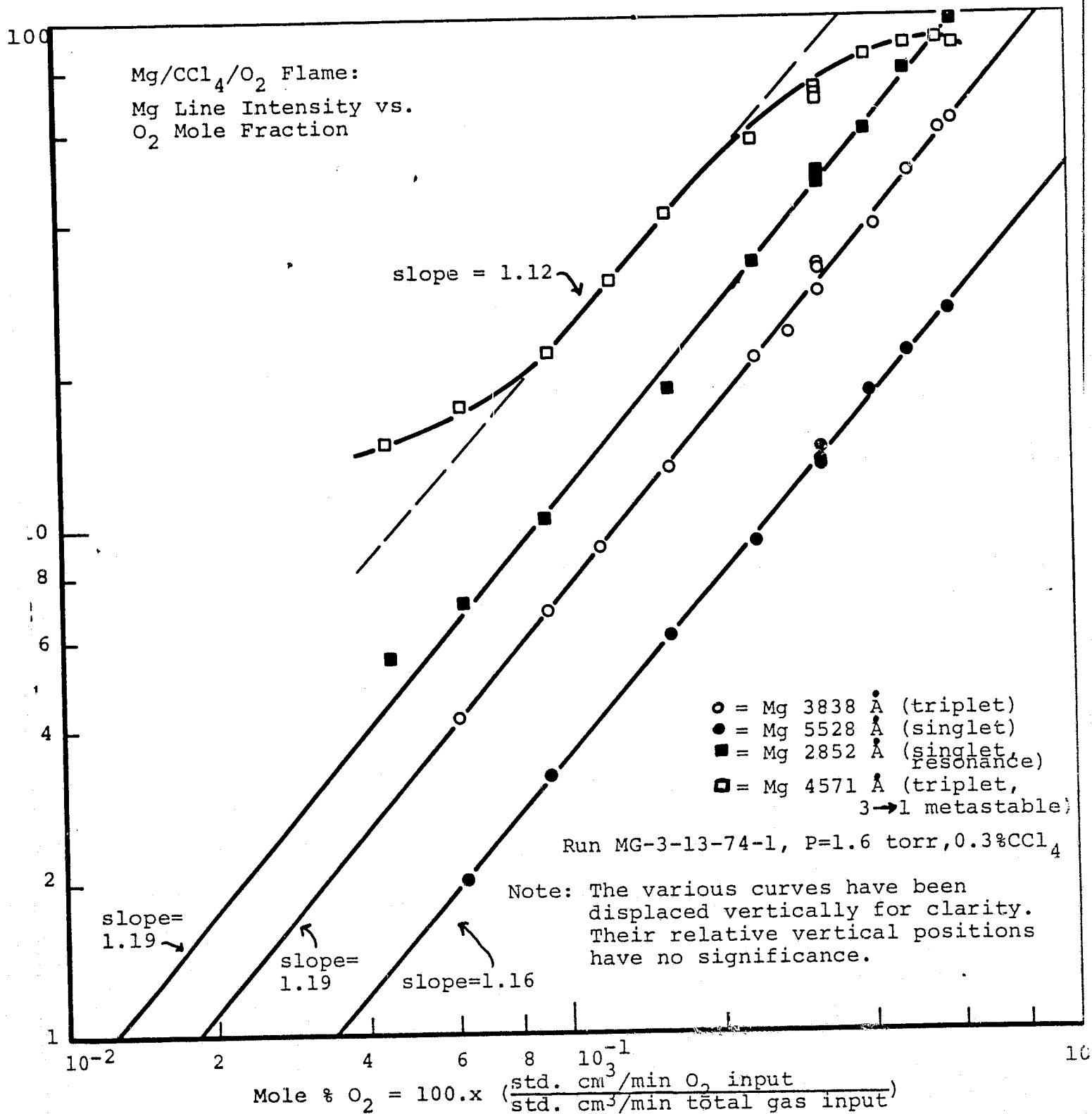
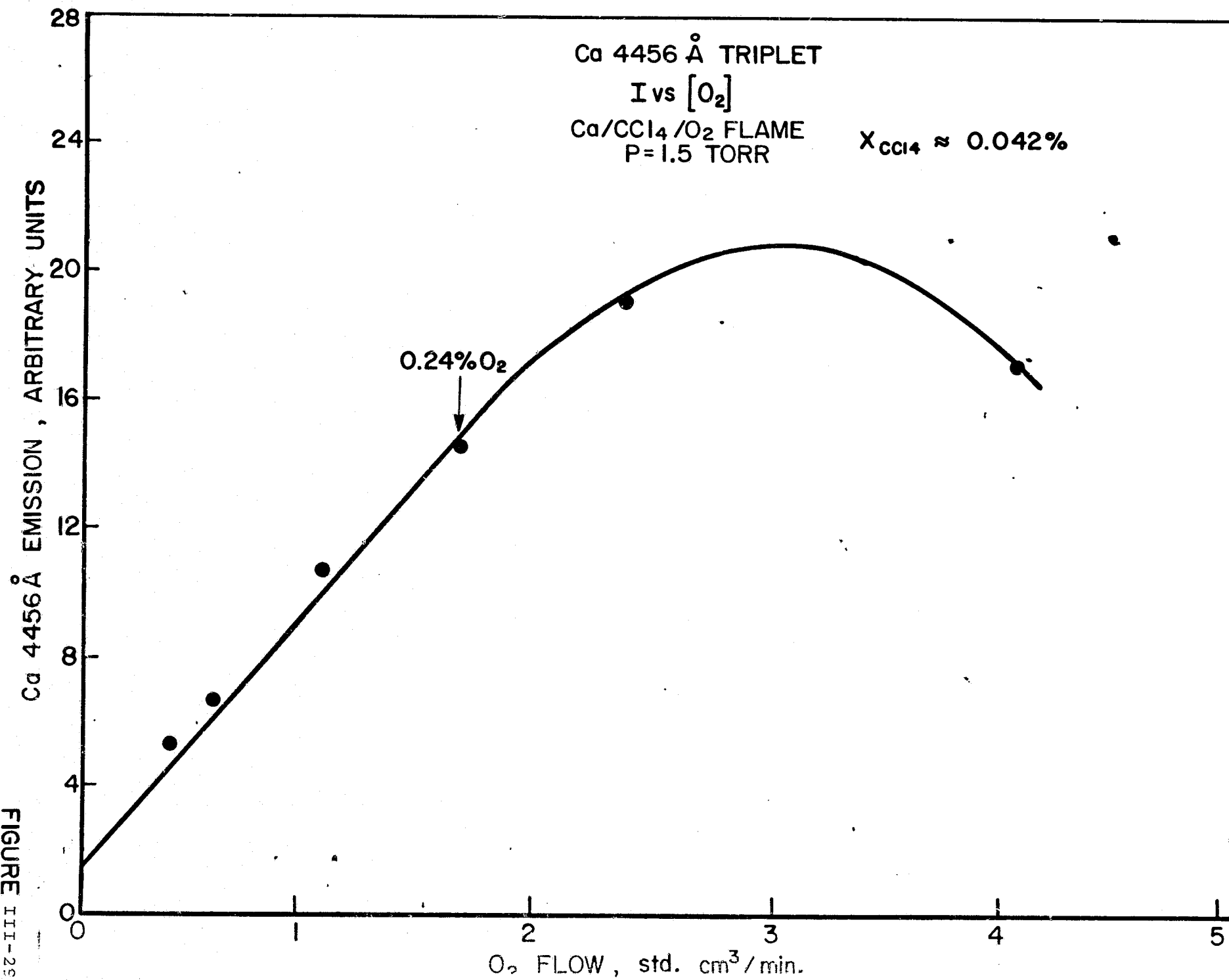


FIGURE III-28



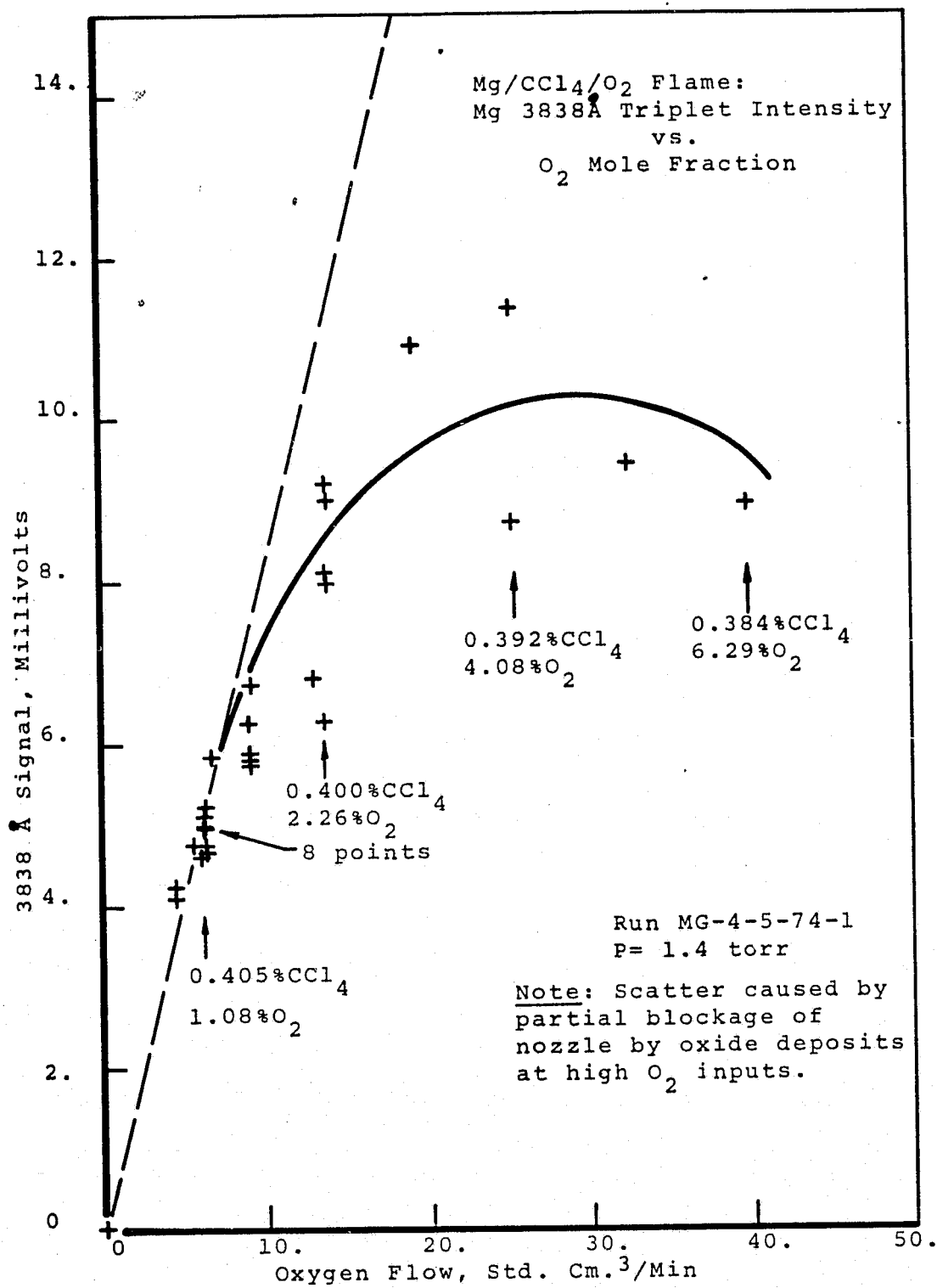


FIGURE III-30

C.5

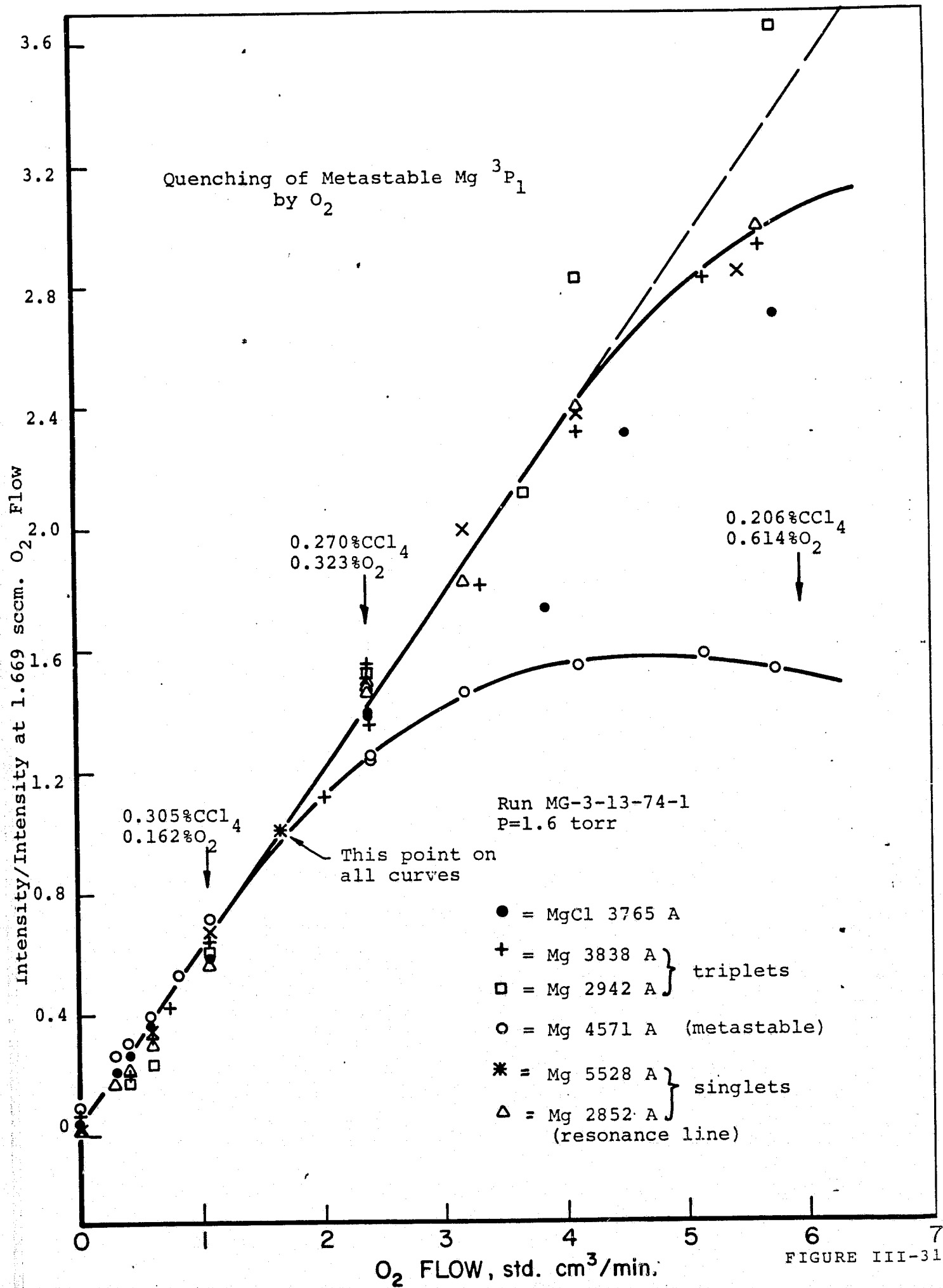


FIGURE III-31

Quenching of Ca Line Emission by O_2 :
Comparison of Metastable 3P_1 with Other States.

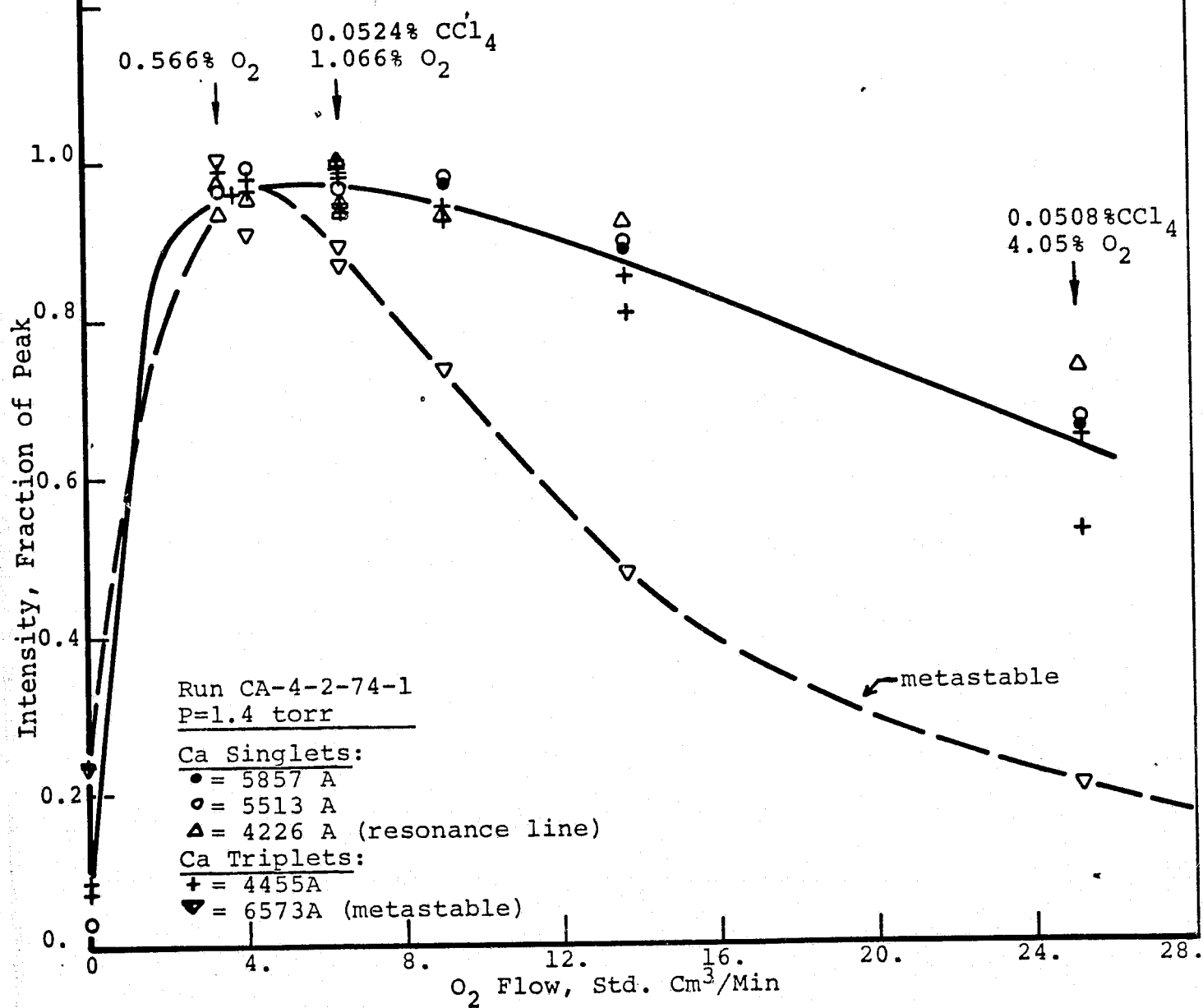


FIGURE III-32

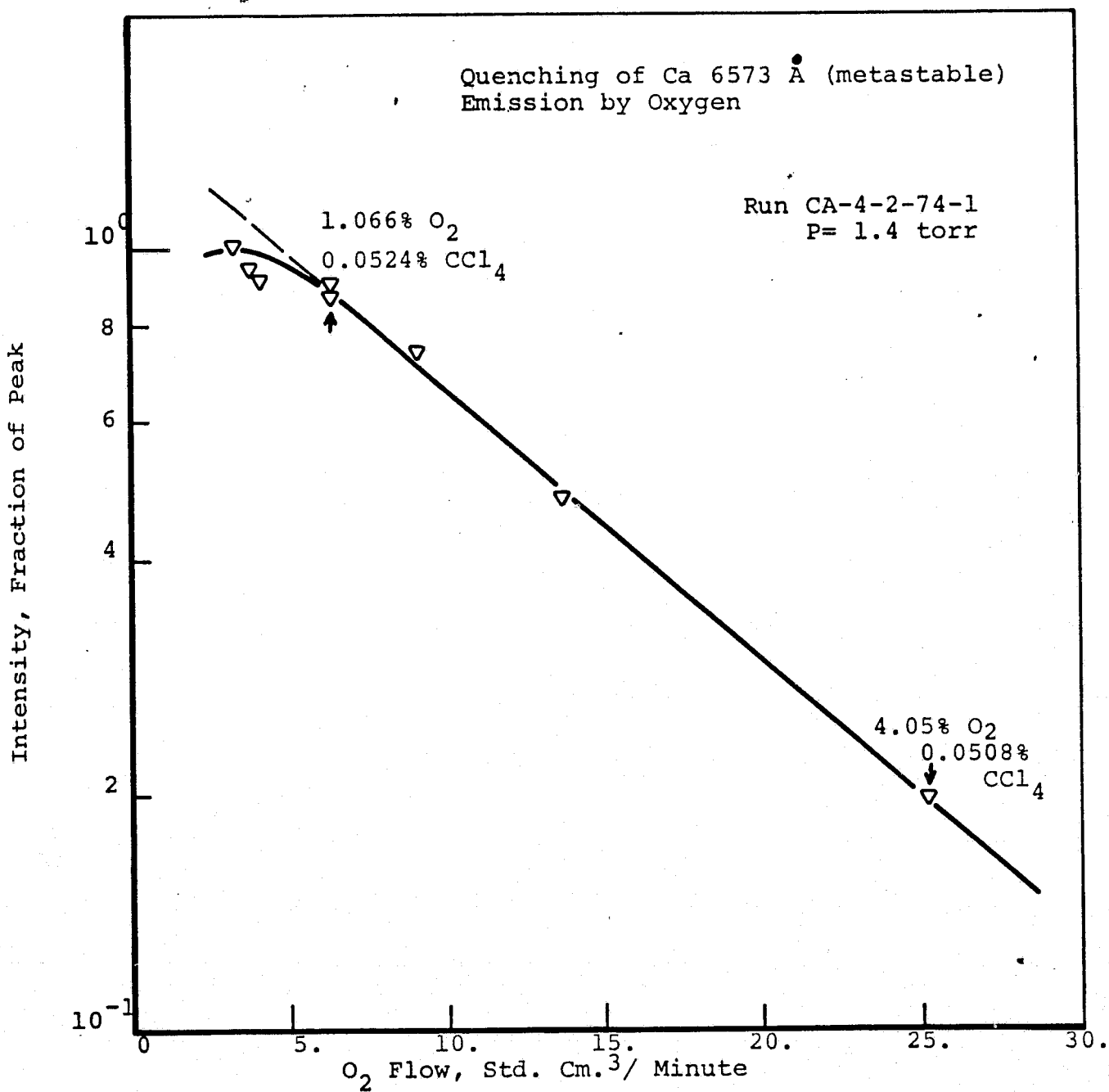


FIGURE III-33

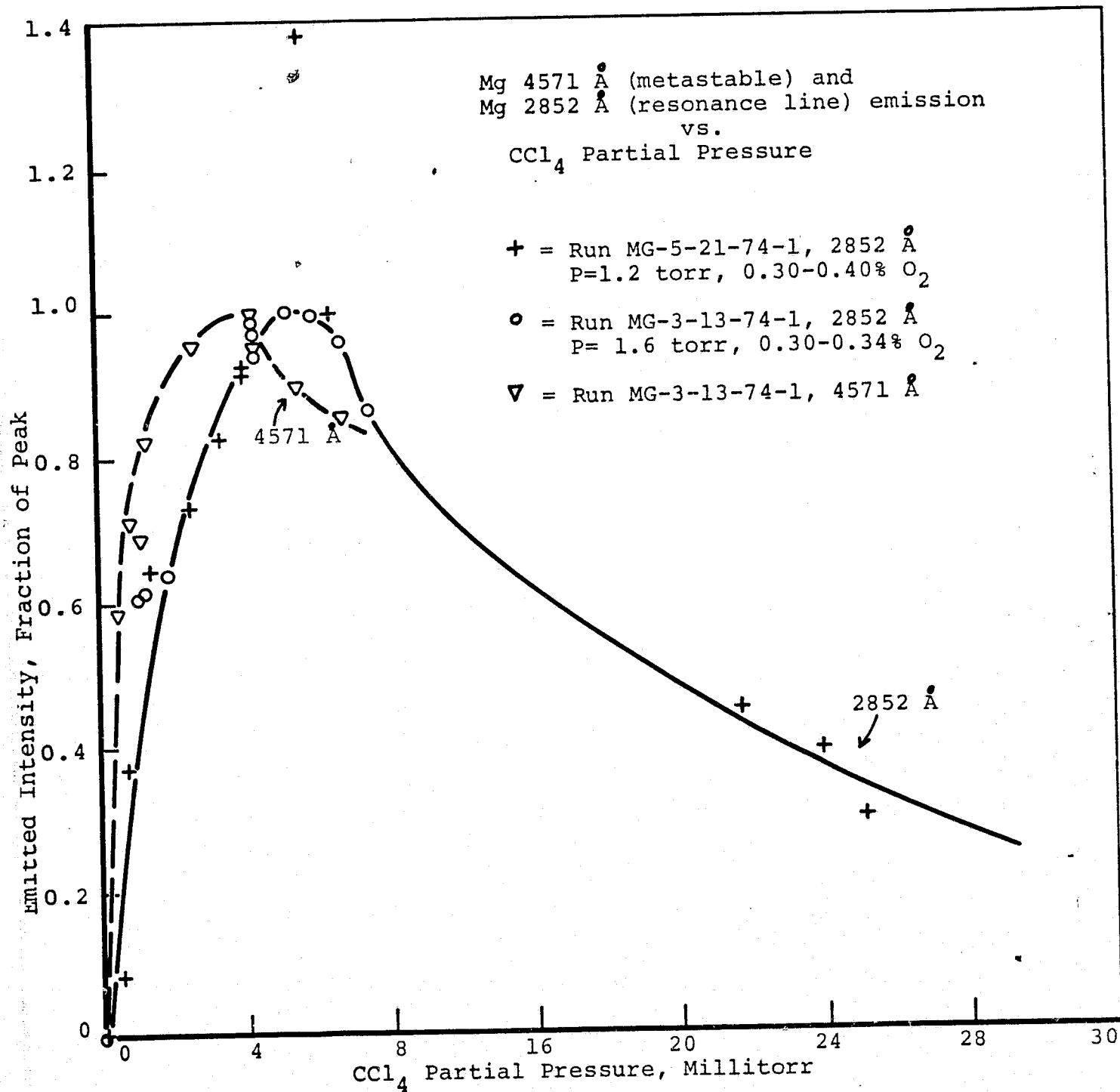


FIGURE III-34

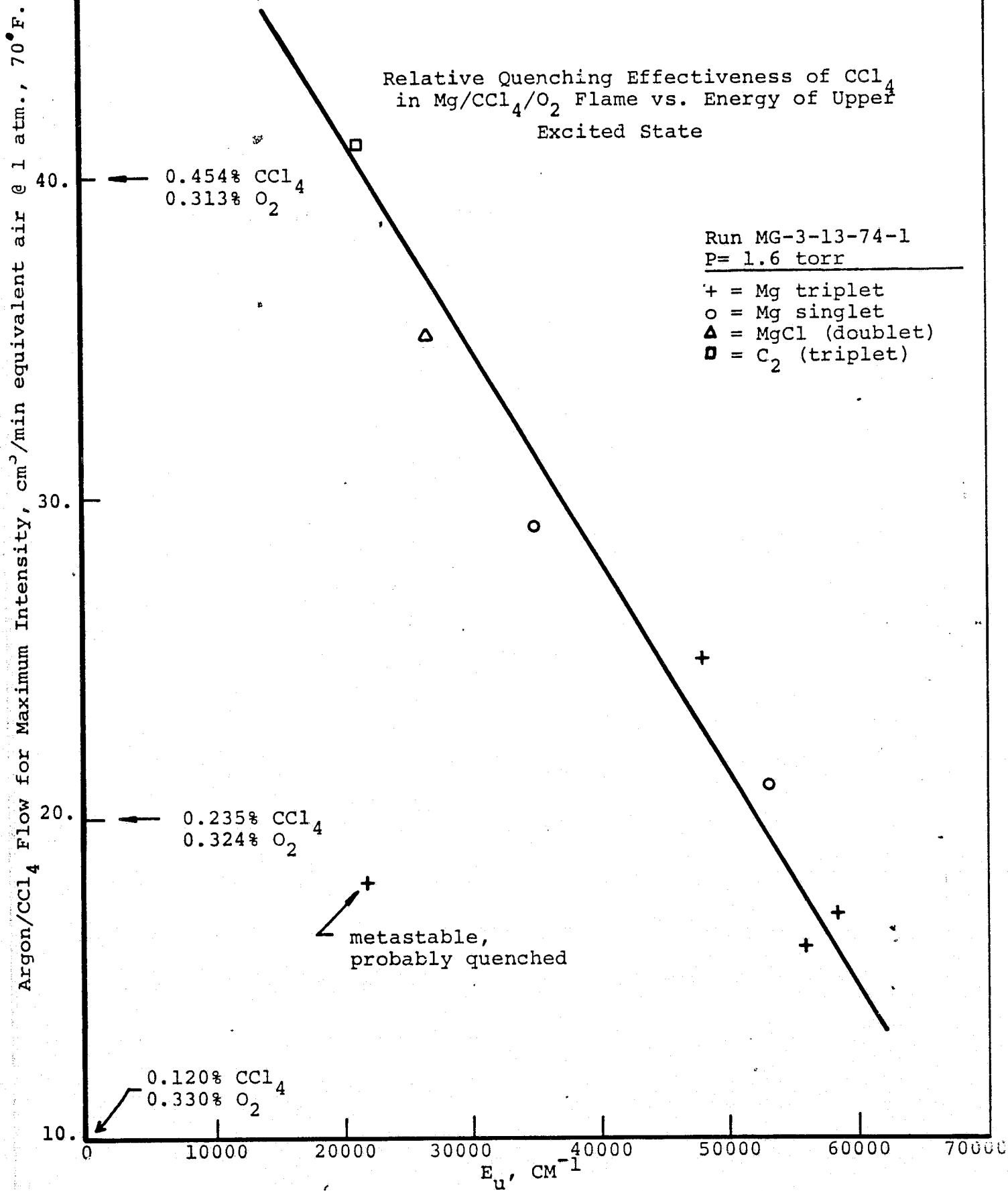


FIGURE III-35

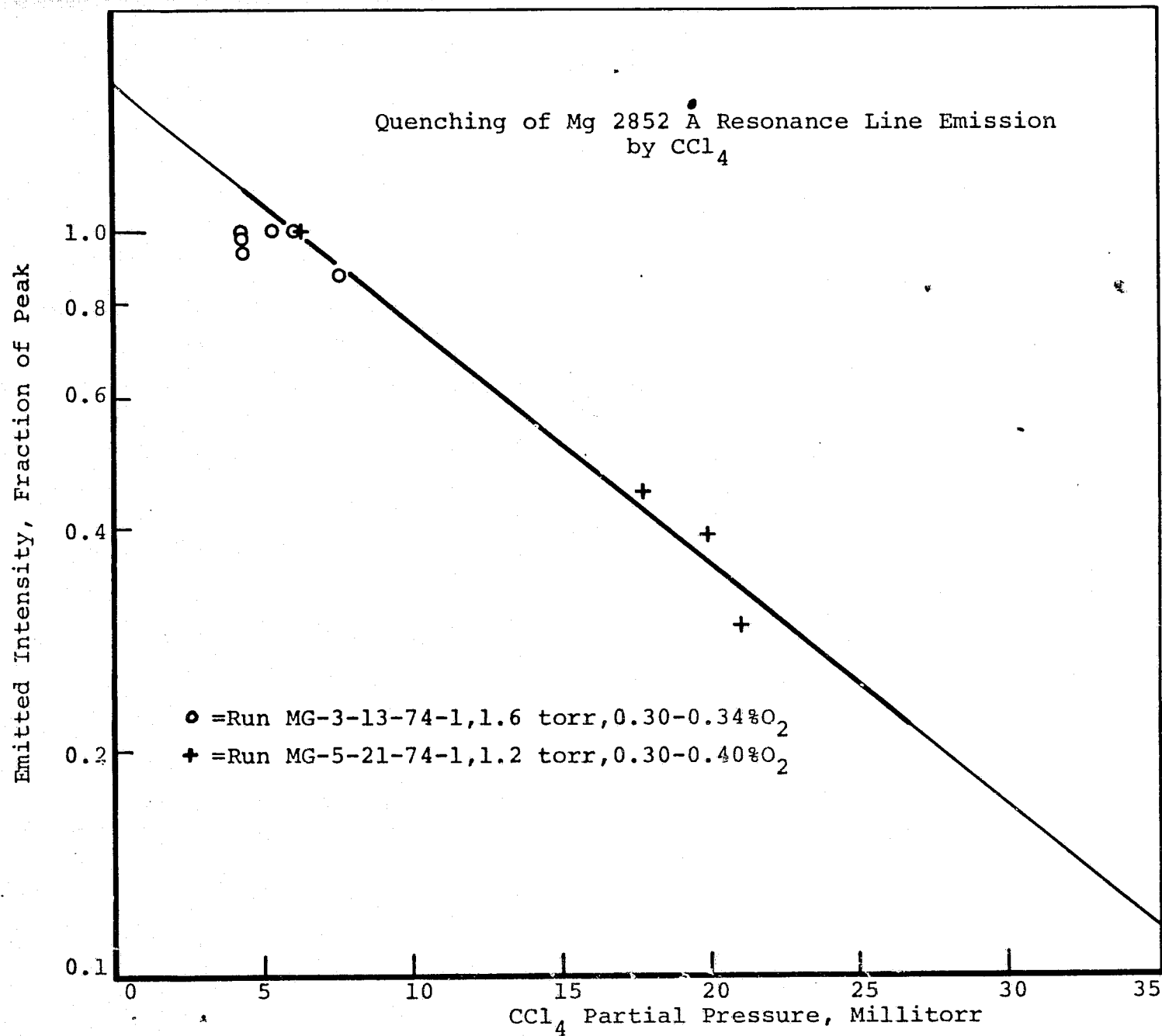


FIGURE III-36

Magnesium Triplet Excitation Temperatures vs. CCl_4 Mole Fraction

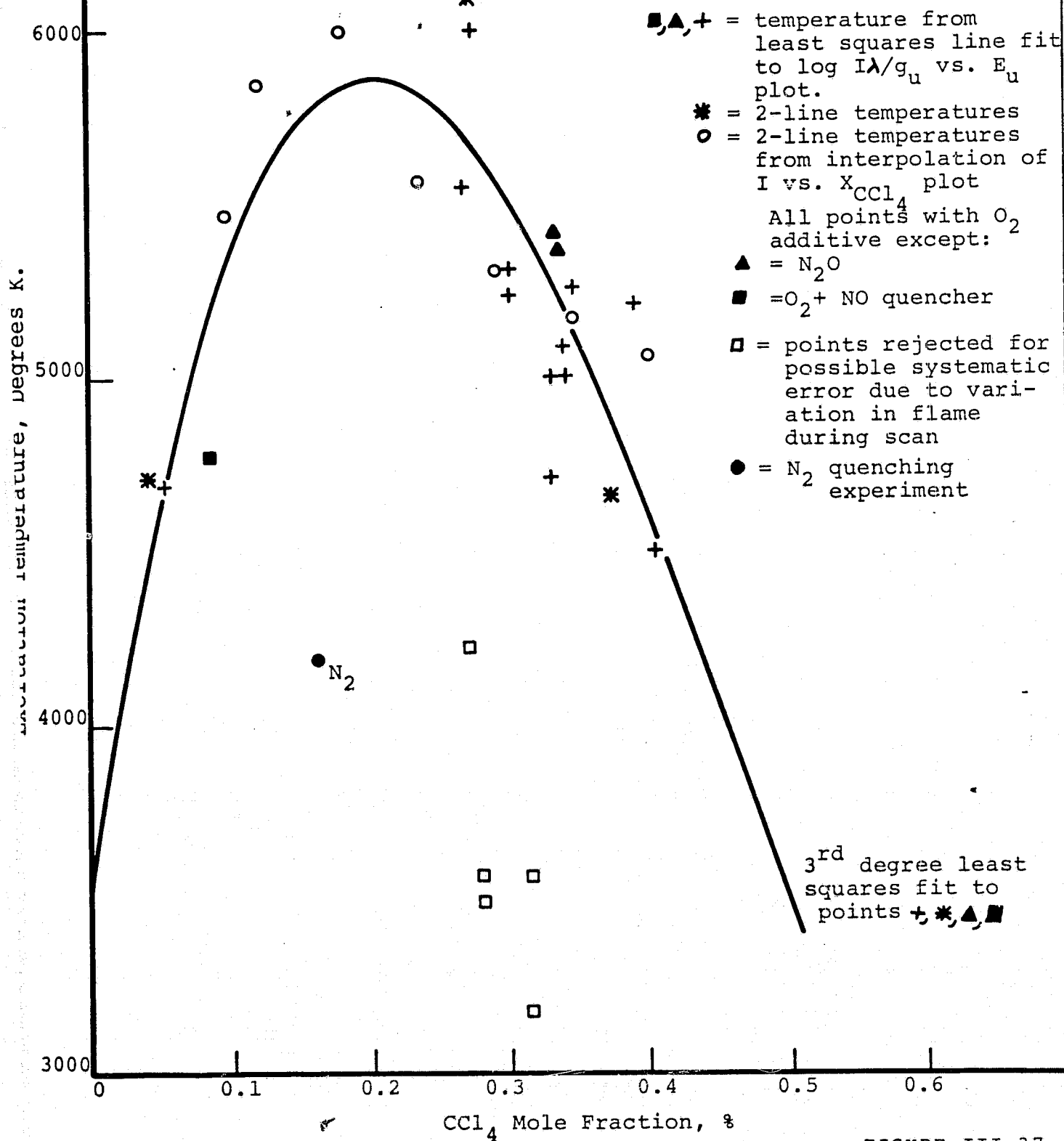


FIGURE III-37

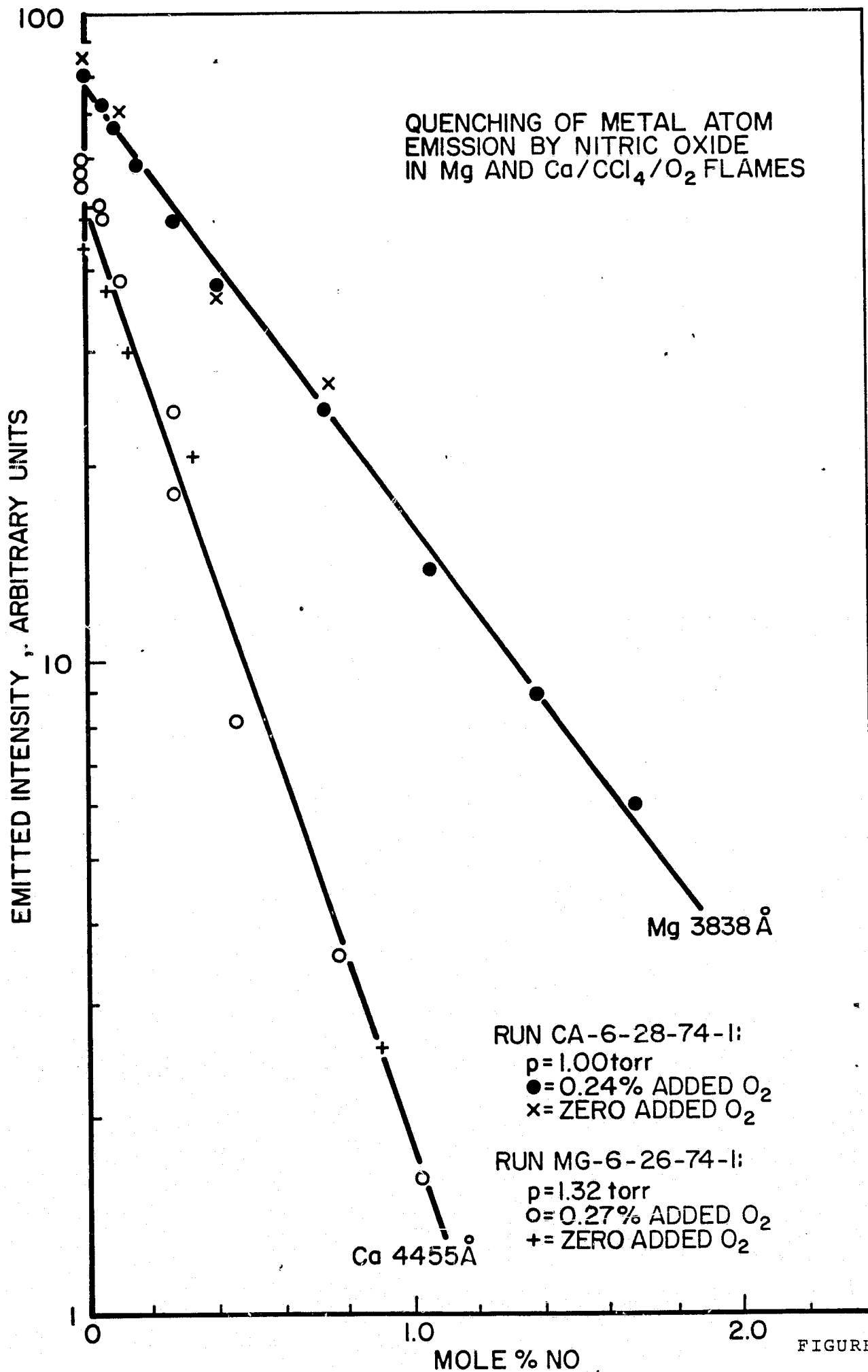


FIGURE III-38

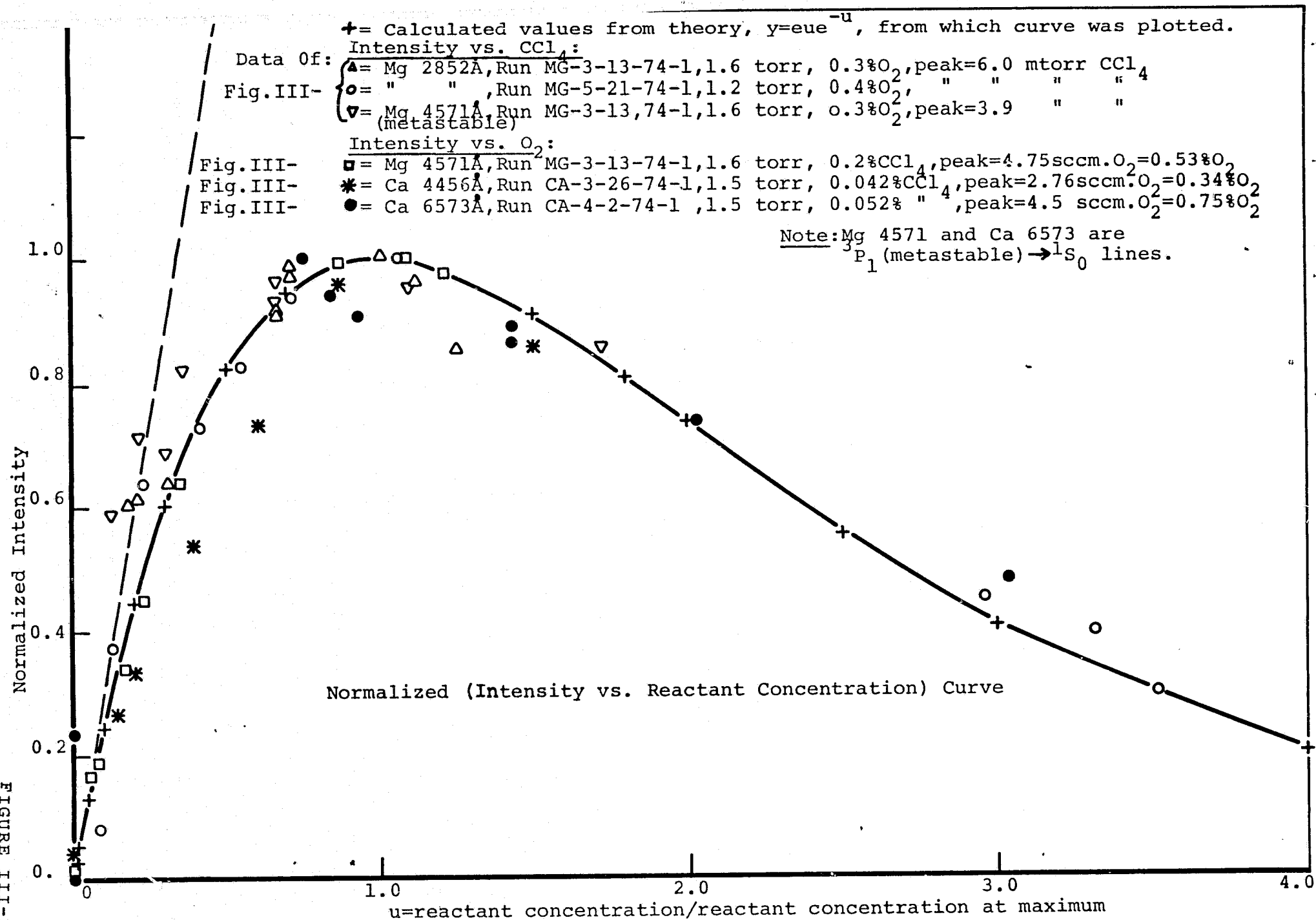
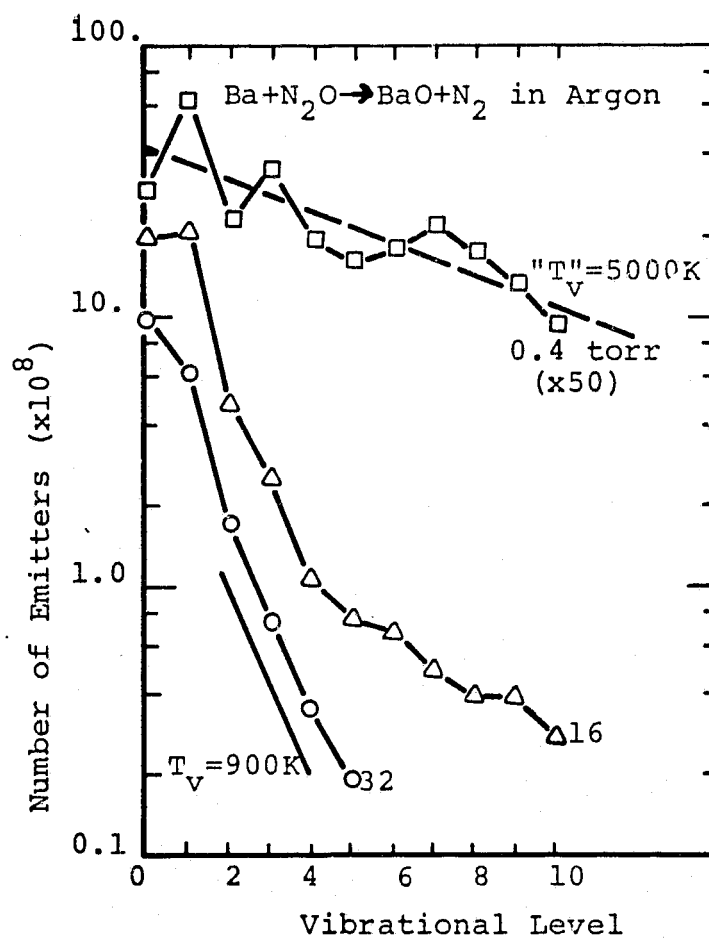


FIGURE III-39



Vibrational Population Distribution
of BaO(A¹Σ⁺) (After Jones and Broida, 1974.
5000K line added)

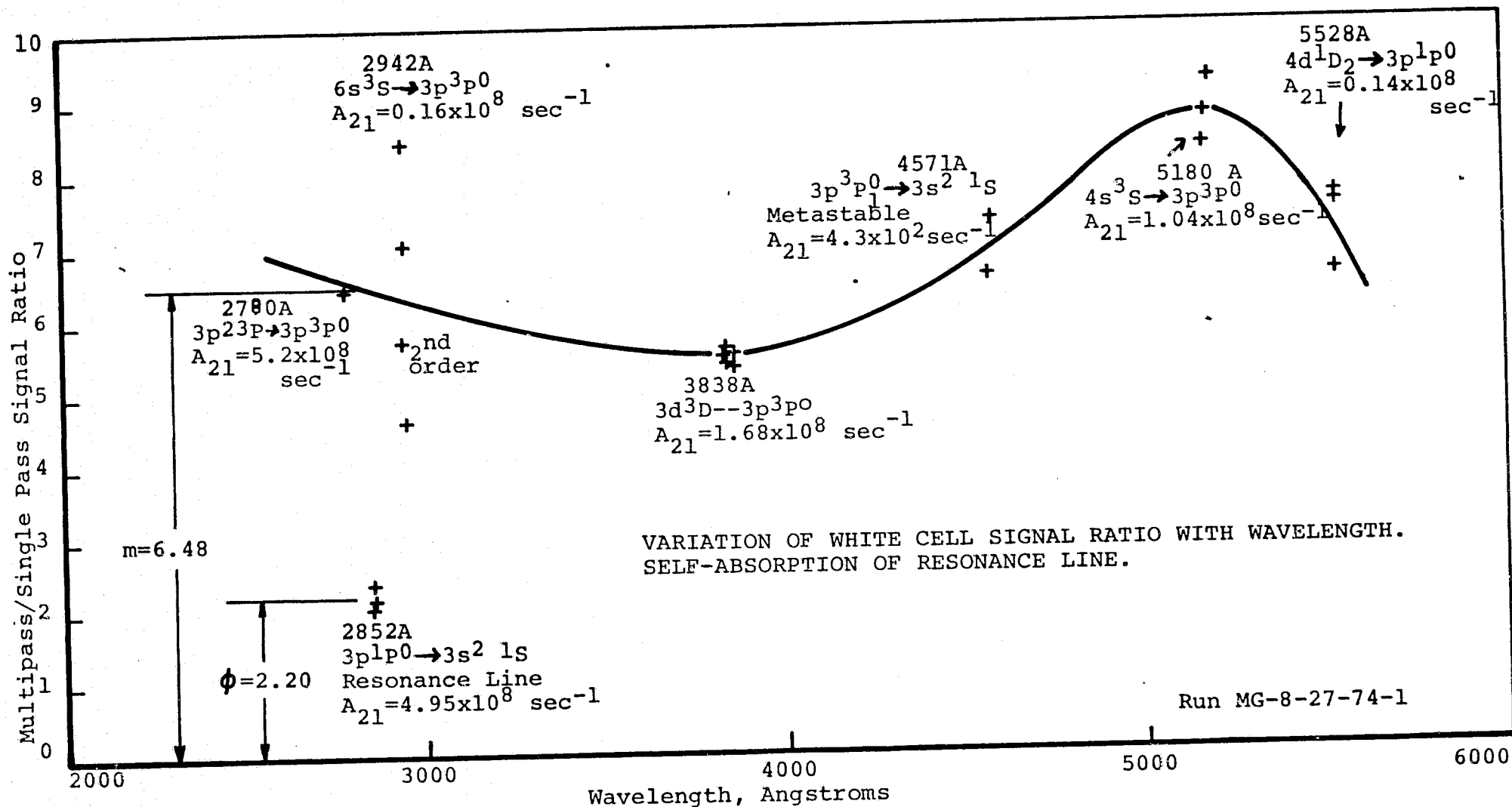
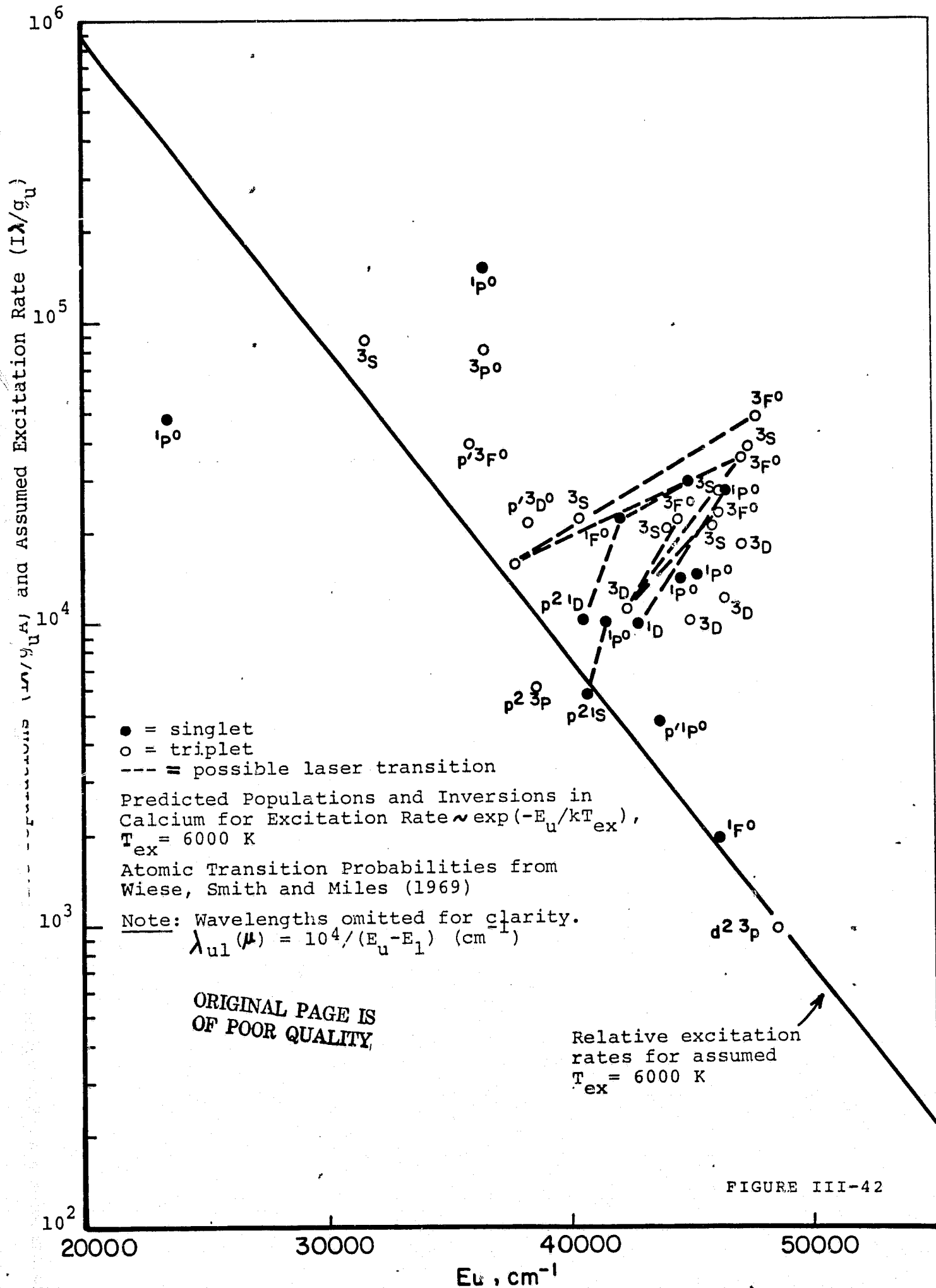


FIGURE III-41



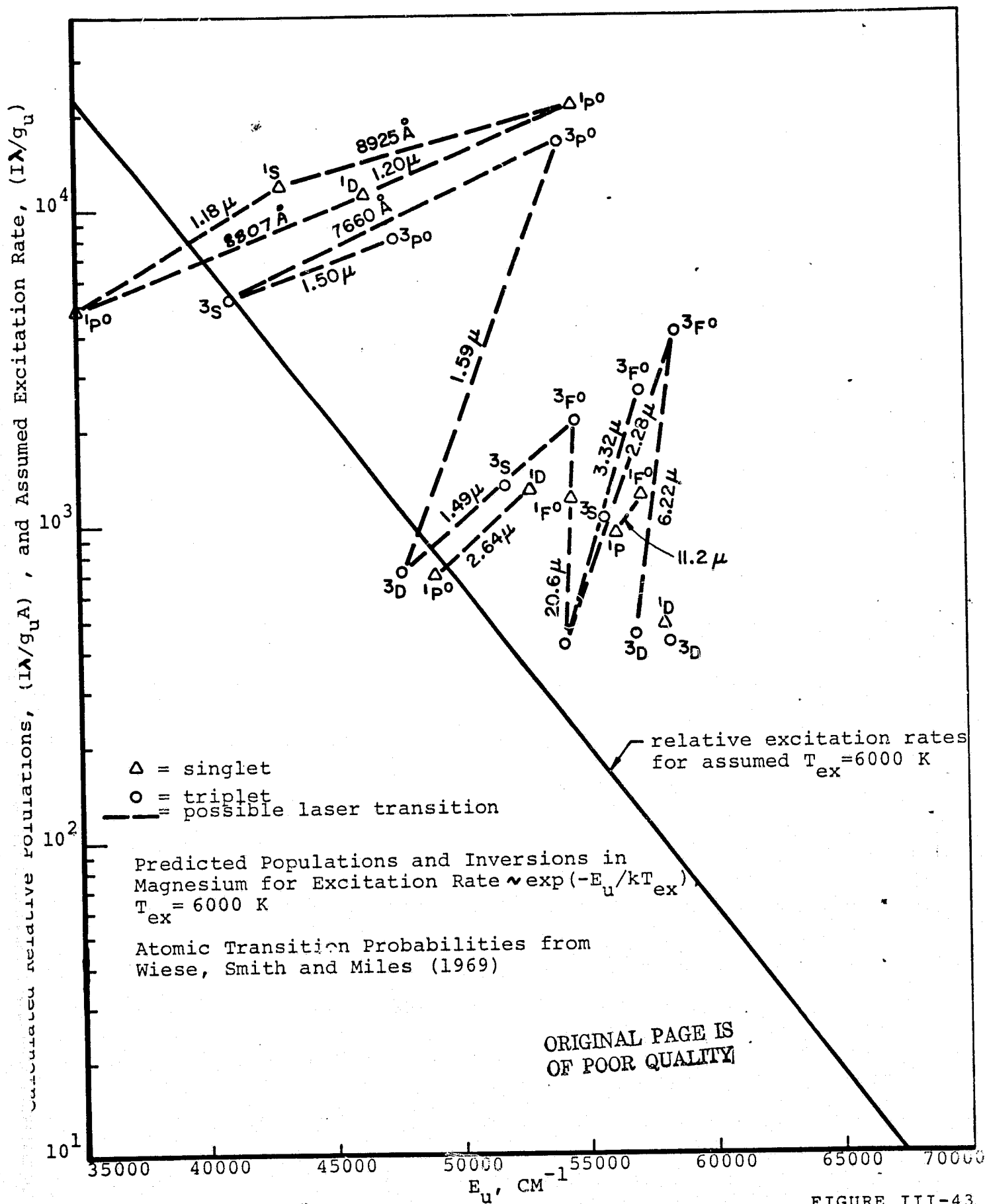


FIGURE III-43

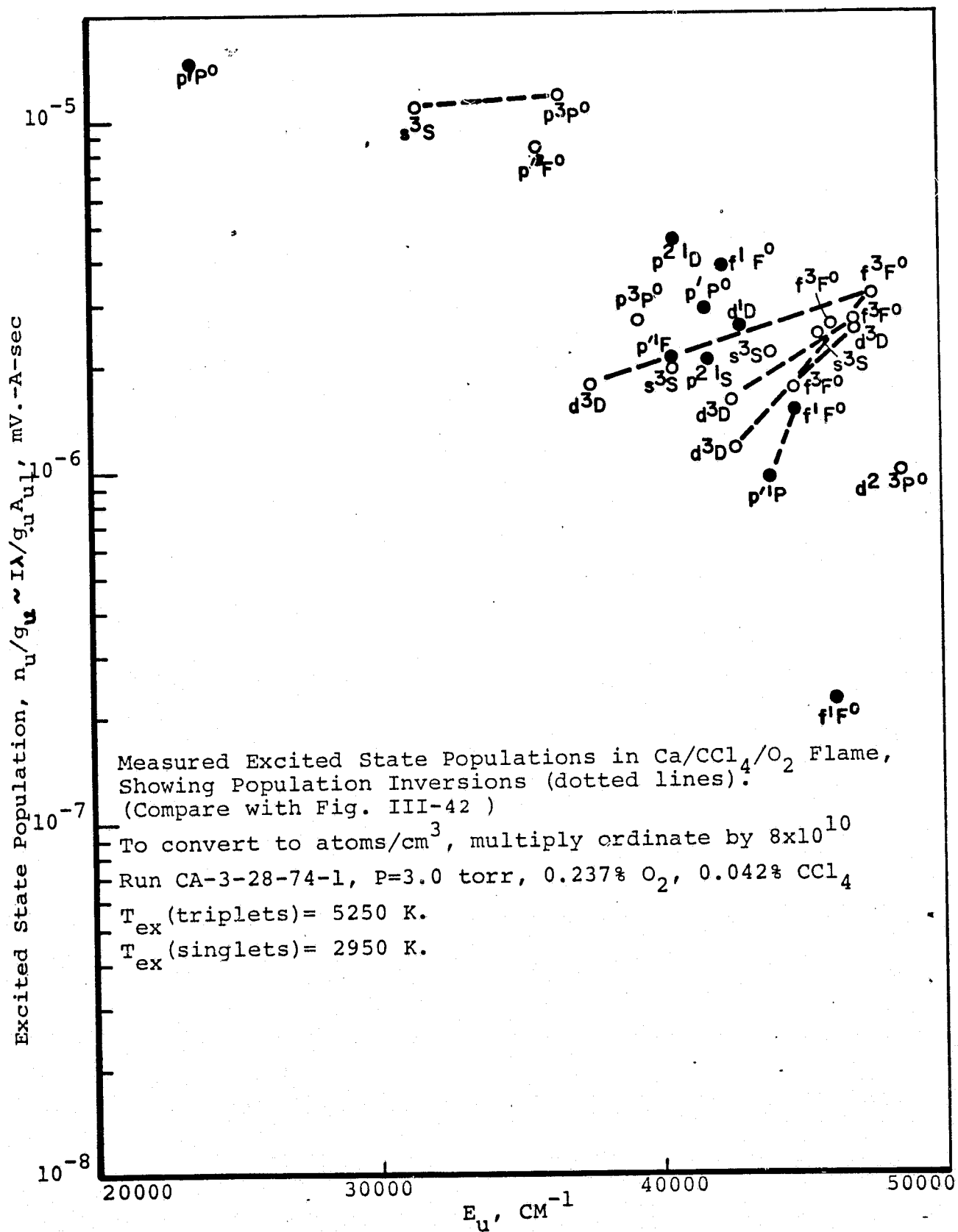
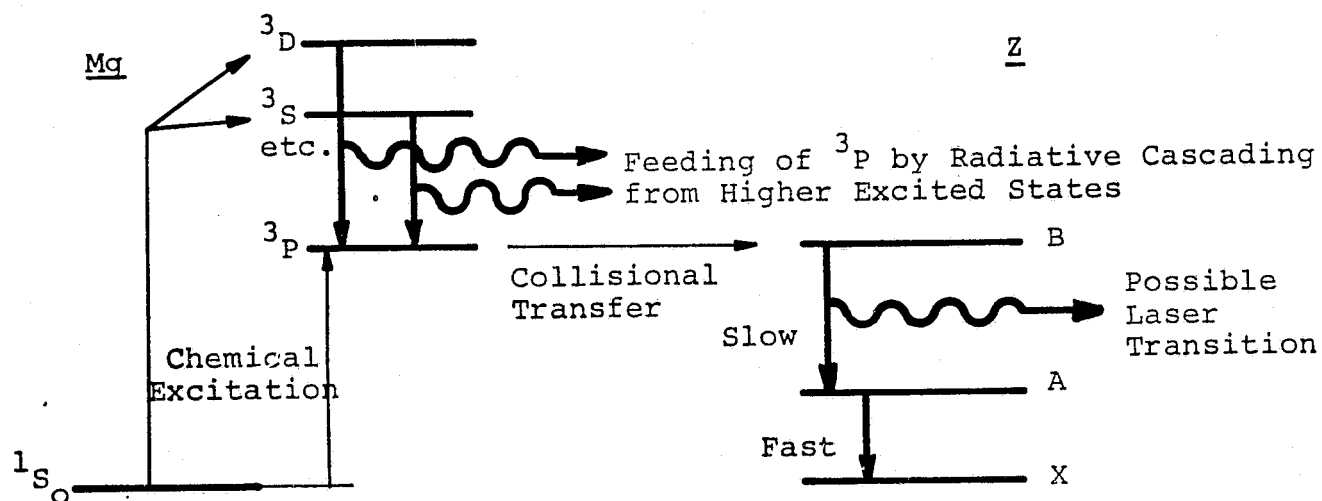
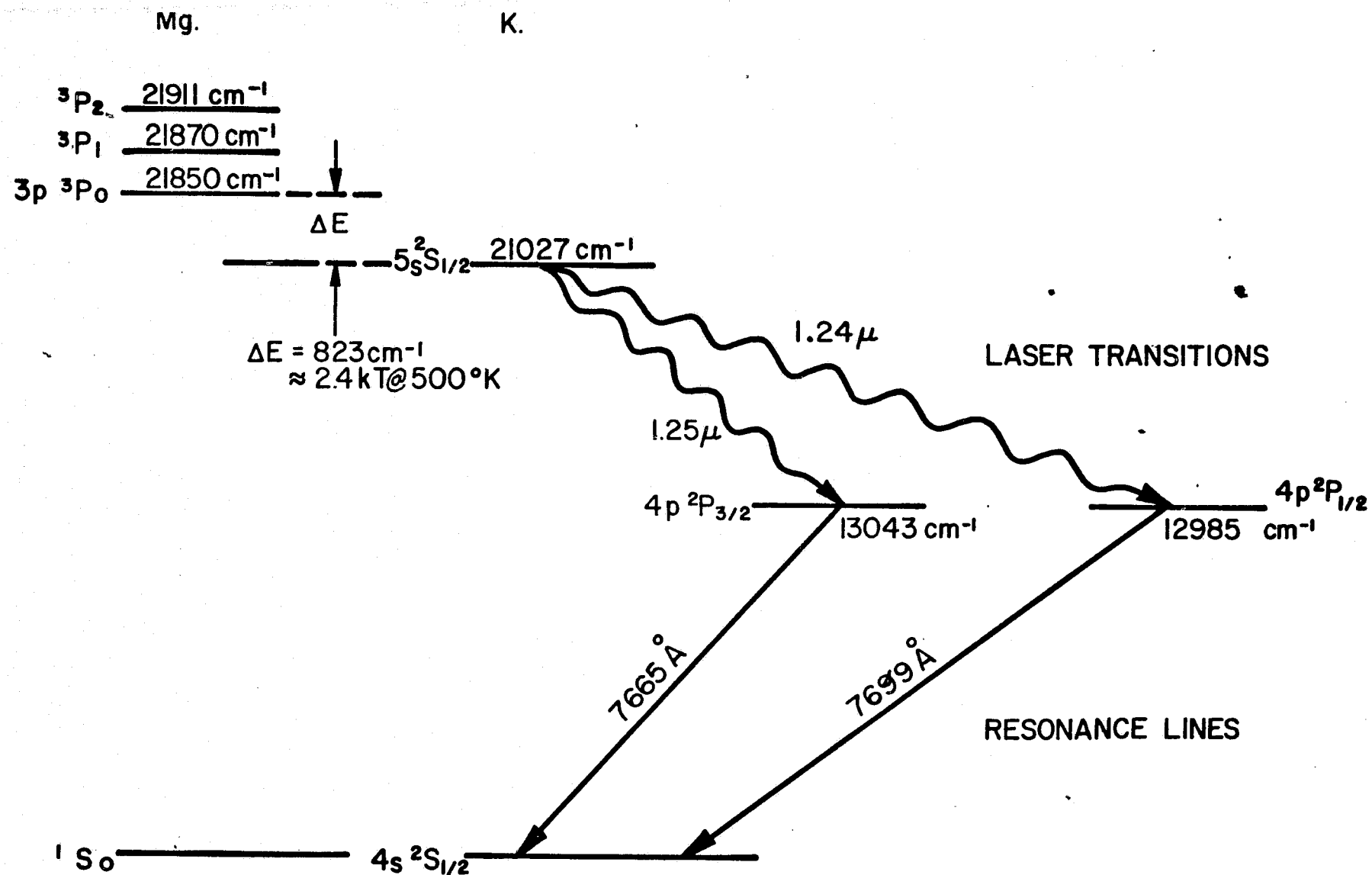


FIGURE III-44



Possible Methods of Producing Laser Action in the $\text{Mg}/\text{CCl}_4/\text{O}_2$ System by Using the $\text{Mg } 3p$ State as an Energy Reservoir for Resonant Excitation of Another Species.

FIGURE III-45



PRODUCTION OF POPULATION INVERSION IN POTASSIUM
BY COLLISIONAL ENERGY TRANSFER FROM $\text{Mg}^*(^3P)$ METASTABLE